Abrogating the G2/M checkpoint with PROTACs to enhance DNA damaging therapies

Lauryn Amy Buckley-Benbow

A thesis submitted for the degree of Doctor of Philosophy in the Faculty of Health and Medicine at Lancaster University

December 2023

Declaration

I hereby declare that this thesis is my own work, except where otherwise

stated, and has not been submitted for the award of a higher degree

elsewhere.

Abstract

Head and neck squamous cell carcinoma (HNSCC) incidence is expected to increase by 30% by 2030. Whilst rare, the five-year survival rate for HNSCC patients is only 50%, with tumours often resistant to genotoxic treatments. Survival data shows that the current treatment modality is ineffective, thus, it is critical to find targets for combinatorial treatment, to increase the efficacy of common tumour therapies against HNSCC. HNSCC tumours often have a dysfunctional G1/S checkpoint due to p53 mutations. Abrogating the G2/M checkpoint, via targeting of Wee1 (a serine/threonine kinase involved at the G2/M checkpoint), in this context would promote tumour cell death via synthetic lethality after radiotherapy or chemotherapy treatment.

Small molecule inhibitors (SMIs) are often used to target proteins clinically and AZD1775, a Wee1 inhibitor (Wee1i), has shown promise in clinical trials. Although potent, the Wee1i has many off-target effects, therefore our group developed Wee1 PROteolysis TArgeting Chimeras (PROTACs) to overcome selectivity issues. PROTACs are heterobifunctional molecules that contain an E3 ubiquitin ligase recruiting domain and a target protein domain. These ligands are connected via a linker and this molecule facilitates the formation of a productive ternary complex to polyubiquitylate the target protein and target it for degradation by the ubiquitin proteasome system (UPS).

Here, characterisation of Wee1 PROTACs in HNSCC with varying p53-status demonstrated that cereblon (CRBN)- and Von Hippel-Lindau (VHL)-based Wee1 PROTACs can successfully and rapidly degrade Wee1 and reduce the phosphorylation of its substrate, pCDK1 (Tyr15). Monotherapy use of Wee1 PROTACs caused a loss of cell viability and the most potent

compounds were used in lung and kidney cancer cell lines to investigate the bearing of E3 ligase expression on efficacy of the molecules. This work found that the ability for PROTACs to degrade their protein of interest was not dependent on absolute levels of E3 ligase present.

Clonogenic survival assays, cell viability assays and apoptosis detection flow cytometry were performed to evaluate the cytotoxicity of the combination of Wee1 inhibition or degradation with genotoxic agents. p53-deficient cell lines displayed more radiation- and cisplatin-induced cell death as a result of sensitization to the genotoxins from Wee1-targeting treatments. In addition, use of Wee1-targeting compounds alone induced apoptosis in the absence of a genotoxic agent.

HNSCC cell lines showed replication stress and irregularities in DNA content, indicative of chromosome missegregation or improper mitosis, when treated with Wee1-targeting compounds as single and combinatorial strategies. These observations provide insight that Wee1 PROTACs have potential to be used in place of SMIs and has provided a good foundation for future work to investigate if increased specificity is an advantageous trait for cancer treatment.

Acknowledgements

Firstly, I would like to thank Prof. Sarah Allinson for her support and guidance throughout my many years at Lancaster University. From my undergraduate dissertation to my PhD, you have consistently encouraged and supported me as well as provided invaluable opportunities to develop both personally and professionally. I would also like to thank my secondary supervisors, Dr Andrew Fielding at Lancaster University and Prof. Jason Parsons at University of Birmingham for their assistance and experimental ideas throughout the project. It has been a pleasure to work with all of you and I appreciate the support that you have given me starting this PhD during COVID-19. I was lucky to work with my initial supervisor Dr Morgan Gadd who provided great advice during the first year of my PhD.

I am grateful to Dr Nikki Copeland and Dr James Tollitt for their comments during and outside of lab meetings.

A special thank you to my fellow lab mates, Dr Amanda Thomaz and Dr Marine Aublette, who are two excellent scientists that I had the pleasure of working on these projects with.

I would also like to thank Emily Clayton and Amelia Bryers. You both never fail to make me smile. "You guys are the best thing that ever happened to me."

Thank you to my high school friends, especially Chloe, Lucy and Liv for their continuous support and kindness.

Thank you to North West Cancer Research for their funding and outreach opportunities. I have thoroughly enjoyed working with the charity.

Finally, I express the biggest thank you to my parents, Karen and Simon, and brothers, Max and Cory, for always listening and comforting me in the toughest of times. I would like to thank my recently departed Nan, Gillian, and godmother, Ellie. Along with my family, you were supportive of my dreams to become a scientist and I miss you both dearly.

Table of Contents

List of Figures

Chapter 1

Chapter 2

Chapter 3

Chapter 4

Chapter 5

Chapter 6

Chapter 7

List of Tables

Chapter 1

Chapter 2

Chapter 3

Chapter 4

Chapter 5

Chapter 6

Abbreviations

ANOVA: Analysis of variance

APC: Anaphase-promoting complex

ATM: Ataxia telangiectasia mutated

ATP: Adeonsine triphosphate

ATR: ATM and Rad3 Related

ATRIP: ATR-interacting protein

BCA: Bicinchoninic acid

BER: Base excision repair

BRCA1/2: Breast cancer associated protein 1/2

BSA: Bovine serum albumin

CDK: Cyclin dependent kinase

Chk1/2: Checkpoint kinase ½

CMG helicase: Cdc45-MCM-GINS helicase

CRBN: Cereblon

$CuSO_4$: Copper sulfate

DAPI: 4',6-Diamidino-2-phenylindole

DDR: DNA damage response

DMEM: Dulbecco's modified eagle medium

DMSO: Dimethylsulfoxide

DNA: Deoxyribonucleic acid

dNTP: Deoxynucleotide triphosphates

DSB: Double strand break

dsDNA: Double-stranded DNA

DTT: Dithiothreitol

EC50: Half maximal effective concentration

EDTA: Ethylenediaminetetraacetic acid

EdU: 5'-Ethynyl-2'-Deoxyuridine

EGFR: Epidermal growth factor receptor

ER: Oestrogen receptor

FA: Fanconi anaemia

FBS : Fetal bovine serum

H2AX : Histone H2AX

H_2O: Water

H_2O_2: Hydrogen peroxide

H_2SO_4: Sulfuric acid

HCl: Hydrochloric acid

HIF: Hypoxia-inducible factor

HNSCC: Head and neck squamous cell carcinoma

HR: Homologous recombination

ICL: Interstrand crosslink

IR: Ionizing radiation

ITC: Isothermal titration calorimetry

LUAD: Lung adenocarcinoma

MQW: MilliQ Water

MRN complex: MRE11-Rad50-Nbs1 complex

mRNA: Messenger RNA

MT: Microtubule

NaCl: Sodium chloride

NaN_3: Sodium azide

NaOH: Sodium hydroxide

NER: Nucleotide excision repair

NHEJ: Non-homologous end joining

ORC : Origin recognition complex

p53 : Cellular tumour antigen p53

PARP-1 : Poly(ADP-ribose) polymerase 1

PBS: Phosphate buffered saline

PCM: Pericentriolar material

PCNA: Proliferating cell nuclear antigen

PFA: Paraformaldehyde

PI: Propidium iodide

PLK: Polo-like kinase

POM: Pomalidomide

PROTAC: Protelysis targeting chimera

PS: Penicillin-Streptomycin

PTM: Post-translational modification

RCC: Renal cell carcinoma

RNA: Ribonucleic acid

RNase: Ribonuclease

ROI: Region of interest

RPM: Revolutions per minute

RPMI: Roswell Park Memorial Institute

SAR: Structure activity relationship

SCF: Skp1-Cullin-F-box protein

SDS : Sodium dodecyl sulphate

SDS-PAGE: Sodium dodecyl sulphate polyacrylamide gel electrophoresis

SPR : Surface plasmon resonance

TBS: Tris buffered saline

TBST: Tris buffered saline with 0.1% Tween-20

TEMED: Tetramethylethylenediamine

TGS: Tris-Glycine-SDS

TPD: Targeted protein degradation

Tyr: Tyrosine

Ub: Ubiquitin

UPS: Ubiquitin proteasome system

v/v: Volume by volume

VHL: Von Hippel-Lindau

w/v: Weight by volume

WT: Wild type

Y: Tyrosine

γH2AX: Gamma H2AX

1 Introduction

1.1 The eukaryotic cell cycle and cancer development

1.1.1 Overview of the eukaryotic cell cycle

The eukaryotic cell cycle is a heavily regulated sequence of signalling pathways that controls cellular replication and growth. The mitotic cycle is sub-divided into interphase, which accounts for 95% of the cycle, and mitosis to ensure the unidirectional replication and segregation of DNA (Araujo et al., 2016). Interphase is comprised of two "gap" phases and one synthesis phase (Figure 1.1).
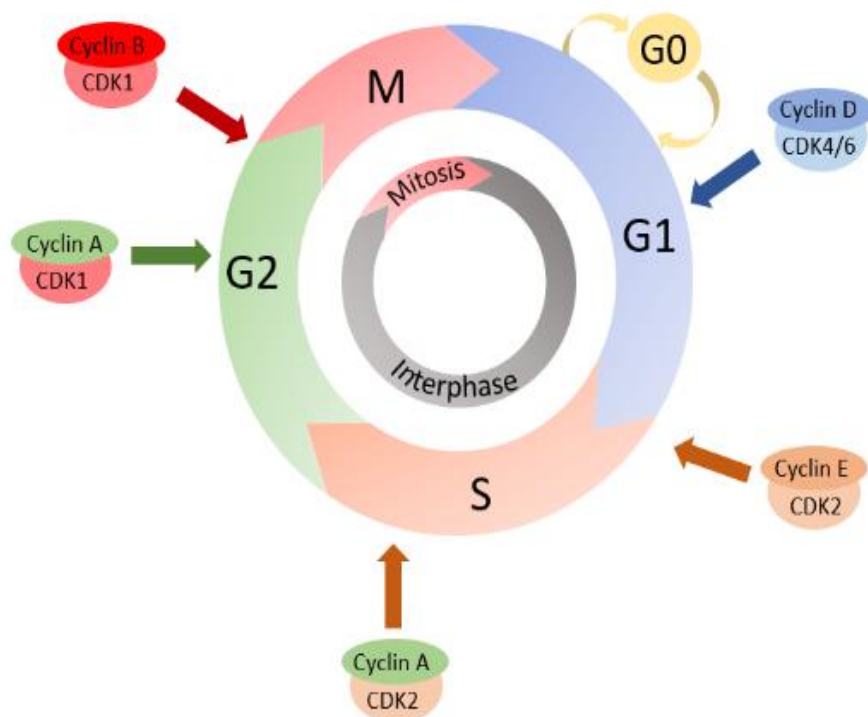
Figure 1.1 The Eukaryotic Cell Cycle stages and their Regulators. Schematic of the four main stages, G1, S, G2 and M, of the eukaryotic cell cycle. The phases G1, S and G2 are part of the broader phase, interphase. G0, also known as quiescence, is a reversible resting phase that lies outside of the replicative cycle. When a cell is in quiescence, it can re-enter the cell cycle into G1, however sometimes cells can enter an irreversible G0 state known as senescence. Cyclins are expressed at key stages to drive the cell through the cycle by activating CDKs, which help regulate these stages and ensure that the cell cycle is unidirectional.

1

The purpose of the pre-replicative gap phase, G1, is to assess if the cell is in a suitable environment to proliferate and, if so, the cell can pass the G1/S transition checkpoint. S phase is where duplication of the genomic DNA occurs and the final checkpoint, the G2/M checkpoint, will determine if the genomic DNA is free of DNA damage and the cell is prepared for division (Matthews et al., 2021). The cell will subsequently progress into mitosis. Mitosis is the physical segregation of the copies of DNA to produce two separate nuclei that each make up their own genetically identical daughter cell after cytokinesis (Figure 1.2) (Yanagida, 2014). During mitosis, the condensed chromosomes migrate towards the metaphase plate before being pulled apart, with the aid of mitotic spindles, to pull the DNA to separate poles of the cell (Alberts et al., 2002). This ensures that the daughter cells will have the correct quantity of genetic information.
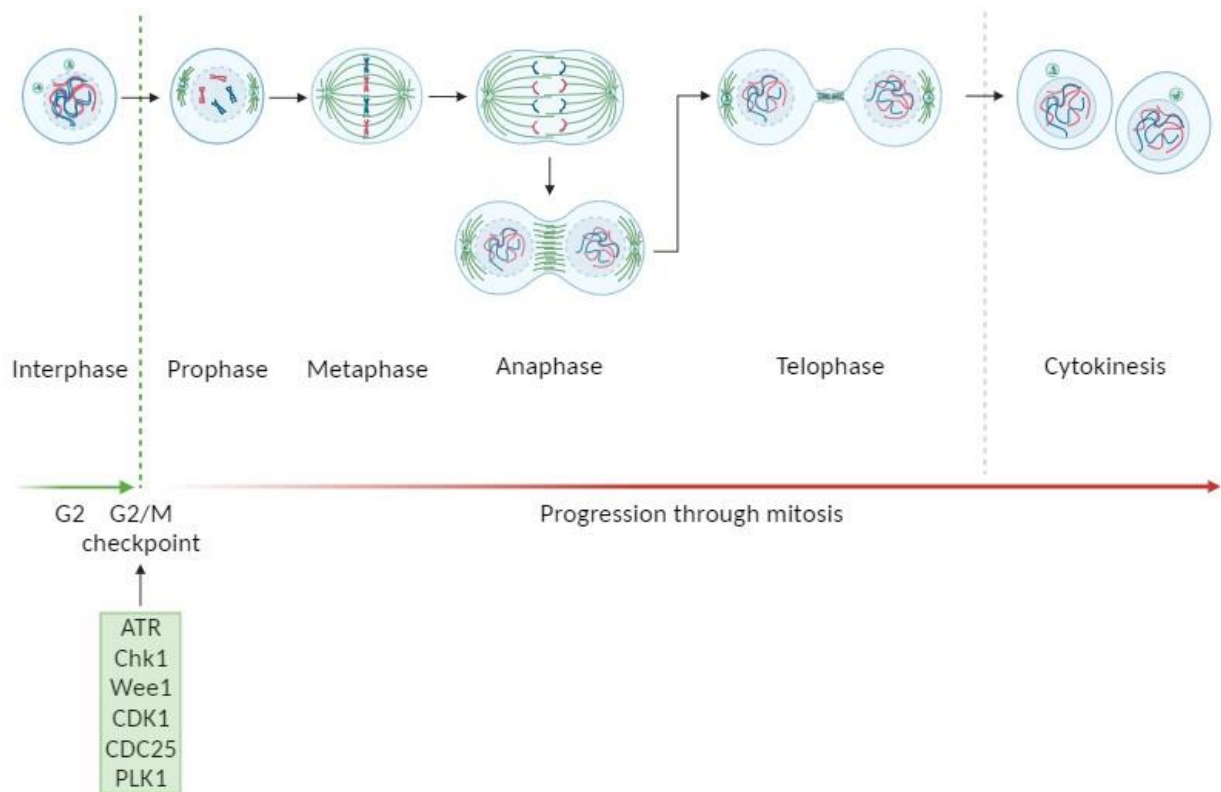
Figure 1.2 Cell division by mitosis in eukaryotes. Schematic of progression of the cell through different stages of mitosis. Once the cell has passed the G2/M checkpoint, regulated by a plethora of kinases and phosphatases, the chromosomes condense (prophase) and line up along the metaphase plate (metaphase). Progression past the spindle formation checkpoint into anaphase allows sister chromatids to be pulled apart and the nuclear envelope begins to reform around the DNA in each daughter cell (telophase). Cytokinetic abscission allows for the intercellular bridge to be severed and the physical separation of the two daughter cells (cytokinesis). Figure produced using BioRender.com.

Cell cycle arrest at the G1/S transition, intra-S phase and the G2/M checkpoints can occur upon the cells sensing DNA damage in order to maintain genomic stability (Iyer and Rhind, 2017). Dormant cells are found in G0, where the cell is in quiescence or senescence which are reversible and irreversible G0 states, respectively. Cells may enter quiescence if they are fully differentiated, such as neurons, or they can enter cellular senescence due to a constant DNA damage response (DDR) or environmental stress factors (Rodier and Campisi, 2011).

Cellular senescence is an alternative to apoptosis for cells when DNA damage has been detected.

Cyclin-dependent kinases (CDKs) play a crucial role in ensuring the cell cycle is appropriately controlled to prevent DNA damage going unnoticed and resulting in genome instability. The activation of CDKs is tightly regulated and they are highly expressed throughout the cell cycle (Arooz et al., 2000). Their binding partners, known as cyclins, are differentially expressed (Figure 1.3) throughout the cell cycle and their main role is to ensure unidirectional progression of the cell cycle (Satyanarayana and Kaldis, 2009).
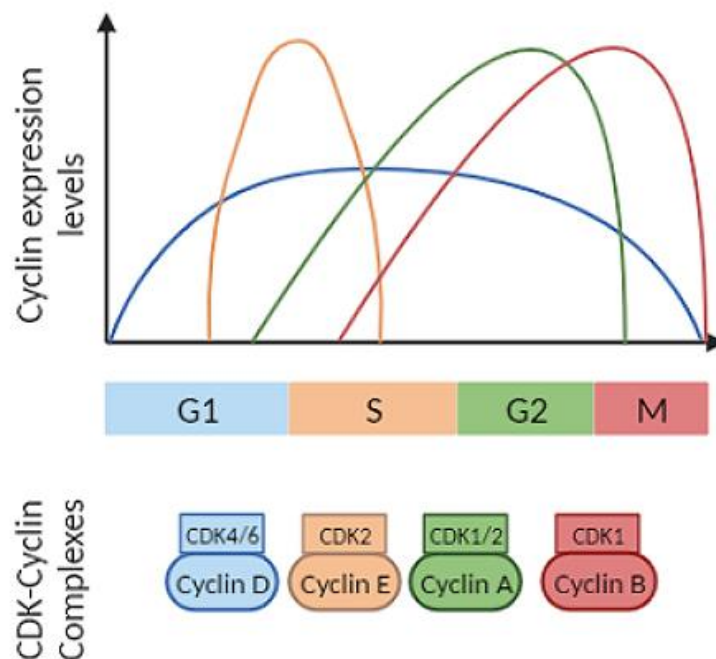
Figure 1.3 Cyclin Expression in eukaryotic cell cycle. Cyclin D, associated with CDK4/6, is crucial for progression through G1. Cyclin E, associated with CDK2, helps to progress the cell into S by preparing for DNA replication and cyclin A, associated with CDK1/2, activates DNA replication in S phase. Cyclin B, associated with CDK1, drives progression into M phase by promoting the assembly of the mitotic spindle. Adapted from (Hochegger et al., 2008). Figure made using BioRender.com

4

CDK inhibitors, various phosphatases and other regulators are key to opposing the activity of CDKs, demonstrating the complexity and numerous mechanisms that control the cell cycle (Vermeulen et al., 2003). As dysregulation of the cell cycle is a major factor in cancer, cell cycle checkpoints and the molecules that regulate them are potential targets for therapeutics that could lead to better prognoses.

1.1.2 Cell cycle checkpoints and cancer development

Cell cycle checkpoints play a major role in preventing tumorigenesis and maintaining genome stability. The G1/S transition is the first and key checkpoint; once a cell has passed this checkpoint, it is committed to the cell cycle. As previously discussed, the cell cycle and its checkpoints are heavily regulated by CDK activity, and this section will go into more detail about these at each checkpoint.

At the G1/S and G2/M checkpoints, cascades of protein phosphorylation can be activated as a response to conditions such as DNA damage accumulation or incomplete DNA replication as a result of stalled replication forks (Figure 1.4) (Reinhardt and Yaffe, 2009). Common checkpoint signalling pathways mainly function to ensure CDKs remain in their inactive state until the DNA damage has been repaired and, dependent on the type of DNA lesion, specific DNA repair pathways will be later activated (Barnum and O'Connell, 2014). These signalling mechanisms are within two major kinase cascades that start with the master regulators, ATR, and ATM. These PI3-kinase-like kinases (PIKKs) initiate the checkpoint response by phosphorylating the downstream effector kinases Chk1 and Chk2, respectively (Abraham, 2001; Bartek and Lukas, 2003). If any of these cell cycle checkpoints are defective, this can lead to inappropriate cell division, mutations, and the initiation of cancer.
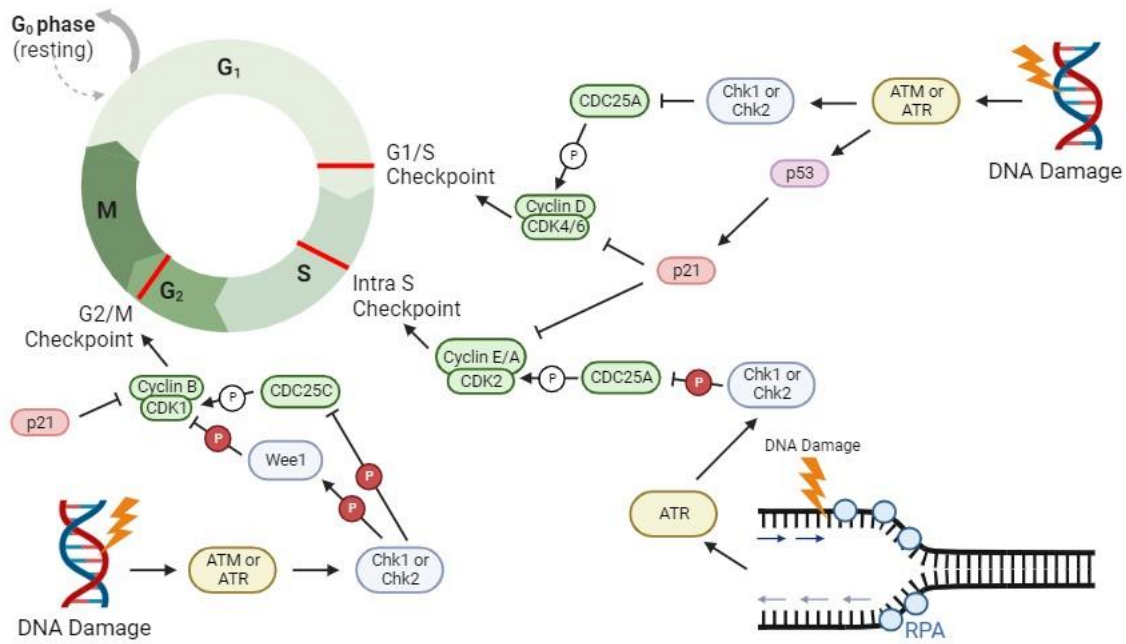
Figure 1.4 Phosphorylation cascades at cell cycle checkpoints. Diagram showing how DNA damage is sensed at each checkpoint and the signalling pathways that lead to the DNA damage repair response. Apical kinases, ATM and ATR, will be activated by DNA lesions which subsequently phosphorylate downstream targets, leading to arrest at checkpoints in the cell cycle. Although there has been some discussion of interplay between these kinases, classically ATM phosphorylates Chk2 and ATR phosphorylates Chk1 upon DNA damage. At the G1/S transition, these activated checkpoint kinases (Chk1 and Chk2) phosphorylate and inhibit phosphatase CDC25A, therefore the inhibitory phosphate is not removed from CDK4/6 and the Cyclin D-CDK4/6 complex cannot form. This causes arrest at the G1/S transition. This cascade is similar to the arrest at the intra-S phase checkpoint, however it is the Cyclin E/A-CDK2 complex that cannot form and allow for S-phase progression. Finally, Chk1/2 can also phosphorylate and activate Wee1, which results in phosphorylation of CDK1 by Wee1, and the Cyclin B-CDK1 complex cannot form leading to G2/M arrest. Furthermore, tumour suppressor protein p53 becomes activated when there is DNA damage present. This results in upregulation of p21 expression, a CDK inhibitor, which further helps to arrest cells at checkpoints before DNA damage is repaired. Unrepaired damage will lead to mutations and, if these are in proteins involved in these signalling cascades, uncontrolled cell division will result in tumorigenesis. Figure made using BioRender.com.

1.1.2.1 G1/S transition

The G1/S checkpoint, also known as the Restriction Point (RP), is the first checkpoint of the eukaryotic cell cycle (Figure 1.4). This checkpoint is responsible for a cell to become

committed to cell division once it has progressed past this point and into S phase (Norbury and Nurse, 1992; Skotheim et al., 2008). If the cell is well prepared for growth, G1/S transcriptional activation occurs in order to begin replication of G1/S genes and promote S phase entry (Bertoli et al., 2013b). G1/S transcriptional activation peaks at the G1/S transition and a positive feedback loop, heavily regulated by CDKs, ensures that gene expression continues to rise and is fully activated in S phase. The main function of the cyclin-CDK complexes is to phosphorylate pocket proteins, such as Retinoblastoma (RB), that usually bind to E2F family members to inhibit the expression of E2F-regulated genes (Hatakeyama and Weinberg, 1995; Helin, 1998; Helin et al., 1993). The transcriptional repressors RB, p107 and p130 are usually bound to E2F transcription factors, however once phosphorylated by Cyclin D-CDK4/6 complexes, the conformation of the protein changes and transcription of G1/S target genes is no longer inhibited (Bertoli et al., 2013b). This emphasises the importance of CDK-dependent phosphorylation for the regulation of the cell cycle. Additionally, the ATR-Chk1 DDR pathway at G1/S ensures phosphorylation of key effector proteins, such as p53, to stall G1/S progression (Tibbetts et al., 1999). This demonstrates the crucial involvement of ATR/Chk1 for promoting genome integrity at the G1/S transition before the cell is committed to the cell cycle. The ATM-Chk2 pathway responds to DNA damage accumulation to ensure that cells do not enter the cell cycle. For example, and upon ionising radiation-induced DNA damage, ATM phosphorylates Chk2 which in turn phosphorylates Cdc25A to target the protein for degradation (Figure 1.4). The activation of ATM also leads to phosphorylation of p53 and Mdm2 which causes G1/S arrest (Maya et al., 2001; Zhang and Xiong, 2001).

A common mutated gene that regulates the G1/S transition checkpoint is *TP53*, encoding the tumour suppressor protein, p53. p53 is known as the "guardian of the genome" due to

its key regulation at the G1/S transition, performing as a DNA damage sensor (Lane, 1992).

First detected in complexes with SV40 T-antigen, p53 was initially classified as an

"immortalising oncogene" as it could work with the oncoprotein Ras to transform primary

rat embryo fibroblasts (Lane and Crawford, 1979; Linzer and Levine, 1979; Olivier et al.,

2002; Oren and Levine, 1983). Co-expression of mutant p53, resulting in loss of p53, and H-

Ras^{G12V} has displayed synergistic effects that leads to upregulation of downstream target

genes of Ras, causing aggressive transformation of phenotypes (Buganim et al., 2010;

Parada et al., 1984). It was discovered that p53 functions at the G1/S checkpoint to cause

cell cycle arrest when DNA damage is detected, behaving as a protector for the cells against

genotoxic damage (Kastan et al., 1991). p53 will become activated via posttranslational

modifications (PTMs) as a result of intrinsic and/or extrinsic stress signals, resulting in

cellular senescence, apoptosis or cell cycle arrest, depending on the severity of the signal

(Jin and Levine, 2001). A specific function of the p53 pathway is expression and activation of

proteins to repair DNA damage, therefore if p53 is mutated or null in cells, DNA damage can

remain unchecked and will lead to cancer development (Harris and Levine, 2005).

Furthermore, this transcription factor upregulates expression of genes that induce apoptosis

and oppose proliferation in response to cellular stress, oncogene activation and genotoxic

damage induced by drugs, irradiation, or hypoxia. Thus, p53 is key for regulating cellular

growth and, if it becomes dysfunctional, a key cell cycle checkpoint will be lost, and cancer is

more likely to develop.

These pathways are crucial to the G1/S transition to maintain genome stability, hence in

many cancers these proteins, especially p53, will be mutated to allow tumour growth

(Levine, 1997; Petitjean et al., 2007). This leads to such cancer cells becoming heavily reliant

on the G2/M checkpoint to repair DNA damage so that their genome does not become so unstable that viable daughter cells cannot be produced.

1.1.2.2 Intra S-phase checkpoint

The G1/S transition is crucial to detect DNA damage before the cell commits to the cell cycle however, S phase is when the most DNA damage will occur. This makes the intra-S phase checkpoint crucial to maintenance of genomic stability. The ATR-Chk1 pathway plays an important role in response to replication stress in S phase. On activation, Chk1 inhibits E2F6, a E2F repressor, by phosphorylating it and releasing it from promoter regions to allow reactivation of the G1/S transcriptional programme to respond to the replication stress (Bertoli et al., 2013a). Furthermore, ATR negatively regulates origin firing, which it performs in both damaged and unperturbed S phase cells (Saldivar et al., 2017). ATR, however, can be activated by multiple different types of DNA lesions which suggests that there is a common intermediate involved in the response to these abnormalities. This has been suggested as the replication protein A (RPA)-single-stranded DNA (ssDNA) complex (Paulsen and Cimprich, 2007). RPA is recruited to protect single stranded DNA (ssDNA) when a lesion causes a stalled replication fork and causes the unwinding of DNA. This binding protein covers the ssDNA to produce a protective coating, and this subsequently recruits ATR-interacting protein (ATRIP) and ATR (Zou and Elledge, 2003). Because RPA-coated ssDNA is produced as a normal intermediate during replication, the intra-S phase checkpoint is activated during every S phase and monitors fork progression and origin firing. However, the amount of Chk1 activation differs dependent on if the cell is unperturbed or a checkpoint response is required due to the presence of DNA damage (Iyer and Rhind, 2017). Therefore,

the greater the amount of ssDNA present in a perturbed fork, the more Chk1 activation and

a stronger checkpoint response is required (Byun et al., 2005). This highlights the

importance of ATR and Chk1 for preventing aberrant DNA replication and in supressing

potential tumour development.

ATM is less important than ATR for the intra-S phase checkpoint, but provides a fast

response that involves phosphorylation of Nbs1 and Chk2 after DNA damage (Zhou et al.,

2002). Here, ATM activates Chk2 which subsequently phosphorylates Cdc25A to target it for

degradation and to stop activation of Cdk2, which subsequently causes arrest at the intra-S

checkpoint (Falck et al., 2002). It has been shown that defects within the ATM-Chk2-Cdc25A

or ATM-Nbs1-Mre11 pathways cause the S-phase checkpoint to become dysfunctional,

therefore showing the importance of ATM in DNA damage repair at this checkpoint (Falck et

al., 2002). For the purposes of this thesis, the regulatory mechanisms of the S phase

checkpoint, such as the maintenance of transcription of G1/S phase genes, will not be

discussed in detail however, more comprehensive reviews on this topic are available (Ciardo

et al., 2019; Errico and Costanzo, 2012; Iyer and Rhind, 2017).

1.1.2.3 G2/M checkpoint

The G2/M checkpoint has an important function in maintaining genome stability as it utilises

the DNA damage response to ensure that daughter cells are not produced with mutations

present. The key regulator of the G2/M checkpoint is CDK1 (Cdc2 in fission yeast). When

CDK1 successfully interacts with its binding partner, cyclin B, this creates the maturation

promoting factor (MPF) which is the main complex that drives cells into mitosis (Figures 1.1

and 1.4) (King et al., 1994). For the cell to arrest at the G2/M checkpoint, inhibition of MPF

is crucial. Similar to the other checkpoints, ATR and ATM are key apical kinases that begin the phosphorylation cascade to halt cell cycle progression, therefore defects in these enzymes will significantly affect the DDR as well as apoptosis and cell cycle arrest (Ngoi et al., 2021; Shiloh, 2003). When DNA damage is present at the G2/M checkpoint, ATR is activated to phosphorylate Chk1, which subsequently promotes the Cdk1 inhibitory kinase, Wee1, and inhibits the phosphatase, Cdc25c (Figure 1.4) (Parker and Piwnicaworms, 1992). Consequently, inhibitory phosphorylation of tyrosine-15 (Y15) of CDK1 by Wee1 occurs, thus rendering the CDK unable to bind to cyclin B and drive cell cycle progression (Nurse, 1975; Russell and Nurse, 1987). This ultimately leads to arrest at the G2/M checkpoint to allow time for DNA damage repair to occur. The G2/M checkpoint represents the last opportunity to ensure that all DNA damage is repaired, however if this signalling pathway becomes defective, this can lead to the introduction of mutations but also mitotic catastrophe.

Collectively, this demonstrates the importance of the key regulatory proteins of the cell cycle checkpoints, such as ATR/ATM, Wee1 and Chk1, in normal physiology. However, these enzymes also show great potential as therapeutic targets through which inducing mitotic progression in cancer cells that have DNA damage present can stimulate cell death via mitotic catastrophe (Chen et al., 2012; Toledo et al., 2017; Visconti et al., 2016).

1.2 Genome instability and carcinogenesis

The importance of a heavily regulated cell cycle, discussed in section 1.1, is crucial for the successful repair of DNA damage and for the maintenance of genomic stability. Successive alterations of the genome can result in advantageous mutations that allow for cells to grow in the absence of mitogens. This makes genome instability and mutation a key hallmark of cancer (Hanahan and Weinberg, 2011). The hallmarks of cancer are continuously being updated and there are currently 14 hallmarks of cancer that encompass a wide array of characteristics of cancer ranging from inflammatory responses to resistance of cell death (Figure 1.5) (Hanahan, 2022). Targeting of these hallmarks of cancer to increase cancer cell death is continuously a well-researched field (Hanahan and Weinberg, 2011).
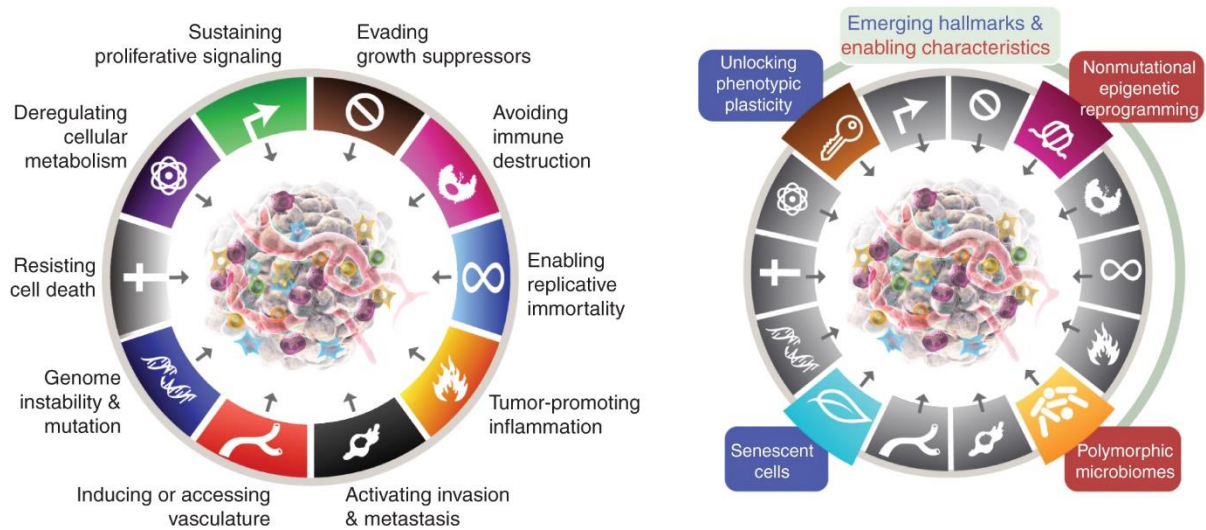
Figure 1.5 The fourteen hallmarks of cancer. In 2000, it was proposed that there were six acquired capabilities of cancer; sustaining proliferative signalling, evading growth suppressors, activating invasion and metastasis, resisting cell death, inducing or accessing vasculature and enabling replicative immortality. In 2011, two more emerging hallmarks, deregulating cellular metabolism and avoiding immune destruction, and an additional two enabling characteristics, tumor-promoting inflammation and genome instability and mutation, were suggested. These can be seen in the left-hand figure. On the right, in the most recent review in 2022, four additional proposed emerging hallmarks and enabling characteristics are senescent cells, polymorphic microbiomes, unlocking phenotypic plasticity and nonmutational epigenetic reprogramming. Figure taken from Hanahan (2022).

1.2.1 Types of DNA damage

DNA is highly receptive to modifications by exogenous and endogenous factors, therefore types of damage can be broadly characterised into these two main categories (Chatterjee and Walker, 2017). Exogenous DNA damage occurs due to physical, chemical or environmental agents, such as ionizing radiation and carcinogens in tobacco smoke, whereas endogenous DNA damage is produced as a result of the reactive DNA interacting with its surroundings, such as with water and reactive oxygen species (ROS) (Figure 1.6).
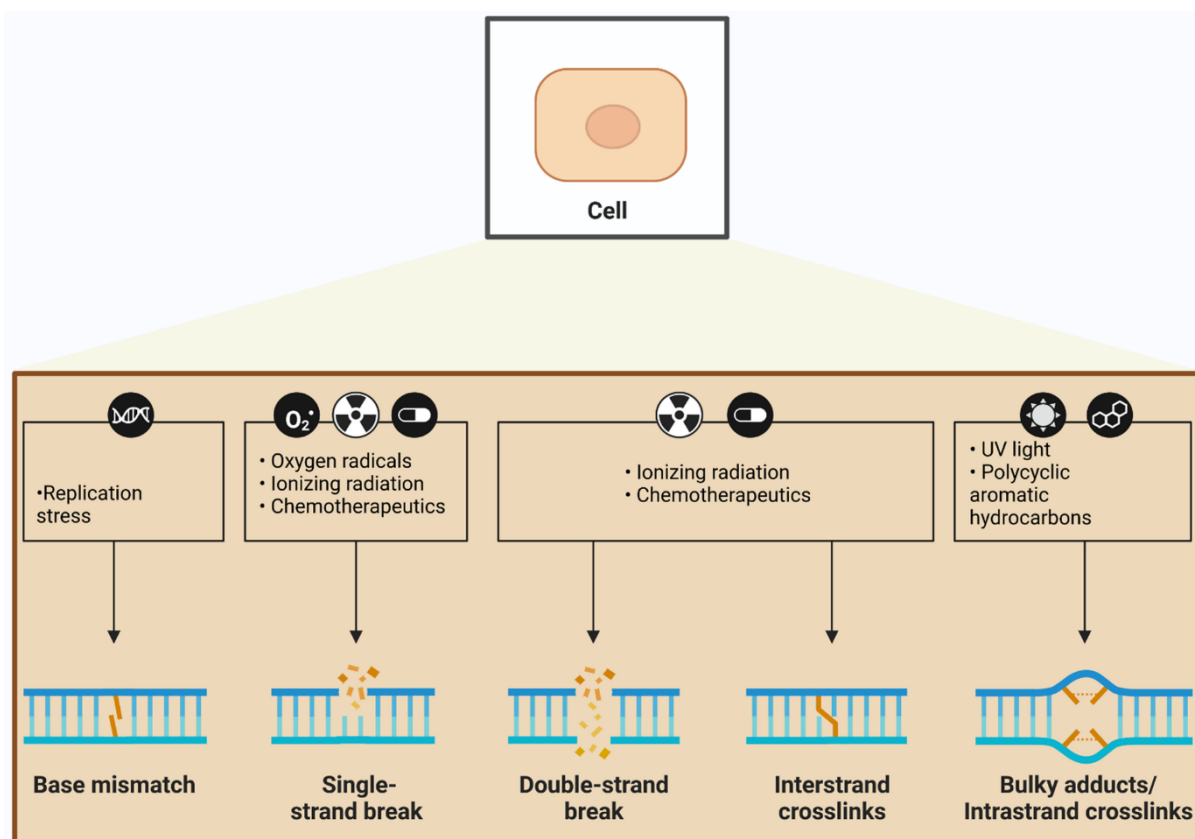
Figure 1.6 Types of DNA damage. Ionizing radiation and chemotherapeutics induce SSBs, DSBs and interstrand crosslinks. Free radicals mainly induce SSBs and bulky DNA adducts/intrastrand crosslinks form as a result of damage by UV radiation. Replication stress often causes base mismatches. Figure taken from (Shadfar et al., 2023).

For example, ionizing radiation (IR), an exogenous agent, can damage DNA directly or indirectly by producing highly reactive hydroxyl radicals as a result of radiolysis of water

(Desouky et al., 2015), hence why it can form different types of DNA damage. Approximately 65% of radiation-induced DNA damage is base lesions as a result of hydroxyl radicals and the most common lesions are 8-oxo-guanine, thymine glycol and formamidopyrimidines (Vignard et al., 2013). Although ionizing radiation causes DNA damage which can enhance tumorigenesis, IR is often used to treat cancers to decrease the stability of the genome and lead to cancer cell death. Cisplatin, a platinum-based chemotherapeutic, is another agent that inflicts DNA damage and is used as a treatment for cancers. Cisplatin binds to the N7 reactive centre on purine residues causing intrastand crosslinks between cisplatin and DNA. This leads to blocking of DNA replication and cell division, often resulting to cell death (Dasari and Tchounwou, 2014). In some cases, a single type of agent can induce multiple types of DNA damage, therefore established repair pathways that repair specific DNA damage lesions are crucial to maintain genome stability.

1.2.2 DNA damage repair pathways

1.2.2.1 Base excision repair (BER)

One of the major DNA damage repair pathways is base excision repair (BER). Established by Tomas Lindahl, BER is initiated by a specific DNA glycosylase for the type of DNA damage present, for example OGG1 is the DNA glycosylase that repairs 8-oxo-guanine lesions (Jacobs and Schär, 2012; Lindahl, 1974). Once a DNA glycosylase has excised the damage and formed an abasic (AP) site, there are a number of routes that BER can take (Figure 1.7).
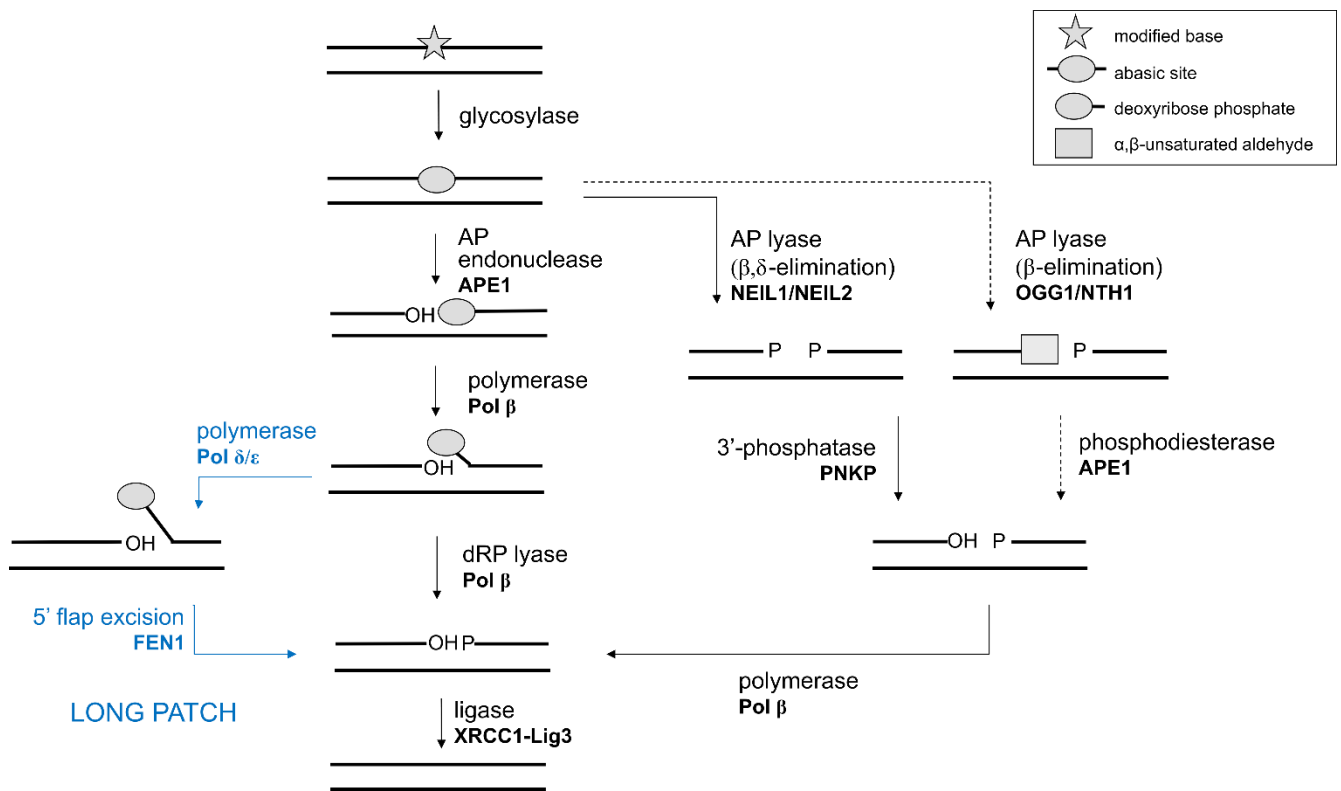
Figure 1.7 Repair of DNA damage by base excision repair (BER) pathways. The first step in base excision repair (BER) is generation of an abasic (AP) site by a damage-specific glycosylase. Subsequently, damage can be repaired via alternative pathways dependent on the catalytic action of the initiating glycosylase. Incision of the DNA backbone at the AP site by APE1 leads to a nick with a 5'-deoxyribosephosphate and a 3'-hydroxyl in the "classical" BER pathway. In the long patch pathway, Pol β inserts a single nucleotide and Pol δ/ε is further recruited to extend this chain before FEN1 catalyses the removal of the flap to produce a ligatable DNA junction. Whereas, short patch BER recruits a dRP lyase after the addition of the single nucleotide by Pol β, to remove the deoxyribose phosphate and allow for ligation by XRCC-Lig3 to occur. The righthand-route produces a 3'-phosphate via cleavage of the backbone by NEIL1/NEIL2 and is heavily dependent on the phosphatase activity of PNK. Glycosylases, OGG1 and NTH1, have weaker AP lyase activity and often BER initiated by these glycosylases proceeds via the "classical" mechanism.

The correction of deamination, alkylation, abasic single base and oxidative damage by BER is important to prevent the occurrence of mutations and the potential for tumorigenesis.

1.2.2.2 Nucleotide excision repair (NER)

Bulky DNA lesions caused by UV irradiation and other environmental mutagens are mainly repaired by Nucleotide excision repair (NER). Discovered in the 1960s by Howard-Flanders and Boyce at Yale University and Setlow and Swenson and Carrier at Oak Ridge National Laboratory, NER was identified when *E. coli* were found to remove fragments of DNA with UV-radiation induced lesions from their genome (Boyce and Howard-Flanders, 1964; Setlow and Carrier, 1964). Broadly, NER is carried out by over 30 proteins and encompasses four steps: recognition, excision, resynthesis and ligation (Figure 1.8) (Fu et al., 2023).
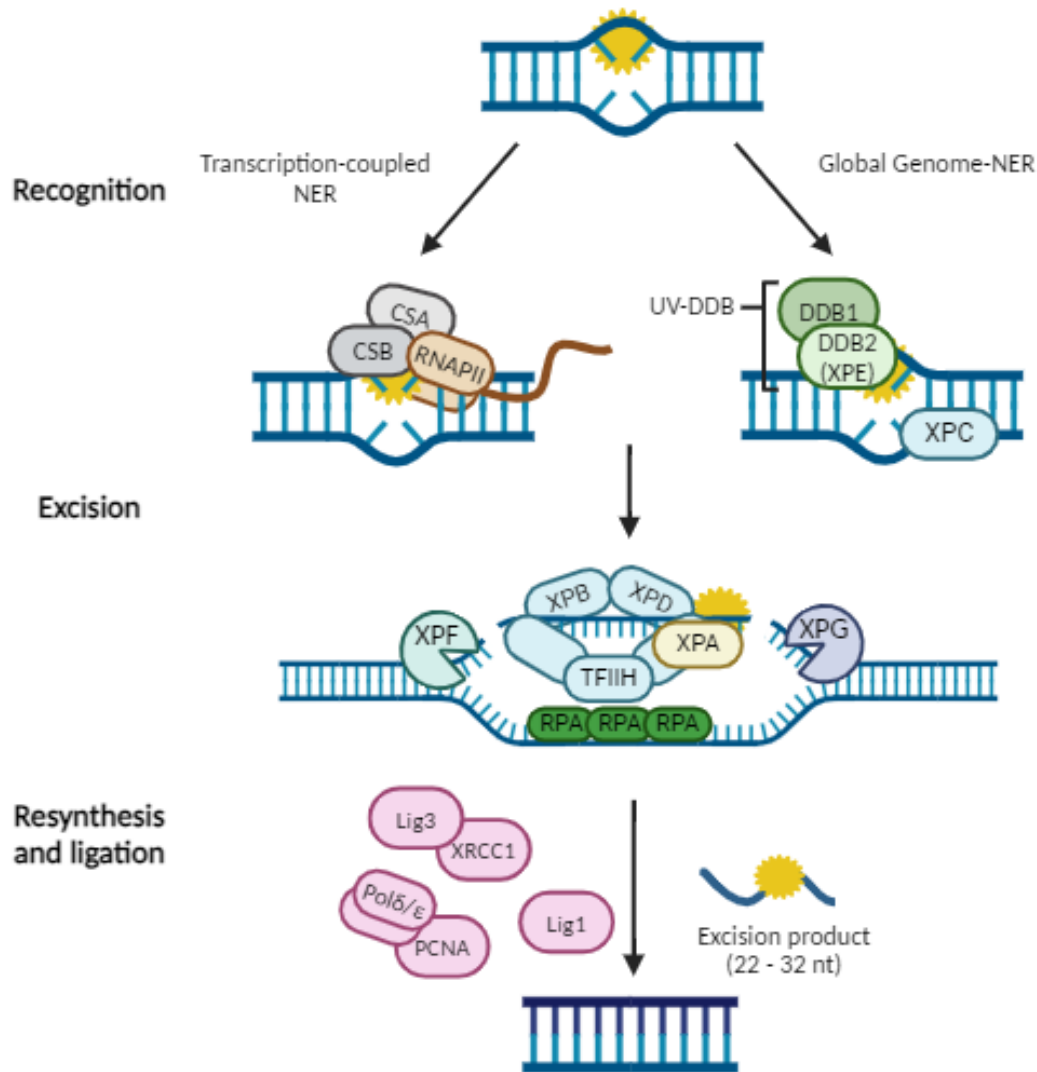
Figure 1.8 Repair of DNA damage by nucleotide excision repair (NER) pathways. Bulky DNA adducts are most commonly repaired by NER. Upon detection, there are two main routes that the lesion can be repaired by either transcription-coupled NER (TC-NER) or global genome-NER (GG-NER). In TC-NER, RNA polymerases will be halted, resulting in recruitment of CSB and CSA, whereas in GG-NER, the lesion is detected by UV-DDB and XPC. Once recognition has occurred, the TFIIH complex and XPA are recruited to the lesion, as well as endonucleases XPF and XPG and ssDNA binding protein, RPA. This marks the completion of the preincision complex. Dual incision can then be performed to excise the damaged DNA and DNA gap-filling synthesis and ligation by DNA ligase 1 (or XRCC1), DNA ligase 3, PCNA, Polε and Polδ can be carried out. Figure made using Biorender.com and adapted from (Lee and Kang. 2019).

Bulky DNA lesions, such as cyclobutane pyrimidine dimers (CPD) caused by UV or intrastrand crosslinks inflicted by cisplatin, are excised through a "cut-and-patch" mechanism by NER. This begins by either TC-NER, whereby DNA lesions in transcribed strands are repaired during active transcription to ensure the activity of RNA polymerase II is not blocked, or GG-

18

NER, whereby repair can take place throughout the genome, however with the caveat of varying repair efficiency (Fousteri and Mullenders, 2008). In TC-NER, after recognition of the helix-distorting lesion by the stalled RNA polymerases, CSB is recruited to the site, which subsequently recruits CSA (Figure 1.8). Whereas in GG-NER, UV-damaged DNA-binding protein complex (UV-DDB) initially recognises the damaged DNA and recruits XPC to the site (Kusakabe et al., 2019). Subsequently after recognition has occurred, the TFIIH complex (consisting of 10 subunits, such as XPB and XPD) directly interacts with XPC and orchestrates unwinding of the DNA helix. Finally, XPA, RPA, XPG and XPF are recruited to complete the preincision complex, XPF and XPG endonucleases perform a dual incision generating a 3'-hydroxyl and 5'-phosphate, respectively (Schärer, 2013). Finally, once the 22-32 nucleotide-long oligomer containing the lesion is excised, DNA gap-filling synthesis and ligation is facilitated by DNA ligase 1 (or XRCC1), DNA ligase 3, PCNA, Polε and Polδ (Lee and Kang, 2019).

1.2.2.3 Interstrand crosslink repair (ICL) and the Fanconi anemia (FA) pathway

DNA interstrand cross-links (ICLs) are highly cytotoxic and often occurs as a result of IR or chemotherapeutics, such as cisplatin, therefore overexpression of ICL repair proteins in cancers is commonly associated with chemotherapy resistance (Semlow and Walter, 2021). Repair of ICLs is a very complex molecular mechanism as this type of lesion affects both DNA strands. In quiescent G0/G1 phase cells, the first and second incisions to excise the ICL is carried out by NER (Figure 1.8; section 1.2.2.2) (Hashimoto et al., 2016). The ssDNA gap generated by the first incision via NER is bypassed by translesion synthesis (TLS) polymerases, particularly DNA polymerases ζ and κ and REV1 (Sarkar et al., 2006). After TLS, the second round incision by NER is performed, excising the ICL and the remaining ssDNA

gap is repaired by Pol δ and PCNA (Hashimoto et al., 2016). Repair of ICLs in S-phase cells, also known as replication-coupled ICL repair, is now more commonly recognised as the Fanconi anaemia (FA) pathway (Figure 1.9) (Kottemann and Smogorzewska, 2013).
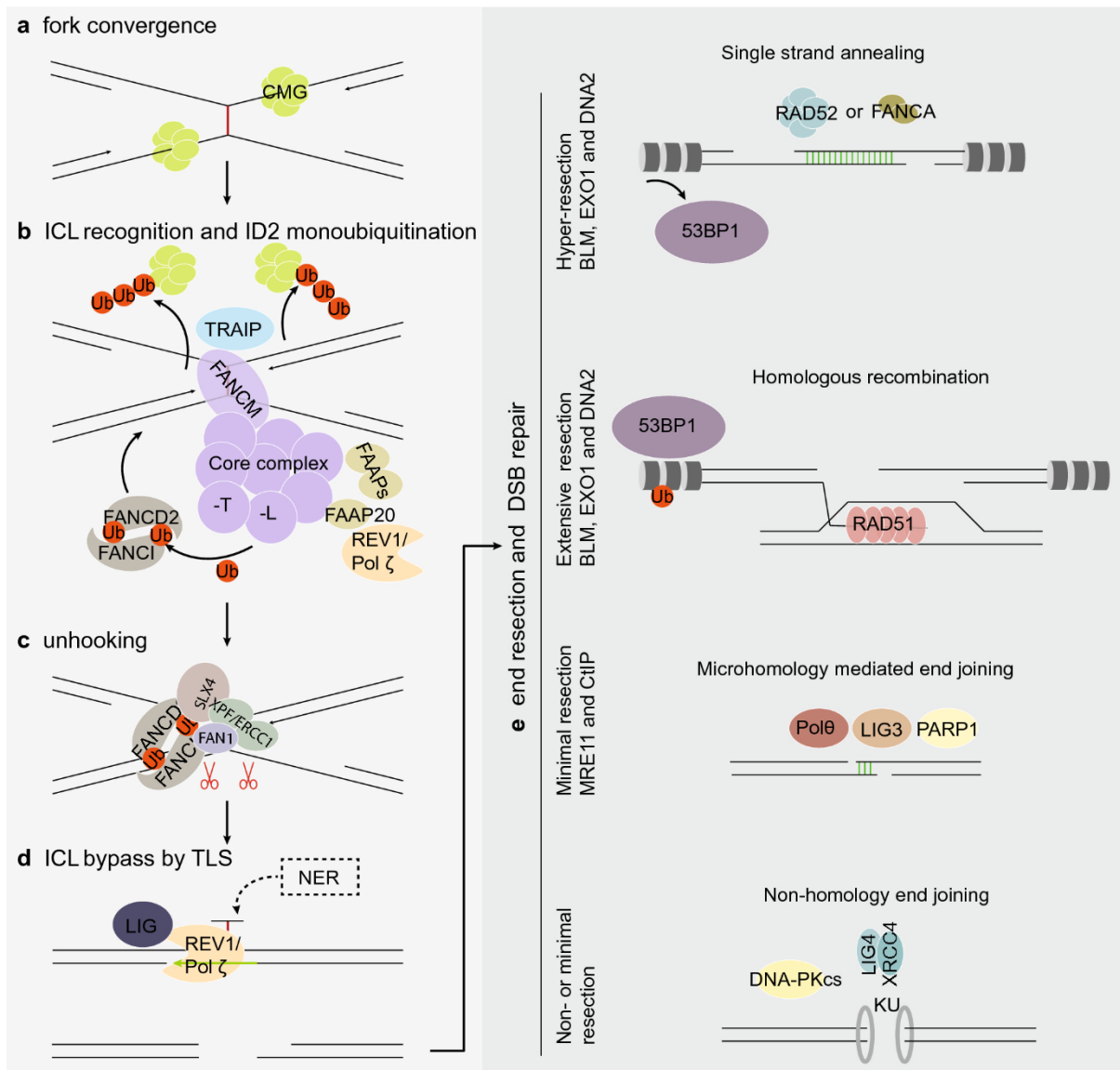
Figure 1.9 The Fanconi anemia (FA) pathway. (A) An ICL is when the two DNA strands become covalently bonded to each other and this is detected with the convergence of two replication forks at the lesion site. (B) The X shaped DNA structure is recognised by FANCM/FAAP24 and this protein subsequently recruits other proteins involved in the FA core complex and FAAPs. The FA pathway is activated upon monoubiquitination of the ID2 complex, leading to recruitment of FAN1 and structure specific nucleases to (C) incise and unhook the ICL. (D) TLS and NER will repair at the site of the unhooked ICL and DSB repair pathways will repair DSB intermediates. Figure taken from (Liu et al., 2020).

ICLs halt fork progression as replication forks cannot separate covalently cross-linked DNA strands (Niraj et al., 2019). Fork convergence initiates the ubiquitination of the CMG complex by TRAIP, an E3 ubiquitin ligase, and this leads to unloading of the CMG helicase (Liu et al., 2020). The anchoring complex, comprised of FANCM and some Fanconi anemia core complex associated proteins (FAAPs), are crucial for the detection and activation of the FA pathway by monoubiquitination of the ID2 complex (FANCI and FANCD2). The monoubiquitination of the ID2 complex is orchestrated via proteins in the FA core complex, FANCT, the E2-conjugating enzyme, and FANCL, the E3-ubiquitin ligase (Rickman et al., 2015). Repair proteins, such as TLS polymerases and structure-specific nucleases, can dock to ID2-Ub to allow for nucleolytic cleavage and incision of the ICL, known as unhooking (Figure 1.9). FANCQ (XPF/ERCC1), MUS81/EME1 and FANC1 have been shown to be crucial for this unhooking mechanism (Liu et al., 2020). Subsequently, TLS polymerases are recruited to the gap where the ICL has been unhooked and these bypass the damage. The final DSBs are then repaired via various DSB break repair pathways, more frequently by HR or NHEJ when FA pathway-mediated ICL repair has occurred.

1.2.2.4 Double strand break (DSB) repair pathways

Dependent on the type of DNA damage, different pathways exist that repair the various lesion types and ensure the maintenance of genome stability. DNA double strand breaks (DSBs) are the most cytotoxic DNA lesions, which are repaired in a cell cycle-dependent manner by non-homologous end joining (NHEJ) or homologous recombination (HR) (Figure 1.10).
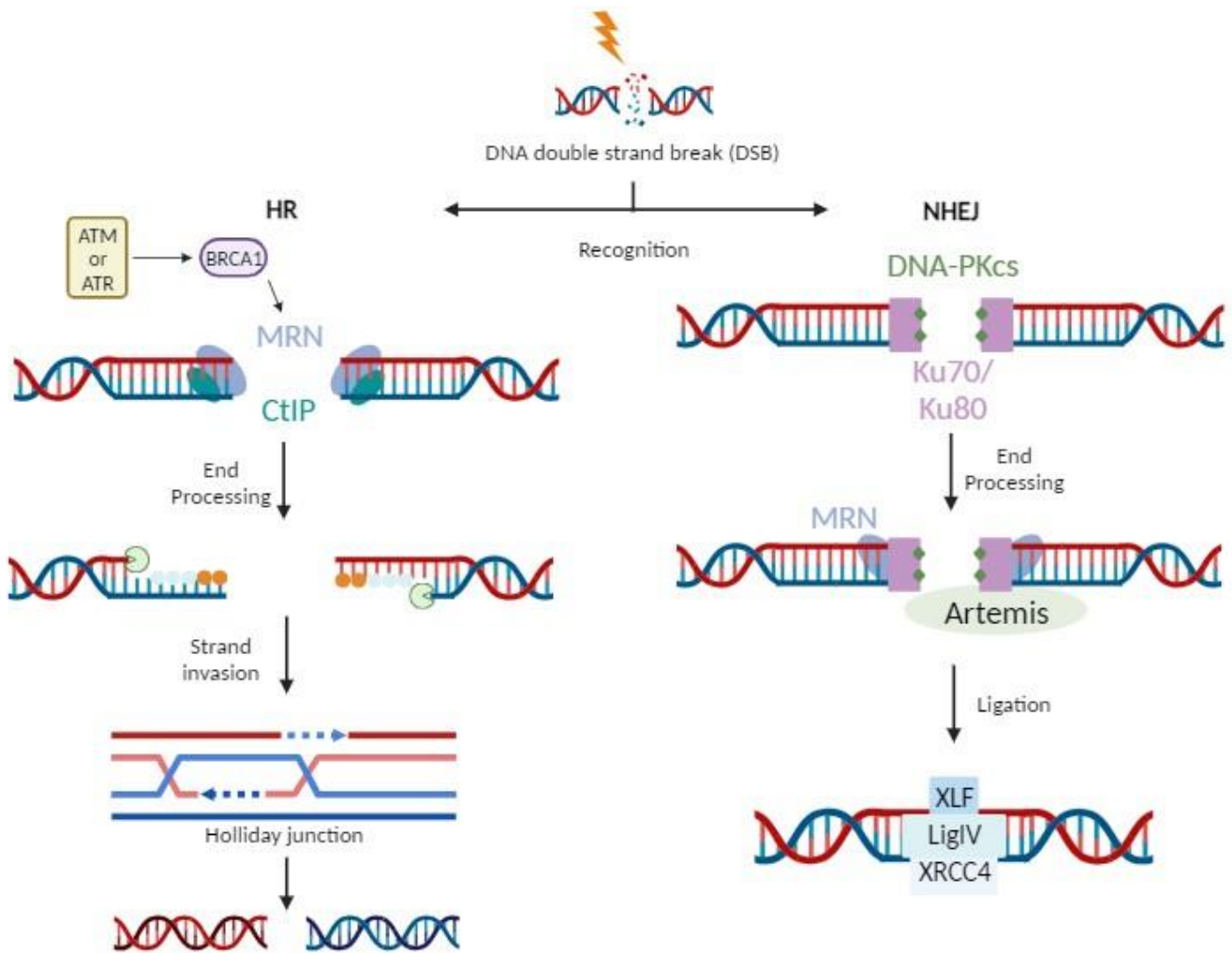
Figure 1.10 Signalling cascade of DSB repair mechanisms, NHEJ and HR. Diagram showing the homologous recombination (HR) and classical Non-homologous end joining (NHEJ) pathways to repair DSBs. MRE11-RAD50-NBS1 (MRN)-CtIP complex and Exo1 endonuclease (green pacman) resects DNA and recruits RPA (light blue circles), RAD51 (orange circles) and BRCA1 to ssDNA at the start of HR. Strand invasion forms Holliday junctions which are then ligated to form two copies of DNA. NHEJ is a more error prone pathway where Ku70/80 binds to DSBs and recruits Artemis, DNA-PKcs and XRCC4/LIGIV/XLF to ligate DNA ends. Figures created using BioRender.com.

There is much interplay and crossover of proteins involved in these repair pathways, although as previously mentioned ATM and ATR are the main transducers in the DDR signalling pathways (Maréchal and Zou, 2013). On DSB formation, either ATM or ATR phosphorylates the histone H2A variant H2AX on serine 139 to form γH2AX, which binds to and induces a DNA damage signalling response on chromatin (Burma et al., 2001; Ward and Chen, 2001). The MRE11, RAD50 and NBS1 (MRN) complex activates ATM to form active monomers via auto-phosphorylation (Bakkenist and Kastan, 2003; Gately et al., 1998; Uziel et al., 2003). Whilst ATM phosphorylates and activates its effector protein, Chk2, ATM also activates the nuclease CtIP (CtBP (carboxy-terminal binding protein) interacting protein) which, in combination with Chk2 and MRE11, facilitates end resection in HR (Gusho and Laimins, 2021).

Although ATM is very specific to DSBs, ATR has a broader range of DNA lesions that can activate the enzyme. ssDNA is produced by DSB end-processing or stalled replication forks, therefore agents that produce these, such as platinum-based compounds and UV light, will recruit ATR (Swift and Golsteyn, 2014). RPA-ssDNA recruits the ATR-ATRIP complex to initiate a DDR response by phosphorylating its effector protein, Chk1. Without the recruitment of ATR, repair of ssDNA would not occur and this highlights ATR's important function in the protection against replication stress, as well as other key processes, such as coordinating substrates involved with fork progression and origin firing, that contribute to genome stability (Maréchal and Zou, 2013). Chk1 and Chk2 are serine/threonine kinases that functionally overlap even though they do not possess similar structures (Bartek et al., 2001). Both kinases are involved in the phosphorylation cascade at checkpoints downstream from ATR and ATM which phosphorylate Chk1 and Chk2, respectively. However, crosstalk between the pathways has been shown as Chk1 can be activated by ATM in response to

ionising radiation and ATM-independent Chk2 activation has been observed (Bartek and

Lukas, 2003).

1.3 The effect of targeting the DDR via inhibition as a treatment of various cancer types

Many small molecule inhibitors (SMIs) have been developed to target ATM, ATR, Chk1, Chk2

and Wee1 that control cell cycle progression and the cellular DDR, and which have moved

forward into clinical trials (summarised in Table 1.1). This section will additionally highlight

some of the key findings related to the SMIs, and the most recent preclinical evidence

demonstrating the importance of targeting these kinases in cancer treatment.

Table 1.1 Current DDR protein inhibitors in clinical trials. Trials are grouped by target protein and the EC50 value of the SMIs is displayed when available. Details of if the clinical trials are actively recruiting and what phase they are in has been noted.

Target	Inhibitor	EC50	ClinicalTrials.gov Identifier (Stage and phase)	Tumour type
ATM	KU-60019 (improved analogue of KU-55933)	6.3 nM (Golding et al., 2009)	NCT03571438 (Recruiting – Phase N/A)	Kidney
	M4076	600 ± 40 nM (Stakyte et al., 2021)	NCT04882917 (Completed – Phase I)	Advanced solid tumours
	XRD-0394 (also DNA-PKi)	UNKNOWN	NCT05002140 (Not yet recruiting – Phase I)	Metastatic, locally advanced, or recurrent solid tumours
	AZD1390	0.78 nM (Durant et al., 2018)	NCT03423628 (Recruiting – Phase I) NCT03215381 (Completed – Phase I) NCT05182905 (Recruiting – Early Phase I) NCT05116254 (Recruiting – Phase I)	Glioblastoma N/A (Healthy volunteers) Glioblastoma Adult soft tissue sarcoma NSCLC Metastatic solid tumour cancer

			NCT04550104 (Recruiting – Phase I) NCT05678010 (Recruiting – Phase I)	
	AZD0156	0.58 nM (Pike et al., 2018)	NCT02588105 (Completed – Phase I)	Locally advanced/metastatic cancer
	WSD0628	0.42 nM (Tuma et al., 2022)	NCT05917145 (Not yet recruiting – Phase 0/I)	Glioblastoma
ATR	ART0380	UNKNOWN (Artios, 2022)	NCT04657068 (Recruiting – Phase I) NCT05798611 (Recruiting – Phase I)	Advanced/metastatic solid tumours
	Ceralasertib (AZD6738)	1 nM (Vendetti et al., 2015)	NCT03682289 (Recruiting – Phase II) NCT03330847 (Active, not recruiting – Phase II) NCT02630199 (Completed - Phase I) NCT02576444 (Active, not recruiting – Phase II) NCT02264678 (Recruiting – Phase I/II) NCT04704661 (Recruiting – Phase I) NCT05514132 (Recruiting – Phase I) NCT05469919 (Recruiting – Phase I) NCT05450692 (Recruiting – Phase III) NCT05061134 (Recruiting – Phase II) NCT04417062 (Recruiting – Phase II) NCT04699838 (Recruiting – Phase II) NCT03801369 (Recruiting – Phase II) NCT03878095 (Recruiting – Phase II) NCT03328273 (Active, not recruiting – Phase I) NCT04564027 (Recruiting – Phase II) NCT04090567 (Recruiting – Phase II) NCT03022409 (Completed – Phase I)	Renal/Pancreatic/Urothelial Metastatic TNBC Refractory cancer Solid tumours Advanced solid malignancies Solid tumours Advanced solid tumours Advanced solid malignancies Advanced/metastatic NSCLC Melanoma Osteosarcoma Extensive small cell lung cancer Metastatic TNBC Refractory malignant solid neoplasm CLL Advanced solid tumours BRCA mutated breast cancer HNSCC Ovarian/Peritoneal/Fallopian tube Prostate NSCLC NSCLC Platinum (Pt) refractory extensive stage small cell lung cancer Myelodysplatic Syndrome or Chronic Myelomonocytic Leukaemia Biliary tract

		NCT03579316 (Recruiting – Phase II) NCT03787680 (Active, not recruiting – Phase II) NCT03334617 (Recruiting – Phase II) NCT03833440 (Recruiting – Phase II) NCT02937818 (Active, not recruiting – Phase II) NCT03770429 (Recruiting – Phase Ib) NCT0429008 (Recruiting – Phase II) NCT03428607 (Recruiting – Phase II) NCT02223923 (Not yet recruiting – Phase I) NCT04298021 (Recruiting – Phase II) NCT03462342 (Recruiting – Phase ?)	
	Gartisertib (M4344, VX-803)	< 150 pM (Ki) (Zenke et al., 2019)	NCT02278250 (Completed – Phase I)	Advanced solid tumours
	Elimusertib (BAY1895344)	78 nM (Mei et al., 2019)	NCT03188965 (Active, not recruiting – Phase I) NCT04491942 (Recruiting – Phase I) NCT04535401 (Recruiting – Phase I) NCT04514497 (Recruiting – Phase I) NCT04095273 (Active, not recruiting – Phase I) NCT05071209 (Recruiting – Phase I/II) NCT04267939 (Recruiting – Phase I) NCT04576091 (Recruiting – Phase I) NCT04616534 (Recruiting – Phase I)	Advanced solid tumours/Lymphomas Advanced solid tumours (urothelial) Stomach/Intestines Solid tumours Advanced solid tumours Relapsed or refractory solid tumours Advanced solid tumours (ovarian) Recurrent HNSCC Advanced solid tumours (pancreatic/ovarian)
	M1774	UNKNOWN (Yap et al., 2021)	NCT05396833 (Recruiting – Phase I) NCT04170153 (Recruiting – Phase I) NCT05882734 (Not yet recruiting – Phase Ib/IIa)	Advanced unresectable solid tumours NSCLC Advanced breast cancers SPOP-mutant prostate cancer Ovarian and endometrial cancer Merkel cell skin cancer

		NCT05986071 (Not yet recruiting – Phase I/II) NCT05828082 (Recruiting – Phase II) NCT05691491 (Recruiting – Phase I/II) NCT05950464 (Recruiting – Phase Ib) NCT05947500 (Not yet recruiting – Phase II)	
Berzosertib (M6620, VX-970, VE-822)	19 nM (Fokas et al., 2012)	NCT02487095 (Active, not recruiting – Phase I/II) NCT03309150 (Active, not recruiting – Phase I) NCT05246111 (Recruiting – Phase I) NCT04216316 (Recruiting – Phase I/II) NCT04768296 (Active, not recruiting – Phase II) NCT04802174 (Recruiting – Phase I/II) NCT04052555 (Recruiting – Phase I) NCT04826341 (Recruiting – Phase I/II) NCT02567422 (Active, not recruiting – Phase I) NCT04807816 (Recruiting – Phase II) NCT02567409 (Active, not recruiting – Phase II) NCT02589522 (Active, not recruiting – Phase I) NCT03517969 (Active, not recruiting – Phase II) NCT03641313 (Recruiting – Phase II) NCT02627443 (Active, not recruiting – Phase I) NCT02595931 (Recruiting – Phase I) NCT04266912 (Recruiting – Phase I/II) NCT02723864 (Completed – Phase I) NCT02595892 (Active, not recruiting – Phase II)	Small cell lung cancer Advanced solid tumours Solid tumours Advanced NSCLC Relapsed Pt-resistant SCLC SCLC & high-grade neuroendocrine Breast cancer Advanced solid tumours (SCLC/HRD cancer) HNSCC Adult leiomyosarcoma Metastatic urothelial cancer NSCLC/SCLC/neuroendocrine tumours Metastatic castration-resistant prostate cancer TP53 mutant gastric cancer Recurrent and metastatic solid tumours Solid tumours DDR deficient Solid tumours Refractory solid tumours Ovarian/Peritoneal/Fallopian tube
Camonsertib (RP-3500)	1 nM (Roulston	NCT05405309 (Recruiting – Phase I/II)	CLL Advanced solid tumours Advanced solid tumours

			NCT04972110 (Recruiting – Phase I/II) NCT04855656 (Recruiting – Phase I) NCT04497116 (Recruiting – Phase II)	
Chk1/2	PHI-101	UNKNOWN (Han et al., 2021)	NCT04678102 (Recruiting – Phase I) NCT04842370 (Recruiting – Phase I)	Pt-resistant Ovarian/Fallopian tube/Peritoneal Refractory AML
	Prexasertib (LY2606368, ACR-368)	< 1 nM (Chk1), 8 nM (Chk2) (King et al., 2015)	NCT02873975 (Completed – Phase II) NCT02514603 (Completed – Phase I) NCT04032080 (Active, not recruiting – Phase II) NCT02808650 (Completed – Phase I) NCT02778126 (Completed – Phase I) NCT03414047 (Completed – Phase II) NCT04095221 (Active, not recruiting – Phase I/II) NCT02735980 (Completed – Phase II) NCT02860780 (Completed – Phase I) NCT03057145 (Completed – Phase I) NCT02555644 (Completed – Phase I) NCT03495323 (Completed – Phase I) NCT02649764 (Completed – Phase I) NCT04023669 (Active, not recruiting – Phase I) NCT01115790 (Completed – Phase I) NCT02124148 (Completed – Phase I) NCT05548296 (Recruiting – Phase I/II)	Advanced solid tumours Advanced solid tumours Metastatic TNBC Refractory solid tumours Advanced solid tumours Ovarian Desmoplastic small round cell tumour & Rhabdomyosarcoma SCLC Colorectal & NSCLC Ovarian & Fallopian tube HNSCC Advanced solid tumours AML & Myelodysplastic Refractory medulloblastoma Advanced solid tumours Advanced cancer Pt-resistant ovarian/Endometrial adenocarcinoma/Urothelial
	SRA737 (CCT245737)	1.4 nM (Walton et al., 2016)	NCT02797964 (Completed – Phase I/II) NCT02797977 (Completed – Phase I/II)	Advanced solid tumours/Non-Hodgkin's Lymphoma (NHL) Advanced solid tumours
	LY2880070	UNKNOWN	NCT05275426 (Recruiting – Phase II)	Ewing sarcoma/Ewing-like sarcoma

Wee1	Adavosertib	5.2 nM (Hirai et al., 2009)	NCT03330847 (Active, not recruiting – Phase II)	Metastatic TNBC
			NCT02576444 (Active, not recruiting – Phase II)	Solid tumours
			NCT03579316 (Recruiting – Phase II)	Ovarian/Peritoneal/Fallopian tube
			NCT02937818 (Active, not recruiting – Phase II) (61 studies total)	Pt refractory extensive-stage SCLC
	Zn-c3	3.9 nM (Huang et al., 2021)	NCT05198804 (Recruiting – Phase I/II)	Pt-resistant Ovarian/Peritoneal/Fallopian tube
			NCT04814108 (Recruiting – Phase II)	Uterine serous carcinoma
			NCT05368506 (Not yet recruiting – Early Phase I)	Metastatic TNBC/Ovarian
			NCT05128825 (Recruiting – Phase II)	Malignant tumours
			NCT04158336 (Recruiting – Phase I)	Solid tumours
			NCT04833582 (Recruiting – Phase I/II)	Osteosarcoma
			NCT04516447 (Recruiting – Phase I)	Pt-resistant Ovarian
			NCT04972422 (Recruiting – Phase I)	Solid tumours
			NCT05431582 (Not yet recruiting – Phase I)	Solid tumours
			NCT05682170 (Recruiting – Phase I/II)	Acute myeloid leukaemia

1.3.1 ATM

Given ATM has a major role in mediating cell cycle checkpoints and its apical position in DDR

pathways, this makes it an ideal drug target (Bensimon et al., 2011; Golding et al., 2004;

Tang et al., 2020). Studies have shown that ATM inhibition greatly sensitizes cells to

genotoxic agents that cause DSBs, such as ionising radiation and topoisomerase inhibitors

(García et al., 2022; Hickson et al., 2004). Hickson et al (2004) reported the first selective

ATM inhibitor (ATMi), KU-55933, demonstrating that it was able to suppress ionising

radiation-dependent p53 phosphorylation and radiosensitize U2OS and HeLa cancer cell

lines. Unfortunately, while KU-55933 and subsequent early compounds KU-59403 and KU-60019 showed high selectivity towards ATM compared to the closely related kinases mTOR, ATR, PI3K and DNA-PK, they also exhibited low oral bioavailability, low aqueous solubility and moderate cellular potency. Therefore, translating these compounds from bench to clinic has proved not feasible (Batey et al., 2013; Hickson et al., 2018; Hickson et al., 2004). These early ATMi's have been superseded by a more selective and potent compound, AZD0156 (Pike et al., 2018). AZD0156 has been shown to have excellent general kinome selectivity, a sub-nanomolar cell EC50 (0.57 nM) and to potentiate the effects of chemotherapeutics such as the PARP inhibitor, olaparib and the topoisomerase inhibitor irinotecan (Pike et al., 2018). To directly compare the effect of AZD0156 on mTOR, PI3K, ATM and ATR, and thus their EC50, the same cell line should have been used. Indeed, olaparib in combination with AZD0156 led to tumour regression in a colorectal cancer (SW620) xenograft model of nine out of ten mice versus only four out of ten mice with olaparib as a monotherapy. AZD0156 has now moved forward into Phase I clinical trials in advanced solid tumours (NCT02588105). AZD1390 is another promising inhibitor for ATM that has not only shown radiosensitization of nine glioma cell lines, with p53-mutant cells being significantly more sensitive, but it has also exhibited the ability to cross the blood brain barrier in cynomolgus monkey brain PET imaging (Durant et al., 2018). The EC50 was determined in HT29, however it was not in the other cell lines used in this study.

M3541 and M4076 are the first members of a new class of 1,3-dihydro-imidazo[4,5-c]quinolin-2-one ATMi's that reportedly show similar selectivity and potency over AZD1390 (Zimmermann et al., 2022) (Fuchss et al., 2018). M3451 was designed to be orally administered and showed selectivity when a panel of 292 protein kinases were tested, as only four additional kinases (CLK2, ARK5, FMS and FMS[Y969C]) were inhibited over 50% at 1

μM (Fuchss et al., 2018). Treatment of A549 cells with M3541 caused inhibition of radiation-dependent phosphorylation of ATM and its downstream targets, attenuation of DSB repair and decreased clonogenic survival (Zimmermann et al., 2022). Additionally, the response of 79 cancer cell lines to M3541 alone and in combination with IR was performed, where it was observed that synergistic effects were evident in all cell lines independent of p53-status and tumour origin. This study also demonstrated excellent potentiation of radiotherapy in mouse xenograft models. M3541 entered phase I clinical trials as a combination treatment with radiotherapy for solid tumours (NCT03225105) however, its clinical development has now been halted due to unfavourable pharmacokinetic properties indicative of poor absorption at higher doses (Waqar et al., 2022). M4076 shows similar activity to M3541, although it has been demonstrated to have an increased solubility and potency. Like M3541, it is able to enhance radiotherapy sensitivity in both cellular and xenograft models of advanced solid tumours. It is also able to induce synergistic effects when combined with either topoisomerase or PARP inhibitors. M4076 is currently being investigated as a monotherapy in a phase I clinical trial of patients with advanced solid tumours (NCT04882917). Zimmerman et al., 2022 tested a large panel of cell lines to investigate cell viability with the mono- and combination treatments, determined the EC50 value and quantified the synergy of the compounds but immunofluorescence studies, immunoblotting and colony formation assays only used A549 cells. Inhibitors can be variable across tumour types and even in cell lines within the same tumour type so we are uncertain if the same effect on the DSB repair pathway will be observed across other cell lines.

There is currently only one clinical trial investigating M4076 and future studies should focus on this inhibitor as this may overcome the problems mentioned above with M3541. It will also be interesting to compare M4076 with AZD1390 as they both show similar potency. The

natural progression of using these inhibitors is to test their effectivity as a combination with other genotoxic treatments, therefore once the pharmacokinetic properties have been determined they should be tested with radiotherapy as a treatment plan. Radiotherapy and small molecule inhibition are likely to show more tumour regression than either therapy alone and can be more targeted to tumours, improving the quality of life of the patient.

1.3.2 ATR

The ATR/CHK1 pathway is essential for the survival of cells, therefore therapeutically targeting this pathway particularly in combination with other therapies should be advantageous to kill cancer cells by inhibiting the capacity to repair the DNA damage. The first ATR inhibitor (ATRi) reported was caffeine, however it demonstrated a weak EC50 in the mM range and lacked specificity for ATR as it inhibited multiple PIKKs (Sarkaria et al., 1999). Developing specific ATR inhibitors has been difficult as there is a lack of structural information known about the ATR kinase, although currently there are seven ATRi's in clinical trials (Table 1.1).

HPV-positive head and neck squamous cell carcinomas (HNSCC) have been demonstrated to adapt to utilize the ATR pathway for viral DNA synthesis to ensure cell survival (Anacker et al., 2016). The ATR inhibitor (ATRi), ceralasertib (AZD6738), was found to be unable to inhibit colony growth of any of 21 HNSCC cell lines when administered alone, however it did cause varying sensitization in combination with cisplatin through apoptosis-induced cell death (Leonard et al., 2019). Consistent with these observations, co-treatment of ceralasertib and cisplatin has been shown to result in growth inhibition in two patient derived HNSCC xenograft models (Leonard et al., 2019). This study tested a wide range of

cell lines, which include 4 HPV+ and 17 HPV-, however the colony formation assays were only in HPV- cell lines. This paper did prove the aim and highlighted future work to understand the required dosing and schedule of administration of the inhibitor as well as looking into predictive biomarkers. Ceralasertib has also shown promise in triple negative breast cancer (TNBC) cell lines (Jin et al., 2018). Synergy was observed when combining ceralasertib with the Wee1 inhibitor, AZD1775, to cause a decrease in cell survival and viability through increased apoptosis in MDA-MB-231 and Hs578t cell lines. Both these cell lines are p53 mutant so when comparing the CI values to MCF7 cells, which are p53-WT, they did not show the same co-effect. This highlights the importance that p53 plays when inhibiting these targets and should be considered when choosing cell lines to investigate more closely. Ceralasertib has also demonstrated a synergistic effect with radioimmunotherapy (radiotherapy and anti-PD-L1) in hepatocellular carcinoma mice xenografts (Sheng et al., 2020). Across many studies similar trends are seen, whereby Ceralasertib in combination with other inhibitors or genotoxic agents results in cell death, increased unrepaired DNA damage and an uncontrolled cell cycle (Bradbury et al., 2020; Min et al., 2017; Vendetti et al., 2015).

Whilst Ceralasertib was the second ATRi to enter clinical trials, the first was berzosertib (VX-970, M6620). As a combination treatment with gemcitabine in advanced solid tumours, berzosertib was shown to induce a partial response in one of four TNBC patients (Plummer et al., 2016). Berzosertib as a combination treatment with radiotherapy in chemotherapy-resistant TNBC tumours is currently being investigated in an ongoing clinical trial (NCT04052555). In terms of preclinical evidence, berzosertib has been shown to increase the radiosensitivity of TNBC cell lines (MDA-MB-231, HCC1806 and BT-549), but this effect was not observed in a non-cancerous human breast epithelial cell line (MCF10A) (Tu et al.,

2018). Furthermore, berzosertib-treated BT-549 cells showed persistent unrepaired DNA damage and the drug appeared to abrogate the G2/M checkpoint in MDA-MB-231, BT-549 and HCC1806 cell lines. To further display the potential of berzosertib, it was demonstrated that patient-derived xenograft models were radiosensitized by the ATRi irrespective of HR-proficiency. Berzosertib has furthermore been shown to promote radiation-induced cytotoxicity in non-small cell lung cancer cell lines via increased mitotic cell death, associated with an abrogation of the G2/M checkpoint and elevated levels of micronuclei (Baschnagel et al., 2021). This study used cell lines that had p53-mutations that were KRAS-WT and vice versa, therefore testing if the inhibitors are more or less potent dependent on the mutations harboured by the tumour. This work is now being moved forward in patients with brain metastasis from NSCLC whereby Berzosertib in combination with radiotherapy is being investigated in an ongoing clinical trial (NCT02589522).

The latest generation ATRi, elimusertib (BAY1895344), is currently in 9 clinical trials (Table 1.1) and has been reported as being effective as both a mono and combination therapy (Wengner et al., 2020). Elimusertib was suggested to display a stronger *in vivo* anti-tumour efficacy as a monotherapy in comparison to ceralasertib and berzosertib in GRANTA-519 tumours in mice. Furthermore, in combination with various PARP inhibitors, elimusertib showed synergistic effects in BRCA1-deficient MDA-MB-436 breast cancer cells (Wengner et al., 2020). In various PDX models, elimusertib has displayed potent antiumour activity as a monotherapy, specifically in models harbouring mutations in DDR proteins, such as ATM and BRCA (Pico et al., 2021). As this compound has been assessed in multiple solid tumour cancer cell lines and shown similar results at reducing tumour proliferation in both cell lines and clinical trials, it is likely that this specific ATRi will be efficacious in DDR altered cancers (Lücking et al., 2020).

ATR has more inhibitors currently in clinical trials compared to ATM. These studies have all tested the inhibitor in a wide range of cell lines and *in vivo* work has been performed with a range of PDX models. Similarly, to the future of ATMi research, there needs to be predictive biomarkers discovered to signify a response to ATR inhibition. Most clinical trials are early phase and larger studies need to be performed in order to assess the administration schedules and dosing.

1.3.3 Chk1/Chk2

The Ser/Thr protein kinase Chk1 is phosphorylated at Ser-317 and Ser-345 by ATR, leading to its activation and which begins the DDR and checkpoint signalling cascade of the ATR-Chk1-dependent pathway (Walworth and Bernards, 1996). The therapeutic potential of Chk1 inhibition has been explored since 1996 where the first defined Chk1 inhibitor, UCN-01, was shown to induce cell death in Chinese hamster ovary cell lines and enhance radiosensitivity in p53-deficient lymphoma and colon carcinoma cells (Bunch and Eastman, 1996; Graves et al., 2000; Wang et al., 1996). Although Chk1 inhibition has shown some promise as a monotherapy, synergistic inhibitory effects have also been seen when using Chk1 inhibitors in combination with genotoxic agents. For example UCN-01 was previously demonstrated in combination with gemcitabine to result in cancer cell death in TNBC through overriding of the G1/S phase checkpoint (Bennett et al., 2012). PF-477736 was entered into a phase I clinical trial in combination with gemcitabine (NCT00437203), however the study was terminated due to business reasons. It is apparent that no more clinical trials have started using this compound, particularly as there are other second generation Chk1/2 dual inhibitors that have shown a better response (see below).

Interestingly though in melanoma cells, A375 and WM9, Chk1 inhibition has been shown to overcome resistance to the BRAF inhibitor vemurafenib, and that the combination of BRAF and Chk1 inhibition (PF477736) can synergistically decrease cell survival and viability (Hwang et al., 2018). Both selected cell lines in this study were p53-WT which means this study did not identify a different response would occur in p53-mutant cells which has been seen in previous Chk1i studies, however the PTEN status of the cells was different.

Chk2 is activated through phosphorylation at Thr68 by ATM when sensing DSBs (Matsuoka et al., 2000), and so inhibiting Chk2 can lead to dysfunctional DNA repair and enhanced genome instability. However, this is a lesser studied enzyme and target for inhibitors, compared to the ATR-Chk1 pathway. BML-277, the most recently developed Chk2 inhibitor, has been demonstrated to reduce the growth of oxaliplatin-resistant (OR) colorectal cancer cells *in vitro* and xenograft tumours *in vivo* in an HR-dependent manner (Hsieh et al., 2022). Prexasertib (LY2606368), a second-generation dual ATP-competitive Chk1/2 inhibitor, in early studies was shown to increase levels of γH2AX indicating elevated DSB levels (Thompson and Eastman, 2013). As a combination treatment, prexasertib has been demonstrated to improve the effectiveness of olaparib or cisplatin in ovarian cancer and small cell lung cancer cell lines (Brill et al., 2017; Sen et al., 2017), particularly through increases in apoptosis. Prexasertib has also been shown to display anti-tumour effects as a monotherapy in TNBC cells regardless of p53 mutation status, and a phase II pilot study is being conducted in sporadic TNBC and *BRCA1/2*-mutated breast cancer (Curigliano et al., 2016; Lazaro et al., 2016). Early data shows 4 out of 9 patients have attained stable disease. A co-treatment approach of prexasertib, EGFR inhibitor cetuximab and radiotherapy has demonstrated anti-tumour activities and reduced proliferation of HPV-positive HNSCC cells and a phase Ib clinical trial investigating this approach in locally advanced tumours is

ongoing (NCT02555644) (Zeng et al., 2017). Prexasertib is currently showing good results in clinical trials and these are discussed more extensively in other reviews (Angius et al., 2020).

Overall, Chk2i clinical trials are in early phase and have small sample sizes, therefore more clinical data needs to be obtained to identify if targeting Chk2 will be a viable treatment strategy. More research has been conducted on Chk1i in comparison to Chk2i and work on dual-targeting inhibitors would ensure that more pathways are hit and could be more effective.

1.3.4 Wee1

Wee1 is a serine/threonine kinase that acts at the G2/M checkpoint to phosphorylate CDK1 to inactivate MPF and arrest the cell cycle when DNA damage has been detected. Targeting Wee1 is thought to result in synthetic lethality through abrogation of the G2/M checkpoint in p53-deficient cancers that have an inherent disrupted G1/S checkpoint. Adavosertib (AZD1775) is the current best in class inhibitor targeting Wee1, and has shown particular promise in treating a variety of p53-deficient cancer types when used in combination with genotoxic treatments and other agents (Kong and Mehanna, 2021). The majority of trials are examining adavosertib as a combination treatment with concurrent chemotherapy. An open-label phase I clinical trial of adavosertib has been assessed for use in borderline-resectable or unresectable stage III/IVB HNSCC suitable for definitive chemoradiation (Mendez et al., 2018). The study demonstrated that a combination treatment of adavosertib, docetaxel and cisplatin did not negatively impact patients, whilst having anti-tumour effects. The first trial to study definitive-dose radiotherapy with Wee1 inhibition and cisplatin demonstrated that using cisplatin at the standard-dose proved too toxic, therefore

a smaller dose of cisplatin was more beneficial (Chera et al., 2021). As the study highlighted, the major limitation of this trial was the unknown p53-status of the patients given that Wee1 inhibition would be expected to have a greater impact on p53-deficient tumours.

In terms of preclinical studies, the effect of adavosertib in combination with olaparib in two gastric adenocarcinoma cell lines, MKN45 and AGS, showed that increasing doses of adavosertib resulted in decreased viability and enhanced apoptosis through increased mitotic DNA damage (Lin et al., 2018). The combination also led to inhibited tumour proliferation of xenograft models, suggesting a synthetic lethality effect by inhibiting Wee1 and PARP. Both these cell lines are p53-WT so the dependency on p53 for the effectiveness of these treatments was not discussed in this study. Not only does adavosertib appear to enhance the effect of olaparib, it has been reported to overcome PARP inhibitor resistance in CAPAN1 (pancreatic cancer) and SUM149 (breast cancer) models that have HR-reactivating secondary BRCA1/2 mutations (Dréan et al., 2017). TNBC has shown a decreased capacity to repair DNA DSBs when adavosertib is used as a monotherapy or as a combination with inhibitors, such as olaparib and ceralasertib (Ha et al., 2020). MDA-MB-157, MDA-MB-231, HCC1143 and BT-549 cells were found to be sensitive to Wee1 inhibition (EC50 values of <0.5 μmol/L), whereas MDA-MB-468 and Hs 578 T cells were only moderately sensitive (EC50 values of >0.5 μmol/L), and p53-status seemed to have no effect on adavosertib sensitivity. Adavosertib was shown to reduce DSB repair, and increase both micronuclei formation and apoptosis as a monotherapy. In combination with olaparib, adavosertib showed synergy in inhibiting the growth of MDA-MB-231 xenograft tumours. In addition to breast, gastric and HNSCC, adavosertib has shown the ability to sensitize p53-deficient lung and prostate cancer cell lines to genotoxic agents (Bridges et al., 2011; Hirai et al., 2009).

Although adavosertib has shown excellent potency in causing cytotoxicity in various cell lines and xenograft models, the molecule has been reported to have off-target effects, including inhibition of the mitotic regulator PLK1 (Wright et al., 2017). Therefore, the Wee1 inhibitor ZN-c3 has recently been developed (Huang et al., 2021). In a lung cancer cell line (A-427) derived xenograft model, ZN-c3 had a similar EC50 to adavosertib (75 nM and 78 nM respectively), indicating that ZN-c3 has similar cellular potency to adavosertib. However, ZN-c3 also showed better kinase selectivity. There have yet to be published studies that have investigated ZN-c3 as a combination treatment in cancer cells. ZN-c3 is orally bioavailable and is currently in clinical trials for use in solid tumours (NCT04158336), and in women with recurrent or persistent uterine serous carcinoma (NCT04814108) and platinum-resistant ovarian cancer (NCT04516447), with early results being positive (Fu et al., 2021).

As has been previously discussed with ATRi and Chk1i, there are no predictive biomarkers to investigate the response to Wee1i. AZD1775 is currently being investigated in over 60 early clinical trials but, although AZD1775 has shown promising results in many cancer types, it has many off-target effects that could be hindering how effective targeting Wee1 could be. ZN-c3 has shown better kinase selectivity so it will be interesting to see if this will be more efficacious in preclinical and clinical data.

1.4 Proteolysis targeting chimeras (PROTACs)

1.4.1 Structure and function of PROTACs

Proteolysis-targeting Chimeras (PROTACs) are heterobifunctional protein degraders that
conjugate an E3 ubiquitin ligase-targeting domain and a protein of interest (POI)-binding
ligand via a linker (Sun et al., 2019). This brings the target protein into close proximity to the
E3 ubiquitin ligase, to promote the formation of a ternary complex and target the POI for
degradation by the ubiquitin proteasome system (UPS) to generate a chemical knockdown
phenotype (Figure 1.11) (An and Fu, 2018; Gao et al., 2020; Konstantinidou et al., 2019).
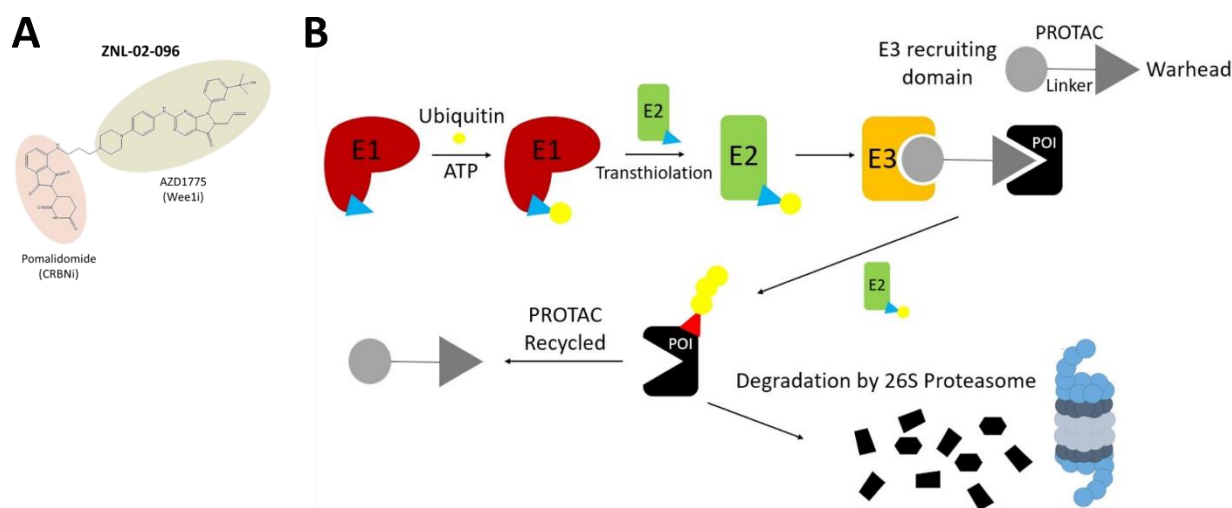
Figure 1.11 Hijacking the UPS system with a heterobifunctional molecule. (A) PROteolysis TArgeting Chimeras
(PROTACs) contain two binding domains that recruit a protein of interest, also known as the warhead, and an
E3 ligase. Here, the pink oval highlights the inhibitor used, pomalidomide, as the E3 ligase binding domain to
recruit CRBN and the light green oval highlights the inhibitor used as the protein of interest (POI) targeting
domain, also known as the warhead, AZD1775, to recruit Wee1 in Wee1 PROTAC, ZNL-02-096. (B) The PROTAC
forms a productive ternary complex with the E3 ubiquitin ligase and POI recruited to allow for
polyubiquitylation of the POI, targeting it for degradation by the 26S proteasome.

In some cases, when using high doses of PROTACs, unproductive binary complexes of the
PROTACs with the protein of interest or with the E3 ligase can form, resulting in the

degrader acting solely as an inhibitor and not inducing protein degradation. This phenomenon is more commonly known as the hook effect (Pettersson and Crews, 2019).

The UPS's main role is to regulate cellular pathways by degrading proteins that are no longer required or if they are faulty and cannot perform their desired function. Some of the pathways that it helps to regulate include cell cycle progression and cell death, which are crucial pathways for a cancer cell to be able to divide. Furthermore, the knowledge that the 20S proteasome, the core particle of the 26S proteasome, is highly conserved across organisms, clearly demonstrates the importance of the UPS in the proper maintenance of many biological pathways (Valas and Bourne, 2008). Hijacking the UPS is a useful target to inhibit cancer growth and potentially stimulate cancer cell death.

The first step in the UPS cascade is an E1 activating enzyme involved in an ATP-dependent mechanism to conjugate itself to ubiquitin via a thioester bond (Schulman and Harper, 2009). Subsequently, a transthiolation (trans-thioesterification) reaction occurs to produce the E2-ubiquitin conjugate via an E2 ubiquitin conjugating enzyme. Finally, the transfer of the ubiquitin from the E2-ubiquitin conjugate to a lysine residue on the protein being targeted for degradation, is mediated by the E3 ubiquitin ligase (Hershko and Ciechanover, 1992; Hershko et al., 1983; Kleiger and Mayor, 2014; Komander and Rape, 2012; Ye and Rape, 2009). As mentioned above, PROTACs manipulate the signal cascade of the UPS by binding and inducing the ternary complex formation between the POI and E3 ligase in order to stimulate the transfer of ubiquitin from an E2-conjugating ligase to the POI (Paiva and Crews, 2019).

Protac-1 was the first PROTAC synthesised and showed that it can successfully induce ubiquitination of a POI, in this case the POI was MetAP-2. Protac-1 has been shown to

41

degrade MetAP-2 and proved that the UPS could be hijacked to degrade substrates that the E3 ligases do not usually target (Sakamoto et al., 2001; Sakamoto et al., 2003; Schneekloth et al., 2004). These small molecule degraders have demonstrated that they can hijack the "undruggable" proteome and proteins that the pharmaceutical industry have struggled to target, such as Tau and KRas, which displays the potential applications of PROTACs in many different diseases, from cancer to Alzheimer's (Bond et al., 2020; Silva et al., 2019; Wang et al., 2021a; Wang et al., 2021b). Therefore, the need to create a large library of ligands that can target proteins to the UPS by infiltrating the ubiquitin signal cascade is crucial for the future of drug development.

1.4.2 Development, optimisation and enhanced target selectivity

PROTACs are small molecules with a complex mechanism to target proteins to the UPS for degradation and due to their complexity, the design and optimisation of PROTACs is still an emerging field. PROTAC design contains three major components, the POI-recruiting ligand, the linker and the E3 ligase-recruiting ligand (Sakamoto et al., 2001). Each of these components is important to the functioning of the PROTAC as they all play a role in binding affinities, ternary complex formation, and the ability to bring the two proteins into close proximity with one another. Cancer research has discovered many proteins that could be degraded to help kill cancer cells, notably Wee1 seems to be an excellent POI as it is upregulated in many cancer types (section 1.3.4). However, there are over 600 E3 ubiquitin ligases within the body with three broad classes (RING, RBR and HECT), and some of these may be specifically upregulated in certain cancer types (Blaquiere et al., 2020; Cohen and Tcherpakov, 2010). E3 ligases may be the key to providing cancer therapies that are

personalised to the cancer type due to their substrate specificity, which leads to the first obstacle when producing PROTACs, E3 ligase ligand discovery.

PROTAC ligands are usually based on SMIs that are already targeted to binding the desired protein and, unfortunately, there are currently limited E3 ligase binders in targeting E3 ligases (Ishida and Ciulli, 2021). PROTACs have been developed recruiting RING E3 ligases VHL (von Hippel–Lindau protein), CRBN (Cereblon), IAPs (specifically cIAP) and MDM2, but most PROTACs have been synthesised to recruit VHL and CRBN as these are the E3 ligases that have the best characterised ligands (Buckley et al., 2012; Ito et al., 2010). MDM2 has had a library of inhibitors produced against it termed the 'Nutlins' which were developed by Roche (Vassilev et al., 2004). PROTACs have been designed to recruit MDM2 using nutlin 3 as the ligand to degrade the androgen receptor, however, the research into MDM2-recruiting PROTACs is a less developed area compared to investigating VHL-recruiters and thalidomide-based ligands to recruit cereblon. For this reason, this work will utilise CRBN- and VHL-recruiting PROTACs. Currently, the majority of PROTAC discovery is trying to find inhibitors that can be used to recruit the POI; however, a key concept may be to utilize products that have previously been shown to bind to the POI but not effectively inhibit it. For a PROTAC to successfully induce ternary complex formation, the warhead only needs to bring the POI into close proximity with the E3 ligase (Gerry and Schreiber, 2020). This understanding may speed up PROTAC development and allow for specific proteins in certain cancers to be targeted, potentially allowing for the compounds to be used as both a single-agent and combination therapy.

PROTACs are more complex molecules in comparison to inhibitors, therefore it is unsurprising that they can generate selectivity for target engagement. Analysing the ternary

complex formation and kinetics via x-ray crystallography, isothermal titration calorimetry

(ITC) and surface plasmon resonance (SPR) will aid the understanding of how protein-

protein interactions (PPIs) and the availability of lysine residues that can be ubiquitinated

contribute towards a PROTACs enhanced target selectivity (Gadd et al., 2017; Hughes and

Ciulli, 2017; Kostic and Jones, 2020; Maniaci and Ciulli, 2019; Roy et al., 2019). The most

effective cooperativity and PPIs observed can then be recreated in future compounds. These

techniques have been successfully exploited to produce Wee1-targeted PROTACs that

exhibit enhanced selectivity for Wee1 in comparison to AZD1775 (Aublette et al., 2022; Li et

al., 2020; Wright et al., 2017). Thus, Wee1 modulation via selective PROTACs needs to be

investigated in comparison to inhibition to assess if the different mechanism of action alters

how cells respond to the absence of Wee1 activity.

1.4.3 Degradation via PROTACs as an alternative to classic inhibitors

It is clear from the extensive amount of literature that inhibition of proteins involved in cell

cycle checkpoints and the cellular DDR can help sensitize cancers to radiotherapy and/or

chemotherapy and which are being moved forward into clinical trials. Although inhibitors

have proven to be effective, there are disadvantages to this approach in that relatively high

doses are required at saturating concentrations, and binding needs to be sustained in order

to cause the desired effect. Also, cancer cells often can become resistant to inhibitors and

traditional anti-cancer drugs. This makes targeted protein degradation an interesting

avenue to explore as an alternative treatment pathway. An advantage of utilising targeted

protein degradation versus SMIs is that PROTACs only need to weakly bind to the POI to

enable the formation of the ternary complex, and they do not have the limitation of needing

to bind to an active or allosteric site to have their desired effect. In addition, as discussed in section 1.4.2, PROTACs show enhanced selectivity to POIs in comparison to inhibitors due to the increased serendipitous interactions created (Martín-Acosta and Xiao, 2021).
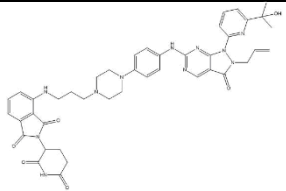
The potential phenotypic differences between knockout versus inhibition of proteins has always been an interesting topic, and indeed studies have investigated this in the context of the DDR pathway. As ATM and ATR are the first proteins to respond to DNA damage in the cascade, it is not surprising that complete loss of function of ATR leads to genomic instability and early embryonic lethality, and ATM-deficient mice also show growth retardation and neurologic dysfunction (Barlow et al., 1996; Yamamoto et al., 2012). Kinase-dead ATM protein expression seemed to be more damaging to the mice in comparison to knockout ATM mice that can remain viable for much longer (Barlow et al., 1996; Elson et al., 1996; Yamamoto et al., 2012). These studies suggest that inhibition of ATM may be more advantageous than knockout of ATM and that cells could choose an alternative route if recognising that ATM is not present. Although the increased sensitization is advantageous, knock down of the target or degradation via PROTACs ensures increased specificity to the target and will have less off-target effects. Therefore, the question is whether the benefits of increased selectivity by small molecule degraders outweigh the drawbacks that so far it is slightly less cytotoxic than inhibition.
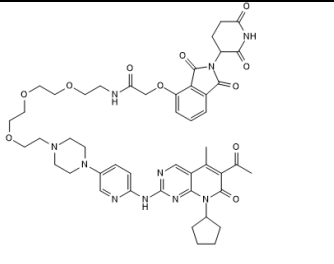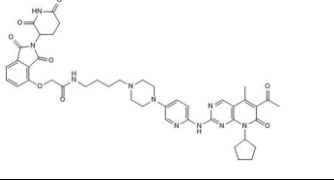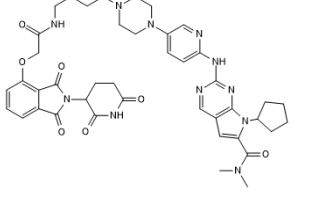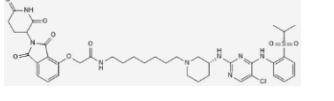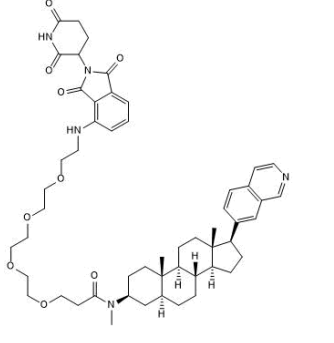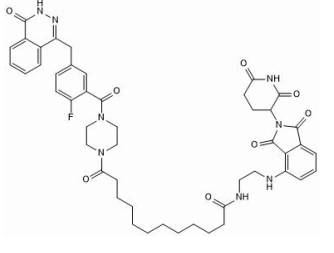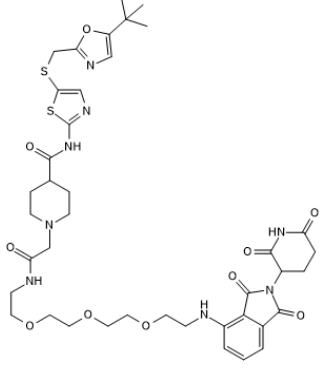
ATR knockout leads to embryonic lethality that is thought to be due to chromosomal fragmentation and cell death (Brown and Baltimore, 2000). It has been demonstrated that ATR does not need to be fully deficient or inhibited in order to cause toxicity to cancer cells. Hypomorphic ATR signalling (decreased to 10% of normal levels) caused synthetic lethality in oncogenic RAS-driven tumours and functional loss of ATR through overexpression of
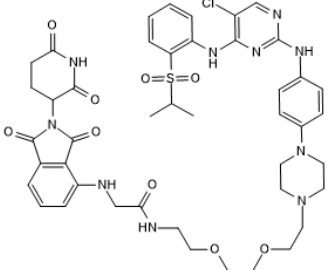
kinase-dead ATR displays enforced mitotic progression and sensitisation to DNA damaging agents (Cliby et al., 1998). Although it has been shown that inhibition and knockout phenotypes show promise with ATR and ATM causing enhanced levels of DNA damage, it has not been directly compared to investigate if knockout or "degradation" provides more cytotoxic effects than inhibition. In terms of Wee1, an siRNA-mediated knockdown has been shown to sensitize p53-mutant colon cancer cell lines to ionising radiation like the effects of pharmacological Wee1 inhibition that have previously been discussed (Bridges et al., 2011; Cuneo et al., 2016; Yin et al., 2018). It is yet to be thoroughly investigated if the treatment of cancers benefits more from a knockdown phenotype of Wee1 compared with SMIs, however Wee1-degrading PROTACs, namely ZNL-02-96, at 10-fold lower doses to AZD1775 have shown promise at synergizing with PARP inhibition (Li et al., 2020).

PROTAC degraders that target various proteins involved in regulating the cell cycle and the DDR are actively in development (Table 1.2), with more targeted towards cell proliferation, including degraders for JAK2 and EGFR. These have been studied in cell lines, showing promising results for targeted protein degradation (TPD) as a future treatment method to improve the effectiveness of genotoxic treatments.

Table 1.2 Current PROTACs targeting proteins involved in the cell cycle or DNA damage response

PROTAC Name	Structure	E3 ligase	Protein of Interest
ZNL-02-096 (Li et al., 2020)		CRBN	Wee1

		CRBN	Cdk6
BSJ-03-123 (Brand et al., 2019)		CRBN	Cdk6
BSJ-03-204 (Jiang et al., 2019)		CRBN	Cdk4/6
BSJ-04-132 (Jiang et al., 2019)		CRBN	Cdk4
BSJ-4-116 (Jiang et al., 2021)		CRBN	Cdk12
JH-XI-10-02 (Hatcher et al., 2018)		CRBN	Cdk8
SK 575 (Cao et al., 2020)		CRBN	PARP1
THAL SNS 032 (Olson et al., 2018)		CRBN	Cdk9

TL 12-186 (Huang et al., 2018)		CRBN	Multikinase degrader (incl. AURKA and AURKB)

Although cell cycle or DDR targeting PROTACs are relatively new, several other PROTACs for treating cancer are further along the drug development pipeline. ARV-110 is an Androgen Receptor (AR)-targeting PROTAC that has displayed >90% AR degradation in mouse xenograft models and inhibition of tumour growth in prostate cancer patient derived xenograft (PDX) models (Neklesa et al., 2019). ARV-471 is another PROTAC that has shown high potency ($DC_{50} \sim 2nM$) at degrading its POI, Oestrogen Receptor Alpha (ERα), in multiple ER-positive breast cancer cell lines. Using ARV-471 in PDX models proved effective at halting tumour growth (Flanagan et al., 2019). ARV-110 is currently in Phase I and ARV-471 is in Phase 2 clinical trials due to their ability to efficiently stop tumour growth and are being administered as oral therapeutics (Table 1.2) (Pfizer and Arvinas, 2021). These results have helped increase the amount of pre-clinical work with other promising compounds, such as SD-36 targeting STAT3 and BETd-260 targeting the BET family proteins, displaying a regress in tumour growth in PDX, Osteosarcoma cell line-derived and Molm-16 xenograft models (Shi et al., 2019; Zhou et al., 2019). Both SD-36 and BETd-260 are CRBN-recruiting PROTACs but there have been promising effects in xenograft models with VHL-recruiting PROTACs, such as DT2216 (Khan et al., 2019). This proves that PROTAC technology is translatable to the clinic, therefore the concept that PROTACs can be used as a therapy is achievable and this work may further demonstrate these compounds' ability to effectively do this.

1.5 Head and neck cancer

1.5.1 Overview of head and neck cancer

Head and neck cancer occurs in over 30 locations, there are ~12,000 new cases in the UK each year (Cancer Research, 2021) and 325,000 deaths annually (Gormley et al., 2022). The most common malignancy for head and neck cancer is head and neck squamous cell carcinoma (HNSCC), which develops from the mucosal epithelium. The incidence of HNSCC is expected to increase by 30% by 2030 (Johnson et al., 2020). Most commonly these tumours arise in the pharynx, larynx, and oral cavity. The burden of HNSCC is different in each country as many causes are preventable. Although not very common, HNSCC five-year survival rate is only 50% and they are relatively tolerant towards genotoxic agents (Denaro et al., 2018). Thus, it is critical to find treatments that make HNSCC more susceptible to radiotherapy and chemotherapy to improve prognosis.

1.5.2 Causes, symptoms and diagnosis

Most HNSCC are preventable as they are caused by carcinogens within certain lifestyle factors. Tobacco and alcohol use accounts for approximately 75% of all head and neck cancers, however, viral infections, such as human papillomavirus (HPV) and Epstein-Barr virus (EBV) have been linked to HNSCC (Bouvard et al., 2009; Testino, 2011). In addition, excessive alcohol consumption is often linked with tobacco use and there also appears to be a synergistic effect between these factors in inducing tumorigenesis (Hashibe et al., 2009; Talamini et al., 2002). HPV, specifically HPV-16 and HPV-18, mainly causes tumours in the

oropharynx and these develop due to the E5, E6 and E7 viral oncoproteins stimulating

expression of genes that lead to immune evasion (DiMaio and Petti, 2013; Grabowska and

Riemer, 2012). In addition, these viral oncoproteins stimulate cell cycle progression to

induce tumorigenesis in the host cell (Estevao et al., 2019). For example, E6 forms a complex

with E6-AP, a cellular ubiquitination protein, and p53 in order to target it for degradation by

the UPS (Scheffner et al., 1993). This results in the tumour suppressor being absent at the

G1/S transition, therefore a DDR will not be initiated, and the cell will be forced through the

cell cycle. Mutations in *TP53* are the most common mutation in HPV-negative HNSCC,

therefore many treatment plans targeting the G2/M checkpoint may be beneficial in these

G1/S transition dysfunctional cancers (Zhou et al., 2016).

Symptoms of head and neck cancers are often like those of less serious conditions;

therefore, these symptoms are often overlooked by primary care physicians. Most patients

complain of hoarseness and general throat pain but, depending on the site of the cancer,

some may see a neck lump, have tongue pain, or could have dysphagia (difficulty

swallowing) (Alho et al., 2006; Robertson and Hornibrook, 1982). It was thought that

misdiagnosis of these symptoms by primary care physicians led to poorer prognoses,

however, the literature shows inconsistency for whether delayed diagnosis correlates with

overall survival (Schutte et al., 2020; Thomas et al., 2021). Diagnosis of HNSCC is often

through tactile examination, CT-scans and panendoscopy, however, it is clear that there is a

need for biomarkers that can be detected in a clinical setting for earlier diagnosis

(Economopoulou et al., 2019; Guizard et al., 2017). There have been several studies

investigating salivary microRNA, tissue-based, such as PD-L1, and genetic-based biomarkers,

but these lack specificity to solely diagnose in a clinical setting (De Keukeleire et al., 2021; Kang et al., 2021).

1.5.3 Current treatments

HNSCCs are complex tumours that are difficult to treat and often aggressive which contributes to the poor prognoses of this cancer. Treatments against these malignancies are quite unsuccessful with the main recommendations being surgery to eradicate the tumour, radiotherapy and platinum-based chemotherapeutic agents (Alsahafi et al., 2019). Many HNSCCs show resistance towards radiotherapy, thus this type of treatment often reduces quality of life whilst proving ineffective at killing the cancer. Unfortunately, as there are few targeted therapies, such as Cetuximab (an EGFR-targeting antibody that inhibits the binding of EGF to its receptor), to prove effective against genetic alterations in HNSCCs, radiotherapy is the main treatment pathway (Alsahafi et al., 2019; Dietz et al., 2009).

The need to create more effective treatments against head and neck cancers is clear as they are the sixth most common malignancy globally and these cancers also have a poor survival rate (Parkin et al., 2005). Furthermore, without the development of clinical biomarkers to diagnose these cancers earlier, mortality and morbidity from these cancers will continue to rise. Therefore, it is crucial to investigate ways to improve current therapies against HNSCC to increase the survival rate.

1.6 Project aims

It is clear that head and neck cancer is becoming a greater public health concern as it has poor prognoses, is caused by lifestyle factors, such as tobacco use or alcohol consumption, and the incidence is due to increase. Therefore, the overall aim of this project was to investigate the use of Wee1 PROTACs compared to Wee1 inhibitor, AZD1775, to increase cancer cell death *in vitro* as single and combinatorial strategies with the following experimental aims:

- Characterise the Wee1 PROTACs in HNSCC and analyse their impact on cell survival as single agents compared to Wee1i, AZD1775 (Chapter 3)

- Evaluate the cytotoxicity of Wee1 PROTACs alone and in addition to radiotherapy or chemotherapeutics in HNSCC cells, and compare this to Wee1 inhibition (Chapter 4)

- Identity the consequences that Wee1 PROTACs have on mitosis and the DNA damage response, compared to Wee1 inhibition and the similarities or differences observed between cell lines with varying p53-status (Chapter 5)

- Investigate the dependence of Wee1 PROTACs on E3 ligase expression to degrade their target in a broader range of cancer cell types (Chapter 6)

2 Materials and Methods

2.1 Materials

2.1.1 Reagents

All reagents were purchased from Thermo Fisher Scientific (Massachusetts, USA) and Sigma Aldrich (Missouri, USA), or as otherwise specified. All tissue culture media, PS, FBS and Trypsin were purchased from Gibco (Thermo Fisher Scientific). Cell culture flasks and cell culture dishes were from Thermo Fisher Scientific (Massachusetts, USA), Corning Incorporated (New York, USA) or SARSTEDT AG & Co. (Nümbrecht, Germany).

2.1.2 Antibodies

Table 2.1 Table of primary antibodies for Western blotting and IF staining

Primary antibody	Manufacturer/Information	Concentration	Application
Wee1 (Rb)	CST (Massachusetts, USA), #4936, polyclonal	1:1,000	WB
β-actin (Rb)	CST, #8457, monoclonal	1:10,000	WB
β-actin (M)	CST, #3700, monoclonal	1:10,000	WB
α-tubulin (M)	Sigma Aldrich, T6199, monoclonal	1:10,000	WB
pCDK1 (Tyr15) (Rb)	CST, #9111, polyclonal	1:1,000	WB
CRBN (Rb)	CST, #71810, monoclonal	1:1,000	WB
VHL (Rb)	CST, #68547, monoclonal	1:1,000	WB
PLK1 (M)	Abcam (Cambridge, UK), ab17057, monoclonal	1:500	WB
γH2AX (pS139) (M)	Abcam, ab26350, monoclonal	1:1000, 1:250	WB, IF
PARP (Rb)	CST, #9542, polyclonal	1:1000	WB
Caspase-3 (Rb)	CST, #14220, monoclonal	1:1000	WB

pChk1(Ser345) (Rb)	CST, #2348, monoclonal	1:1000	WB
pChk2(Thr68) (Rb)	CST, #2197, monoclonal	1:1000	WB
Chk1 (M)	CST, #2360, monoclonal	1:1000	WB
Chk2 (M)	CST, #3440, monoclonal	1:1000	WB
pATR(Ser428) (Rb)	CST, #2853, polyclonal	1:1000	WB
Pericentrin (Rb)	Abcam, ab4448, polyclonal	1:1,000	IF
Cyclin B1 (M)	Millipore (Massachusetts, USA), 05-373, monoclonal	1:1,000	IF
Tubulin (Rt)	Millipore, MAB1864, monoclonal	1:1,000	IF
CENPA [3-19] (M)	GeneTex (California, USA), GTX13939, monoclonal	1:200	IF
BLM (Rb)	Invitrogen, PA5-27384, polyclonal	1:200	IF

Table 2.2: Table of secondary antibodies for Western blotting and IF staining.

Secondary antibody	Manufacturer/Information	Concentration	Application
Anti-mouse IgG, HRP-linked	CST #7076	1:3,000 or 1:30,000	WB
Anti-rabbit IgG, HRP-linked	CST, #7074	1:3,000	WB
Anti-mouse, Alexa Fluor Plus 488	Invitrogen, A32723, polyclonal	1:500	IF
Anti-rabbit, Alexa Fluor Plus 488	Invitrogen, A11034, polyclonal	1:500	IF
Anti-rabbit, Alexa Fluor Plus 555	Invitrogen, A32732, polyclonal	1:500	IF
Anti-mouse, Alexa Fluor Plus 555	Invitrogen, A32727, polyclonal	1:500	IF
Anti-rat, Alexa Fluor 647	Invitrogen, A21247, polyclonal	1:500	IF

2.2 Buffers and Solutions

Table 2.3: Table of recipes for buffers and solutions.

Solution	Recipe
Blocking Solution	5% (w/v) skimmed milk powder in TBST or 5% (w/v) BSA in TBST
Crystal violet solution	0.5% (w/v) crystal violet in ultra-pure water (MQW)
Hot Lysis (Laemmli) Buffer	50 mM Tris-Cl, 2% (w/v) SDS, 10% (v/v) glycerol, pH 6.8 in MQW
Immunoblotting solution for antibodies dilution	5% (w/v) BSA, 0.05% (w/v) NaN_3 in 1X TBST
Mounting media for immunofluorescence	0.2 M Tris-HCl, pH 8.5 in MQW, 24% (v/v) glycerol, 9.6% (w/v) Mowiol 4-88, 2 µg/mL DAPI
Resolving gel Tris buffer	1.5 M Tris-Cl, pH 8.8 in MQW
Sample Loading Buffer for SDS-PAGE gels (6X)	375 mM Tris-HCl, 9% (w/v) SDS, 50% (v/v) glycerol, 0.03% (w/v) bromophenol blue in MQW
Stacking gel Tris buffer	0.5 M Tris-Cl, pH 6.8 in MQW
Tris-Borate-EDTA Buffer (5X TBE)	90 mM Tris, 2 mM EDTA, pH 8.3 in MQW
Tris-Buffer Saline (10X TBS)	50 mM Tris-Cl, 150 mM NaCl, pH 7.5 in MQW
Tris-Buffer Saline with Tween (1X TBST)	10% (v/v) 10X TBS, 0.1% (v/v) Tween-20
Tris-Glycine Running Buffer (10X TGS)	250 mM Tris, 1.92 M glycine, 1% (w/v) SDS, pH 8.3 in MQW

2.3 Polyacrylamide gels preparation

Table 2.4 shows how gels with SDS were prepared using combs and glass plates from the Bio-Rad Mini-Protean system. The resolving gel was made and poured, absolute ethanol was added to the top to even out the gel and stop it from drying out and gels were left to set for ~ 25 min. Once set, ethanol was removed and the stacking gel was poured on top. The comb was inserted into the casting plates and the gel was allowed to set for a further ~ 20 min. Once set, the gels were stored at 4 °C wrapped in damp blue roll until use. PageRuler™ Plus Prestained Protein Ladder (Thermo Fisher Scientific, 26619) was used as the molecular weight marker to run the gels.

Table 2.4: Table of composition of SDS-PAGE gels used for Western blotting.

	Resolving SDS-PAGE (20 mL)	Resolving SDS-PAGE (20 mL)	Stacking SDS-PAGE (5 mL)
Percentage	16%	10%	4%
MQW	6.7 mL	9.7 mL	3.17 mL
Resolving Tris buffer	5 mL	5 mL	-
Stacking Tris buffer	-	-	1.25 mL
Acrylamide (40%)	8 mL	5 mL	0.5 mL
SDS (10%)	200 µL	200 µL	50 µL
APS (10%)	100 µL	100 µL	25 µL
TEMED	20 µL	20 µL	5 µL

2.4 Tissue culture

2.4.1 Routine mammalian cell culture

UM-SCC-6, UM-SCC-12, UM-SCC-74A and UM-SCC-81B were obtained from Tom Carey, University of Michigan and FaDu and A-253 were purchased from ATCC. These are all head

and neck squamous cell carcinoma (HNSCC) cell lines, however are resected from different tumour sites. These sites are the tongue (UM-SCC-6 and UM-SCC-74A), larynx (UM-SCC-12), tonsils (UM-SCC-81B), salivary gland (A-253) and hypopharynx (FaDu). All cell culture work was performed using an aseptic technique in a class II laminar flow hood. The hood was disinfected with 70 % ethanol before and after use. HNSCC cell lines were cultured in Dulbecco's modified eagle's medium (DMEM) (Gibco) with 10% (v/v) of fetal bovine serum (FBS) (Sigma-Aldrich), 4 mM L-glutamine, 25 mM D-glucose, 1 mM sodium pyruvate and 1% (v/v) penicillin/streptomycin (PS) (100 units penicillin and 10 μg streptomycin/mL) (Gibco). Cells were routinely STR profiled and grown in an incubator at 37 °C and 5% CO_2.

NCI60 cell lines (A-498, SN-12C, A-549 and NCI-H23) were purchased from the National Cancer Institute (NCI) and were cultured in Roswell Park Memorial Institute (RPMI) 1640 medium (Gibco) with 10% (v/v) FBS (Sigma-Aldrich), 2 mM L-glutamine, 11 mM D-glucose and 1% PS (100 units penicillin and 10 μg streptomycin/mL) (Gibco). Cells were grown in an incubator at 37 °C and 5% CO_2.

2.4.2 Passaging cells

Cells were passaged every 3 to 4 days when they reached 70 – 80 % confluency. To passage the cells, old medium was removed from the flask and cells were then washed with PBS and incubated for 5-10 min, depending on cell line, with 1 mL 0.05 % trypsin in a T75 at 37 °C, 5 % CO_2. Once all cells had detached from the bottom of the flask, 5 mL medium was added to the trypsinised cells to neutralise the trypsin and to create a single-celled suspension. Cells were usually split 1:6 with 1 mL of cell suspension and 9 mL medium added to a new T75 flask. To seed plates, the cell suspension was counted using a haemocytometer (Counting

chamber, Hawksley, AC1000) and a microscope (AE2000, Motic) to determine the cells/mL and calculate the volume of cell suspension required for the desired seeding density of the experiment.

2.4.3 Thawing cells and storage

Cells were grown to ~70 % confluency in T75 flasks and a single-cell suspension was produced as described in section 2.4.2. The cell suspension was centrifuged at 1500 rpm for 5 minutes and the supernatant was discarded. The cell pellet was re-suspended in 5 mL of a 10 % (v/v) solution of cell culture medium and DMSO before pipetting 1 mL aliquots into cryovials. Cryovials were inserted into a Mr. Frosty™ freezing container (Thermo Fisher Scientific) and incubated at -80 °C overnight. Cell stocks were then transferred to liquid nitrogen for long-term storage.

To thaw cell stocks, once removed from liquid nitrogen, cell stocks were heated quickly and 1 mL warm medium was added to the cryovial. The 2 mL cell suspension was then transferred to a 15 mL falcon and centrifuged at 1500 rpm for 5 minutes. The supernatant was discarded and the cell pellet was resuspended in 5 mL medium and transferred to a T25 cell culture flask. Fresh medium was added to the flask the next day and cells were transferred to a T75 for routine cell culture once they had reached a confluency of 70 – 80 %.

2.5 Cell treatments

2.5.1 For immunoblotting

Cells were trypsinised and seeded (see Section 2.4.2) at 3×10^5 cells in 2 mL of media per well on a NuncTM Cell-Culture Treated multidishes 6- well plate (Fisher Scientific) and incubated at 37 °C and 5% CO_2 overnight. Cells were treated with PROTACS for the desired length of time at 37 °C and 5% CO_2 and with DMSO (0.1% v/v) to serve as a control with the same conditions. Cells were washed with PBS (Sigma-Aldrich) twice before harvesting.

For co-treatment with mechanistic inhibitors, MG132 (5 or 10 μM) (Tocris), VH298 (100 μM) (Sigma-Aldrich), pomalidomide (5 or 10 μM) or AZD1775 (1 μM) (Cayman Chemical) was added to the desired wells three hours before PROTAC treatment. Cells had a final concentration of DMSO (0.1% v/v). Plates were incubated for a further 21 h at 37 °C and 5% CO_2 prior to harvesting.

2.5.2 For flow cytometry

Cells were trypsinised and seeded (see Section 2.4.2) at 1×10^5 cells in 1 mL of media per well on a NuncTM Cell-Culture Treated multidishes 12-well plate (Fisher Scientific) and incubated at 37 °C and 5% CO_2 overnight. Cells were treated with 300 nM PROTACS for 24 h at 37 °C and 5% CO_2 and with DMSO (0.1% v/v) to serve as a control with the same conditions.

For co-treatment with irradiation, cells were treated with 300 nM PROTACS for 2 h prior to irradiation (CellRad, Faxitron Bioptics), then cells were further incubated with the compounds for 22 h at 37 °C, 5% CO_2, for a total treatment time of 24 h.

2.5.3 For clonogenic survival assays

Cells were trypsinised and seeded (see Section 2.4) at a desired density in triplicates on a

24-well plate and incubated overnight at 37 °C, 5% CO_2. Single-celled suspensions were

prepared as described in section 2.4.2. Cells were plated at a low desired density (Table 2.5)

in triplicate into a 24-well plate and was increased relative to the treatment. For

chemotherapeutic clonogenic assays, the co-treatment wells seeded double the number of

cells to the single agent treatment. Cells were treated with the compounds (300 nM for

PROTACs and AZD1775, 300 nM for cisplatin and 10 µg/mL for bleomycin) for 24 h at 37 °C,

5% CO_2 then the compound-supplemented media was removed and replaced with fresh

media and cells were allowed to grow for 6 - 10 days to form colonies.

Table 2.5 Seeding densities for clonogenic assays relative to ionising radiation dose. These seeding densities were used in triplicate for DMSO or Wee1-targeting drug at each radiation dose in a 24-well plate

	Number of cells seeded per well			
IR dose (Gy)	0	1	2	4
UM-SCC-6	400	400	400	400
A-253	400	800	1600	3200
FaDu	400	800	1600	3200

2.5.4 For immunofluorescence

Cells were trypsinised and seeded (see Section 2.4) at 1×10^5 cells per well (UM-SCC-74A, A-

253 and FaDu) or 1.2×10^5 cells per well (UM-SCC-6) in a 12-well plate on round coverslips.

Cells were then treated with the PROTAC, AZD1775 or DMSO control (0.1% (v/v) DMSO) and

incubated for 24 h.

For co-treatment with irradiation, cells were treated with PROTAC, AZD1775 or DMSO control (0.1% (v/v) DMSO) for 2 h prior to irradiation. Samples were then irradiated and remained in drug-supplemented media for a further 22 h.

2.6 Cell proliferation assay

UM-SCC-6, UM-SCC-12, UM-SCC-74A, UM-SCC-81B, A-253, FaDu, A-498, SN-12C, A-549 and NCI-H23 were seeded into 96 well plates (see Table 2.6) and incubated at 37 °C and 5% CO_2 overnight. Cells were treated with the test compounds at the desired dose, ranging from 0 to 20 µM (for PROTAC treatments, AZD1775 and Cisplatin) or 0 to 500 µg/mL (for bleomycin), and used DMSO (PROTAC and AZD1775), PBS (bleomycin) or deionised water (Cisplatin) as a vehicle control. Compounds were supplemented into 100 µL of media and incubated at 37 °C and 5% CO_2 for 72 h. 20 µL of CellTiter 96® AQueous One Solution Cell Proliferation Assay (MTS) (Promega) reagent was added to each well. Plates were incubated for 1-3 h in 37 °C and 5% CO_2 incubator and the formazan product were measured by absorbance at 490 nm every 1 h using a Wallac 1420 Viktor^2 multilabel counter (PerkinElmer). Data analysis was performed using GraphPad Prism 9.2.0 and curves were plotted using non-linear regression to a [Agonist] vs. response – Variable slope (four parameters).

Table 2.6 Table of seeding densities for cell lines when performing 72 h MTS assay

Cell line	Seeding density per well in 96 well plate
UM-SCC-6 (HNSCC)	3×10^3
UM-SCC-12 (HNSCC)	1×10^3
UM-SCC-74A (HNSCC)	1×10^3
UM-SCC-81B (HNSCC)	1×10^3
A-253 (HNSCC)	2×10^3
FaDu (HNSCC)	3×10^3
A-498 (RCC)	2×10^3
SN-12C (RCC)	3×10^3
A-549 (LUAD)	1×10^3
NCI-H23 (LUAD)	5×10^3

2.7 Immunoblotting

2.7.1 Hot lysis sample preparation

See section 2.5.1 for how cells were treated. Hot lysis was performed by adding 75-150 μL (depending on confluency of cells) of hot lysis buffer, heated for 30 minutes prior, to each well over a heat block at 105°C. The hot lysis buffer contained 50 mM Tris (pH 6.8), 2% SDS (Alfa Aesar) and 10% glycerol (see Table 2.3) (Melford Laboratories). A cell scraper was used to detach the cells from the bottom of the well and to collect the lysate. The lysate was left on the heat block for 10 minutes, vortexed every 2 minutes. The protein concentration of the lysates was determined by the Pierce™ BCA Protein Assay Kit (Fisher Scientific) using the 2 h incubation at room temperature method. The absorbance of the solution was measured at 520 nm using a Nanodrop 2000c (Fisher Scientific). The lysate was used immediately or stored at -20°C until use.

2.7.2 SDS-PAGE

Samples were run on either 7.5 % or 4 – 20 % Bio-Rad Mini-PROTEAN® TGX™ Precast Protein gels or 10 % or 16 % self-cast resolving gels with 5 % stacking gels (Section 2.3). Gels were run in a Mini-PROTEAN® Tetra Cell Tank (Bio-Rad) at 45 mA per gel for approximately 1 h, or until sample dye reached the base of the gel.

2.7.3 Transferring protein to nitrocellulose membrane and probing

SDS-PAGE gels (Section 2.7.2) were transferred using a Trans-Blot® Turbo™ Transfer System to either an Amersham™ Protran™ 0.45 µm nitrocellulose blotting membrane (GE Healthcare Life Sciences) or membrane provided in the Trans-Blot Turbo RTA Mini 0.45 µm Nitrocellulose Transfer Kit. Transfer stacks, membrane and SDS-PAGE gels were soaked in transfer buffer provided in the kit before assembling in the cassette in the following order: transfer stack, nitrocellulose membrane, protein gel, transfer stack. Blots were ran on the turbo, mixed molecular weight (MW), 1 or 2 mini gels setting for 7 minutes.

Following transfer, membranes were blocked for 2 hr in 50 mL falcon tubes in 10 mL blocking buffer (Section 2.2) on a roller. After blocking, membranes were incubated with primary antibody made to the appropriate concentration in magic mix (section 2.2) overnight at 4 °C on a roller. After primary antibody incubation, membranes were washed in PBS for 5 minutes thrice before adding HRP-conjugated secondary antibody made to the appropriate concentration in blocking buffer for 2 h. After secondary antibody incubation, membranes were washed thrice in PBS and developed with the Bio-Rad Chemidoc MP imaging system or Invitrogen ™ iBright™ FL1500 imaging system.

2.7.4 Normalisation of band intensity

Protein levels were equalised by measuring the signal intensity of the loading control and calculating a ratio between the samples. This ratio was used to normalise the signal intensity measured of the protein of interest. The signal intensities were normalised relative to DMSO or to other samples dependent on the experiment. The signal intensity was measured by using the iBright™ Analysis Software or Bio-Rad Image Lab.

2.8 Flow cytometry

2.8.1 EdU and DAPI staining for cell cycle profile analysis

See section 2.5.2 for how cells were treated. After treatment, cells were incubated with 10 µM EdU for 1 h. After incubation, cells were washed with PBS (Sigma-Aldrich) before harvesting with trypsin for 5 min at 37 °C, 5% CO_2. Cells were resuspended in 1 mL media and transferred to a microcentrifuge tube and centrifuged at 500 x g for 5 min. The media was removed and the pellet was resuspended in 1 mL of PBS and then centrifuged for 5 min at 500 x g. The cells were fixed, permeabilized and fluorescently labelled the EdU using the Click-iT™ EdU Alexa Fluor™ 647 Flow Cytometry Assay Kit. After step 5.5 of the kit, cells were incubated with 1 µg/mL DAPI on ice for 30 min.

Samples were ran using the CytoFLEX (Beckman Coulter) Flow Cytometer. 10,000 events after gating out debris (cells) and excluding doublets (singlets) were collected per sample (see Figure 2.1). An EdU only stain was used to determine where EdU-positive cells would appear on the axis. A DAPI only stain was used to confirm that all cells were EdU-negative and to analyse where the cells would fall on the axis. Furthermore, untreated cells were

stained with both dyes to confirm that there was no overlap between the dyes and to

compensate if necessary.
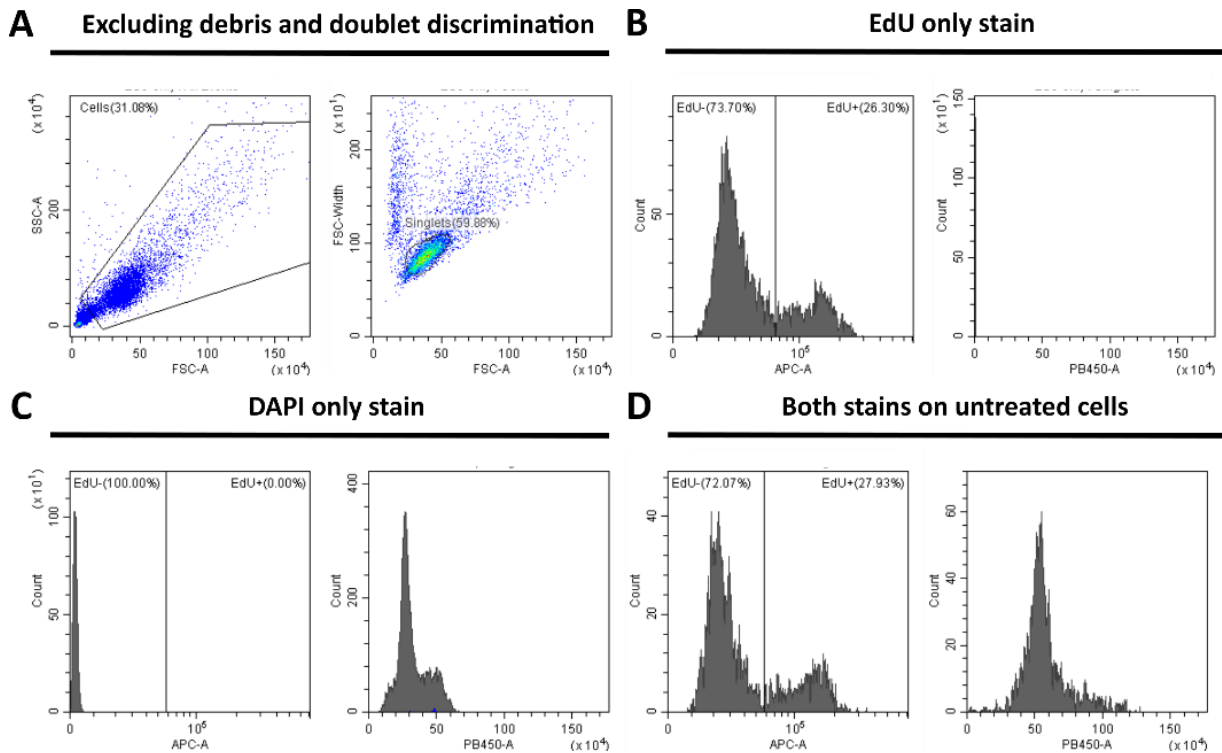
Figure 2.1 Cell gating for EdU and DAPI flow cytometry. UM-SCC-6 cells have been used here as an example for how cells are gated to correctly compensate and only analyse individual cells for cell cycle stage flow cytometry. (A) Debris was gated out and the cells gate was applied to the FSC-A versus FSC-width plot. A tight gate around the singlet population was made and this was applied to all future plots. (B) EdU only stain shows that no signal is seen in the DAPI channel (PB450) and two peaks can be seen for EdU-negative cells (G1 and G2/M) and EdU-positive cells (S). (C) DAPI only stain shows that no signal is seen in the EdU channel (APC) and a cell cycle profile can be seen in the DAPI plot. (D) Both stains on untreated cells to confirm previous gating has been correctly done.

Data were analysed using CytExpert software and cells were gated with DNA content

(PB450-A) versus EdU incorporation (APC-A) to separate cells in G1, S (EdU positive) and

G2/M cells.

2.8.2 Annexin V and PI staining for apoptosis/necrosis detection

See section 2.5.2 for how cells were treated. After treatment, cells were washed with PBS (Sigma-Aldrich) twice before harvesting with trypsin for 5 min at 37 °C, 5% CO_2. Cells were resuspended in 1 mL media and transferred to a microcentrifuge tube and centrifuged at 500 x g for 5 min. The media was removed and the pellet was resuspended in 1 mL of PBS and then centrifuged for 5 min at 500 x g. The pellet was then resuspended in Annexin V-binding buffer (Abcam) supplemented with 5 µL of Annexin V-FITC detection reagent (Abcam) and 5 µL of Propidium Iodide (PI) (Abcam).

Samples were ran using the CytoFLEX (Beckman Coulter) Flow Cytometer. 15,000 events after gating out debris were collected per sample. Data were analysed using CytExpert software and cells were gated with positive staining for phosphatidylserine molecules (apoptosis detection) (FITC-A) versus DNA content (PE-A) to separate cells that were live (-/-), early apoptotic (+/-), late apoptotic (+/+) and necrotic (+/-) by staining for Annexin V/PI.

2.9 Clonogenic assay

Following section 2.5.3 for cell treatments in clonogenic assays, the media was removed and wells washed twice in PBS. The colonies were then fixed in 4% PFA for 1 h before staining with 0.5 % crystal violet (Acros organics) for 1 h. Colonies were washed and left to air dry before counting by eye and images were taken using a light box. The plating efficiency was calculated by counting the number of colonies for unirradiated control and dividing by the seeding density of the unirradiated control. Plating efficiencies ± SEM for the cells were as follows: UM-SCC-6 (12.7 ± 1.4 %), A-253 (17.3 ± 3 %) and FaDu (13 ± 5.6 %). The surviving fraction was determined by the following calculation:

Surviving fraction = Number of colonies for selected condition / (Seeding density of selected

condition x average plating efficiency)

2.10 Immunofluorescence

See section 2.5.4 for how cells were treated. After treatment, cells were gently washed

twice with PBS before being fixed with 1 mL 4% PFA in PBS per coverslip for 15 min. PFA was

removed and coverslips were washed in PBS twice. 2 mL 50 mM ammonium chloride in PBS

was added per coverslip for 10 min. The ammonium chloride was removed and coverslips

were washed once with PBS. To permeabilize the cells, 2 mL of 0.2% (v/v) Triton X-100 in

PBS was added to each coverslip for 5 min. Once the Triton had been removed, 1 mL of 5%

(v/v) goat serum in PBS was added to each well for 30 min at room temp to block. After 30

min, blocking solution was removed from each coverslip and 50 μL of primary antibody mix

was added per coverslip for 2 h at room temp protected from light. After the primary

incubation, each coverslip was washed thrice with PBS for 5 min. 50 μL of secondary

antibody mix was added per coverslip for 1 h at room temp protected from light. After 1 h

incubation, coverslips were washed with PBS and mounted onto ~ 10 μL mounting medium

(see Table 2.7). Slides were left to dry overnight before storing at 4 °C protected from light.

See Table 2.1 for primary and secondary antibody solutions.

A Zeiss-LSM880-Airyscan confocal microscope and Zen software (or Leica Stellaris 5 (DMI18)

and LASX software (4.5.0) were used to image the immunofluorescence of stained cells on

glass coverslips, using a 40× objective dry lens (Plan-Apochromat 40×/0.95) for micronuclei

detection or 10x objective dry lens (Plan-Apochromat 10x/0.4) for γ-H2Ax. A 63x oil-

immersion lens (Plan-Apochromat 63x/1.4) was used to obtain better images for foci. Three

fields of view were imaged per condition (coverslip) and an average of these was taken to

compare repeats. Images were analysed in FIJI software (2.3.0). Micronuclei were counted by eye, total cells and nuclei size were calculated by marking nuclei in the DAPI channel as regions of interest (ROI) and the ROIs were saved as an overlay to calculate the γ-H2Ax intensity.

Table 2.7: Table of primary and secondary antibody solutions for IF staining.

Experiment	Primary antibody mix	Secondary antibody mix
Detection of micronuclei and ultrafine anaphase bridges	BLM (Rb), 1:200 CENP-A [3-19] (M), 1:200 Tubulin (Rt), 1:1,000	Anti-rabbit, Alexa Fluor Plus 488, 1:500 Anti-mouse, Alexa Fluor Plus 555, 1:500 Anti-rat, Alexa Fluor Plus 647, 1:500
γ-H2Ax foci	γ-H2Ax (M), 1:250	Anti-mouse, Alexa Fluor Plus 488, 1:500
Detection of G2/M arrest via cyclin B1 intensity	Cyclin B1 (M), 1:1,000 Pericentrin (Rb), 1:1,000 Tubulin (Rt), 1:1,000	Anti-rabbit, Alexa Fluor Plus 555, 1:500 Anti-mouse, Alexa Fluor Plus 488, 1:500 Anti-rat, Alexa Fluor Plus 647, 1:500

3 Analysing the degradation profile of Wee1 PROTACs in Head and Neck Squamous Cell Carcinoma (HNSCC)

3.1 Introduction

3.1.1 Wee1 kinase as a target for cancer therapy

As discussed in section 1.1.2, dysregulation of the cell cycle will often lead to carcinogenesis. Many cancers, including HNSCC, have mutations in p53, which has a role in the G1/S and S phase checkpoints, therefore cancer cells heavily rely upon arrest at the G2/M checkpoint to repair DNA damage and may overexpress Wee1 to accomplish this. Furthermore, patients with Wee1 overexpression have shown poorer prognoses and survival (Matheson et al., 2016). Targeting of Wee1 kinase in cancer treatments has shown potential and the best inhibitor for Wee1, AZD1775, is currently being tested in over 60 clinical trials (Table 1.1). Single-agent AZD1775 clinical trials have reached Phase Ib, however these have not yet progressed to Phase II (Bauer et al., 2023; Do et al., 2015). AZD1775 in combination with standard genotoxic treatments, such as gemcitabine, radiotherapy and platinum-based chemotherapeutics, as well as with other inhibitors, such as PARP and ATR inhibitors (Kong and Mehanna, 2021; Leijen et al., 2016; Madariaga et al., 2022). These clinical trials have shown that Wee1 is a good therapeutic target, however, further efforts are required to minimise toxicities, such as haematologic and gastrointestinal toxicities, associated with Wee1 inhibition (Takebe et al., 2021). One way that this could be done is by investigating if more selective compounds, such as Wee1 PROTACs, have fewer off-target effects and thus can reduce these toxicities (Aublette et al., 2022; Li et al., 2020).

3.1.2 Targeting domains for E3 ubiquitin ligases and the protein of

interest

3.1.2.1 Wee1 inhibitor, AZD1775

AZD1775 competes with the ATP-binding site on Wee1, which results in inhibition of the

phosphorylation of CDK1 and renders the G2/M checkpoint dysfunctional (Hirai et al., 2009).

This inhibitor has shown to chemosensitize and radiosensitize tumours, as well as work in

combination with other small molecule inhibitors to induce apoptosis and prevent G2/M

arrest (Kong and Mehanna, 2021). Although a potent inhibitor of Wee1, AZD1775 has shown

many off-target effects, such as inhibition of PLK1 (Zhu et al., 2017). A more potent

inhibitor, Zn-c3, discovered through structure-activity relationship (SAR) exploration from

AZD1775 as a starting point, is currently undergoing phase II clinical trials and will hopefully

show less toxicity to patients as it is more specific than AZD1775 (Huang et al., 2021). Work

on Zn-c3 was not published until the end of the project that synthesised these Wee1

PROTAC compounds, therefore AZD1775 was used as the warhead for these molecules

(Aublette et al., 2022).

3.1.2.2 Cereblon inhibitor, pomalidomide

Pomalidomide is a derivative of thalidomide, a controversial drug that has found widespread

clinical use in recent decades (Bartlett et al., 2004). Developed by Celgene and approved for

use by the FDA in 2013, pomalidomide has been used as an anti-cancer drug in combination

with dexamethasone for the treatment of multiple myeloma and has exhibited

immunomodulatory effects (Chen et al., 2023; Dredge et al., 2002). The binding of

pomalidomide to CRBN does not simply inhibit the E3 ligase, but it alters the specificity of

CRBN by inducing it to ubiquitylate various neosubstrates, such as Ikaros transcription

factor, which are important for its anticancer activity in the treatment of multiple myeloma

(Zhao et al., 2023). As it can strongly bind to CRBN and other CRBN-recruiting PROTACs have

shown success when using pomalidomide in the compound, this seemed to be a good

binder to use as the ligand for CRBN in Wee1 PROTACs (Cieślak and Słowianek, 2023;

McCurdy and Lacy, 2013).

3.1.2.3 VHL inhibitor, VH032

VH032 inhibits the interaction of VHL and HIF1-α, activates the HIF transcription factor and

temporarily induces a hypoxic response (Frost et al., 2016). However, more recent evidence

suggests that prolonged treatment results in increased levels of VHL and decreased HIF1-α

(Frost et al., 2021). VHL-recruiting PROTACs using the VH032 ligand have shown significant

success over many years by often displaying a narrower target selectivity profile than CRBN-

based PROTACs (Gadd et al., 2017; Mi et al., 2023; Zengerle et al., 2015), therefore this

ligand was used to create another library of Wee1 PROTACs to maximise the potential to

produce effective Wee1-degrading compounds (Aublette et al., 2022).

Previous work performed in the Gadd/Allinson lab (Dr Marine Aublette) produced two

different Wee1 PROTAC series that targeted Wee1 for degradation by the recruitment of

the E3 ligases, CRBN or VHL. Various PROTACs in each first generation series showed the

ability to degrade Wee1 and reduce levels of Tyr15 phosphorylation of CDK1 in HeLa S3,

prostate cancer cell lines (PC3 and LNCaP) and breast cancer cell lines (BT549 and MCF7)

(Aublette et al., 2022). PROTAC degradation has appeared to be cell line dependent, and it

has been hypothesised that this could reflect levels of the target E3 ligases and other proteins. Preliminary experiments shown in this thesis investigated the relative levels of CRBN and VHL between HNSCC cell lines to aid conclusions on if this could be the case. The ability of first generation Wee1 PROTACs to degrade Wee1 and reduce pCDK1 levels, and the time taken for normal levels of Wee1 to return after removal of the PROTACs was investigated in HNSCC cell lines of varying p53-status. Furthermore, a more potent second-generation series of CRBN- and VHL-recruiter PROTACs was synthesised and assessed in the same HNSCC cell lines. First and second generation Wee1 PROTACs as monotherapy treatments were investigated in cell viability assays to analyse their effectiveness at inhibiting cell proliferation alone.

3.2 Aims and objectives

In this chapter, the viability of using Wee1-degrading PROTACs in head and neck cancer cells will be assessed via a number of aims:

1. Assess CRBN- and VHL-based PROTACs in head and neck cancer cell lines and determine if the first and second generation PROTACs induce Wee1 degradation specifically in each of these cell lines.

2. Compare the degradation profiles of the first generation (MA048 and MA055) to the second generation (MA163 and MA199) PROTACs in head and neck cancers and confirm target engagement.

3. Investigate the effect of the Wee1-targeting compounds (Wee1i (AZD1775) and Wee1 PROTACs) as monotherapy treatments on cell viability and determine the optimal dosage of the compounds for use in combination with other genotoxic agents.

3.3 Results and discussion

3.3.1 Expression levels of E3 ubiquitin ligases in HNSCC cell lines

UM-SCC-6, UM-SCC-74A, A-253 and FaDu cells were allowed to grow under normal growth conditions to evaluate the relative expression levels of E3 ubiquitin ligases, CRBN and VHL, to understand if the amount of E3 ubiquitin ligase present in the cell line has an effect on the PROTACs ability to elicit degradation. Western blots were probed for CRBN, α-Tubulin and VHL. α-Tubulin was used as the loading control for this experiment as there was less variability in α-Tubulin levels across the cell lines in comparison to β-actin (Figure 3.1).
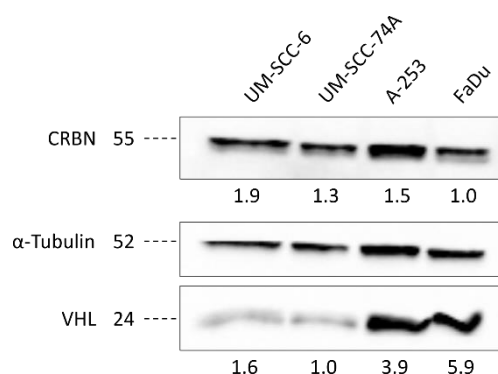
Figure 3.1 Relative expression levels of E3 ubiquitin ligases, CRBN and VHL, in HNSCC cell lines. Western blot showing levels of CRBN and VHL in untreated lysates of UM-SCC-6, UM-SCC-74A, A-253 and FaDu cells. The membrane was blotted for CRBN, α-Tubulin (as the loading control) and VHL, n = 2. Quantitation of relative expression levels corresponding to CRBN or VHL can be seen underneath the bands.

CRBN levels are consistent between cell lines, whereas there are lower levels of VHL, roughly 2 – 6-fold lower in p53-WT cell lines, UM-SCC-6 and UM-SCC-74A, compared with p53-deficient cell lines, A-253 and FaDu.

3.3.2 Assessment of first generation Wee1 PROTACs

3.3.2.1 Dose response of HNSCC cell lines to first generation PROTAC treatment

To assess the Wee1 degradation profiles of the first-generation Wee1 PROTACs (Figure 3.2), UM-SCC-74A (p53-WT) and A-253 (p53-null) cells were treated with varying doses from 20 µM to 1 nM for 24 h. The 24 h treatment time was previously determined as, at this time point, there was complete degradation of the target across different cell lines (M. Aublette – personal communication). Western blots were probed for Wee1, β-actin (as the loading control) and pCDK1 (Tyr15) (Figure 3.3).
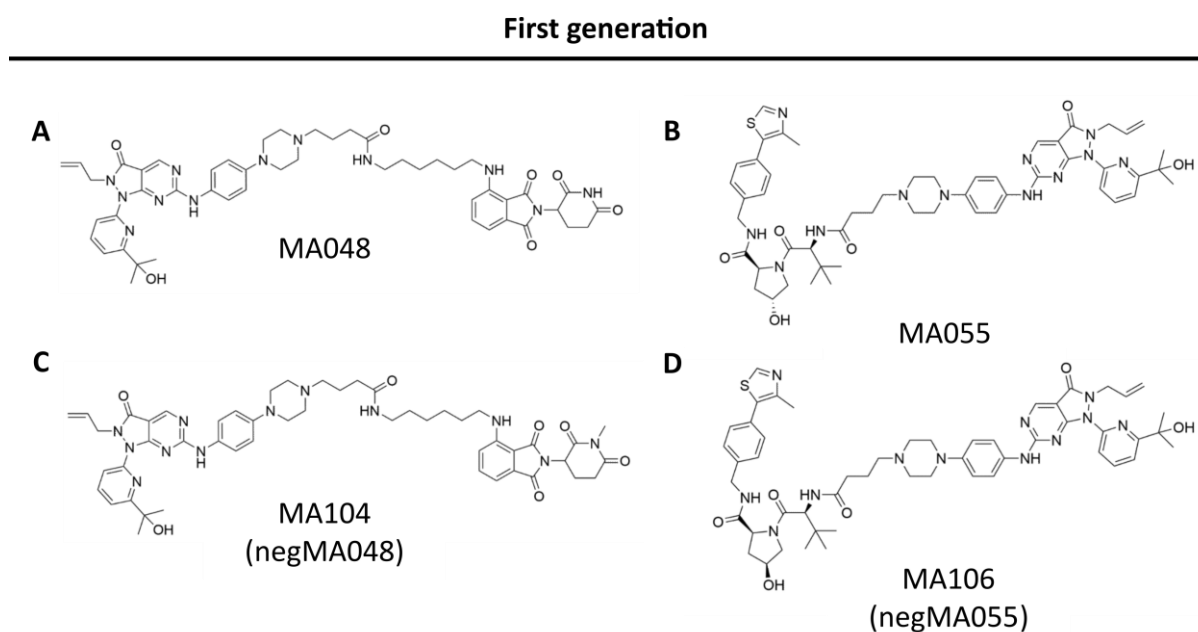
Figure 3.2 Structures of first generation Wee1 PROTACs. Structures of the Wee1 PROTACs displayed above show (A) MA048, (B) MA055, (C) MA104 and (D) MA106. MA104 and MA106 are the negative controls for MA048 and MA055, respectively. MA048 is a CRBN-recruiter and its negative control (MA104) cannot recruit CRBN but can bind Wee1. MA055 is a VHL-recruiter and its negative control (MA106) cannot recruit VHL but can bind Wee1.
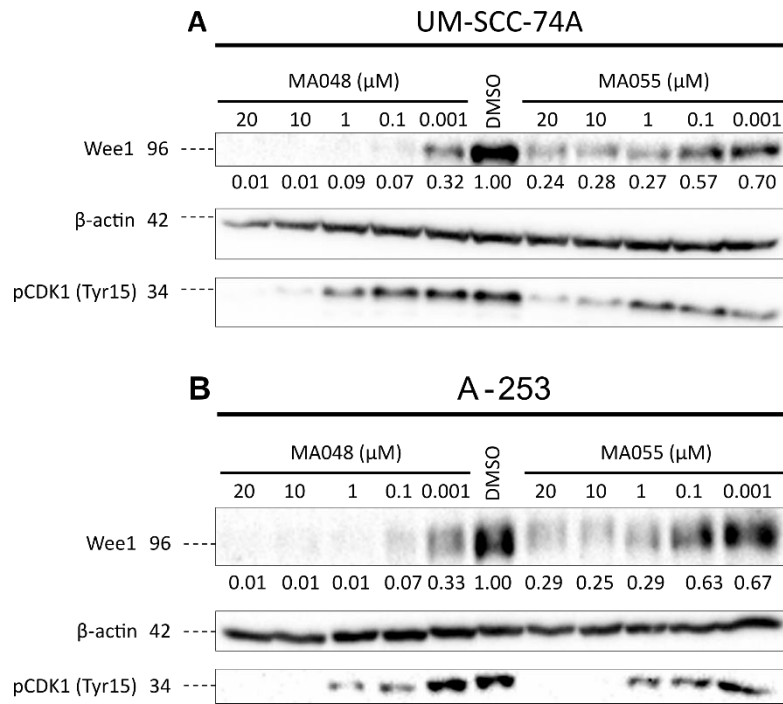
Figure 3.3 Degradation profiles of CRBN-recruiter, MA048, and VHL-recruiter, MA055 in UM-SCC-74A and A-253. (A, C) Western blots of two HNSCC cell lines that were treated with PROTACs for 24 h prior to the production of lysates. (B, D) Quantitation of western blots in (A) and (C) showing the decrease in % Wee1 remaining with the increase of PROTAC concentration. The membrane was blotted for Wee1, β-actin (as the loading control) and pCDK1 (Tyr15), n = 1. Quantitation of relative levels of Wee1 normalised to actin and the DMSO control are presented underneath the corresponding Wee1 band.

MA048, a first generation CRBN-recruiter, is shown as a more potent degrader of Wee1 compared to MA055, a first generation VHL-recruiter, in both UM-SCC-74A (p53-WT) and A-253 (p53-null) (which corroborates previous data in other cell lines). For example, maximal degradation by MA048 results in 99.9 % Wee1 degradation at 20 μM in both cell lines, whereas MA055 at 20 μM degrades 76 % and 71 % Wee1 in UM-SCC-74A (p53-WT) and A-253 (p53-null) respectively. MA055 degraded Wee1 to 24 - 29 % at doses of 20, 10 and 1 μM in both cell lines. MA048 treatment depletes pCDK1 (Tyr15) levels in both cell lines at 20 μM and 10 μM with the depletion effect beginning to weaken at 1 μM. The bands were less intense at 1 μM and 100 nM for pCDK1 (Tyr15) in A-253 (p53-null) in comparison to UM-

SCC-74A (p53-WT), but no change was seen compared to the control at 1 nM. MA055

showed the same trends but was overall less potent.

3.3.2.2 Time taken for PROTACs to degrade Wee1 and return of Wee1 levels

after removal of PROTAC treatment

To determine how long it would take for the PROTACs to degrade Wee1, UM-SCC-74A (p53-

WT) and A-253 (p53-null) cells were treated with 1 µM of CRBN-recruiter, MA048, and VHL-

recruiter, MA055, for 1 h, 2 h and 4 h. Cells were also treated for 4 h with the negative

control PROTACs, MA104 and MA106, for MA048 and MA055, respectively. Western blots

were probed with Wee1 and β-actin as a loading control (Figure 3.4).
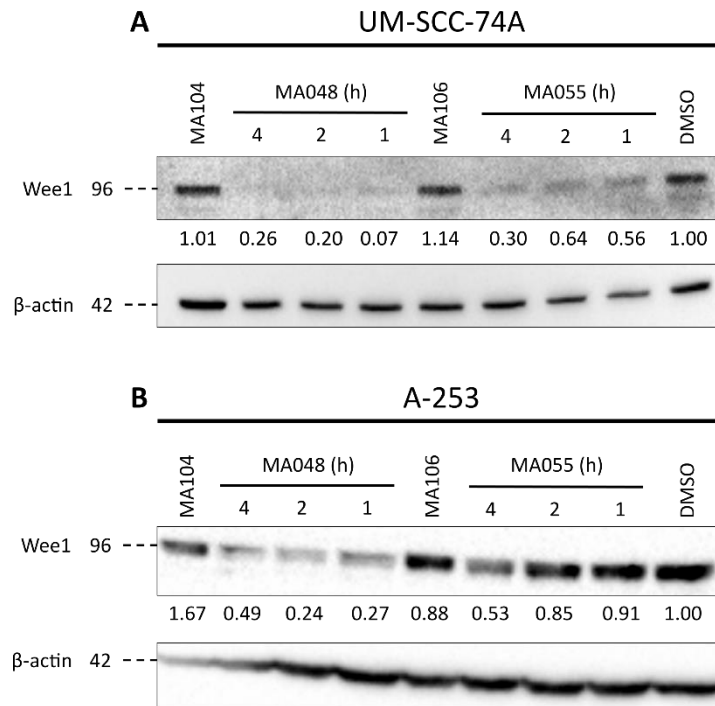
Figure 3.4 Degradation of Wee1 by first generation PROTACs over 4 h time course. Western blots of two HNSCC cell lines that were treated with 1 μM PROTACs for indicated lengths of time prior to the production of lysates. The membrane was blotted for Wee1 and β-actin (as the loading control), n = 1. Quantitation of relative levels of Wee1 normalised to actin and the DMSO control are presented underneath the corresponding Wee1 band.

In UM-SCC-74A (p53-WT), MA048 degraded 93 % of Wee1 and MA055 degraded 44 % of Wee1 within the first hour of treatment (Figure 3.4A). MA048 elicited more degradation of Wee1 compared to MA055 in UM-SCC-74A (p53-WT) which is a similar trend to the PROTACs in A-253 (p53-null) (Figure 3.4B). MA055 was much slower at degrading Wee1 in A-253 (p53-null) compared to MA048, which corresponds with previous data in the lab, (Aublette et al., 2022), that VHL-recruiters appear to take a longer time to reach maximal degradation of their target than CRBN-recruiters. It is clear that MA048 elicits more complete degradation of Wee1 compared to MA055 in both cell lines. After confirming that Wee1 can be degraded in a relatively short time period (<24 h), it led to the question of how

quickly Wee1 protein levels return after removing the degrader to further inform how treatments should be performed.

The time taken for the cell lines to re-establish Wee1 protein levels is important for understanding how Wee1 PROTAC treatments could be performed to assess their potential as a cancer treatment. This would determine how long degradation activity persists in the cells after removing the PROTAC-treated media. Cells were treated with the PROTACs before "washing-out" the PROTAC-treated media and replacing with fresh media after 24 h, with samples taken at time intervals over an 8 h period (Figure 3.5).
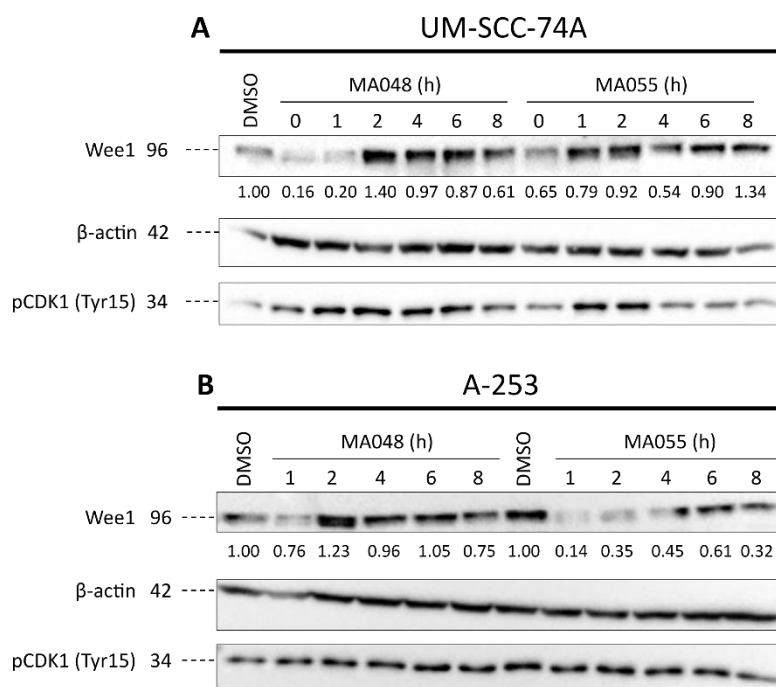
Figure 3.5 Return of protein levels after washing out of PROTAC treatment over 8 h time period. Western blots of two HNSCC cell lines that were treated with PROTACs for 24 h at 1 μM before replacing with fresh media and allowing to sit for different intervals over 8 h. Blots were probed for Wee1 and β-actin as the loading control, n = 1. Quantitation of relative levels of Wee1 normalised to actin and the relevant DMSO control are presented underneath the corresponding Wee1 band.

In UM-SCC-74A (p53-WT), when removing MA048, Wee1 levels had a sharp increase (140 %

Wee1 compared to 100 % levels in DMSO) at 2 h and then stabilized to the normal level

(Figure 3.5). When removing MA055 Wee1 had returned by the 1 h time point (79 % Wee1

compared to 100 % in DMSO control) and, although the changes are slight, pCDK1 (Tyr15)

levels show a similar pattern. pCDK1 (Tyr15) levels appeared lower in he DMSO control

compared to treatments with MA048 and MA055 in both PROTACs at 0 h in both cell lines,

however this is likely due to erroneous loading. In A-253 (p53-null), the opposite happens

where MA055's activity is more prolonged after washing out but levels return rapidly after

MA048 washout. This led to the consideration that the linker length or the E3 ligase ligand

could be affecting the rate at which the PROTACs leave and enter the cell. Another theory

could be that the stoichiometry of MA055 and its partner proteins could maintain the

ternary complex for longer in A-253 (p53-null). Potentially there is a difference between the

cell lines that accounts for the opposing trends observed, and this difference could be

affecting target engagement as this is only seen in the wash-out experiments. A 2018 study

performed a longer washout of 24 h and 48 h with a VHL-based PROTAC and displayed

prolonged reduction of c-Met (POI) levels which was rescued by the addition of free VHL

(Burslem et al., 2018). Our findings conflict this study as A-253 (p53-null) exhibit higher

levels of VHL compared to UM-SCC-74A (p53-WT), therefore, if it were to follow the

observed trend in the previous study, we would anticipate MA055's activity to be more

prolonged in the cell line with lower VHL levels.

3.3.2.3 Effect of linker length on degradation activity of Wee1 PROTACs

The observation that treatment with different PROTACs showed different Wee1 recovery rates following their removal led to the question whether this was due to linker length or E3 ligase recruitment. To investigate this, cell lines were treated with CRBN-recruiting PROTACs that had different linker lengths. MA048 is a shorter linker of 10 carbon atoms and TH012 is a longer linker of 18 carbon atoms.

PROTACs with shorter and longer linker lengths are more potent at degrading Wee1 than those with intermediate lengths (Aublette et al., 2022), but whether these linker lengths also affect how sustained the PROTAC activity is following washout is not currently known. UM-SCC-74A (p53-WT) were treated for 24 h prior to washing out the PROTAC-supplemented media with fresh media. To see if Wee1 levels return to normal after a longer time period, a 24 h washout was performed (Figure 3.6) as the previous washout experiment with MA048 and MA055 showed higher levels of Wee1 compared to the DMSO control (Figure 3.5).
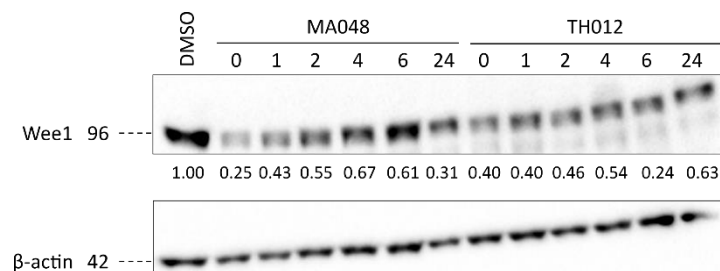
Figure 3.6 Investigating the effect of varying linker lengths on the PROTACs ability to sustain Wee1 degradation after removal. UM-SCC-74A were treated with 1 µM of MA048 or TH012 for 24 h. Drug-supplemented media were replaced with fresh media at time points over 24 h to observe when Wee1 levels returned to normal after removal of PROTAC treatment. Blots were probed for Wee1 and β-actin as the loading control, n = 2. Quantitation of the relative levels of Wee1 normalised to actin and relative to the DMSO control for this representative blot are below the bands in the figure.

Quantitation of Wee1 levels in TH012-treated cells revealed that Wee1 levels were slowly increased from 40 % at 0 h washout to 63 % at 24 h washout. Percentage remaining Wee1 levels increased by 18 % in the first hour of MA048 washout and reached similar levels of Wee1 as the TH012 washout treatment by 24 h (Figure 3.6). Wee1 levels for both PROTACs were still suppressed in this cell line by 24 h after wash out of compound. This is a limitation by comparing protein levels by Western blot as even though the same cell line and conditions were used, Figure 3.5 shows higher levels of Wee1 (>100 %) after 2 h washout of MA048, whereas Figure 3.6 shows lower levels (55 %). Further investigation into how PROTAC linker length affects target protein levels is required and due to the variability between cell lines, this future study should start by comparing cell lines with different expression levels of the E3 ligases to provide more insight.

3.3.2.4 Competition assays of PROTACs with E3 ubiquitin ligase inhibitors

After investigating the degradation ability of MA048 and MA055 PROTACs, a competition assay was performed to investigate if we could block ternary complex formation by using ligands to the E3 ubiquitin ligases. This would confirm that the observed degradation is dependent on E3 ligase activity. Pomalidomide, the parent CRBN ligand for MA048 was used to bind to CRBN, VH298 (a more potent analogue of VH032, the parent VHL ligand for MA055) was used to bind to VHL and MG132 was used to inhibit the proteasome. Pomalidomide was used at a ratio of 10:1 to PROTAC, VH298 100:1 and MG132 at 10:1 (Figure 3.7). Cells were pre-treated with inhibitors for 2 h prior to adding PROTACs to inhibitor-supplemented media for a further 22 h.
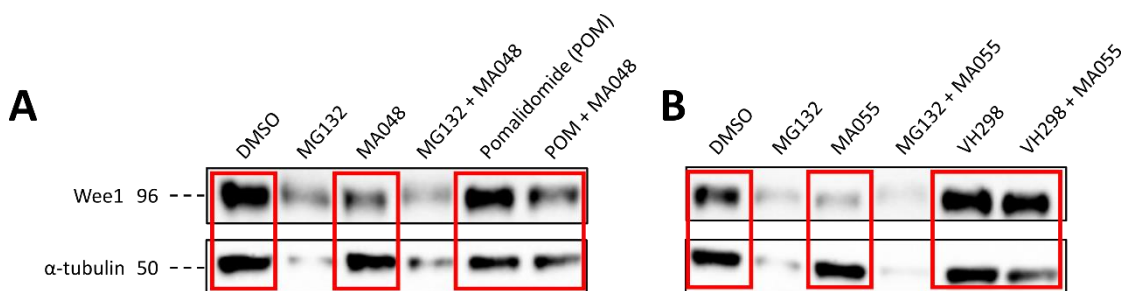
Figure 3.7 Competition assays of first generation Wee1 PROTACs. Investigating the affinity of (A) MA048 and (B) MA055 for their E3 ubiquitin ligases, CRBN and VHL, respectively. A-253 cells were pre-treated with MG132 (10 µM), pomalidomide (10 µM) or VH298 (100 µM) for 2 h prior to PROTAC treatment for a further 22 h. The red boxes show the lanes that will be discussed: DMSO control, PROTAC, E3 ligase inhibitor and PROTAC + E3 ligase inhibitor, from left to right, on each blot. The membrane was blotted for Wee1 and α-tubulin as the loading control, n = 1. Quantitation of Wee1 to calculate remaining Wee1 levels relative to DMSO is as follows: (A) DMSO = 1.00, MA048 = 0.39, POM = 1.61 and MA048 + POM = 1.16 and (B) DMSO = 1.00, MA055 = 0.22, VH298 = 1.82 and VH298 + MA055 = 3.22.

MG132 was very toxic to cells at this concentration and treatment time, resulting in a low protein concentration for those samples. Using this proteasome inhibitor for the same length of pre-treatment as the PROTACs was not feasible to observe inhibition of degradation by MG132 in these cell lines. Quantitation confirmed that pre-treatment with VH298 and pomalidomide prevented Wee1 degradation by MA055 or MA048, respectively (Figure 3.7).

3.3.3 Assessment of second generation Wee1 PROTACs

After testing of first generation PROTACs, Dr Marine Aublette synthesised a second generation of Wee1 degraders based on optimisation of the first generation. Furthermore, a negative control to MA163 (where negMA163 has an additional methyl group on the

82

pomalidomide ligand to prevent negMA163 ubiquitinating and degrading Wee1) was also produced.

3.3.3.1 Dose response of HNSCC cell lines to second generation PROTAC treatment

Cells were treated with varying doses of the second generation PROTACs (Figure 3.8) from 10 µM to 1 nM for 24 h to assess their Wee1 degradation profiles. An additional p53-proficient and p53-deficient cell line was selected to test the second-generation PROTACs as, due to previous data in the lab, they were expected to be more potent and used as the compounds in future combination treatments. Western blots were probed for Wee1, β-actin and pCDK1 (Tyr15) (Figure 3.9 & Figure 3.10).
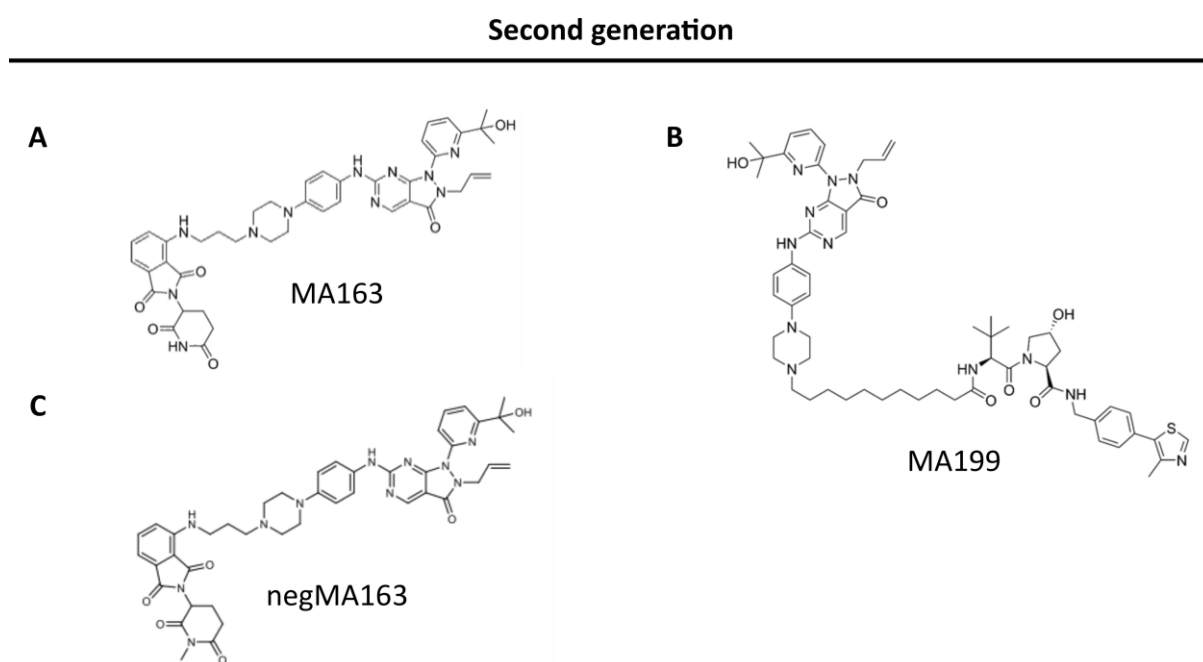
Second generation

Figure 3.8 Structures of second generation Wee1 PROTACs. Structures of the Wee1 PROTACs displayed above show (A) MA163, (B) MA199 and (C) negMA163. A negative control for MA199 was not synthesised due to time constraints. MA163 is a CRBN-recruiter and its negative control cannot recruit CRBN but can bind Wee1, MA199 is a VHL-recruiter.
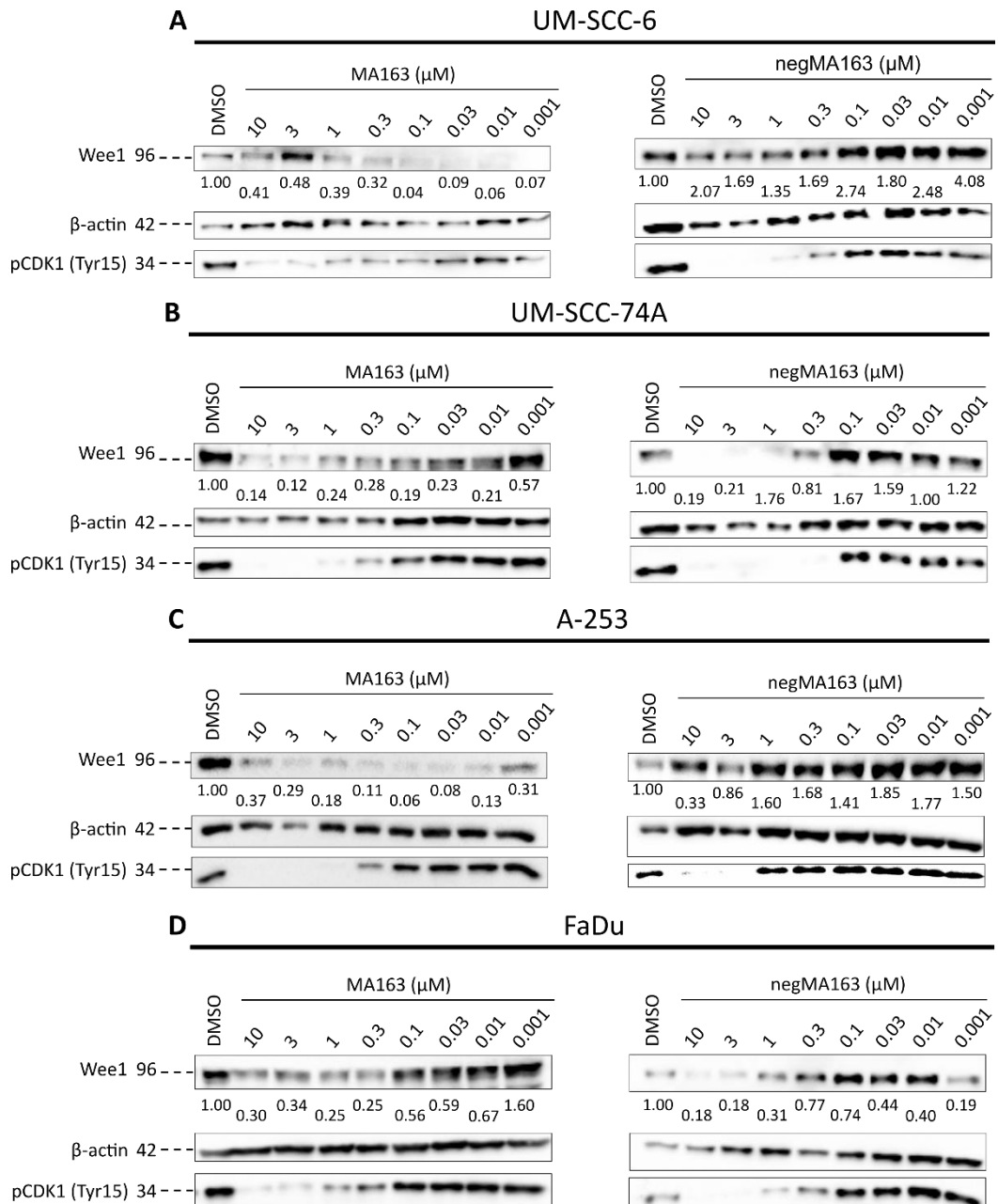
Figure 3.9 Degradation profiles of CRBN-recruiter, MA163, and its negative control in HNSCC cell lines. Western blots of four HNSCC cell lines (p53-WT, UM-SCC-6 and UM-SCC-74A, and p53-deficient, A-253 and FaDu) that were treated with PROTACs for 24 h prior to the production of lysates. The membrane was blotted for Wee1, β-actin (as the loading control) and pCDK1 (Tyr15), n=1. Relative levels of Wee1 normalised to actin and relative to the DMSO control for this representative blot are staggered below the bands in the figure.

MA163, a second generation CRBN-recruiter, is shown to be a potent degrader in all cell

lines. The hook effect, where unproductive binary complexes between the PROTAC and

either the POI or E3 ligase is formed at high PROTAC doses, is observed in UM-SCC-6 (p53-

WT) and A-253 (p53-null), with degradation of Wee1 seen until 300 nM in all cell lines.

Normal levels of Wee1 begin to return by 100 nM in UM-SCC-74A (p53-WT) and FaDu (p53-

mutant) whilst degradation is sustained in UM-SCC-6 (p53-WT) and A-253 (p53-null). In UM-

SCC-6 (p53-WT) and A-253 (p53-null) we see no degradation of Wee1 by the negative

control, however we see reduced levels of Wee1 in UM-SCC-74A (p53-WT) and FaDu (p53-

mutant). The unexpected decrease of Wee1 seen for the negative control could be due to

changes in synthesis of Wee1 protein upon adding a Wee1i in those cell lines and this was

further investigated in A-253 (p53-null) (Figure 3.11). Reduction of pCDK1 (Tyr15) levels are

seen from 10 μM to 100 nM in all cell lines.
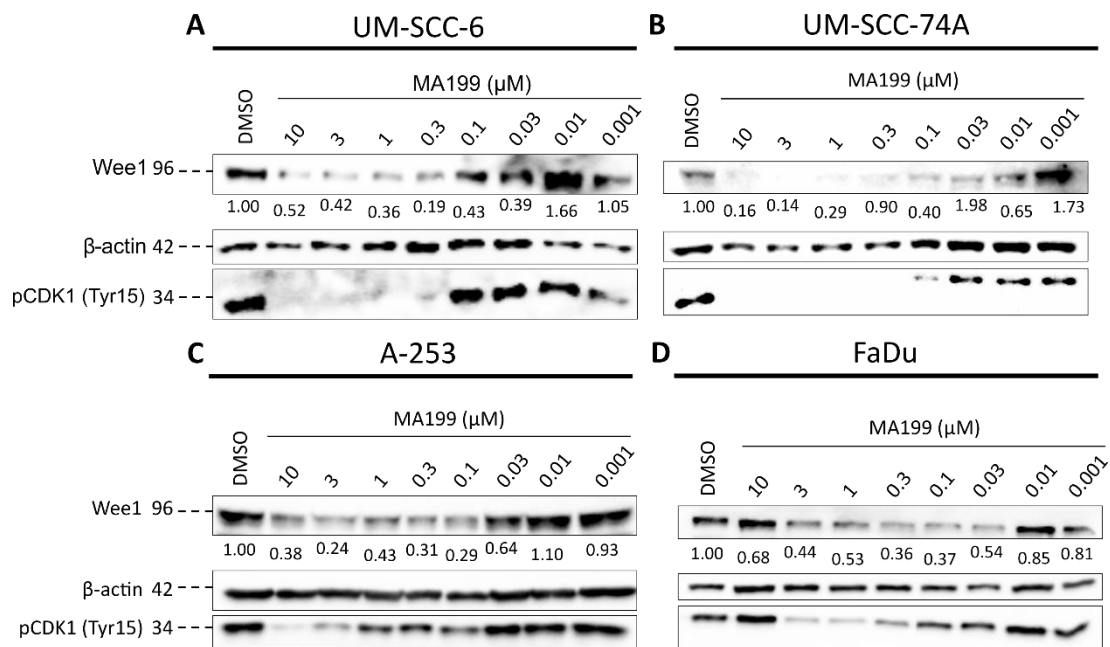
Figure 3.10 Degradation profiles of VHL-recruiter, MA199, in HNSCC cell lines. Western blots of four HNSCC
cell lines that were treated with MA199 for 24 h prior to the production of lysates. The membrane was blotted
for Wee1, β-actin (as the loading control) and pCDK1 (Tyr15), n=1. Relative levels of Wee1 normalised to actin
and relative to the DMSO control for this representative blot are staggered below the bands in the figure.

MA199, a second generation VHL-recruiter, has shown increased potency compared to the

first generation PROTAC, MA055, in all cell lines. For example, treatment with 100 nM

MA055 led to 63 % remaining Wee1, whereas treatment at the same dose with MA199

resulted in only 29 % remaining Wee1 in A-253 (p53-null). The hook effect is observed in

FaDu (p53-mutant) with degradation of Wee1 seen until 300 nM in all cell lines. Normal

levels of Wee1 begin to return by 100 nM in UM-SCC-6 (p53-WT) and 30 nM in A-253 (p53-

null) and UM-SCC-74A (p53-WT) and 10 nM in FaDu (p53-mutant). Reduction of pCDK1

(Tyr15) levels are seen from 10 μM to 100 nM in UM-SCC-6 (p53-WT), UM-SCC-74A (p53-

WT) and FaDu (p53-mutant) but sufficient reduction can only be seen up to 1 μM in A-253

(p53-null).

As there was no negative control available for MA199, a dose response of AZD1775 was

performed in A-253 (p53-null) cells. AZD1775 was used as it will be able to inhibit Wee1, and

thus reduce its substrate pCDK1 (Tyr15), however it cannot induce ubiquitination and

degradation of Wee1. This experiment should demonstrate that degradation of Wee1 is

seen as a result of the PROTAC and that levels of pCDK1 (Tyr15) will still be observed due to

the inhibitory effect of Wee1 (Figure 3.11).
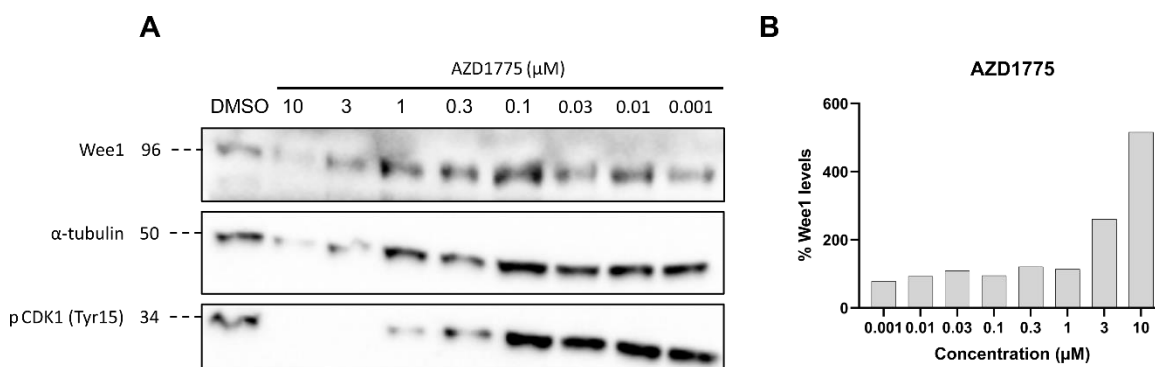
Figure 3.11 Dose response of AZD1775 in A-253 cells. Western blot of A-253 cells that were treated with
AZD1775 for 24 h prior to the production of lysates. The membrane was blotted for Wee1, α-tubulin (as the
loading control) and pCDK1 (Tyr15), n=1.

Although levels of Wee1 appear lower in 10 μM and 3 μM AZD1775 treatment, after normalising the band intensities to tubulin and calculating Wee1 levels relative to the DMSO control, no degradation of Wee1 was observed (Figure 3.11B). Therefore, we can assume that the reduced Wee1 levels observed in Figure 3.9 are due to PROTAC-induced degradation. This experiment should be repeated and performed in other cell lines before making conclusions about if Wee1 inhibition effects expression levels of Wee1 (discussed with respect to the loss of Wee1 by negMA163 in Figure 3.9).

This section has concluded that degradation of Wee1 occurs within 24 h, however we do not know how rapidly these PROTACs can degrade Wee1 in comparison to the first generation PROTACs, MA048 and MA055 (Figure 3.4).

3.3.3.2 Time taken for PROTAC treatment to degrade Wee1

The time taken for the more potent, second generation PROTACs to degrade Wee1 needs to be considered when planning future experiments investigating co-treatments and ensuring that we are comparing inhibition of Wee1 versus degradation. Therefore, A-253 (p53-null)
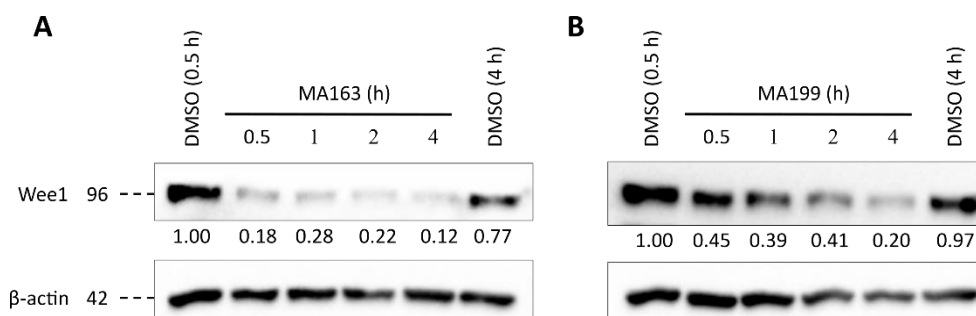
Figure 3.12 Degradation of Wee1 over 4 h time course by CRBN-recruiter, MA163, and VHL-recruiter, MA199, in A-253 cells. Western blot of A-253 cells that were treated with MA163 or MA199 for 0.5 h, 1 h, 2 h and 4 h prior to the production of lysates. The membrane was blotted for Wee1 and β-actin (as the loading control), n=1. Relative levels of Wee1 normalised to actin and relative to the DMSO control for this representative blot are staggered below the bands in the figure.

cells were treated with CRBN-PROTAC, MA163, and VHL-PROTAC, MA199, for 0.5 h, 1 h, 2 h and 4 h (Figure 3.12).

MA163 was able to cause maximal degradation of Wee1 to 18 % remaining Wee1 within 30 minutes, whereas MA199 was slower, with degradation continuing to increase, with maximal degradation of Wee1 by 80 %, up until the final time point.

3.3.3.3 Competition assays of PROTACs with E3 ubiquitin ligase inhibitors

To determine that the PROTACs exhibit dependency on the UPS to degrade Wee1, their ability to degrade Wee1 was compared to co-treatments with E3 ligase ligands (pomalidomide for CRBN and VH298 for VHL). A-253 (p53-null) cells were pre-treated with pomalidomide (10 μM) and VH298 (100 μM) for 2 h before adding the PROTAC or Wee1i (300 nM) for a further 22 h. The E3 ligase ligands do disrupt both MA163- and MA199-induced degradation of Wee1, but over a 24 h period we see that it cannot fully block Wee1 degradation (Figure 3.13). This suggests that the affinity of pomalidomide to CRBN or VH298 to VHL is weaker than the second generation PROTACs to their relative E3 ligases.
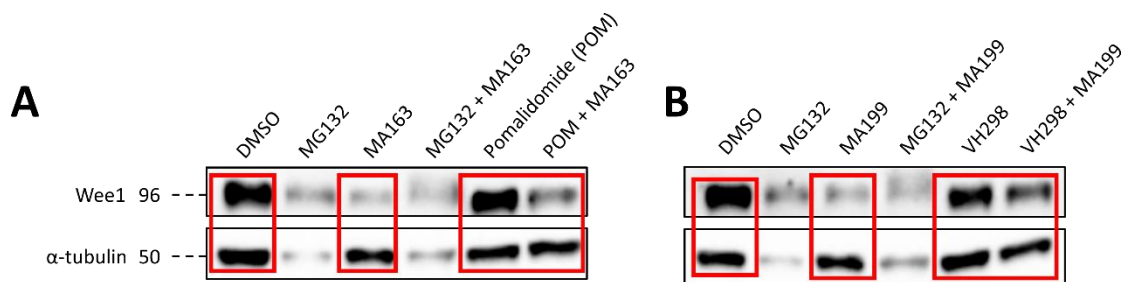
Figure 3.13 Competition assays of second generation Wee1 PROTACs. Investigating the affinity of (A) MA163 and (B) MA199 for their E3 ubiquitin ligases, CRBN and VHL, respectively. A-253 cells were pre-treated with pomalidomide (10 µM) or VH298 (100 µM) for 2 h prior to PROTAC treatment for a further 22 h. The red boxes show the lanes that will be discussed: DMSO control, PROTAC, E3 ligase inhibitor and PROTAC + E3 ligase inhibitor, from left to right, on each blot. The membrane was blotted for Wee1 and α-tubulin, n = 1. Remaining Wee1 levels were calculated normalised to tubulin and relative to DMSO are as follows: (A) DMSO = 1.00, MA163 = 0.23, POM = 1.64 and POM + MA163 = 0.56 and (B) DMSO = 1.00, MA199 = 0.17, VH298 = 0.49 and VH298 + MA199 = 0.45.

As can be seen in Figure 3.7, MG132 was too toxic for the cells when treated for this treatment length at this concentration and resulted in a low protein concentration in the sample. In the case of the VHL-based PROTACs, previous work in the lab revealed that the PROTAC ternary complex binds the E3 ligase more tightly than a binary complex of the PROTAC and E3 ligase alone. This was with MA055 where the K_d(VBC:MA055) = 360 ± 130 nM whereas K_d (Wee1:MA055:VBC) = 190 ± 90 nM (M. Aublette, unpublished results). Given its higher potency over MA055, MA199 likely has a much higher affinity for forming ternary complexes, therefore this could explain why in these competition experiments we still see some degradation with MA199, whereas excess VH298 seemed capable of fully blocking MA055 from forming a ternary complex. The K_d for the ternary complex for Wee1:MA199:VBC is 60 ± 30 nM (M. Aublette, unpublished results), therefore almost two-fold lower than Wee1:MA055:VBC (the equivalent binary complex for MA199 could not be determined due to solubility issues – M. Aublette, personal communication).

3.3.4 Effect of monotherapy treatments on cell viability

3.3.4.1 First generation PROTACs

To assess the ability of first generation PROTACs to inhibit cell proliferation, UM-SCC-74A (p53-WT), A-253 (p53-null) and FaDu (p53-mutant) cells were treated with varying doses of PROTAC from 20 µM to 1 nM for 72 h. The plates were analysed with MTS reagent and dose-response curves were produced (Figure 3.14).
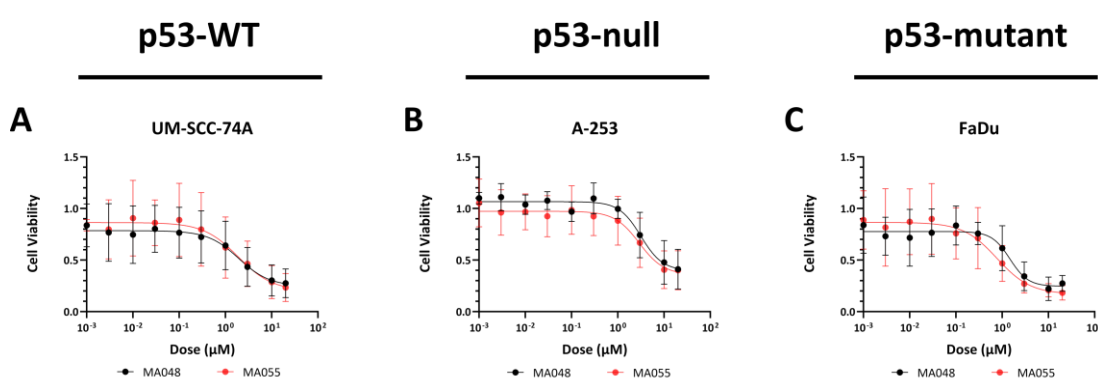
Figure 3.14 Cell viability assays of first generation PROTACs in HNSCC cell lines. Cells were treated for 72 h with CRBN-recruiter, MA048, or VHL-recruiter, MA055. Cell viability assays were normalised with vehicle control, DMSO. Plots are presented as mean ± SD of n = 4 biological repeats.

Both MA048 and MA055 were able to reduce cell viability across all three cell lines tested (Figure 3.14). Both compounds were most potent in p53-mutant cell line, FaDu (p53-mutant), with EC50 values of 1.8 µM for MA048 and 0.9 µM for MA055 (Table 3.1). UM-SCC-74A (p53-WT) and A-253 (p53-null) had similar EC50 values for MA055 (2.4 µM and 2.9 µM respectively), however, UM-SCC-74A (p53-WT) were more sensitive to MA048 in comparison to A-253 (p53-null) (2.0 µM and 3.6 µM respectively).

Table 3.1 Table of EC50 values of cell viability assays (MTS) in HNSCC cell lines for first generation PROTACs. UM-SCC-74A, A-253 and FaDu were treated with MA048 and MA055 for 72 h (n = 4) and dose response curves for these values can be seen in Figure 3.14.

Treatment	EC50 (µM) ± SD		
	UM-SCC-74A	A-253	FaDu
MA048	2.0 ± 0.4	3.6 ± 0.7	1.8 ± 0.4
MA055	2.4 ± 1.0	2.9 ± 0.3	0.9 ± 0.2

As observed in Section 3.3.3.1, the second generation Wee1 PROTACs elicit stronger degradation of Wee1 in the Western blots, therefore cell viability assays were performed for MA163 and MA199 and Wee1i, AZD1775, to investigate the effect on cell proliferation and to confirm the increased potency of the compounds by analysing the EC50 values.

3.3.4.2 Second generation PROTACs

 To assess the ability of second generation PROTACs to inhibit cell proliferation, UM-SCC-6, UM-SCC-74A, A-253, UM-SCC-12, FaDu and UM-SCC-81B cells were treated with varying doses of PROTAC from 20 µM to 0.1 nM for 72 h. The plates were analysed with MTS reagent and dose response curves were produced (Figure 3.15).
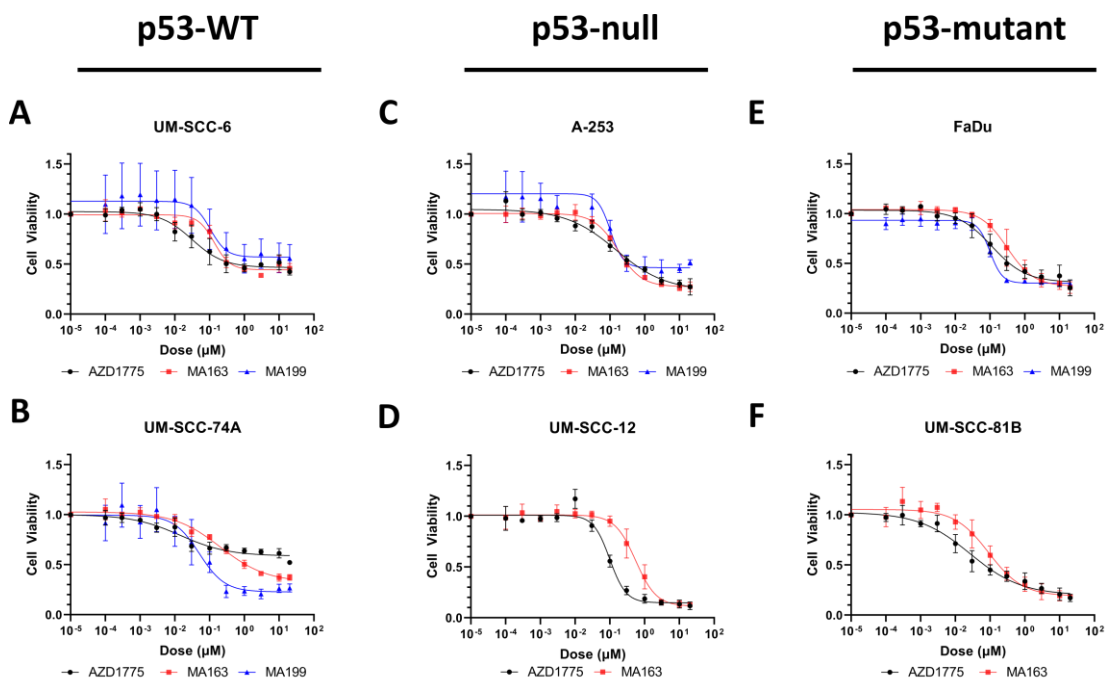
Figure 3.15 Cell viability assays of second generation PROTACs in HNSCC cell lines. Cells were treated for 72 h with Wee1i, AZD1775, CRBN-recruiter, MA163, and VHL-recruiter, MA199. Cell viability assays were normalised with vehicle control, DMSO. Plots are presented as mean ± SD of n = 4 biological repeats.

Sensitivity to both PROTACs was seen across all six cell lines tested and sensitivity to AZD1775 was seen in five cell lines. The overall viability of UM-SCC-74A (p53-WT) does decrease with PROTAC treatment more than with AZD1775 treatment, suggesting a proportion of the population displays resistance to AZD1775. However, there are limitations to the MTS technique, therefore other cell viability assays should be performed in future work to confirm or deny this observation. The lowest EC50 for MA163 was seen in UM-SCC-81B (p53-mutant) at 113 nM (Table 3.2). MA199 was equally potent in UM-SCC-6 (p53-WT), A-253 (p53-null) and FaDu (p53-mutant) at ~ 100 nM. For AZD1775, the lowest EC50 was 46 nM in UM-SCC-81B (p53-mutant). In most cases, MA163 and MA199 PROTACs were at least an order of magnitude more potent than the first-generation recruiters tested.

Table 3.2. Table of EC50 values of cell viability assays (MTS) in HNSCC cell lines for second generation PROTACs. UM-SCC-12 and UM-SCC-81B were treated with AZD1775 and MA163. UM-SCC-6 (p53-WT), UM-SCC-74A, A-253 and FaDu were treated with AZD1775, MA163 and MA199. All treatments were 72 h (n = 4) and dose response curves for these values can be seen in Figure 3.15.

Treatment	EC50 (µM) ± SD					
	UM-SCC-6	UM-SCC-74A	A-253	UM-SCC-12	FaDu	UM-SCC-81B
AZD1775	0.085 ± 0.044	0.082 ± 0.060	0.131 ± 0.049	0.097 ± 0.0070	0.109 ± 0.027	0.046 ± 0.026
MA163	0.155 ± 0.040	0.234 ± 0.058	0.166 ± 0.015	0.630 ± 0.146	0.395 ± 0.154	0.113 ± 0.043
MA199	0.116 ± 0.028	0.055 ± 0.012	0.093 ± 0.0040	-	0.102 ± 0.0044	-

The EC50 values seen in Table 3.2 allows us to select the appropriate dose of the Wee1-targeting compounds to use for future treatments. Cell viability assays of the chemotherapeutic treatments were performed in order to select the appropriate dose of these compounds in Chapter 4.

3.3.5 Discussion

Wee1 PROTACs can successfully degrade Wee1 and reduce levels of its product, pCDK1 (Tyr15), in HNSCC cell lines (Figures 3.3, 3.9 and 3.10). MA048 and MA055 PROTACs showed successful degradation of Wee1 from 20 µM to 1 µM for the VHL-recruiter (MA055) and the CRBN-recruiter (MA048) showed even greater potency with sustained degradation of Wee1 to 100 nM (Figure 3.3) Both PROTACs exhibited the same effectiveness at reducing pCDK1 (Tyr15) levels with an increase in pCDK1 at 1 µM PROTAC treatment and comparable levels of pCDK1 in 100 nM PROTAC treatment compared to DMSO when degradation is absent. The CRBN-recruiters (MA048 and MA163) showed that they could more completely degrade Wee1 compared to VHL-recruiters (MA055 and MA199) in HNSCC cell lines. Furthermore,

MA163 degrades Wee1 faster than MA199, which corroborates previous lab data that CRBN-recruiters are usually faster degraders than VHL-recruiters. MA163 and MA199 PROTACs showed enhanced potency compared to the first-generation PROTACs (Figures 3.9 and 3.10). Generally, Wee1 degradation was sustained until 30 nM in most cases when using the CRBN-recruiter (MA163) and 10 nM when using the VHL-recruiter (MA199). Furthermore, pCDK1 (Tyr15) levels remained absent until 300 nM, with control levels appearing by 100 nM. Therefore, despite enhanced potency we still see a similar pattern of return of pCDK1 (Tyr15) levels. The first-generation Wee1 PROTACs seem to specifically target Wee1 as the negative controls for these compounds did not exhibit Wee1 degradation (Figure 3.4). MA163 can degrade Wee1 within 0.5 h and MA199 shows some degradation by 2 h (Figure 3.12). This allows us to consider how long pre-treatment with PROTACs should be before adding other genotoxic agents to compare inhibition versus degradation in Chapter 4.

Ternary complex formation for both first and second generation PROTACs was inhibited in the competition assays, with the inhibitors being able to completely block the degradation of Wee1 by MA048 and MA055 and partially block the degradation of Wee1 in the cases of MA163 and MA199 (Figures 3.7 and 3.13). Although the ratio of inhibitor to PROTAC was much higher for MA163 and MA199 compared to the former compounds, these second-generation compounds are much more potent and so may form ternary complexes more effectively than MA048 and MA055, leading to only partial inhibition. These findings confirm target engagement of the PROTACs to the E3 ligases.

AZD1775 has several off-target effects, for example it inhibits PLK1 (Wright et al., 2017; Zhu et al., 2017). However, some studies have shown that, at nanomolar concentrations,

AZD1775 only inhibits Wee1 and not PLK1 (Serpico et al., 2019). Previous work in other cell lines (Aublette et al., 2022; Li et al., 2020) showed enhanced selectivity of the PROTACs, in that they only targeted and degraded Wee1 out of a panel of kinases, however, future work should investigate that the PROTACs remain selective in HNSCC cell lines. For example, treatments with AZD1775, Wee1 PROTACs and BI-6727 (PLK1i) to produce lysates and then Western blotting for Cdc25C (Ser198) could highlight if the PLK1-dependent phosphorylation of Cdc25C is inhibited by the PROTACs.

Interestingly, UM-SCC-6 (p53-WT) and UM-SCC-74A (p53-WT) have lower expression levels of VHL in comparison to A-253 (p53-null) and FaDu (p53-mutant), therefore we can assume that the absolute levels of E3 ligase is not important for the PROTAC to function: MA055 exhibits the similar degradation profiles in UM-SCC-74A (p53-WT) and A-253 (p53-null) cell lines, whereas MA199 shows the most sustained Wee1 degradation in UM-SCC-74A (p53-WT). Perhaps the stereochemistry of the ternary complex is more important for effective PROTAC-dependent degradation, rather than expression of E3 ligase. How the levels of E3 ligase effect PROTAC potency will be further investigated in Chapter 6.

In order to use PROTACs to improve treatment modalities, the sustained degradation of Wee1 after PROTAC removal should be considered for how often PROTAC doses are administered. Furthermore, the effect of linker length on cell penetration and sustained degradation needs to be understood to determine the trend between linker length and return of normal Wee1 levels when considering future methods of drug delivery. A limitation of using MA048 versus TH012 in the Wee1 recovery experiments is that they display different potencies, therefore it may not be a direct comparison, as the initial amount of degradation induced by each PROTAC was different (Figure 3.6). PROTACs with

similar potencies but different linker lengths or designs should be compared to exclude other variables.

As monotherapy treatments, MA048 and MA055 PROTACs exhibit EC50 values of around 1–4 µM, whereas MA163 and MA199 PROTACs exhibit values of around 50–550 nM (Figures 3.14 and 3.15). This approximately 2 – 20-fold improvement further confirms the enhanced potency of the second generation PROTACs. From this data, the second generation PROTACs, MA163 and MA199, will be used to investigate combination treatments and a dose of 300 nM will be selected to perform these treatments. This is higher than the EC50 values (~100 nM) in the cell lines that will be tested (UM-SCC-6 (p53-WT), UM-SCC-74A (p53-WT), A-253 (p53-null) and FaDu (p53-mutant)), however, this is a concentration where a reduction of pCDK1 (Tyr15) levels is observed. At 100 nM, normal pCDK1 (Tyr15) levels are present in most cases from the Western blots, therefore a treatment dose that has both degraded Wee1 and supressed pCDK1 (Tyr15) would be selected.

The cytotoxicity of Wee1-targeting compounds alone and as a combinatorial strategy with ionizing radiation and chemotherapies will be explored in Chapter 4.

4 Evaluating the cytotoxicity of Wee1 PROTACs in HNSCC with varying p53 status

4.1 Introduction

4.1.1 Cytotoxicity of Wee1 inhibitor, AZD1775, in HNSCC

The advantages of Wee1 as a target for cancer therapy has been discussed in section 1.3.4 of the introduction. Here we will focus on a brief history of how Wee1 inhibition has been tested for efficacy against head and neck cancers in preclinical and clinical studies.

The first publication to report the use of AZD1775 against head and neck cancer demonstrated that the Wee1i sensitized p53-mutant HNSCC cells to cisplatin by bypassing the cisplatin-induced G2/M arrest and causing a senescence-like phenotype (Osman et al., 2015). In October 2015, AZD1775 entered a phase I single agent study in patients with solid tumours (Do et al., 2015). It found that one head and neck patient carrying BRCA mutations had a partial response to AZD1775 treatment. With the knowledge that AZD1775 seemed to work well in HR defective tumours, groups started to combine AZD1775 with other inhibitors to induce more DNA damage. For example, the combination of AZD1775 with Vorinostat, a histone deacetylase (HDAC) inhibitor, caused enhanced replication stress and inhibition of tumour growth in cells with p53 mutations (Tanaka et al., 2015). Furthermore, targeting of Wee1 and Aurora Kinase A, a kinase involved in spindle assembly, enforced mitotic catastrophe in p53-mutant cells and combined inhibition of Wee1 and Rad51 radiosensitized HPV-positive and negative tumours (Lee et al., 2019; Lindemann et al., 2021).

Due to the success of AZD1775's anti-proliferative effects in combination with other genotoxic treatments, AZD1775 is currently in Phase I clinical trials to establish it as a potential treatment of head and neck cancers in combination with cisplatin and radiotherapy. The trial is called WISTERIA and recruitment ended for this trial in 2019. This dose escalation trial is using AZD1775 before surgery with cisplatin or AZD1775 with cisplatin and radiotherapy after surgery. The study's main aims are to understand the optimal and highest safe dose of AZD1775 that can be administered pre- and post-operatively with the above mentioned combinations and potential toxicities of AZD1775 (Kong et al., 2020).

AZD1775 has been demonstrated to be effective from both basic science and clinical literature, however targeting Wee1 more selectively with PROTACs could be more advantageous over small molecule inhibition with AZD1775.

4.2 Aims and Objectives

In this chapter, the cytotoxicity of Wee1-degrading PROTACs alone will be compared to their cytotoxicity in combination with ionizing radiation or chemotherapies, as well as the mode of death that these drugs cause. This will be assessed via a number of aims:

1. Evaluate if Wee1 PROTACs and AZD1775 cause a loss of cell viability over time and determine the appropriate dose of the chemotherapy drugs to use in combination with the PROTACs

2. Assess if PROTAC treatment enhances radiation- or chemotherapy-induced cell death, comparing this to AZD1775 treatment and determining the effects of p53 status.

3. Investigate if the PROTACs induce apoptosis and compare this to AZD1775 treatment.

4.3 Results and discussion

4.3.1 Effect of treatment time of monotherapy PROTACs on cell viability

To calculate EC50 values of drugs, MTS assays are usually performed between 24 – 72 h after drug treatment. Previously in our lab (Aublette et al., 2022) and in initial testing of the compounds in the HNSCC cell lines (Section 3.3.4), the MTS reagent was added 72 h after drug treatment however, we wanted to investigate if the drug reached its maximal effect in reducing cell viability at an earlier time point. Cell viability (MTS) assays were performed in UM-SCC-6 (p53-WT), A-253 (p53-null) and FaDu (p53-mutant) cells treated with varying doses of AZD1775 or PROTAC from 20 μM to 0.1 nM for either 24 h, 48 h or 72 h. Data were normalised to the vehicle control, DMSO, and plotted as dose response curves seen in Figures 4.1 – 4.2.
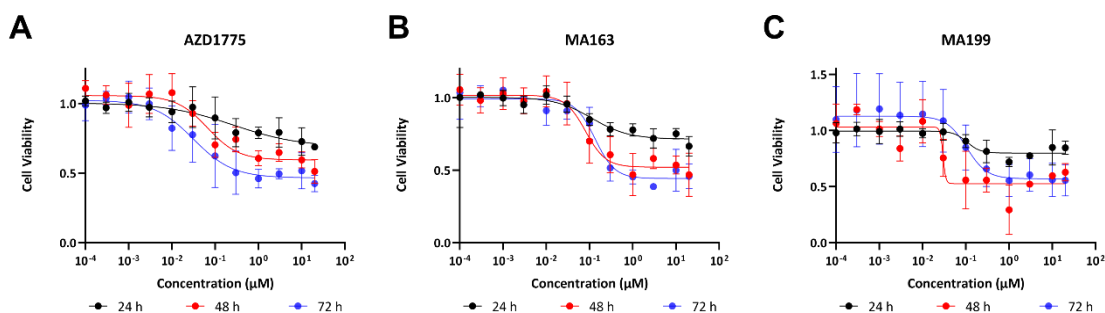
Figure 4.1 Time course cell viability assays showing the effect of AZD1775, MA163 and MA199 on p53-proficient cells. Cells were treated for 24 h, 48 h or 72 h with (A) Wee1i, AZD1775, (B) CRBN-recruiter, MA163, and (C) VHL-recruiter, MA199. Cell viability assays were normalised with vehicle control, DMSO. Plots are presented as mean ± SD of n = 2 - 4 biological repeats (GraphPad Prism).

Figure 4.1 shows the 24 h, 48 h and 72 h dose response curves of the drugs in p53-proficient cells, UM-SCC-6 (p53-WT). Across all treatments, the longer that the drug treatment is left on the cells, the larger the decrease in cell viability. The PROTACs are not very potent at 24 h, with the lowest cell viability being 67% at 20 µM for MA163 and 72% at 1 µM for MA199. AZD1775 and MA163 behave in a similar manner, whereby the longer the treatment is left on, the greater the reduction in cell viability (Figure 4.1A – B). In contrast, MA199 seems to exert its maximal effect on reduction of cell viability by 48 h (cell viability plateaus at 53%) as the 72 h treatment (cell viability plateaus at 56%) does not cause any more reduction in cell viability (Figure 4.1C). The EC50 values at 24 h for AZD1775 and MA163 are the highest at 263 nM and 242 nM, respectively (Table 4.1). At 48 h these decrease to 66 nM and 81 nM and by 72 h the value for AZD1775 decreases to 33 nM and increases for MA163 to 134 nM. The proportional increase between the 48 h and 72 h EC50 values for MA199 (30 nM and 104 nM for 48 h and 72 h, respectively) is much larger than that of MA163. To conclude, only AZD1775 displays a progressive increase in loss of cell viability the longer the treatment time. The PROTACs reach the maximum loss of cell viability sooner.

Table 4.1 Table of EC50 values of time course cell viability assays (MTS) in UM-SCC-6 cells. UM-SCC-6 (p53-WT) were treated with AZD1775, MA163 and MA199 for 24 h, 48 h or 72 h (n = 2 - 4) and dose response curves for these values can be seen in Figure 4.1. *Experiments with only n = 2.

Treatment	EC50 (µM) ± SD		
	AZD1775	**MA163**	**MA199**
24 h	0.263 ± 0.121*	0.242 ± 0.112*	0.107 ± 0.054*
48 h	0.066 ± 0.020	0.081 ± 0.088	0.030 ± 0.072
72 h	0.031 ± 0.090	0.134 ± 0.065	0.104 ± 0.058

To investigate if the behaviour of the compounds had any dependency on p53, we investigated the time course in A-253 (p53-null) and FaDu (p53-mutant) cells (Figure 4.2).
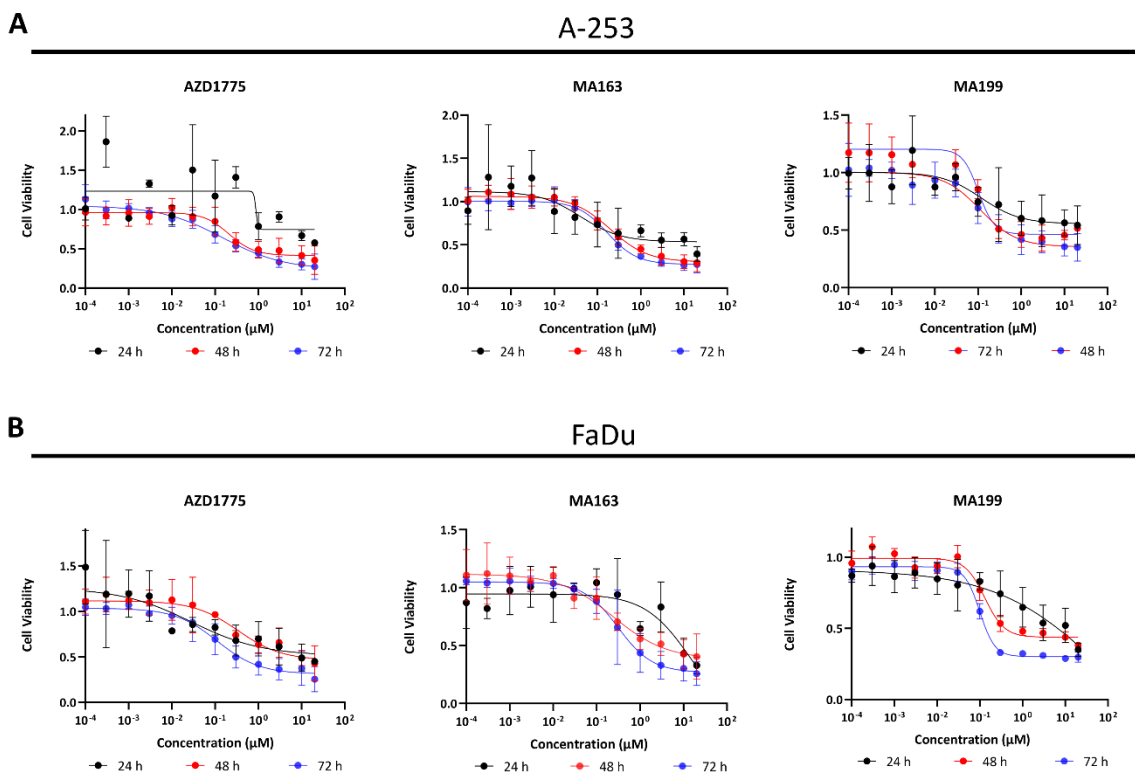
Figure 4.2 Time course cell viability assays showing the effect of AZD1775, MA163 and MA199 on p53-deficient cells. (A) p53-null cells, A-253 and (B) p53-mutant cells, FaDu, were treated for 24 h, 48 h or 72 h with Wee1i, AZD1775, CRBN-recruiter, MA163, and VHL-recruiter, MA199. Cell viability assays were normalised with vehicle control, DMSO. Plots are presented as mean ± SD of n = 2 - 4 biological repeats (GraphPad Prism).

In p53- deficient cells, A-253 and FaDu, all treatments have a similar potency at the 72 h time point (seen in Table 3.2, section 3.3.4.2). Similarly, to UM-SCC-6 (p53-WT) cells (Figure 4.1), the general trend is that the longer the treatment time, the larger the reduction in cell viability. The EC50 values are the smallest for MA199 in A-253 (p53-null) and FaDu (p53-mutant). The EC50 values were of a similar order of magnitude for all three cell lines tested which suggests that p53 status may not have much of an impact on overall cytotoxicity of these compounds. However, to confirm this hypothesis, p53 activity should be restored in A-253 (p53-null) or FaDu (p53-mutant) and the EC50 values of the compounds can be compared. The EC50 values at 24 h for FaDu (p53-mutant) are relatively high for MA163 and

MA199 in comparison to A-253 (p53-null). This is likely due to the variable data collected at this time point, leading to difficulties plotting the dose response curve for this data. Table 4.2 shows the EC50 values for dose response curves in Figure 4.2.

Table 4.2 Table of EC50 values of time course cell viability assays (MTS) in A-253 and FaDu cells. A-253 and FaDu were treated with AZD1775, MA163 and MA199 for 24 h, 48 h or 72 h (n = 2 - 4) and dose response curves for these values can be seen in Figure 4.2. *Experiments with only n = 2. †Experiment where two repeats produced unstable EC50 values when individually plotted.

Treatment	EC50 (µM) ± SD					
	A-253			FaDu		
	AZD1775	MA163	MA199	AZD1775	MA163	MA199
24 h	0.878 ± 0.727*	0.041 ± 0.474	0.120 ± 0.400	0.028 ± 0.066	15.0 ± 16.5	61.0 ± 3.07†
48 h	0.209 ± 0.026	0.197 ± 0.060	0.112 ± 0.101	0.337 ± 0.305	0.241 ± 0.203	0.130 ± 0.042
72 h	0.149 ± 0.086	0.168 ± 0.037	0.102 ± 0.0022	0.112 ± 0.171	0.308 ± 0.304	0.100 ± 0.009

4.3.2 Effect of chemotherapeutics alone on cell viability

In order to select an appropriate dose for future combination treatments of chemotherapeutics and PROTACs, monotherapy cell viability assays were performed in UM-SCC-6, UM-SCC-74A, A-253, UM-SCC-12, FaDu and UM-SCC-81B cells with cisplatin and bleomycin. Previous studies had used cisplatin at a range of doses between 0.5 µM to 50 µM in head and neck cell lines that we were using, therefore we decided to perform the MTS assay with the same concentration ranges that we had tested for the PROTACs and AZD1775 (Li et al., 2022a; Ziemann et al., 2015). Cells were seeded and left to adhere

overnight before treatment with varying doses of cisplatin from 20 μM to 1 nM or varying

doses of bleomycin from 500 μg/mL to 9.6 ng/mL for 72 h. The plates were analysed with

MTS reagent and dose response curves were produced (Figure 4.3 – 4.4).
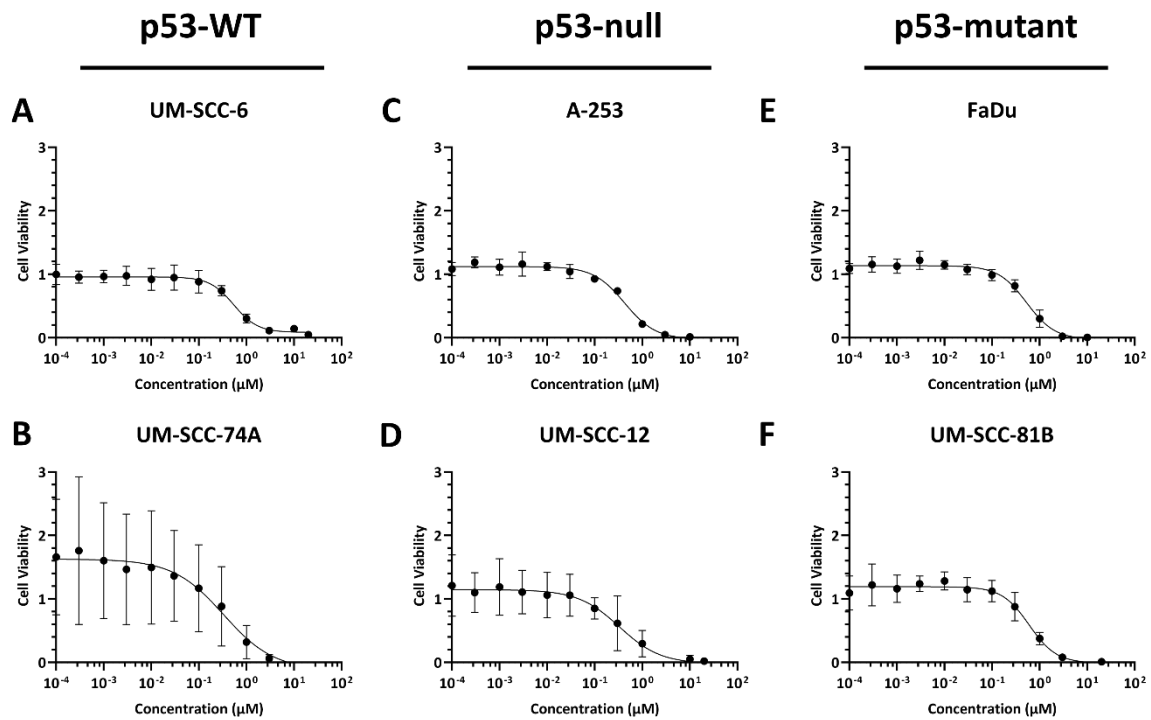
Figure 4.3 Dose response of cisplatin in HNSCC cell lines. Cells were treated for 72 h with cisplatin. Cell viability assays were normalised with vehicle control, DMSO. Plots are presented as mean ± SD of n = 3 biological repeats (GraphPad Prism).

Similar sensitivity to cisplatin was seen across all six cell lines. In UM-SCC-6 (p53-WT) cells,

we saw ~10% viability remaining at the higher doses, whereas in the other five cell lines we

saw 0% cell viability. UM-SCC-6 (p53-WT), A-253 (p53-null), UM-SCC-12 (p53-null) and FaDu

(p53-mutant) cells all exhibit EC50 values between 435 nM and 592 nM (Table 4.3). UM-

SCC-74A (p53-WT) and A-253 (p53-null) exhibit more sensitivity to cisplatin with EC50 values

of 321 and 435 nM, respectively.

Table 4.3. Table of EC50 values of cell viability assays (MTS) in HNSCC cell lines for cisplatin. UM-SCC-6, UM-SCC-74A, A-253, UM-SCC-12, FaDu and UM-SCC-81B were treated with cisplatin for 72 h (n = 3) and dose response curves for these values can be seen in Figure 4.3.

Treatment	EC50 (µM) ± SD					
	UM-SCC-6	UM-SCC-74A	A-253	UM-SCC-12	FaDu	UM-SCC-81B
Cisplatin	0.542 ± 0.029	0.321 ± 0.035	0.435 ± 0.049	0.557 ± 0.208	0.564 ± 0.103	0.592 ± 0.089

Bleomycin showed much more variability between repeats at inhibiting cell proliferation compared to cisplatin treatment. This resulted in some cell lines not exhibiting typical dose-response curves (Figure 4.4).
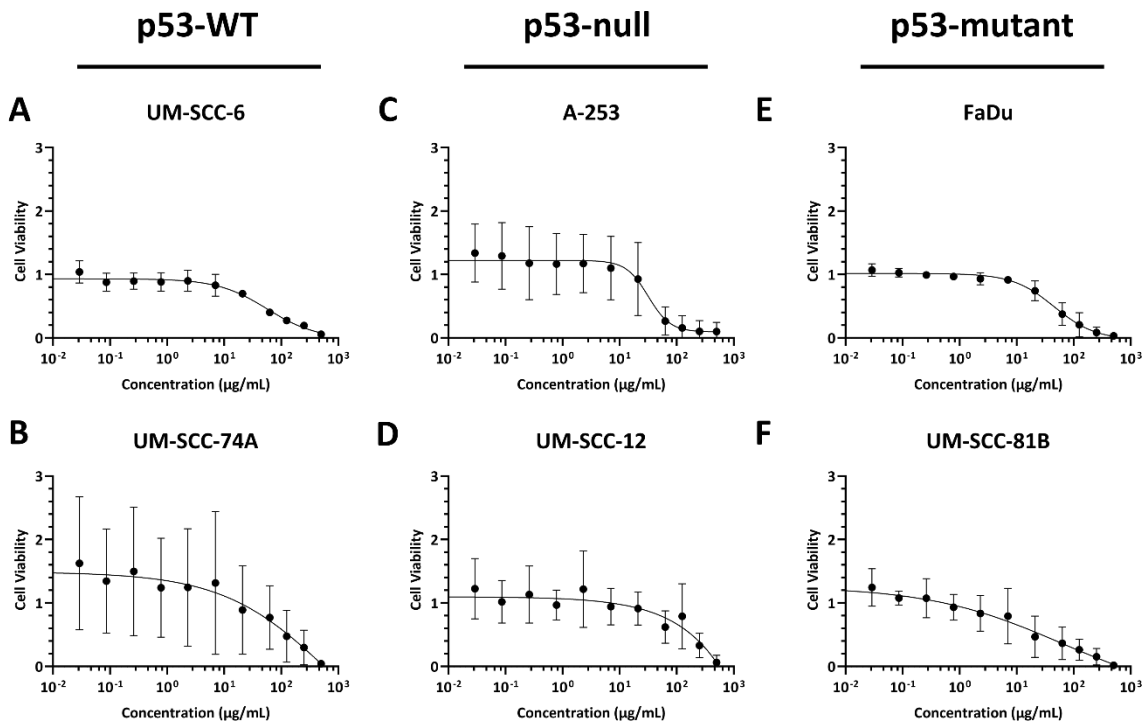
Figure 4.4 Dose response of bleomycin in HNSCC cell lines. Cells were treated for 72 h with bleomycin. Cell viability assays were normalised with vehicle control, DMSO. Plots are presented as mean ± SD of n = 3 biological repeats (GraphPad Prism).

Generally, p53-deficient cells (A-253, UM-SCC-81B, FaDu) were more sensitive to bleomycin treatment compared to p53-proficient cells (UM-SCC-6, UM-SCC-74A). EC50 values were roughly 2 – 8 times higher in p53-proficient cells (105.7 µg/mL and 244.9 µg/mL in UM-SCC-6 and UM-SCC-74A respectively) than in p53-deficient cell types (30.3 µg/mL, 62.5 µg/mL and 59.3 µg/mL in A-253, FaDu and UM-SCC-81B respectively) (Table 4.4). UM-SCC-12 (p53-null) did not fit this pattern and exhibited the highest EC50 value, however this cell line also had the largest standard deviation.

Table 4.4. Table of EC50 values of cell viability assays (MTS) in HNSCC cell lines for bleomycin. UM-SCC-6, UM-SCC-74A, A-253, UM-SCC-12, FaDu and UM-SCC-81B were treated with bleomycin for 72 h (n = 3) and dose response curves for these values can be seen in Figure 4.4.

Treatment	EC50 (µg/mL) ± SD					
	UM-SCC-6	UM-SCC-74A	A-253	UM-SCC-12	FaDu	UM-SCC-81B
Bleomycin	106 ± 29.4	245 ± 96.5	30.3 ± 4.57	392 ± 199	62.5 ± 19.0	59.3 ± 44.0

Cisplatin exhibited EC50 values between 300–600 nM in UM-SCC-6 (p53-WT), UM-SCC-74A (p53-WT), A-253 (p53-null) and FaDu (p53-mutant) cell lines, therefore 300 nM was the selected dose for combination treatments to ensure that the toxicity that we see is not a result of cisplatin treatment alone, but due to the combination with Wee1-targeting compounds. Due to the variability in the bleomycin data, EC50 values for the above-mentioned cell lines ranged from 30 µg/mL to 392 µg/mL. Clonogenic assays with treatments of 10 µg/mL, 50 µg/mL and 100 µg/mL were performed to investigate the cytotoxicity of a 24 h treatment of bleomycin alone. This showed that even at 10 µg/mL there was some cytotoxicity, therefore this dose was selected.

4.3.3 Assessment of cytotoxicity of Wee1-targeting compounds alone and as a combinatorial treatment in p53-proficient cells

4.3.3.1 Effect of mono and combination treatments on clonogenicity

Colony survival assays were performed in UM-SCC-6 (p53-WT) cells to investigate if Wee1 PROTAC treatment in combination with ionizing radiation or chemotherapy decreased cell survival more than the genotoxic treatments alone in a p53-proficient cell type. We determined that a dose of 300 nM would be appropriate for AZD1775 and the PROTACs in

all three cell lines, UM-SCC-6 (p53-WT), A-253 (p53-null) and FaDu (p53-mutant) in Chapter 3 and in section 4.3.1. Furthermore, monotherapy treatments of cisplatin determined a dose of 300 nM was optimal across all cell lines and monotherapy treatments of bleomycin gave EC50 values of 30 µg/mL to 110 µg/mL however, these doses killed all cells in preliminary single treatment clonogenics. Therefore, a dose of 10 µg/mL was tested and selected as some cells survived in preliminary clonogenics and this was below the EC50 values in each cell line. Radiation doses selected were 1 Gy, 2 Gy and 4 Gy based on previous doses that had worked for combination clonogenic assays in Professor Parsons' laboratory.

To investigate combination treatments, AZD1775 and PROTACs were added to cells 2 h prior to either irradiation or addition of the chemotherapy drugs to ensure Wee1 was sufficiently degraded or inhibited. For radiation combination treatments, after irradiation the media was replaced with drug-free media, whereas for the chemotherapy combination all treatments were left for a total of 24 h. From these experiments, we were able to collect data on the effect on clonogenicity of AZD1775 and the PROTACs when they were added for 2 h alone versus 24 h alone.

In UM-SCC-6 (p53-WT) cells, at 2 h, only MA199 was significantly better at reducing cell survival alone in comparison to DMSO (Figure 4.5). MA199 was not significantly better than AZD1775 or MA163 (Table 4.5). At 24 h, AZD1775, MA163 and MA199 were significantly better at reducing colony formation in comparison to DMSO. All of the treatments were as potent as each other at 24 h. Therefore, targeting Wee1 alone appears to be cytotoxic to p53-proficient head and neck cancer cells and degrading Wee1 shows no added benefits in comparison to inhibiting it when considering monotherapy.
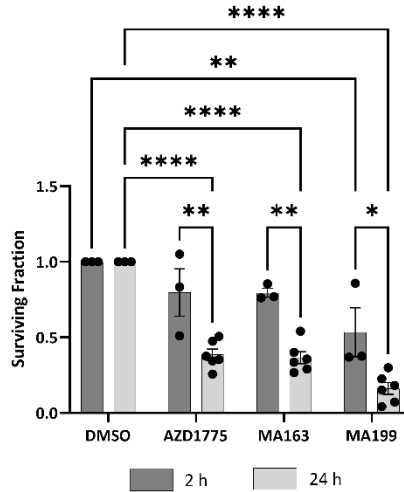
Figure 4.5 Effect of 2 h versus 24 h treatment time with Wee1-targeting treatments on the clonogenicity of UM-SCC-6. Bar graph showing surviving fraction of UM-SCC-6 cells that have been allowed to grow for 6 -10 days post 2h or 24 h treatment with monotherapies, AZD1775, MA163 and MA199. Data were analysed with a one-way ANOVA and Tukey's test. All data plotted is mean ± SD of n = 3 biological repeats.

Table 4.5 Table of adjusted p-values for the monotherapy treatment comparisons at 2 h and 24 h in UM-SCC-6 cells. Colonies were fixed, stained and counted, the plating efficiencies were calculated and values were normalised to the DMSO control as 100% cell survival. Data were analysed by a two-way ANOVA and a Šidák's multiple comparisons test and bar graphs can be seen in Figure 4.5.

	DMSO 2 h	AZD1775 2 h	MA163 2 h	MA199 2 h	DMSO 24 h	AZD1775 24 h	MA163 24 h	MA199 24 h
DMSO 2 h	-	0.8887 (ns)	0.8762 (ns)	0.0069 (**)	>0.9999 (ns)	<0.0001 (****)	<0.0001 (****)	<0.0001 (****)
AZD1775 2 h	0.8887 (ns)	-	>0.9999 (ns)	0.4849 (ns)	0.8887 (ns)	0.0054 (**)	0.0031 (**)	<0.0001 (****)
MA163 2 h	0.8762 (ns)	>0.9999 (ns)	-	0.5037 (ns)	0.8762 (ns)	>0.9999 (ns)	0.0033 (**)	<0.0001 (****)
MA199 2 h	0.0069 (**)	0.4849 (ns)	0.5037 (ns)	-	0.0069 (**)	0.9780 (ns)	0.9177 (ns)	0.0159 (*)
DMSO 24 h	>0.9999 (ns)	0.8887 (ns)	0.8762 (ns)	0.0069 (**)	-	<0.0001 (****)	<0.0001 (****)	<0.0001 (****)

AZD1775 24 h	<0.0001 (****)	0.0054 (**)	>0.9999 (ns)	0.9780 (ns)	<0.0001 (****)	-	>0.9999 (ns)	0.1945 (ns)
MA163 24 h	<0.0001 (****)	0.0031 (**)	0.0033 (**)	0.9177 (ns)	<0.0001 (****)	>0.9999 (ns)	-	0.3302 (ns)
MA199 24 h	<0.0001 (****)	<0.0001 (****)	<0.0001 (****)	0.0159 (*)	<0.0001 (****)	0.1945 (ns)	0.3302 (ns)	-

Although AZD1775, MA163 and MA199 showed a reduction of colony formation alone, when using this in addition to ionizing radiation, we see no enhancement of cell death and no significance between treatments when analysing with multiple unpaired t tests with Welch correction in UM-SCC-6 (p53-WT) cells (Figure 4.6).
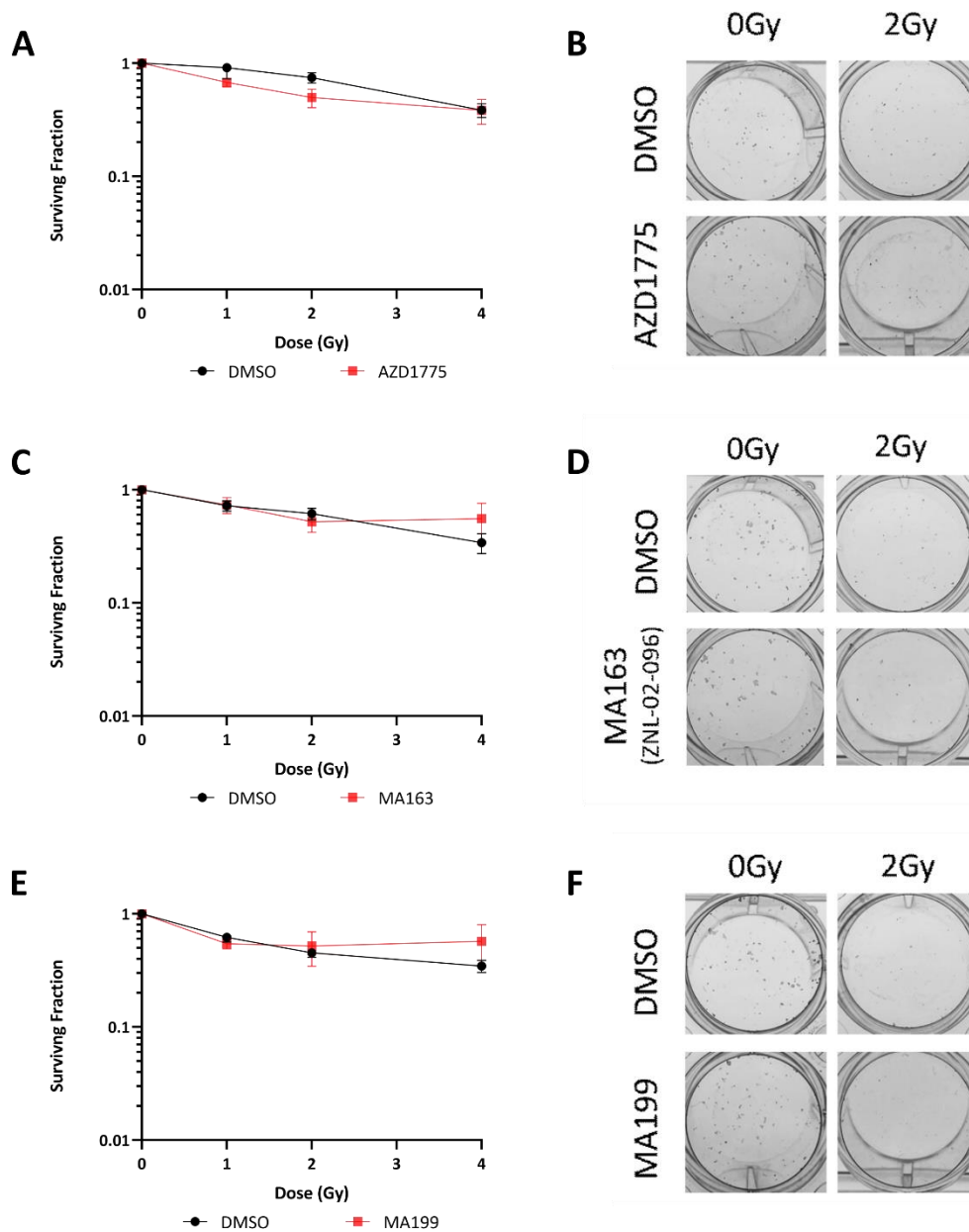
Figure 4.6 Investigation of Wee1-targeting treatments in combination with radiation on clonogenicity of p53-proficient cells, UM-SCC-6. Cells were pre-treated with Wee1-targeting drugs for 2 h prior to irradiation, supplemented with drug-free media post-IR and allowed to grow for 6 – 10 days. (A & B) Survival curve and representative images for AZD1775-treated cells, (C & D) Survival curve and representative images for MA163-treated cells and (E & F) Survival curve and representative images for MA199-treated cells. All data plotted is mean ± SD of n = 3 biological repeats.

Clonogenic survival of Wee1-targeting treatment cells in combination with

chemotherapeutic, cisplatin and bleomycin, in UM-SCC-6 (Figure 4.7).

111
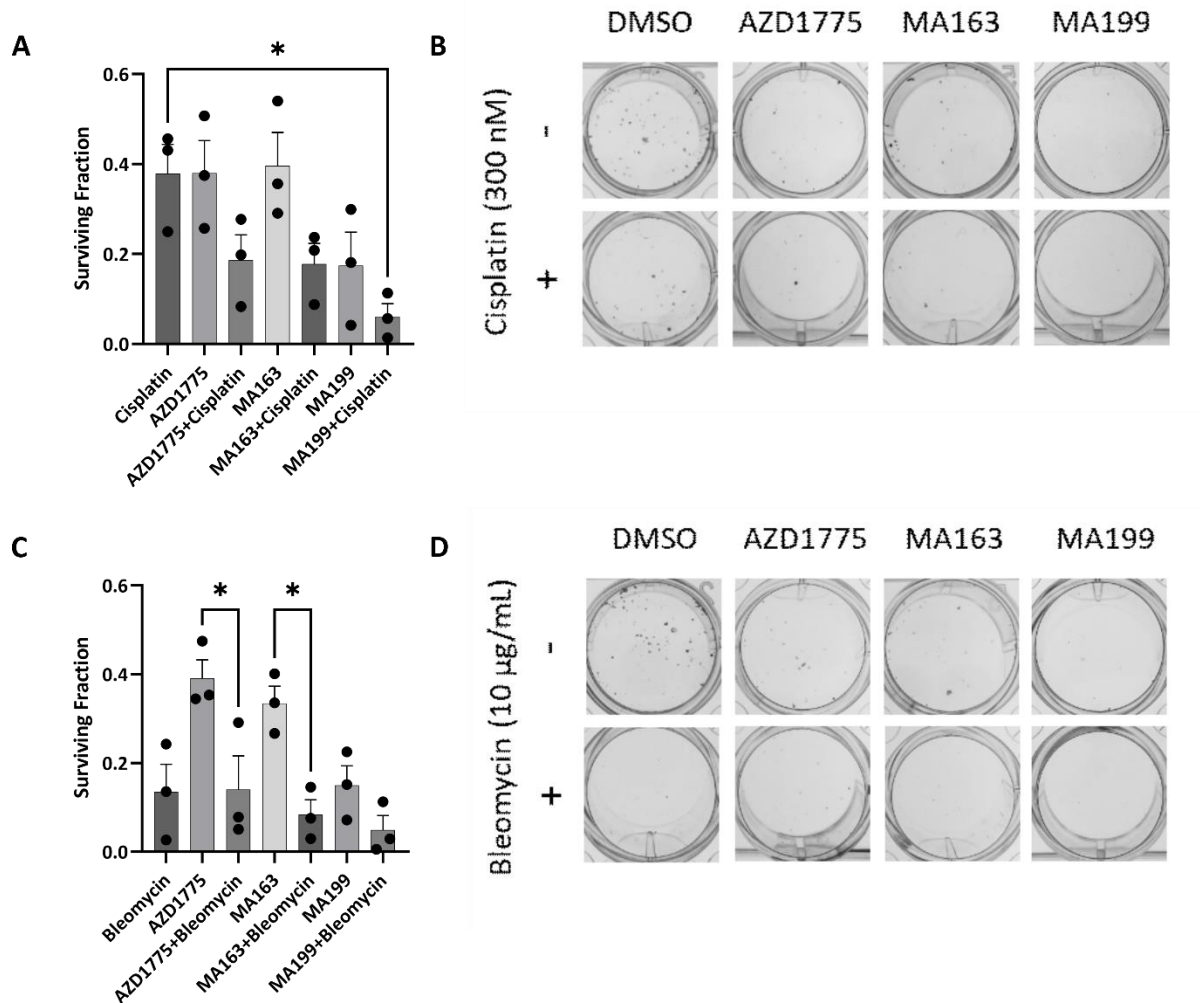
Figure 4.7 Investigation of Wee1-targeting treatments in combination with cisplatin and bleomycin on clonogenicity of p53-proficient cells, UM-SCC-6. Cells were treated with Wee1-targeting compounds and cisplatin or bleomycin for 24 h before replacing with drug-free media and allowed to grow for 6 – 10 days. (A & B) Survival curve and representative images for AZD1775-treated cells, (C & D) Survival curve and representative images for MA163-treated cells and (E & F) Survival curve and representative images for MA199-treated cells. All data plotted is mean ± SD of n = 3 biological repeats.

Cisplatin treatment resulted in a mean cell survival of 38% however, AZD1775 and cisplatin treatment resulted in a mean cell survival of 19%, MA163 and cisplatin caused only 18% cell survival and MA199 and cisplatin caused only 6% of cells to survive. Only MA199 significantly enhanced cisplatin-induced cell death (p = 0.0332) however, AZD1775 and MA163 (p = 0.3495 and p = 0.3062 for AZD1775 and MA163, respectively) also enhanced

cisplatin-induced cell death (Figure 4.7). MA163 and MA199 did cause a slight reduction to the surviving fraction compared to bleomycin alone, but as bleomycin is so toxic to cells alone, the combination of bleomycin with Wee1-targeting compound was significant compared to the Wee1-targeting compound alone. However, the combination was not significant compared to bleomycin alone, therefore none of the treatments significantly enhanced bleomycin-induced cell death (Figure 4.7).

As these experiments confirmed that we saw enhanced cisplatin-induced cell death when using cisplatin in combination with the Wee1-targeting compounds in UM-SCC-6 (p53-WT), we wanted to investigate if we were seeing an additive effect in a dose response curve.

4.3.3.2 Impact of chemotherapeutics, cisplatin and bleomycin, with Wee1-targeting treatments on cell viability

After observing that Wee1 degradation via a VHL-recruiter did significantly enhance cisplatin-induced cell death (Figure 4.7), MTS assays that measure metabolic activity of cells treated with varying doses of AZD1775, MA163 and MA199 were performed with a fixed dose co-treatment of cisplatin (300 nM) or bleomycin (10 µg/mL) to investigate if the combination of the drugs resulted in a synergistic or additive effect (Figure 4.8).
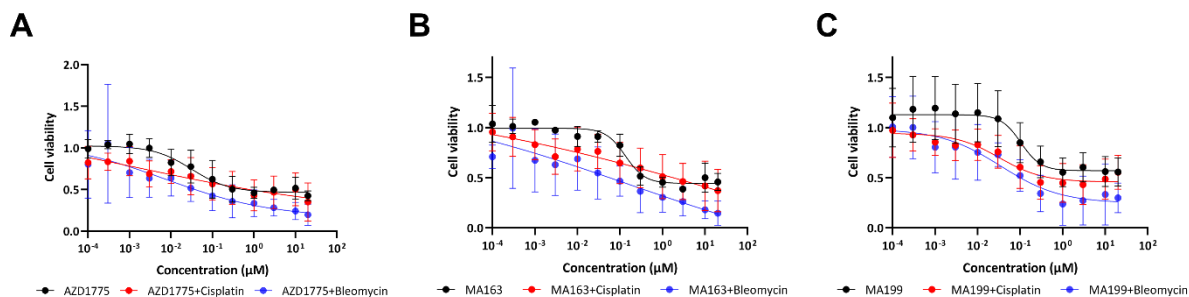
Figure 4.8 Reduction of cell viability of UM-SCC-6 cells by Wee1-targeting compounds alone and in combination with cisplatin or bleomycin. Cell viability assays of UM-SCC-6 cells treated with (A) AZD1775, AZD1775 and cisplatin or AZD1775 and bleomycin, (B) MA163, MA163 and cisplatin or MA163 and bleomycin and (C) MA199, MA199 and cisplatin or MA199 and bleomycin for 72 h. All treatments were normalised with DMSO. Data are presented as mean ± SD of n = 4 biological repeats (GraphPad Prism).

At 300 nM cisplatin treatment in UM-SCC-6 (p53-WT) cells, the mean cell viability was 74% (Figure 4.3A) and at 300 nM AZD1775 treatment, the mean cell viability was 50% (Figure 3.14; section 3.3.4.2). The mean cell viability when these compounds were used together was 52% (Figure 4.8A). At the higher doses of AZD1775, there was no synergy or additive effect from using the drugs in combination, however, at the smaller doses used (<100 nM) we did observe a small additive effect. This is the same as can be seen for MA163 (Figure 4.8B). However, we discovered an additive effect of MA199 with cisplatin at all concentrations (Figure 4.8C). When comparing between the compounds at 300nM, MA199 reduces cell viability the most at 72 h (45%), therefore it makes sense that this is the most significant combination at enhancing cisplatin-induced cell death. AZD1775 and cisplatin has a 13-fold smaller EC50 compared to AZD1775 alone, MA163 and cisplatin dose response curve has a right-shift, therefore an increase in EC50 and MA199 and cisplatin has a 3.3-fold smaller EC50 compared to MA199 alone (Table 4.6). UM-SCC-6 (p53-WT) cells are more sensitive to bleomycin than cisplatin at the doses used, therefore the larger additive effect

observed of the bleomycin combination compared to the cisplatin combination is due to their sensitivity to bleomycin, rather than the compounds working better together.

Table 4.6 Table of EC50 values of cell viability assays (MTS) in UM-SCC-6 cells for chemotherapy combination treatments. UM-SCC-6 were treated with Wee1-targeting compounds alone and in combination with cisplatin or bleomycin for 72 h (n = 4) and the dose response curves that correspond with these values can be seen in Figure 4.8.

Treatment	EC50 (µM) ± SD		
	Alone	+ 300 nM Cisplatin	+ 10 µg/mL Bleomycin
AZD1775	0.03 ± 0.09	0.0023 ± 0.04	0.0075 ± 0.0085
MA163	0.13 ± 0.07	107 ± 0.07	0.16 ± 0.05
MA199	0.10 ± 0.06	0.03 ± 0.06	0.04 ± 0.03

4.3.3.3 Effect of mono and combination treatments on mode of death

In order to investigate if the PROTACs cause differing modes of death compared to inhibition of Wee1 via AZD1775, apoptosis detection via Annexin V staining by flow cytometry was performed in UM-SCC-6 (p53-WT) cells. Annexin V can be used to measure apoptosis as it binds to phosphatidylserine (PS) that becomes exposed on the surface of the cell as a result of the loss of plasma membrane asymmetry (van Engeland et al., 1998). Cells were treated with a DMSO control, AZD1775, MA163 or MA199 at 300 nM for 24 h before trypsinization and staining with Annexin V-FITC and PI. The first gate applied to FSC-A and SSC-A excluded debris from analysis, and compensation was performed by running a staurosporine positive control for apoptosis and an ethanol control for dead cells (Figure 4.7A).
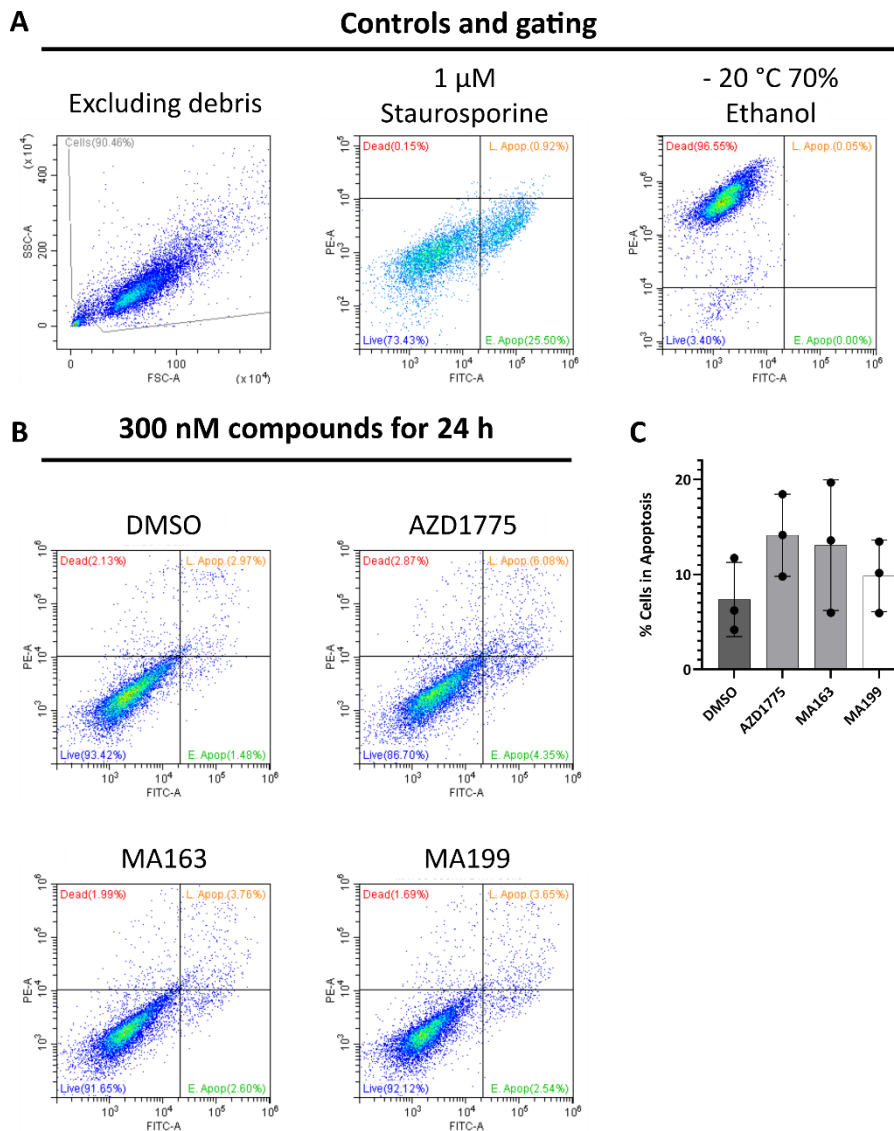
Figure 4.9 Apoptosis detection assay of AZD1775, MA163 and MA199 in UM-SCC-6. Flow cytometry of UM-SCC-6 cells stained with Propidium Iodide (PI) and Annexin V-FITC. Cells were treated with monotherapy agents for 24 h prior to producing samples. (A) Representative dot plots showing gating out of debris to only analyse cells and positive controls for apoptosis (1 µM staurosporine treatment for 24 h) (early apoptotic cells stain positively for Annexin V but negatively for PI and late stain positively for both) and dead cells (-20 °C 70% ethanol for 24 h). (B) Representative dot plots for monotherapy treatments at 300 nM for 24 h. (C) Bar graph showing mean ± SD of n = 3 biological replicates for monotherapy treatments (GraphPad Prism).

AZD1775, MA163 and MA199 all showed slight induction of apoptosis, albeit not statistically significant, in UM-SCC-6 (p53-WT) cells (Figure 4.9B – C). AZD1775 caused a two-fold

increase of annexin-V positive population at 14.1% compared to 7.4% in the DMSO control. MA163 showed a similar level of apoptotic cells at 13.1% and MA199 caused marginally less at 9.8%. This suggests that targeting Wee1 causes some p53-dependent apoptosis in HNSCC, however a longer time point to see the effect after another turn of the cell cycle may reveal if these cells could be arresting or entering a quiescent state to combat the Wee1-deficiency instead of entering apoptosis. With these data, the next step was to investigate if using the compounds in combination with irradiation would result in more or fewer apoptotic cells than the single agents and to investigate the induction of apoptosis with a different technique, western blotting of PARP cleavage. At the onset of apoptosis, initiator caspase (caspase-9) is activated and subsequently activates effector caspases, caspase-3 and caspase-7. Caspase-3 is mainly responsible for PARP cleavage to produce fragments of 89 and 24 kDa during programmed cell death, therefore it has become a useful marker for apoptosis (Boulares et al., 1999).

UM-SCC-6 (p53-WT) cells were treated with 300 nM AZD1775 and MA163 for 2 h prior to irradiation. A dose of 12 Gy was selected to cause enough stress to the cells to send them into programmed cell death as previous irradiation doses (1 Gy, 2 Gy and 4 Gy) would not have inflicted enough apoptosis to detect (J. Parsons – personal communication). Once irradiated, the treatments remained on the cells for a further 22 h prior to the production of lysates. Lysates were probed for PARP-1 (and cleaved PARP-1) and β-actin as a loading control (Figure 4.10).
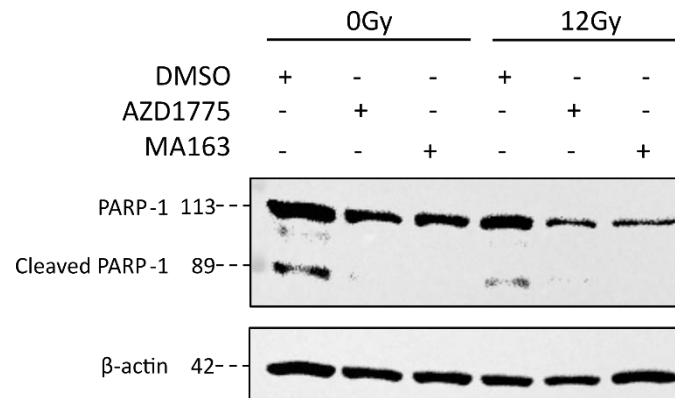
Figure 4.10 Detection of PARP cleavage in UM-SCC-6 cells by AZD1775 and MA163 treatments alone and in combination with 12 Gy irradiation. Western blot of UM-SCC-6 cells that were treated with AZD1775 or MA163 at 300 nM for 2 h prior to irradiation then treatment remained for a further 22 h post irradiation prior to the production of lysates. The membrane was probed for PARP-1, cleaved PARP-1 and β-actin as the loading control, n = 2. Quantitation of full-length PARP-1 can be found in Table 4.7.

Less full-length PARP-1 can be seen in the drug-treated cells in comparison to DMSO or IR alone, suggesting that the protein is being cleaved, however smaller fragments (such as at 50 and 24 kDa) were not observed. There was nearly a 3-fold decrease of full-length endogenous PARP-1 in AZD1775 and MA163-treated cells alone compared to DMSO in UM-SCC-6 (p53-WT) (Figure 4.10 and Table 4.7).

Table 4.7 Quantitation of full-length PARP-1 from Figure 4.8 of UM-SCC-6 cells treated with AZD1775 or MA163 alone or in addition to irradiation. Intensity of full-length PARP-1 was normalised to actin and calculated relative to DMSO. The mean ± SD was produced from n = 2 and is shown in the table below.

Treatment condition	Mean ± SD full-length PARP relative to DMSO
DMSO	1.00 ± 0.00
AZD1775	0.36 ± 0.07
MA163	0.37 ± 0.01
DMSO + 12 Gy	1.00 ± 0.11
AZD1775 + 12 Gy	0.36 ± 0.16
MA163 + 12 Gy	0.35 ± 0.27

Furthermore, a decrease was observed in the combination of Wee1 targeting treatments, only 36 % and 35 % remaining PARP-1 in AZD1775 or MA163 with 12 Gy respectively, in comparison to IR alone (Figure 4.8). This corroborates previous flow cytometry data (Figure

118

4.7) that the Wee1-targeting treatments induce more apoptosis compared to the control. Although the cleavage fragments show fainter or absent bands in these samples, the fainter full-length bands are suggestive of PARP cleavage and indicative of increased apoptosis. It is possible that proteolytic degradation of the cleavage fragments had occurred in the treated samples compared to DMSO or 12 Gy alone, as we only looked at a 24 h time point and apoptosis kinetics are complex. Future experiments should test more time points to investigate if we can see stronger cleavage fragment bands in comparison to the control or irradiation alone. After this result we wanted to perform Annexin V flow cytometry to determine if we see more induction of apoptosis in the combination of AZD1775 or MA163 with irradiation compared to the irradiated alone cells.

Cells were treated in the same manner as the western blotting lysates (Figure 4.10) prior to harvesting and staining with Annexin V-FITC and PI. Data was analysed and gated as described in Figure 4.7A. UM-SCC-6 (p53-WT) cells were most sensitive to AZD1775 and the proportion of apoptotic cells in AZD1775 single treatment and AZD1775 combination were very similar (24.9% and 23.4% for 0 Gy and 12 Gy, respectively) (Figure 4.11). The next highest induction of apoptosis was by the MA163 and 12 Gy combination treatment at 22.1%, followed by MA163 alone at 16.0%. Unfortunately, time constraints only allowed for an n = 2 of these results, therefore the standard deviation of this data is quite large and the experiment needs to be repeated to confirm if these trends that we observed are correct. Furthermore, 12 Gy IR alone should induce a large percentage of apoptosis as it is quite a high dose of ionizing radiation, therefore it is possible that when these experiments were performed, the generator of the irradiator was already broken and having issues with X-ray delivery.

A
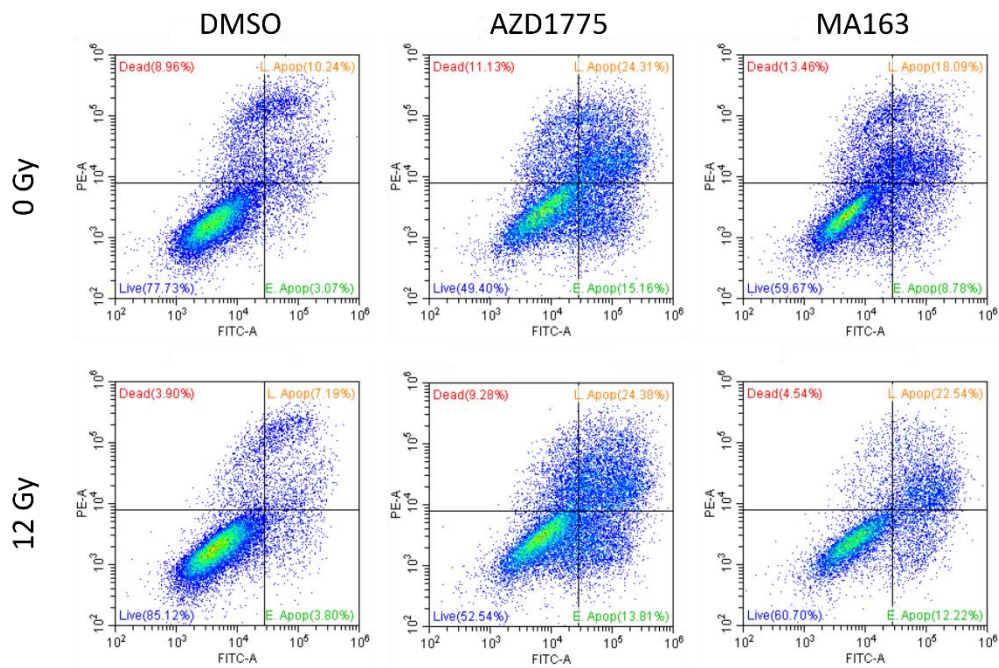
B
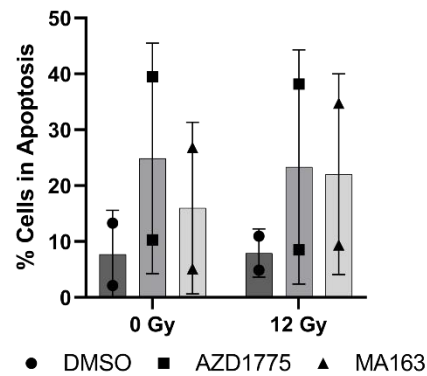
Figure 4.11 Apoptosis detection assay of AZD1775 and MA163 with 12 Gy irradiation in UM-SCC-6. Flow cytometry of UM-SCC-6 cells stained with Propidium Iodide (PI) and Annexin V-FITC. (A) Representative dot plots for DMSO, AZD1775 (300 nM) and MA163 (300 nM) for 24 h alone and with 12 Gy irradiation after initial 2 h treatment prior to staining. (B) Bar graph showing mean ± SD of n = 2 biological repeats (GraphPad Prism).

An increase of cytotoxicity to UM-SCC-6 (p53-WT) cells when using the combination of Wee1-targeting treatments with cisplatin compared to the chemotherapies alone (section 4.3.3.1) led to investigations into how these cells were dying. Western blots were performed to investigate early to mid apoptotic events, such as PARP and caspase-3 cleavage. Cells were treated with DMSO, AZD1775, MA163 or MA199 for 2 h prior to the addition of cisplatin or bleomycin. The cells were further treated for 22 h prior to the production of lysates. Lysates were probed for PARP-1 (and cleaved PARP-1), Caspase-3 (and cleaved caspase-3) and β-actin as a loading control (Figure 4.12).
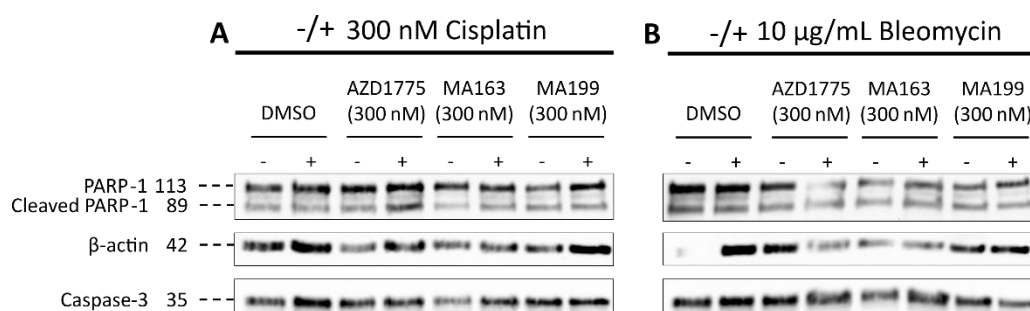
Figure 4.12 Detection of PARP-1 and caspase-3 cleavage in UM-SCC-6 cells by AZD1775, MA163 and MA199 treatments alone and in combination with cisplatin or bleomycin. Western blot of UM-SCC-6 cells that were treated with AZD1775, MA163 or MA199 alone and in combination with cisplatin or bleomycin for 24 h prior to the production of lysates. The membrane was probed for PARP-1, cleaved PARP-1, β-actin as the loading control and caspase-3 (n = 1).

Table 4.8 Quantitation of full-length PARP-1 and caspase-3 from Figure 4.10 of UM-SCC-6 cells treated with Wee1-targeting compounds alone or with chemotherapeutics. Intensity of full-length PARP-1 and Caspase-3 was normalised to actin and calculated relative to DMSO. The relative values are plotted in the table below.

	Band intensity relative to DMSO															
	+ / - Cisplatin								+ / - Bleomycin							
Protein	DMSO		AZD1775		MA163		MA199		DMSO		AZD1775		MA163		MA199	
	-	+	-	+	-	+	-	+	-	+	-	+	-	+	-	+
Full-length PARP-1	1.00	0.93	2.71	1.37	1.71	1.42	1.15	0.66	1.00	0.02	0.02	0.02	0.03	0.04	0.01	0.02
Full-length Caspase-3	1.00	1.02	2.12	1.08	1.03	1.43	1.77	0.66	1.00	0.02	0.04	0.11	0.08	0.10	0.04	0.02

The amount of PARP-1 cleavage appears similar between the single agents across both cisplatin and bleomycin blots, however due to a poor actin band on the bleomycin blot, quantification of full-length PARP cannot confirm this (Figure 4.10). There is an increase in the intensity of cleaved PARP-1 for AZD1775 in combination with cisplatin in comparison to either AZD1775 or cisplatin alone (Figure 4.12A). Furthermore, there is a relative decrease in full-length PARP-1 from 2.71 in AZD1775 to 1.37 in AZD1775 with cisplatin, suggestive of PARP-1 cleavage. MA163 with cisplatin also exhibits more PARP-1 cleavage in comparison to MA163 alone, whereas MA199 as a single agent seems to show less intense total PARP-1 than MA199 combined with cisplatin suggesting that there has been more PARP-1 cleavage in the single agent than the combined treatment. The amount of cleaved PARP-1 does not seem to differ between single treatments and combined treatments with bleomycin (Figure 4.12B). For both blots, smaller cleaved PARP-1 fragments were not detected. Cleaved caspase-3 was also not detected. Due to time constraints, only an n = 1 of this experiment was performed and when it is repeated, more concentrated lysates should be produced in order to be able to load more protein to help with detection of the cleaved fragments. As seen with the radiotherapy combinations, Annexin V flow cytometry was undertaken.

Cells were treated as described above for the western blot prior to harvesting and staining with Annexin V-FITC and PI. Data was analysed and gated as described in Figure 4.9A.
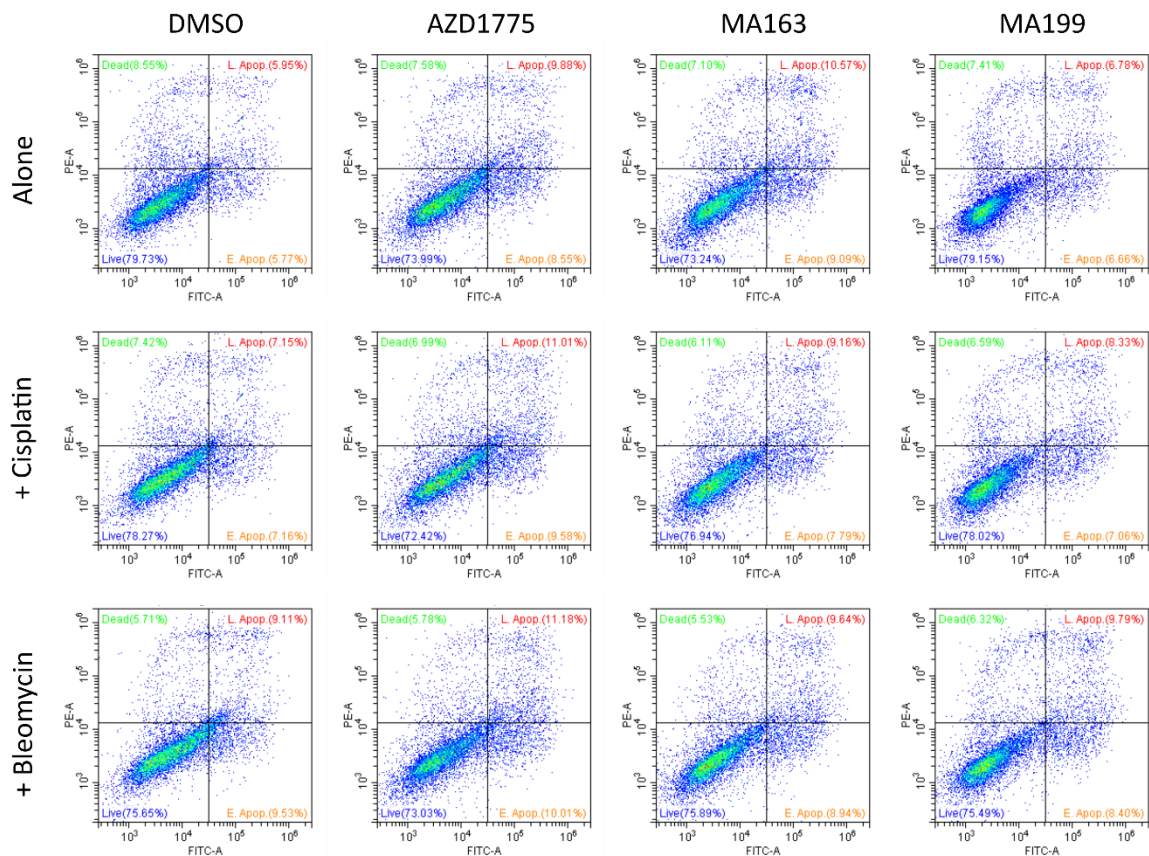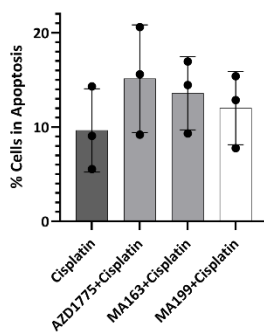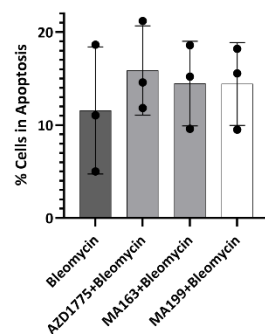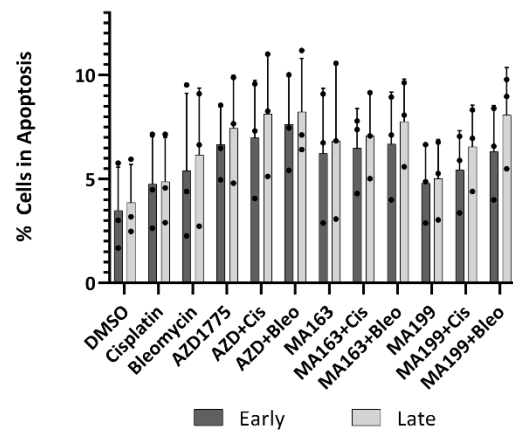
Figure 4.13 Apoptosis detection assay in UM-SCC-6 cells by AZD1775, MA163 and MA199 treatments alone and in combination with cisplatin or bleomycin. Flow cytometry of UM-SCC-6 cells stained with Propidium Iodide (PI) and Annexin V-FITC. (A) Representative dot plots for DMSO, AZD1775 (300 nM), MA163 (300 nM) and MA199 (300 nM) alone and with cisplatin (300 nM) or bleomycin (10μg/mL) for 24 h prior to staining. Bar graph showing the mean % cells in apoptosis of (B) cisplatin combination treatment or (C) bleomycin combination treatment ± SD of n = 3 biological repeats. (D) Bar graph showing the mean % cells in early or late apoptosis in each treatment condition. All graphs made with GraphPad Prism.

UM-SCC-6 (p53-WT) cells showed the most sensitivity to AZD1775 combination treatments (15.1% and 15.9% for cisplatin and bleomycin combination, respectively) (Figure 4.13). The least potent combination treatment to cause apoptosis was MA199 with cisplatin, which only caused ~3% increase in apoptosis compared to cisplatin alone. However, the general trend was that the addition of a Wee1 PROTAC or inhibitor did induce more apoptosis, however this was not statistically significant, than the chemotherapies alone. When plotting early and late stage apoptosis separately, there were no significant differences between treatment conditions (Figure 4.13D).

To easily compare between all of the treatments (single agent, radiotherapy combination and chemotherapy combination), a summary table of the mean % cells in apoptosis observed in the Annexin V flow cytometry assays was produced (Table 4.9). UM-SCC-6 (p53-WT) cells were most sensitive overall to AZD1775 with 12 Gy irradiation and least sensitive to 12 Gy irradiation alone.

Table 4.9 Summary table of mean % cells in apoptosis of Wee1-targeting drugs as a monotherapy and combinatorial strategy with radiotherapy or chemotherapy in UM-SCC-6 cells. UM-SCC-6 were treated with Wee1-targeting compounds alone and in combination with 12Gy irradiation, cisplatin or bleomycin for 24 h (Figures 4.9, 4.11 and 4.13) (n = 3). *Experiments where n = 2.

Treatment	Mean % cells in apoptosis ± SD			
	DMSO	12 Gy	300 nM Cisplatin	10 µg/mL Bleomycin
DMSO	7.51 ± 4.82	7.94 ± 4.31*	9.64 ± 4.41	11.6 ± 6.83
AZD1775	18.4 ± 12.3	23.36 ± 21.0*	15.1 ± 5.71	15.9 ± 4.81
MA163	14.2 ± 4.54	22.1 ± 17.9*	13.6 ± 3.90	14.5 ± 4.54
MA199	9.84 ± 3.76	-	12.0 ± 3.90	14.4 ± 4.46

The low sensitivity that UM-SCC-6 (p53-WT) cells have exhibited to the treatments could be due to the cells having a functional G1/S checkpoint, therefore we reproduced these experiments in section 4.3.4 in p53-deficient cells, A-253 and FaDu.

4.3.4 Assessment of cytotoxicity of Wee1-targeting compounds alone and as a combinatorial treatment in p53-deficient cells

4.3.4.1 Effect of mono and combination treatments on clonogenicity

Clonogenic survival assays were performed in A-253 (p53-null) and FaDu (p53-mutant) cells to investigate if Wee1 PROTAC treatment in combination with ionizing radiation or chemotherapy decreased cell survival more than the genotoxic treatments alone in p53-deficient cell types. The same doses and conditions were used as in section 4.3.3.1.

In A-253 (p53-null) cells, at 2 h, only MA199 was significantly better at reducing cell survival alone in comparison to DMSO (Figure 4.14). This was the same result that was seen in UM-SCC-6 (p53-WT) cells in Figure 4.5 however, in A-253 (p53-null), MA199 was also significantly more potent than AZD1775 and MA163 at 2 h (Table 4.10).
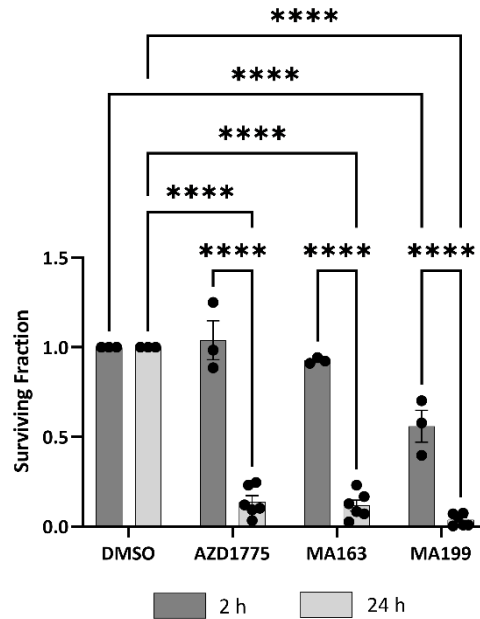
Figure 4.14 Effect of 2 h versus 24 h treatment time with Wee1-targeting treatments on the clonogenicity of A-253. Bar graph showing surviving fraction of A-253 cells that have been allowed to grow for 6 -10 days post 2h or 24 h treatment with monotherapies, AZD1775, MA163 and MA199. Data were analysed with a one-way ANOVA and Tukey's test. All data plotted is mean ± SD of n = 3 biological repeats.

Table 4.10 Table of adjusted p-values for the monotherapy treatment comparisons at 2 h and 24 h in A-253 cells. Colonies were fixed, stained and counted, the plating efficiencies were calculated and values were normalised to the DMSO control as 100% cell survival. Data were analysed by a two-way ANOVA and a Šidák's multiple comparisons test and bar graphs can be seen in Figure 4.14.

	DMSO 2 h	AZD1775 2 h	MA163 2 h	MA199 2 h	DMSO 24 h	AZD1775 24 h	MA163 24 h	MA199 24 h
DMSO 2 h	-	>0.9999 (ns)	>0.9999 (ns)	<0.0001 (****)	>0.9999 (ns)	<0.0001 (****)	<0.0001 (****)	<0.0001 (****)
AZD1775 2 h	>0.9999 (ns)	-	0.9698 (ns)	<0.0001 (****)	>0.9999 (ns)	<0.0001 (****)	<0.0001 (****)	<0.0001 (****)
MA163 2 h	>0.9999 (ns)	0.9698 (ns)	-	0.0006 (***)	>0.9999 (ns)	<0.0001 (****)	<0.0001 (****)	<0.0001 (****)
MA199 2 h	<0.0001 (****)	<0.0001 (****)	0.0006 (***)	-	<0.0001 (****)	<0.0001 (****)	<0.0001 (****)	<0.0001 (****)

DMSO 24 h	>0.9999 (ns)	>0.9999 (ns)	>0.9999 (ns)	<0.0001 (****)	-	<0.0001 (****)	<0.0001 (****)	<0.0001 (****)
AZD1775 24 h	<0.0001 (****)	<0.0001 (****)	<0.0001 (****)	<0.0001 (****)	<0.0001 (****)	-	>0.9999 (ns)	0.7902 (ns)
MA163 24 h	<0.0001 (****)	<0.0001 (****)	<0.0001 (****)	<0.0001 (****)	<0.0001 (****)	>0.9999 (ns)	-	0.9704 (ns)
MA199 24 h	<0.0001 (****)	<0.0001 (****)	<0.0001 (****)	<0.0001 (****)	<0.0001 (****)	0.7902 (ns)	0.9704 (ns)	-

At 24 h, AZD1775, MA163 and MA199 were significantly better at reducing the surviving fraction in comparison to DMSO. All of the treatments were as potent as each other at 24 h. Initial degradation of Wee1 over shorter treatments (2 h) is more beneficial than inhibition in A-253 (p53-null) cells however, degradation of Wee1 shows to be no more advantageous than inhibition when looking at longer treatment times (24 h).

In contrast to UM-SCC-6 (p53-WT) cells, Wee1-targeting treatments did enhance radiation-induced cell death in A-253 (p53-null) cells, however this was not significant after performing multiple unpaired t tests with Welch correction (Figure 4.15).
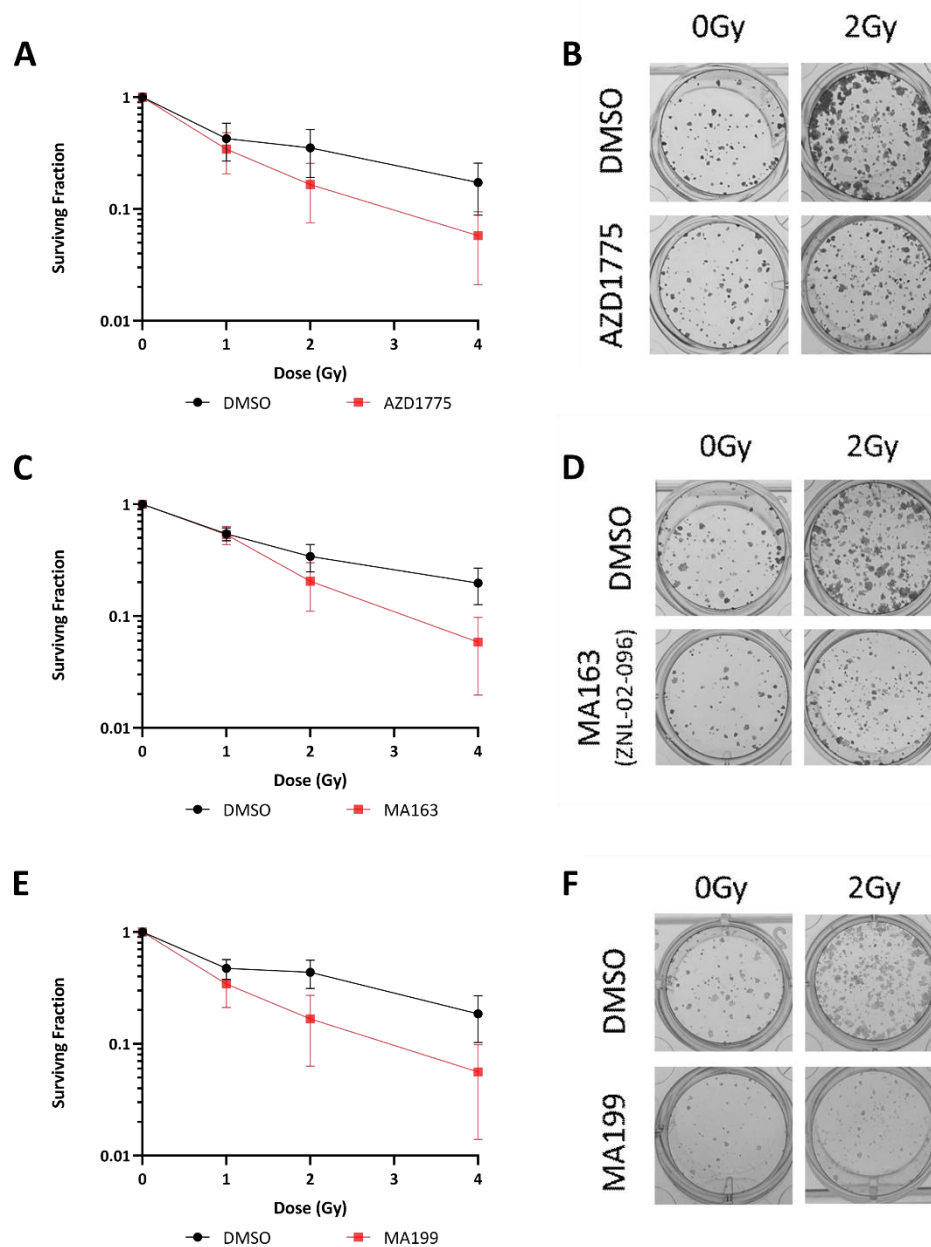
Figure 4.15 Investigation of Wee1-targeting treatments in combination with radiation on clonogenicity of p53-deficient cells, A-253. Cells were pre-treated with Wee1-targeting drugs for 2 h prior to irradiation, supplemented with drug-free media post-IR and allowed to grow for 6 – 10 days. (A & B) Survival curve and representative images for AZD1775-treated cells, (C & D) Survival curve and representative images for MA163-treated cells and (E & F) Survival curve and representative images for MA199-treated cells. All data plotted is mean ± SD of n = 3 biological repeats.

Furthermore, AZD1775, MA163 and MA199 all performed similarly to increase cytotoxicity

with ionizing radiation. So, although the 2 h monotherapy treatment showed that MA199

was more cytotoxic, when combining this with radiotherapy we do not see MA199 reducing colony formation better than the other treatments (Figure 4.15).

Cisplatin treatment was more toxic in A-253 (p53-null) cells in comparison to UM-SCC-6 (p53-WT) with a surviving fraction of 25% (Figure 4.16).
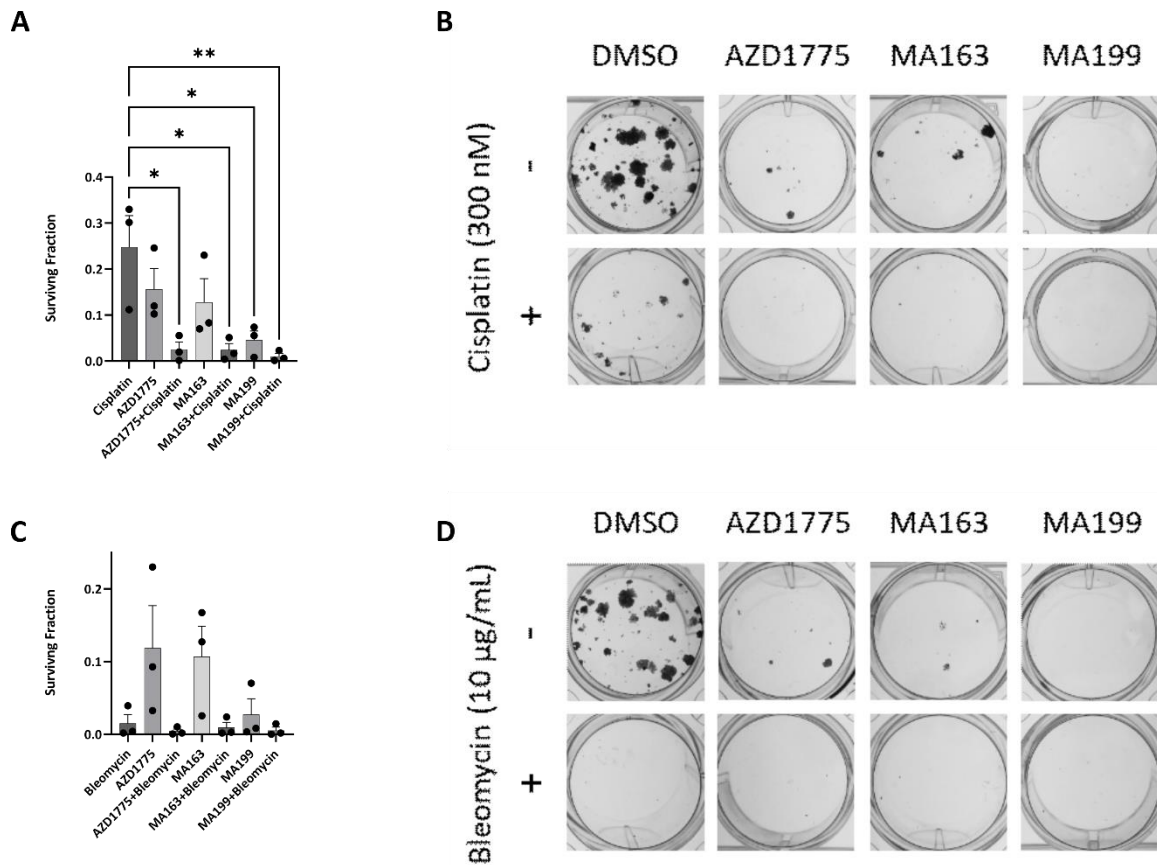
Figure 4.16 Investigation of Wee1-targeting treatments in combination with cisplatin and bleomycin on clonogenicity of p53-deficient cells, A-253. Cells were treated with Wee1-targeting compounds and cisplatin or bleomycin for 24 h before replacing with drug-free media and allowed to grow for 6 – 10 days. (A & B) Survival curve and representative images for AZD1775-treated cells, (C & D) Survival curve and representative images for MA163-treated cells and (E & F) Survival curve and representative images for MA199-treated cells. All data plotted is mean ± SD of n = 3 biological repeats.

All combination treatments were able to significantly enhance cisplatin-induced cell death (surviving fractions were 2.6%, 2.4% and 1.3% for AZD1775, MA163 and MA199 with cisplatin, respectively). Furthermore, the Wee1-targeting treatments alone were also more toxic than cisplatin treatment in A-253 (p53-null). Bleomycin was 10-fold more cytotoxic alone in A-253 (p53-null) compared to UM-SCC-6 (p53-WT), therefore the compounds did not enhance bleomycin-induced cell death (Figure 4.16).

This experiment was carried out in p53-mutant cells, FaDu to corroborate if there is more radiation-induced and cisplatin-induced cell death with the combination treatments in p53-deficient cell lines in comparison to p53-proficient. Furthermore, it would be interesting to see if there are any differences in response between a p53-null and p53-mutant cell line.

In FaDu (p53-mutant) cells, at 2 h, none of the Wee1-targeting treatments were significantly better at reducing colony formation than DMSO however, MA199 does show a similar trend to other cell lines in that the VHL-based PROTAC reduces the surviving fraction more than AZD1775 and MA163, but the difference is not significant (Figure 4.17). At 24 h, AZD1775, MA163 and MA199 were significantly better at reducing the colony formation in comparison to DMSO (Figure 4.17 and Table 4.11). All of the treatments were as potent as each other at 24 h.
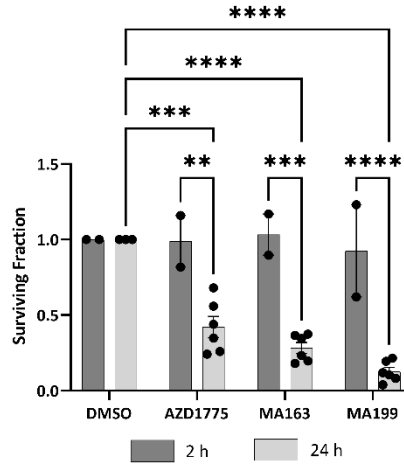
Figure 4.17 Effect of 2 h versus 24 h treatment time with Wee1-targeting treatments on the clonogenicity of FaDu. Bar graph showing surviving fraction of FaDu cells that have been allowed to grow for 6 -10 days post 2h or 24 h treatment with monotherapies, AZD1775, MA163 and MA199. Data were analysed with a one-way ANOVA and Tukey's test. All data plotted is mean ± SD of n = 3 biological repeats.

Table 4.11 Table of adjusted p-values for the monotherapy treatment comparisons at 2 h and 24 h in FaDu cells. Colonies were fixed, stained and counted, the plating efficiencies were calculated and values were normalised to the DMSO control as 100% cell survival. Data were analysed by a two-way ANOVA and a Šidák's multiple comparisons test and bar graphs can be seen in Figure 4.17.

	DMSO 2 h	AZD1775 2 h	MA163 2 h	MA199 2 h	DMSO 24 h	AZD1775 24 h	MA163 24 h	MA199 24 h
DMSO 2 h	-	>0.9999 (ns)	>0.9999 (ns)	>0.9999 (ns)	>0.9999 (ns)	0.0041 (**)	0.0003 (***)	<0.0001 (****)
AZD1775 2 h	>0.9999 (ns)	-	>0.9999 (ns)	>0.9999 (ns)	>0.9999 (ns)	0.0051 (**)	0.0004 (***)	<0.0001 (****)
MA163 2 h	>0.9999 (ns)	>0.9999 (ns)	-	>0.9999 (ns)	>0.9999 (ns)	0.0022 (**)	0.0002 (***)	<0.0001 (****)
MA199 2 h	>0.9999 (ns)	>0.9999 (ns)	>0.9999 (ns)	-	>0.9999 (ns)	0.0171 (*)	0.0012 (**)	<0.0001 (****)
DMSO 24 h	>0.9999 (ns)	>0.9999 (ns)	>0.9999 (ns)	>0.9999 (ns)	-	0.0008 (***)	<0.0001 (****)	<0.0001 (****)
AZD1775 24 h	0.0041 (**)	0.0051 (**)	0.0022 (**)	0.0171 (*)	0.0008 (***)	-	0.9815 (ns)	0.0843 (ns)
MA163 24 h	0.0003 (***)	0.0004 (***)	0.0002 (***)	0.0012 (**)	<0.0001 (****)	0.9815 (ns)	-	0.9310 (ns)
MA199 24 h	<0.0001 (****)	<0.0001 (****)	<0.0001 (****)	<0.0001 (****)	<0.0001 (****)	0.0843 (ns)	0.9310 (ns)	-

Interestingly, only AZD1775 enhanced radiation-induced cell death in FaDu (p53-mutant) cells, although this is not significant after performing multiple unpaired t tests with Welch correction (Figure 4.18).
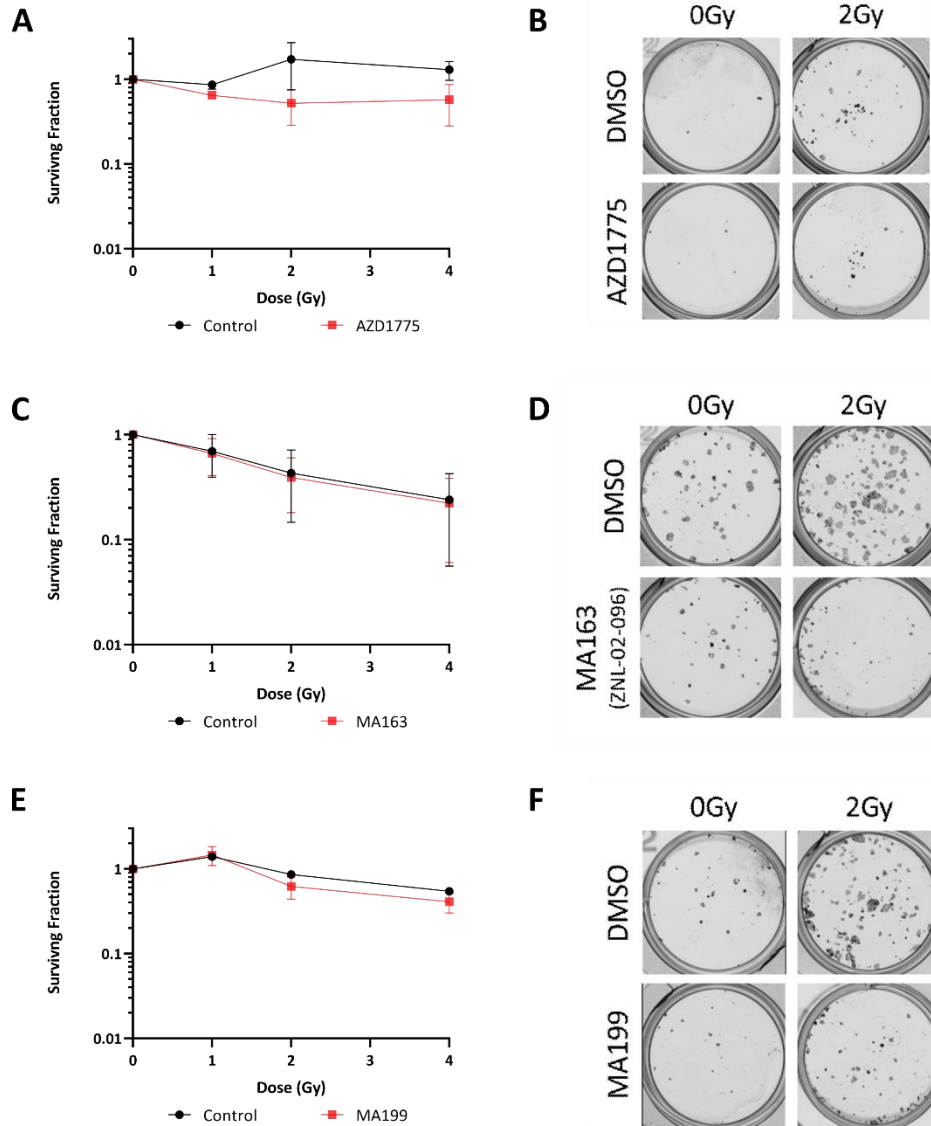
Figure 4.18 Investigation of Wee1-targeting treatments in combination with radiation on clonogenicity of p53-deficient cells, FaDu. Cells were pre-treated with Wee1-targeting drugs for 2 h prior to irradiation, supplemented with drug-free media post-IR and allowed to grow for 6 – 10 days. (A & B) Survival curve and representative images for AZD1775-treated cells, (C & D) Survival curve and representative images for MA163-treated cells and (E & F) Survival curve and representative images for MA199-treated cells. All data plotted is mean ± SD of n = 3 biological repeats.

FaDu (p53-mutant) cells were the least sensitive to cisplatin in comparison to UM-SCC-6 (p53-WT) and A-253 (p53-null) cells however, cisplatin only treatment did kill 56% of the cells (Figure 4.19).
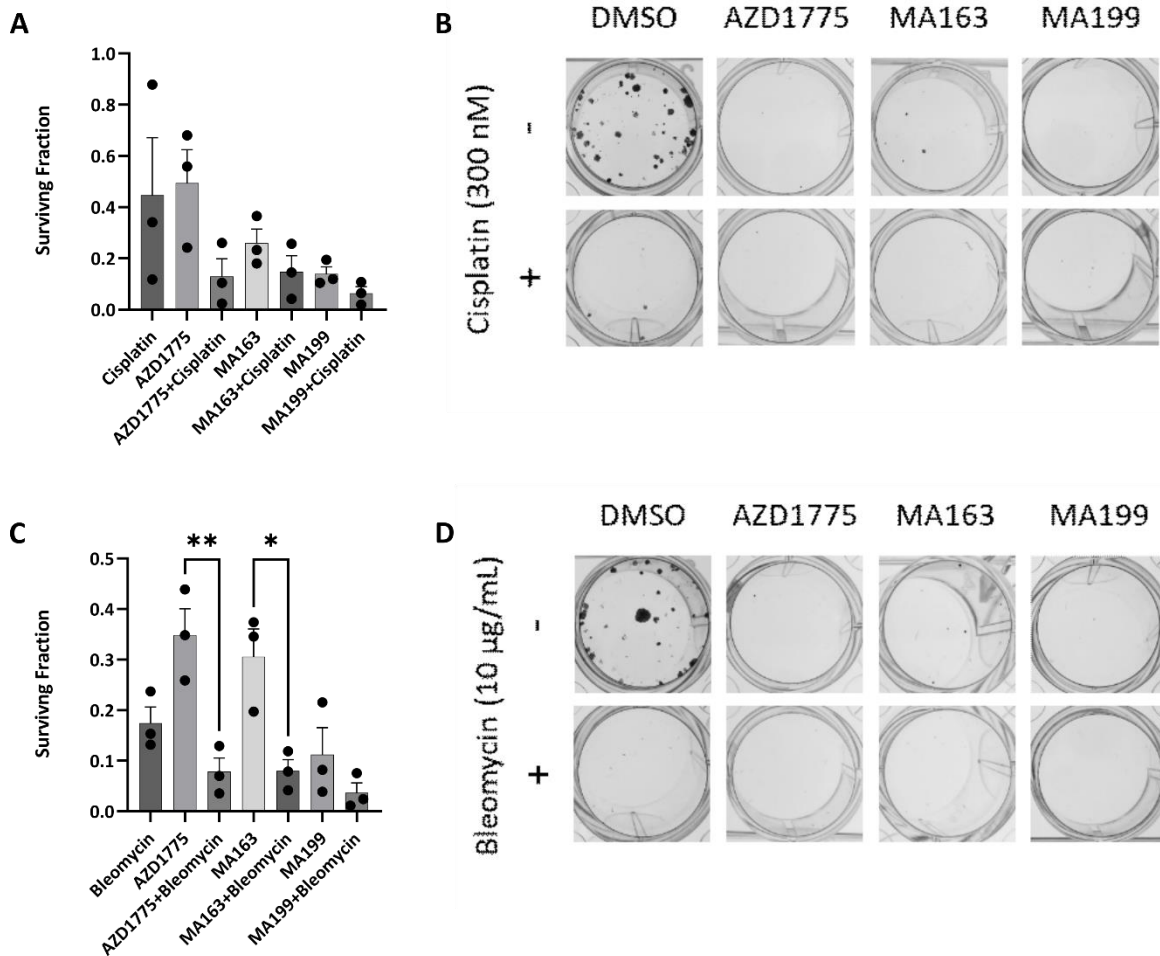
Figure 4.19 Investigation of Wee1-targeting treatments in combination with cisplatin and bleomycin on clonogenicity of p53-deficient cells, FaDu. Cells were treated with Wee1-targeting compounds and cisplatin or bleomycin for 24 h before replacing with drug-free media and allowed to grow for 6 – 10 days. (A & B) Survival curve and representative images for AZD1775-treated cells, (C & D) Survival curve and representative images for MA163-treated cells and (E & F) Survival curve and representative images for MA199-treated cells. All data plotted is mean ± SD of n = 3 biological repeats.

AZD1775, MA163 and MA199 all caused an enhancing effect of cisplatin-induced cell death, with MA199 showing the most cell killing, however the difference is not significant. Furthermore, FaDu (p53-mutant) cells were more resistant to bleomycin treatment (surviving fraction of 17%) compared to A-253 (p53-null) cells (Figure 4.19). We can see some enhancement of bleomycin-induced cell death in FaDu (p53-mutant) (surviving

fractions of 7.8%, 8% and 3.7% for AZD1775, MA163 and MA199 in combination with bleomycin, respectively) compared to the bleomycin only treatment.

As some of these experiments confirmed that we saw enhanced chemotherapy-induced cell death when using the chemotherapies in combination with the Wee1-targeting compounds in p53-deficient cell lines, we wanted to investigate if we were seeing an additive effect in a dose response curve.

4.3.4.2 Impact of chemotherapeutics, cisplatin and bleomycin, with Wee1-targeting treatments cell viability

Similar to the experiments previously carried out for p53 wildtype UM-SCC-6 cells, as discussed in section 4.3.3.2, the synergistic or additive effect of the combination treatments were then investigated for the p53-deficient cell lines, A-253 (p53-null) and FaDu (p53-mutant) (Figure 4.20).
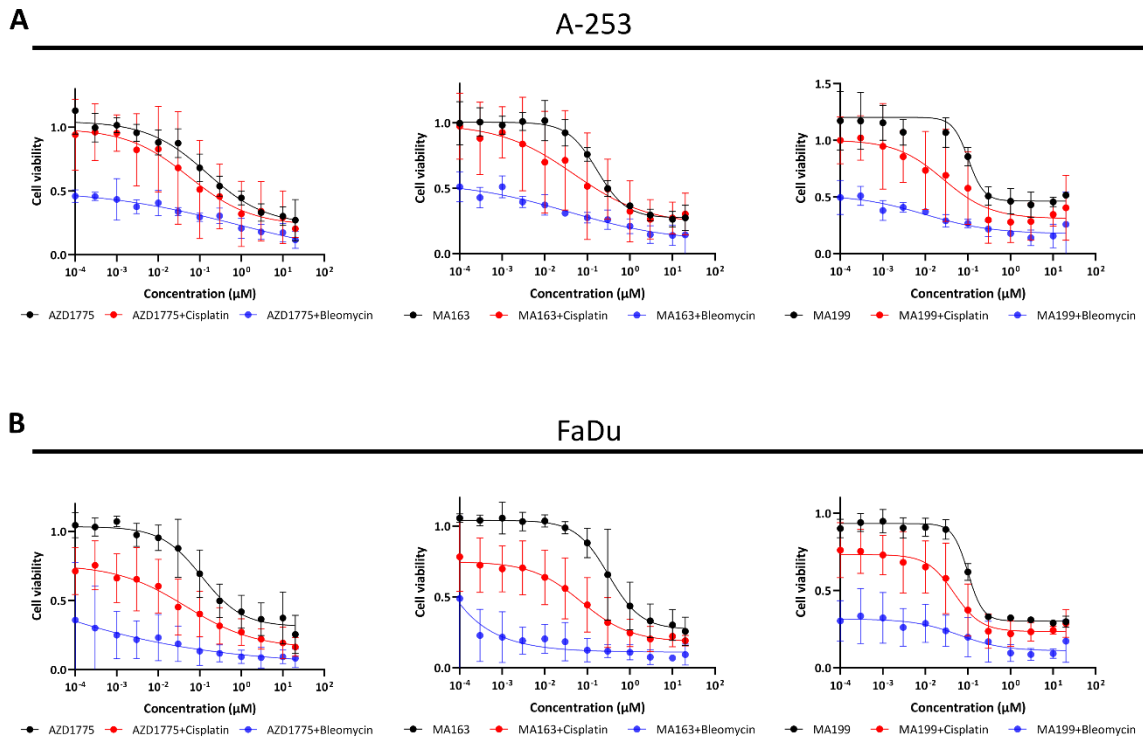
Figure 4.20 Reduction of cell viability of p53-deficient cells by Wee1-targeting compounds alone and in combination with cisplatin or bleomycin. Cell viability assays of (A) A-253 and (B) FaDu cells treated with AZD1775, AZD1775 and cisplatin or AZD1775 and bleomycin, MA163, MA163 and cisplatin or MA163 and bleomycin and MA199, MA199 and cisplatin or MA199 and bleomycin for 72 h. All treatments were normalised with DMSO. Data are presented as mean ± SD of n = 4 biological repeats (GraphPad Prism).

Similarly, to UM-SCC-6 (p53-WT), the combination of the Wee1-targeting compounds with cisplatin or bleomycin has an additive, not synergistic, effect on viability in both A-253 (p53-null) and FaDu (p53-mutant) cells (Figure 4.20). However, we observe that the loss of cell viability is greater for all treatments in A-253 (p53-null) and FaDu (p53-mutant) compared to UM-SCC-6 (p53-WT). In A-253 (p53-null), the combination of AZD1775, MA163 or MA199 with 300 nM cisplatin resulted in a shift of the dose response curve to the left and a reduction in the EC50, with the largest decrease in EC50 from MA163 with cisplatin and MA199 with cisplatin at ~3.4-fold decrease. AZD1775 with cisplatin caused a 2.5-fold decrease of the EC50 compared to AZD1775 alone (Table 4.12). In FaDu (p53-mutant),

136

MA163 combination with cisplatin caused the highest decrease by 4.3-fold, whereas the

AZD1775 and MA199 combinations with cisplatin caused a 2-fold decrease. In both cell

lines, the combination of MA199 and cisplatin showed the greatest loss of cell viability. Both

cell lines were more sensitive to bleomycin alone compared to cisplatin alone, at the

respective doses used, therefore we see that the bleomycin combinations are better at

inhibiting cell proliferation compared to the cisplatin combinations.

Table 4.12 Table of EC50 values of cell viability assays (MTS) in p53-deficient cells for chemotherapy combination treatments. A-253 and FaDu were treated with Wee1-targeting compounds alone and in combination with cisplatin or bleomycin for 72 h (n = 4) and the dose response curves that correspond with these values can be seen in Figure 4.20.

Treatment	EC50 (µM) ± SD					
	A-253			FaDu		
	Alone	+ 300 nM Cisplatin	+ 10 µg/mL Bleomycin	Alone	+ 300 nM Cisplatin	+ 10 µg/mL Bleomycin
AZD1775	0.15 ± 0.09	0.06 ± 0.33	0.84 ± $4.01×10^{16}$	0.1 ± 0.08	0.05 ± 0.04	$3.2×10^{-7}$ ± 0.12
MA163	0.17 ± 0.04	0.05 ± 0.24	0.04 ± 0.02	0.3 ± 0.33	0.07 ± 0.09	$2.3×10^{-12}$ ± 0.27
MA199	0.10 ± 0.0022	0.03 ± 0.07	0.01 ± 0.0061	0.1 ± 0.0090	0.05 ± 0.04	0.06 ± 0.01

4.3.4.3 Effect of mono and combination treatments on mode of death

Western blots detecting for PARP-1 cleavage and caspase-3 cleavage, as well as Annexin V

flow cytometry staining were used to investigate if any of the treatments showed more

promise in inducing apoptosis in p53-deficicent cells over others. To elucidate if these

treatment modalities caused variable induction of apoptosis dependent on p53 status, the

experiments seen in section 4.3.3.1 were performed in p53-deficient cell lines. A-253 (p53-

null) and FaDu (p53-mutant) cells were treated with a Wee1i, AZD1775, and Wee1

PROTACs, MA163 or MA199, at 300 nM for 24 h before harvesting and staining with

Annexin V-FITC and PI. DMSO was used as a control. The gating and controls used for the

Annexin V flow cytometry experiments was as explained before in Section 4.3.3.3. Representative dot plots of this gating and the controls for A-253 (p53-null) and FaDu (p53-mutant) can be seen in Figure 4.21A and Figure 4.22A, respectively.
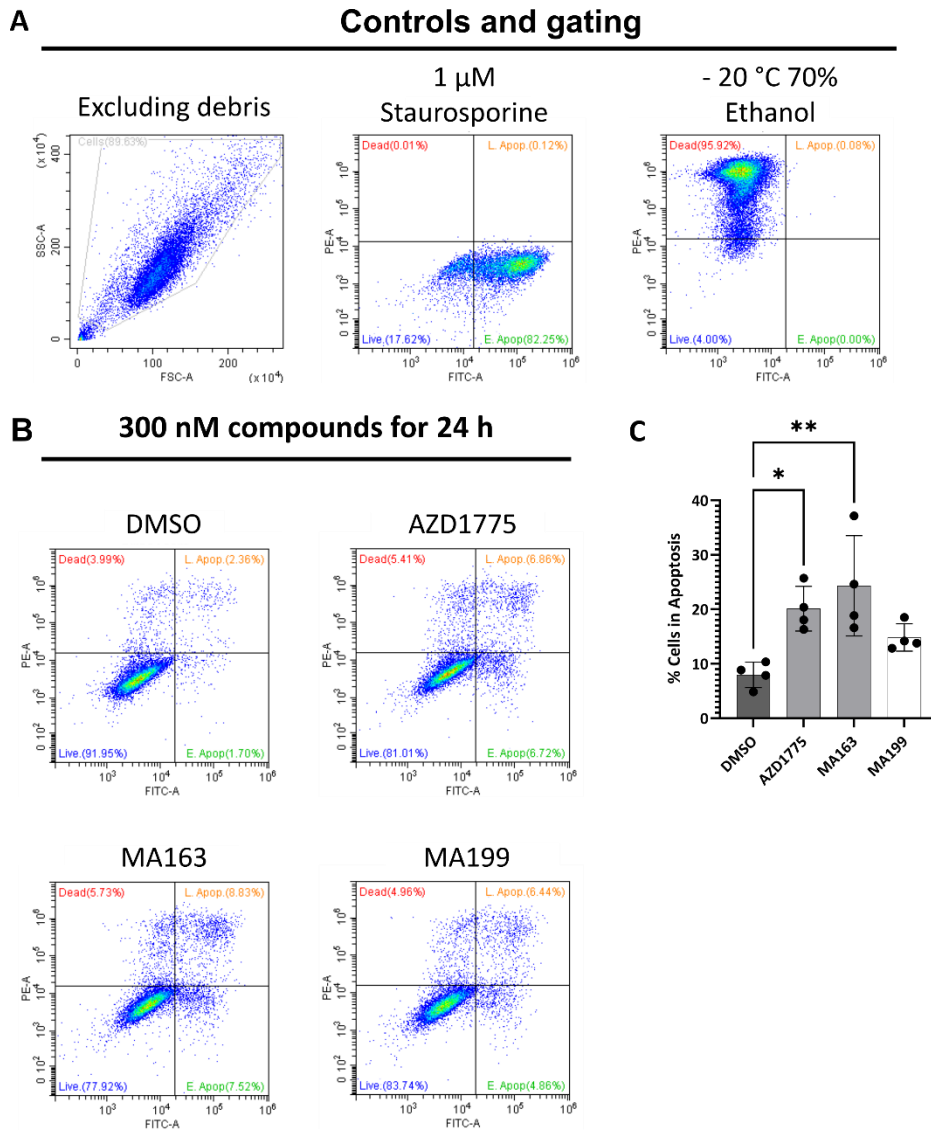
Figure 4.21 Apoptosis detection assay of AZD1775, MA163 and MA199 in A-253. Flow cytometry of A-253 cells stained with Propidium Iodide (PI) and Annexin V-FITC. (A) Representative dot plots showing gating out of debris to only analyse cells and positive controls for apoptosis (1 μM staurosporine treatment for 24 h) and dead cells (-20 °C 70% ethanol for 24 h). (B) Representative dot plots for monotherapy treatments at 300 nM for 24 h. (C) Bar graph showing mean ± SD of n = 4 biological replicates for monotherapy treatments. Data were analysed by a one-way ANOVA and Tukey's post hoc test (GraphPad Prism).

In A-253 (p53-null) cells, AZD1775, MA163 and MA199 all induce apoptosis as single agent treatments (Figure 4.21). AZD1775, MA163 and MA199 cause a 12.1% increase, 16.3% increase and 6.8% increase, respectively, compared to the DMSO control. AZD1775 and MA163 significantly increase the amount of positively stained Annexin V cells, with A-253

(p53-null) cells exhibiting the most sensitivity towards the CRBN-recruiting Wee1 PROTAC, MA163. This suggests that generally targeting Wee1 in a p53-null cell line, whether that is by inhibition or degradation, causes an apoptotic mode of death, leading to synthetic lethality and cell death.

In FaDu (p53-mutant) cells, AZD1775, MA163 and MA199 cause a rise in apoptotic cells as monotherapies (Figure 4.22). We also tested the first-generation PROTACs, MA048 and MA055, to investigate if they caused cells to enter programmed cell death. MA048 and MA055 did not increase the amount of positively-stained Annexin V cells, which further confirms that these compounds are not as effective as the second generation Wee1 PROTACs.

A   Controls and gating

B   300 nM compounds for 24 h

C
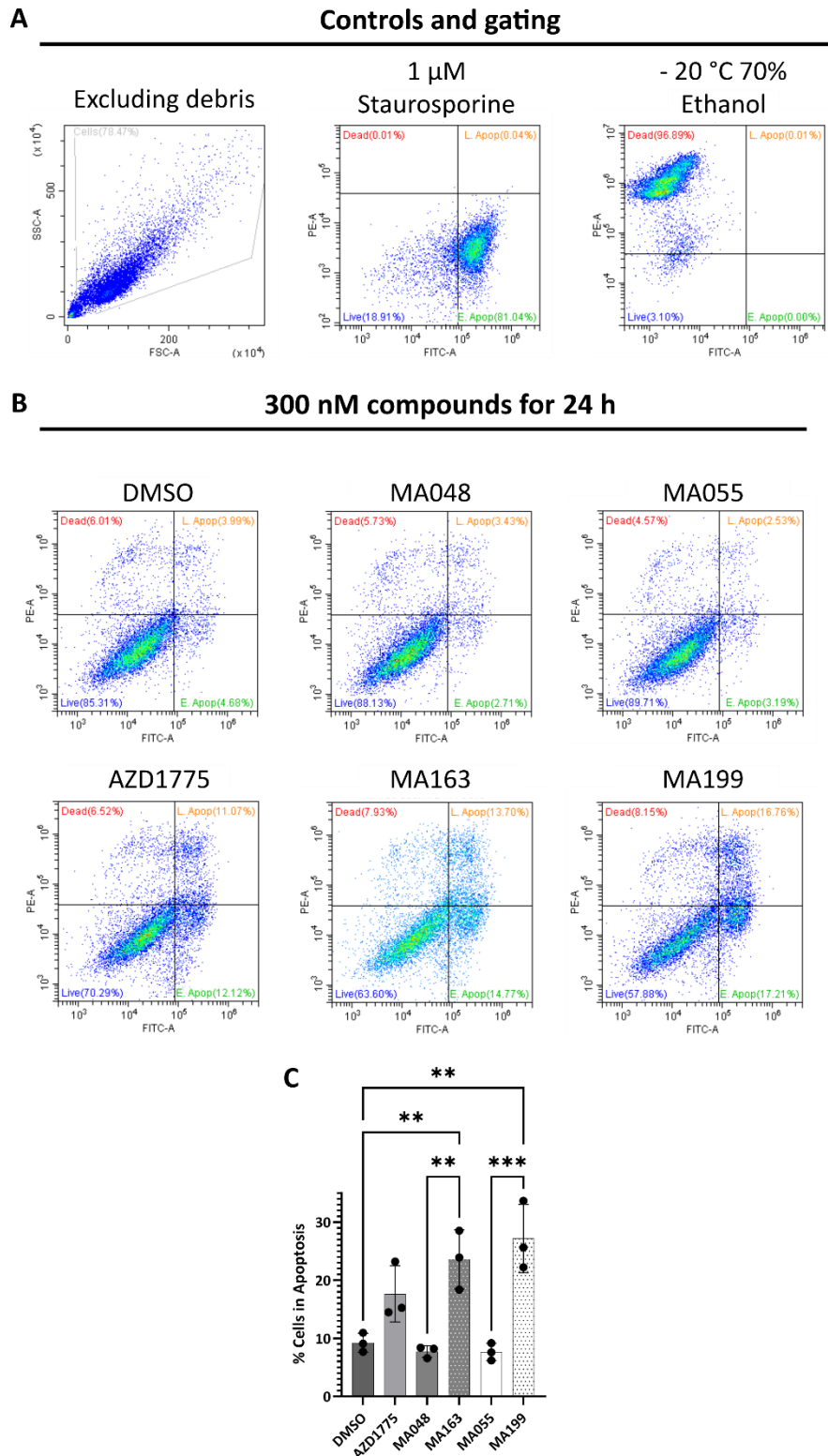
Figure 4.22 Apoptosis detection assay of AZD1775, CRBN-recruiters (MA048 and MA163) and VHL-recruiters (MA055 and MA199) in FaDu. Flow cytometry of FaDu cells stained with Propidium Iodide (PI) and Annexin V-FITC. (A) Representative dot plots showing gating out of debris to only analyse cells and positive controls for apoptosis (1 µM staurosporine treatment for 24 h) and dead cells (-20 °C 70% ethanol for 24 h). (B) Representative dot plots for monotherapy treatments at 300 nM for 24 h. (C) Bar graph showing mean ± SD of n = 3 biological replicates for monotherapy treatments. Data were analysed by a one-way ANOVA and Tukey's post hoc test (GraphPad Prism).

MA163 significantly induces apoptosis by 2.5-fold higher than DMSO and MA199 by 3-fold higher. AZD1775 causes a 2-fold increase in apoptotic cells compared to DMSO. This further corroborates that targeting Wee1 in a p53-deficicent cell line causes a p53-independent apoptotic signalling cascade, which leads to increased cytotoxicity. To investigate if the combination treatments lead to more induction of apoptosis in comparison to the Wee1-targeting compounds alone, we performed western blotting to detect PARP-1 cleavage (and caspase-3 cleavage for the chemotherapeutic combinations) and Annexin V flow cytometry.

Cells were treated for 2 h with 300 nM AZD1775 or MA163 then irradiated and treatment remained for a further 22 h prior to harvesting and producing lysates. Samples were probed for PARP-1 (and cleaved PARP-1) and β-actin as the loading control (Figure 4.23).
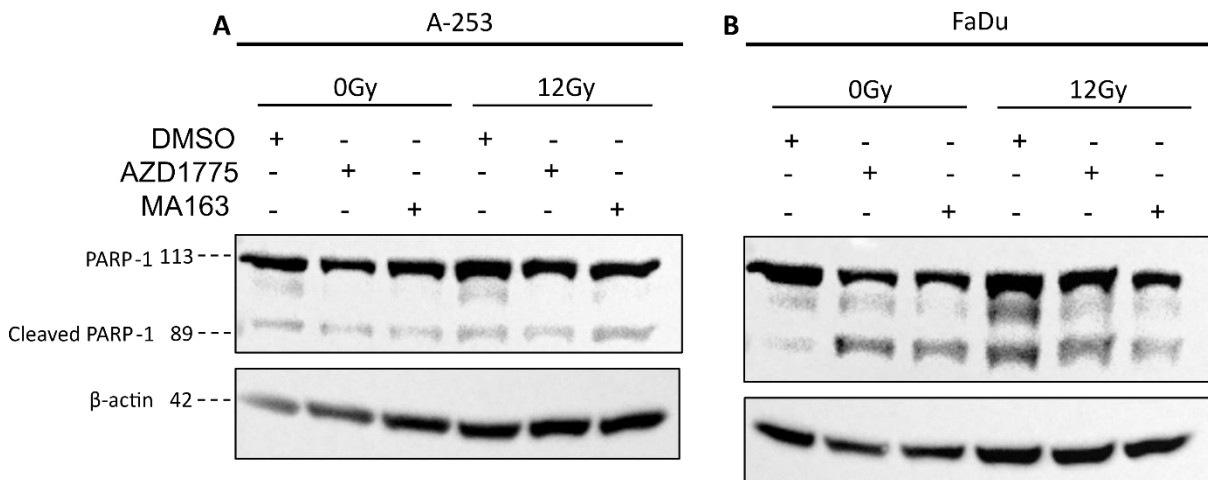
Figure 4.23 Detection of PARP cleavage in A-253 and FaDu cells by AZD1775 and MA163 treatments alone and in combination with 12 Gy irradiation. Western blot of A-253 and FaDu cells that were treated with AZD1775 or MA163 at 300 nM for 2 h prior to irradiation then treatment remained for a further 22 h post irradiation prior to the production of lysates. The membrane was probed for PARP-1, cleaved PARP-1 and β-actin as the loading control, n = 1. Quantitation for full-length PARP-1 can be found in Table 4.13.

In A-253 (p53-null), there was a loss of 66 % of full-length PARP-1 relatively from DMSO to AZD1775 (Table 4.13). In addition, there was a relative decrease of 59 % from DMSO to

MA163, suggesting that AZD1775 and MA163 cause PARP cleavage and induce apoptosis in the absence of IR, consistent with flow cytometry results. The same trend occurs in FaDu (p53-mutant) cells, with an even larger relative loss of total PARP-1.

Table 4.13 Quantitation of full-length PARP-1 from Figure 4.23 of p53-deficient HNSCC cells treated with AZD1775 or MA163 as a single or combination with IR. Intensity of full-length PARP-1 was normalised to actin and calculated relative to DMSO. The relative levels of full-length PARP-1 are shown in the table below.

Treatment condition	Relative band intensity of full-length PARP-1	
	A-253	FaDu
DMSO	1.00	1.00
AZD1775	0.34	0.27
MA163	0.41	0.24
DMSO + 12 Gy	0.58	0.37
AZD1775 + 12 Gy	0.31	0.26
MA163 + 12 Gy	0.43	0.17

For the irradiated cells, there is only a small decrease in full-length PARP-1 when using the Wee1-targeting compounds in addition to irradiation compared to irradiation alone. This implies that the drugs can stimulate a small amount of additional apoptosis. Similarly, to UM-SCC-6 (p53-WT) cells, in both A-253 (p53-null) and FaDu (p53-mutant) we see the amount of total PARP-1 is less in the AZD1775 and MA163 treated samples but do not detect the smaller fragments, therefore there could be reduced transcription/translation of PARP-1 or proteolytic degradation of the cleavage fragments has occurred which would not be detected by western blot.

To identify if any single agent Wee1-targeting drug treatments or combination with irradiation resulted in more PS-presenting cells, Annexin V/propidium iodide flow cytometry was conducted in A-253 (p53-null) cells (Figure 4.24). A-253 (p53-null) cells were treated

with compounds for 2 h prior to irradiation and then were left for a total of 24 h prior to trypsinization and staining with Annexin V-FITC and PI. Data was gated and controls were used as per section 4.3.3.3. This should have been performed in FaDu (p53-mutant) cells and with more repeats for A-253 (p53-null) cells, however the cell irradiator became inoperable which meant that further irradiation experiments were not possible. Similarly to UM-SCC-6 data, 12 Gy IR alone should inflict more apoptosis than has been observed, therefore it is possible that when these experiments were performed, the intended IR dose was not delivered to the cells.

A
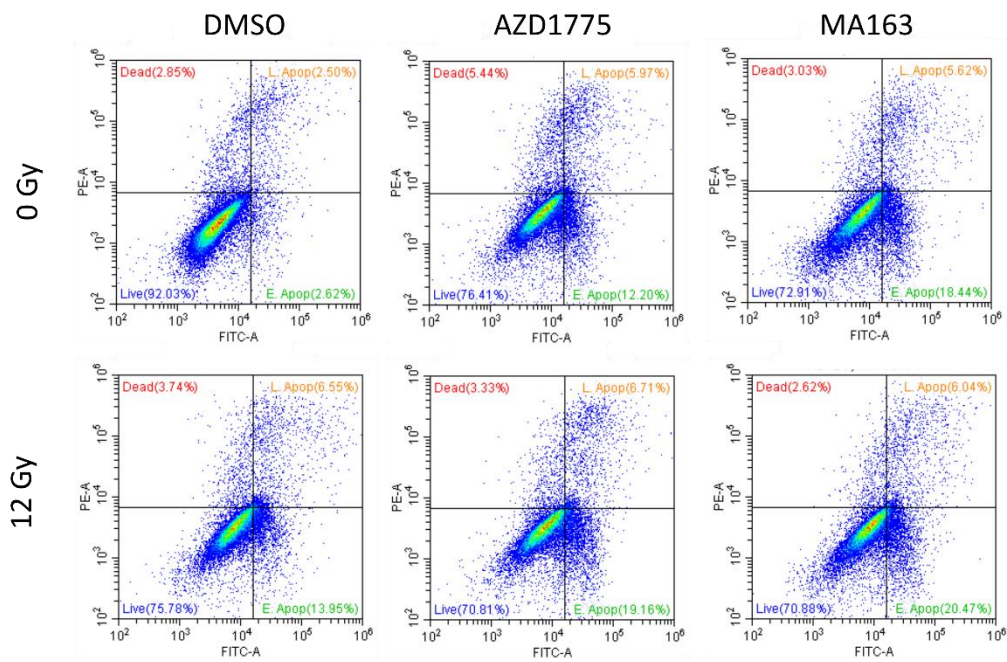
B
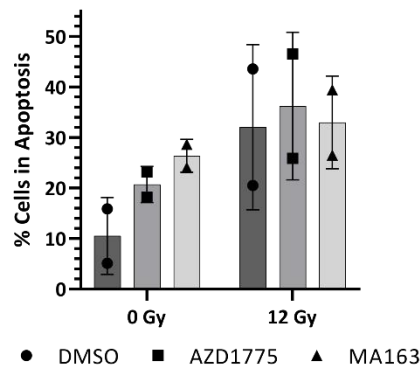
Figure 4.24 Apoptosis detection assay of AZD1775 and MA163 with 12 Gy irradiation in A-253. Flow cytometry of A-253 cells stained with Propidium Iodide (PI) and Annexin V-FITC. (A) Representative dot plots for DMSO, AZD1775 (300 nM) and MA163 (300 nM) for 24 h alone and with 12 Gy irradiation after initial 2 h treatment prior to staining. (B) Bar graph showing mean ± SD of n = 2 biological repeats (GraphPad Prism).

In these preliminary results, AZD1775 and 12 Gy resulted in a slight increase in apoptosis in comparison to 12 Gy alone and MA163 with 12 Gy did not cause a gain or loss of apoptotic cells (Figure 4.24). However, due to the inoperable irradiator, additional repeats of these experiments were not carried out and statistics to support this were not possible to perform.

We next investigated if the combination of the compounds with cisplatin or bleomycin

resulted in the same trends observed with the radiation combination treatments. p53-

deficient cell lines, A-253 (p53-null) and FaDu (p53-mutant), were treated with compounds

for a total of 24 h prior to the production of lysates. Lysates were probed for PARP-1 (and

cleaved PARP-1), caspase-3 (and cleaved caspase-3) and β-actin as a loading control (Figure

4.25).
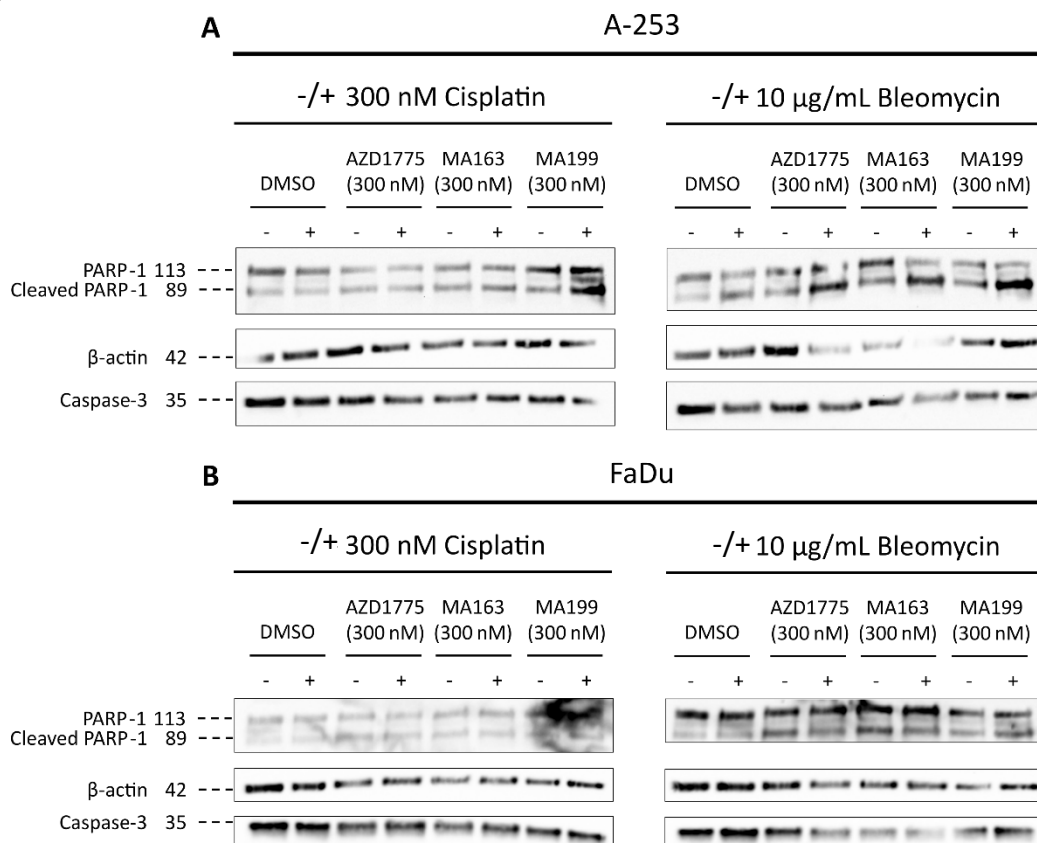
Figure 4.25 Detection of PARP-1 and caspase-3 cleavage in A-253 and FaDu cells by AZD1775, MA163 and MA199 treatments alone and in combination with cisplatin or bleomycin. (A) Western blots of A-253 cells that were treated with AZD1775, MA163 or MA199 alone and in combination with cisplatin or bleomycin for 24 h prior to the production of lysates. (B) Western blots of FaDu cells that were treated with AZD1775, MA163 or MA199 alone and in combination with cisplatin or bleomycin for 24 h prior to the production of lysates. The membrane was probed for PARP-1, cleaved PARP-1, β-actin as the loading control and caspase-3, n = 1. Quantitation for full-length PARP-1 and Caspase-3 for (A) and (B) can be found in Tables 4.14 and 4.15.

In A-253 (p53-null) cells, MA199 and cisplatin resulted in the same intensity of cleaved PARP-1 to total PARP-1 and the cleaved PARP-1 band was much more intense in comparison to MA199 or cisplatin as single agents (Figure 4.25A). When treated with bleomycin, in A-253 (p53-null) cells, all combination treatments with bleomycin inflicted more PARP cleavage in comparison to the single agents of bleomycin or the Wee1-targeting compound. Similarly, to A-253 (p53-null), FaDu (p53-mutant) cells showed a similar trend of consistent levels of total PARP-1 and cleaved PARP-1 between each treatment alone and with cisplatin (Figure 4.25B). There is not an increase in cleaved PARP-1 from AZD1775, MA163 or MA199 alone to the compounds in combination with bleomycin, however they do show a stronger cleaved PARP-1 band in comparison to the bleomycin treatment alone. Finally, no cleaved caspase-3 could be detected in any of the treatments however, we did observe less intense total caspase-3 bands in some of the treatments compared to DMSO. From these data, we performed the apoptosis detection assay using flow cytometry to determine if we see an increase in apoptotic cells, focussing on MA199 with cisplatin and bleomycin combination treatments as these showed the largest increases in PARP cleavage across both A-253 (p53-null) and FaDu (p53-mutant) cells. To discuss the relative levels between treatments of full-length PARP-1 and caspase-3 bands, they were quantified normalised to actin and relative to DMSO for A-253 (p53-null) and FaDu (p53-mutant) in Table 4.14 and Table 4.15, respectively.

Table 4.14 Quantitation of full-length PARP-1 from Figure 4.25A of Wee1-treated A-253 cells alone or in combination with cisplatin or bleomycin. Intensity of full-length PARP-1 and caspase-3 was normalised to actin and calculated relative to DMSO. The relative levels of full-length PARP-1 and caspase-3 in A-253-treated cells are shown in the table below.

Protein	Band intensity relative to DMSO															
	+ / - Cisplatin								+ / - Bleomycin							
	DMSO		AZD1775		MA163		MA199		DMSO		AZD1775		MA163		MA199	
	-	+	-	+	-	+	-	+	-	+	-	+	-	+	-	+
Full-length PARP-1	1.00	0.24	0.10	0.13	0.26	0.29	0.35	1.05	1.00	0.70	0.51	2.36	3.64	5.32	1.00	0.45
Full-length Caspase-3	1.00	0.26	0.18	0.21	0.23	0.27	0.17	0.14	1.00	0.45	0.35	1.28	1.16	2.53	0.48	0.30

Table 4.15 Quantitation of full-length PARP-1 from Figure 4.25B of Wee1-treated FaDu cells alone or in combination with cisplatin or bleomycin. Signal intensity of full-length PARP-1 and caspase-3 was normalised to actin and calculated relative to DMSO. The relative levels of full-length PARP-1 and caspase-3 in FaDu-treated cells are shown in the table below.

Protein	Band intensity relative to DMSO															
	+ / - Cisplatin								+ / - Bleomycin							
	DMSO		AZD1775		MA163		MA199		DMSO		AZD1775		MA163		MA199	
	-	+	-	+	-	+	-	+	-	+	-	+	-	+	-	+
Full-length PARP-1	1.00	0.80	1.63	1.54	2.77	2.10	13.2	14.7	1.00	1.35	1.33	3.19	3.06	2.85	2.47	1.52
Full-length Caspase-3	1.00	1.17	1.38	1.37	1.45	1.33	1.32	1.05	1.00	1.18	1.02	1.03	0.65	0.46	1.35	1.33

Unfortunately, as this is only an n = 1, the quantitation suggests that the relative levels of full-length PARP-1 are higher than DMSO in many of the treatments and does not highlight any trends seen visually from the blots, however this is likely due to the variable loading control and lack of repeats.

The treatment protocol from the previous western blot experiment was carried forward and A-253 (p53-null) and FaDu (p53-mutant) cells were treated prior to harvesting and staining with PI and Annexin V-FITC. Representative dot plots of the gating applied and the controls

for A-253 (p53-null) and FaDu (p53-mutant) can be seen in Figure 4.21A and Figure 4.22A,

respectively.

A
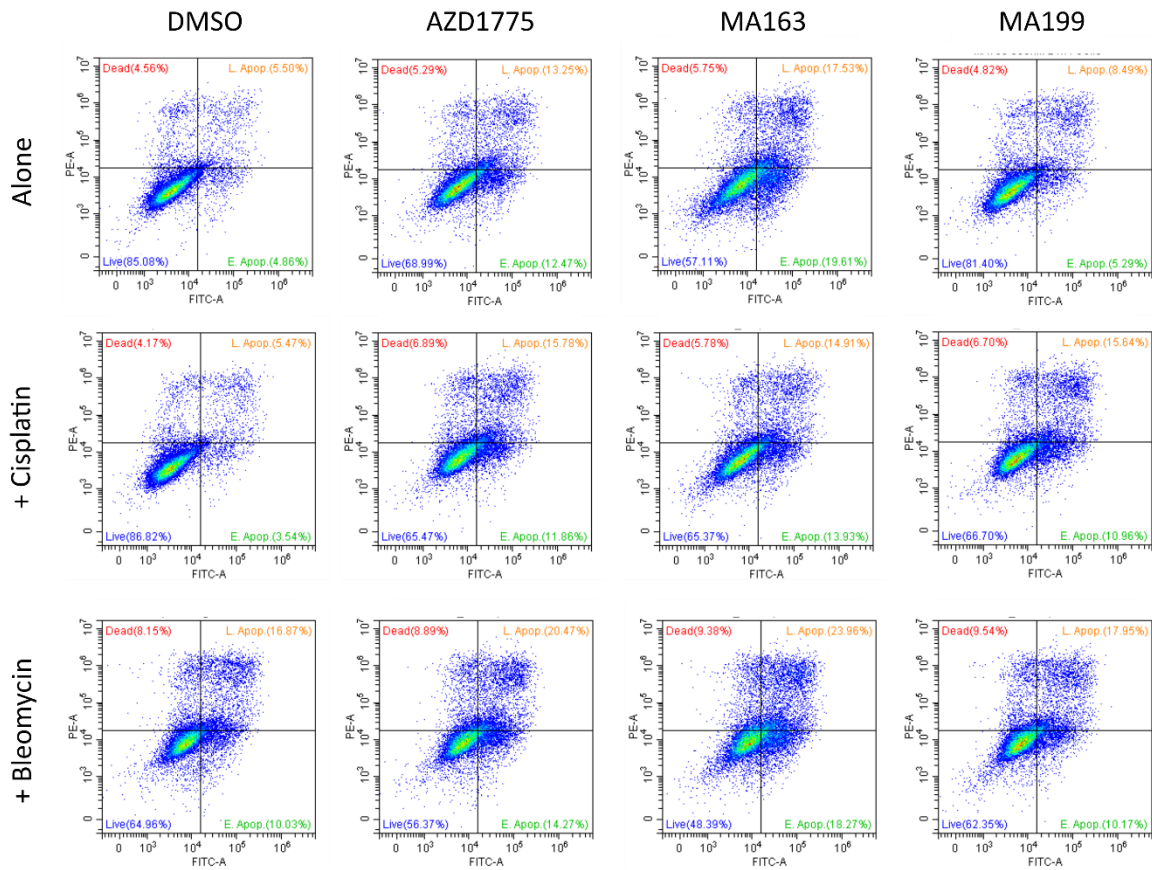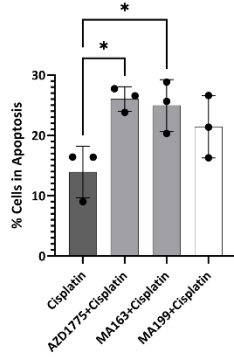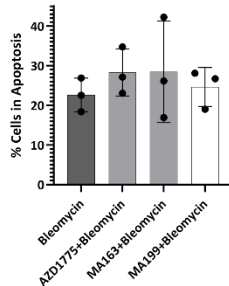
B **C** **D**
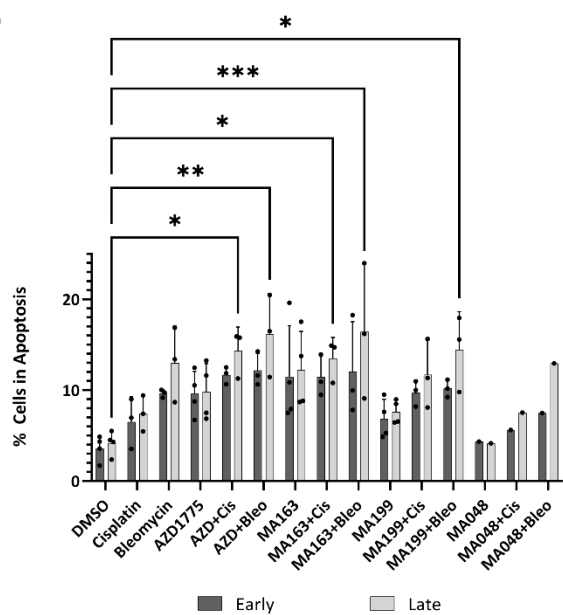
Figure 4.26 Apoptosis detection assay in A-253 cells by AZD1775, MA163 and MA199 treatments alone and in combination with cisplatin or bleomycin. Flow cytometry of A-253 cells stained with Propidium Iodide (PI) and Annexin V-FITC. (A) Representative dot plots for DMSO, AZD1775 (300 nM), MA163 (300 nM) and MA199 (300 nM) alone and with cisplatin (300 nM) or bleomycin (10μg/mL) for 24 h prior to staining. Bar graph showing the mean % cells in apoptosis of (B) cisplatin combination treatment or (C) bleomycin combination treatment ± SD of n = 3 biological repeats. (D) Bar graph showing the mean % cells in early or late apoptosis in each treatment condition. All graphs made with GraphPad Prism.

150

AZD1775 and MA163 co-treated with cisplatin significantly increased the proportion of apoptotic cells compared to cisplatin alone in A-253 (p53-null) (Figure 4.26B). This is a similar trend to the compounds being used as monotherapies, where all three increased the number of apoptotic cells, but AZD1775 and MA163 did this significantly in A-253 (p53-null) cells (Figure 4.21). In A-253 (p53-null) cells, the combination of bleomycin with AZD1775 and MA163 induces ~5% average gain of apoptotic cells and MA199 with bleomycin a 2% increase in comparison to bleomycin alone (Figure 4.26C). When plotting early and late apoptosis separately, we can see that both the early and late apoptotic populations in AZD1775 with bleomycin or MA163 with bleomycin increase from the bleomycin only treated, whereas only the late apoptosis population increases in MA199 with bleomycin cells compared to bleomycin only (Figure 4.26D). The significant inductions of apoptosis can be seen only in the late apoptotic populations; AZD1775 with cisplatin, AZD1775 with bleomycin, MA163 with cisplatin, MA163 with bleomycin and MA199 with bleomycin combinations significantly induced cells staining with both Annexin V and PI, suggestive of late apoptosis. However, necrotic cells present phosphatidylserine (the binding partner of Annexin V) on their surface as well as being able to be stained with propidium iodide. Perhaps, the significant increase of late apoptosis that we see in the combination treatments compared to DMSO is actually an increase in necrosis. Finally, first generation CRBN-recruiter, MA048, was used in combination with the chemotherapeutics once to test if it could induce apoptosis as well as the second generation PROTAC, MA163. MA048 could not induce programmed cell death as effectively as MA163 compared to DMSO in A-253 (p53-null) cells. The bleomycin combinations are better at inducing apoptosis in A-253 (p53-null) in comparison to this cisplatin combinations (Figure 4.26), which is corroborated by the PARP cleavage data (Figure 4.25).

In addition to the main compounds tested, we also tested the first generation PROTACs, MA048 and MA055, in FaDu (p53-mutant) cells as an n = 3. MA048 and MA055 combinations did not induce any more apoptosis in comparison to cisplatin or bleomycin alone (Figure 4.27 and 4.28). The second generation PROTACs significantly increased the proportion of apoptotic cells in comparison to their first-generation relative (MA163 to MA048 and MA199 to MA055). This is likely be as a result of the first generation PROTACs requiring a higher dose as these compounds are not as potent as the second generation. AZD1775 co-treatment with cisplatin and MA163 with cisplatin significantly increased apoptosis induction by 11% and MA199 co-treatment by 16% (Figure 4.27). The same trends were observed with the bleomycin co-treatments. The early and late apoptotic populations from this experiment were plotted separately, however the graph could not fit in the same figure. Therefore, this graph can be seen in Figure 4.28.
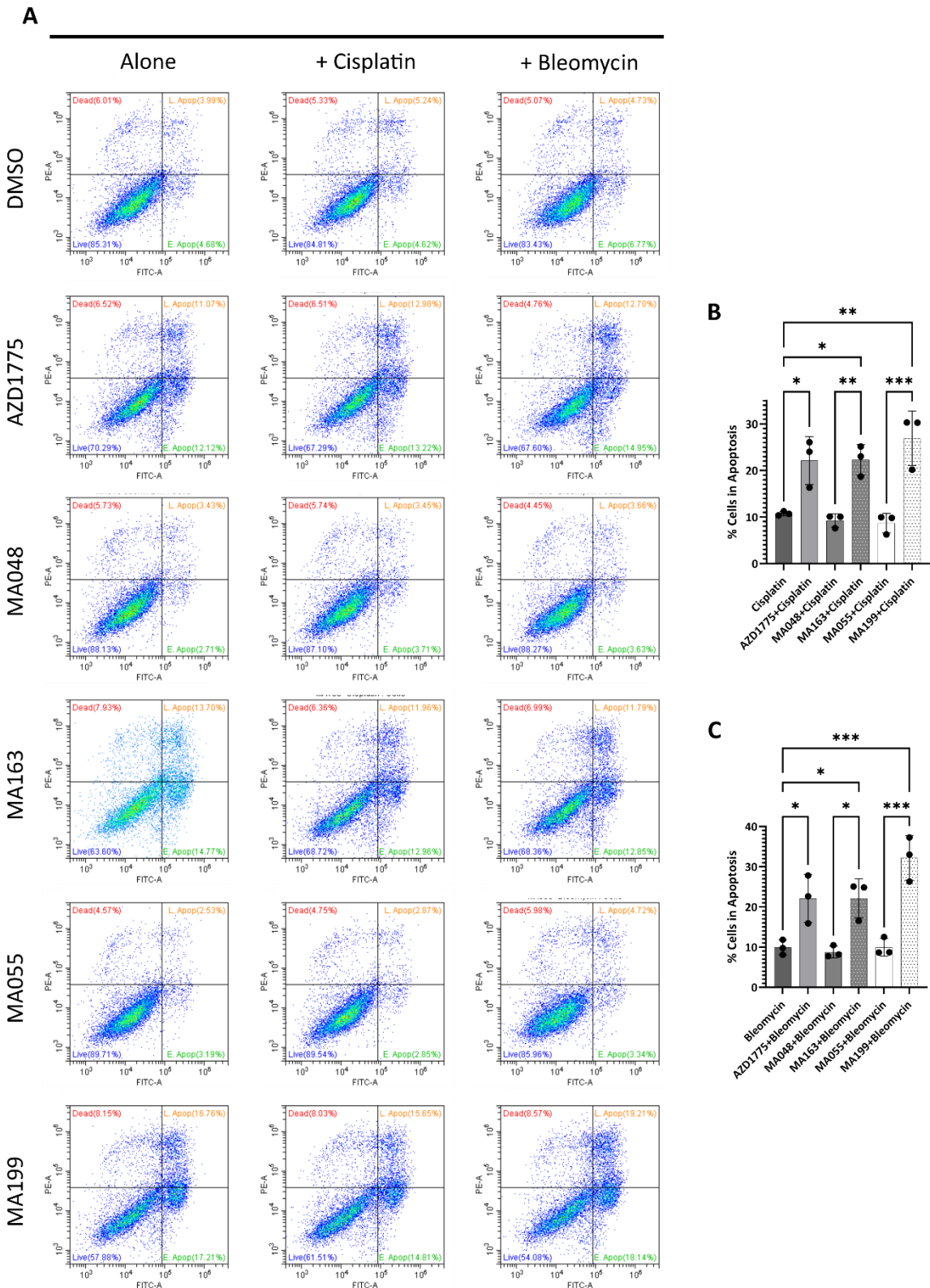
Figure 4.27 Apoptosis detection assay in FaDu cells by AZD1775, CRBN-recruiters (MA048 and MA163) and VHL-recruiters (MA055 and MA199) treatments alone and in combination with cisplatin or bleomycin. Flow cytometry of FaDu cells stained with Propidium Iodide (PI) and Annexin V-FITC. (A) Representative dot plots for treatments that were added for 24 h prior to staining. (B) Bar graph showing the mean % cells in apoptosis of cisplatin combination treatment ± SD of n = 3 biological repeats (GraphPad Prism). (C) Bar graph showing the mean % cells in apoptosis of bleomycin combination treatment ± SD of n = 3 biological repeats (GraphPad Prism).
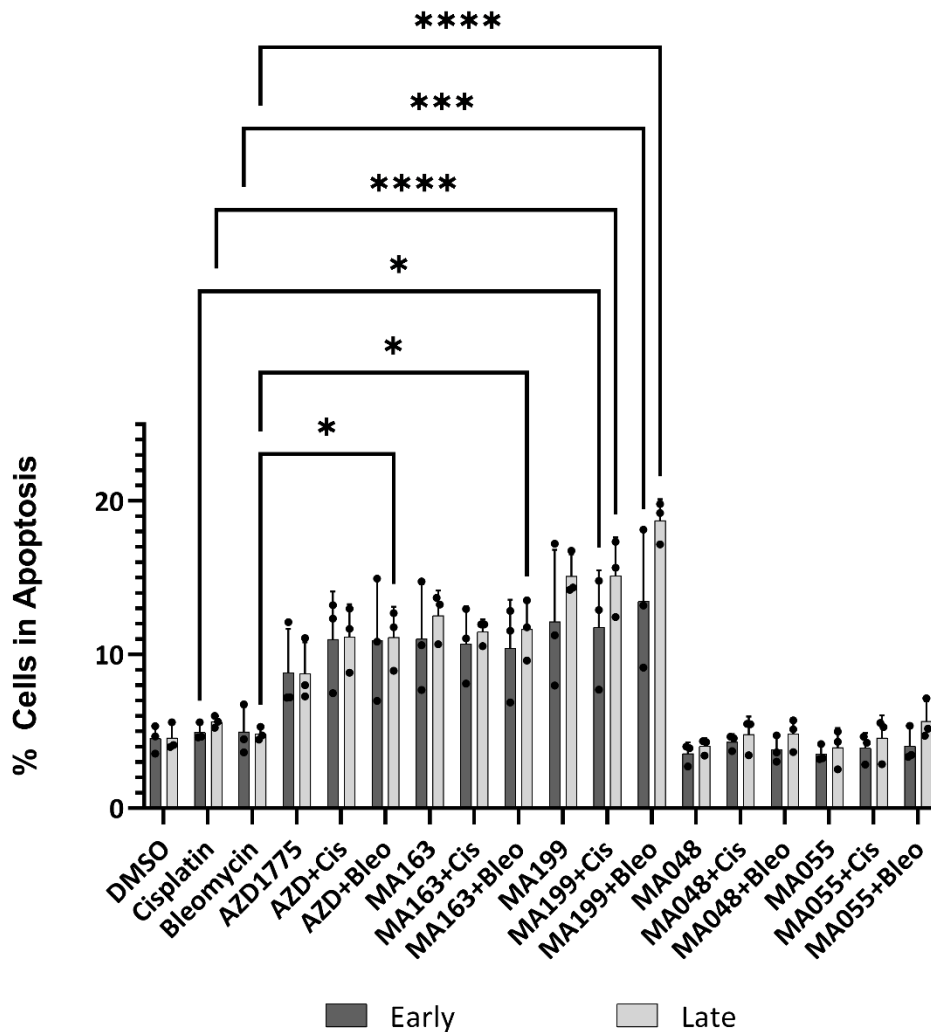
Figure 4.28 Bar graph showing induction of early and late apoptotic populations by chemotherapeutic combination treatments in FaDu cells. Data observed in figure 4.21 has been plotted differently to show the early and late apoptotic populations rather than the sum of both populations as a % apoptosis (GraphPad Prism).

There were many treatment conditions that caused significant apoptosis induction in FaDu (p53-mutant) cells and some of those comparisons have been shown on the bar graph above (Figure 4.28). AZD1775 and cisplatin, AZD1775 and bleomycin, MA163, MA199, MA199 and cisplatin and MA199 and bleomycin significantly increased the early apoptotic population in comparison to DMSO. AZD1775 and cisplatin or bleomycin, MA163 with cisplatin or bleomycin, MA199 with cisplatin or bleomycin and MA163 or MA199 alone all

significantly increased the late apoptotic population in comparison to DMSO. The combination of MA199 with cisplatin or bleomycin compared to the chemotherapeutic induced early and late apoptosis significantly, suggesting that MA199 may be the best PROTAC to use in FaDu (p53-mutant) cells (Figure 4.28).

There is a more intense band for PARP-1 cleaveage fragment at 89 kDa in FaDu (p53-mutant) in the Wee1-targeted cells alone and combination of Wee1-treatment and bleomycin compared to DMSO or bleomycin alone (Figure 4.25). This corresponds with the flow cytometry data that the combination of AZD1775, MA163 or MA199 with bleomycin or cisplatin induces more apoptosis than using the chemotherapeutic as a single agent. To aim to summarise the data from these apoptosis detection assays, Table 4.16 and Table 4.17, for A-253 (p53-null) and FaDu (p53-mutant) respectively, have been created. It highlights that when considering only the flow cytometry data, A-253 (p53-null) are most sensitive to AZD1775 with 12 Gy irradiation and least sensitive to cisplatin treatment only (Table 4.16). AZD1775 and 12 Gy irradiation induces the most apoptosis in both UM-SCC-6 (p53-WT) and A-253 (p53-null).

Table 4.16 Summary table of mean % cells in apoptosis of Wee1-targeting drugs as a monotherapy and combinatorial strategy with radiotherapy or chemotherapy in A-253 cells. A-253 were treated with Wee1-targeting compounds alone and in combination with 12Gy irradiation, cisplatin or bleomycin for 24 h (Figures 4.21, 4.22 and 4.24) (n = 3). *Experiments where n = 2.

Treatment	Mean % cells in apoptosis ± SD			
	DMSO	12 Gy	300 nM Cisplatin	10 µg/mL Bleomycin
DMSO	7.99 ± 2.33	28.7 ± 11.5*	13.9 ± 4.27	22.6 ± 4.25
AZD1775	20.1 ± 4.10	32.6 ± 9.57*	26.0 ± 2.01	28.3 ± 5.93
MA163	24.3 ± 9.20	29.3 ± 3.92*	24.9 ± 4.32	28.4 ± 12.8
MA199	14.8 ± 2.52	-	21.4 ± 5.16	24.6 ± 4.89

Unfortunately, we were unable to conduct the Wee1-targeting compounds with irradiation flow cytometry experiment in FaDu (p53-mutant), therefore, according to this data, the most effective treatment for FaDu (p53-mutant) cells is MA163 as a single agent treatment (Table 4.17). When only considering the second generation PROTACs and AZD1775, the least effective strategy at inducing apoptosis is AZD1775 alone.

Table 4.17 Summary table of mean % cells in apoptosis of Wee1-targeting drugs as a monotherapy and combinatorial strategy with chemotherapy in FaDu cells. FaDu were treated with Wee1-targeting compounds alone and in combination with 12Gy irradiation, cisplatin or bleomycin for 24 h (Figures 4.22 and 4.27) (n = 3).

Treatment	Mean % cells in apoptosis ± SD		
	DMSO	300 nM Cisplatin	10 µg/mL Bleomycin
DMSO	9.24 ± 1.64	10.7 ± 0.46	9.92 ± 1.88
AZD1775	17.6 ± 4.83	22.1 ± 5.14	22.1 ± 5.97
MA048	7.72 ± 1.00	9.26 ± 1.43	8.80 ± 1.47
MA163	23.6 ± 5.08	22.3 ± 3.29	22.1 ± 4.88
MA055	7.65 ± 1.48	8.68 ± 2.09	9.96 ± 2.22
MA199	27.2 ± 5.87	26.9 ± 5.84	32.2 ± 5.52

4.3.5 Discussion

This chapter showed that targeting of Wee1 with AZD1775 or PROTACs causes a progressive loss of cell viability over time in UM-SCC-6 (p53-WT), A-253 (p53-null) and FaDu (p53-mutant) cells regardless of p53-status. MA199 exhibits EC50 values of ~ 100 nM in all cell lines (FaDu is the most sensitive), MA163 gives values of 134 nM to 308 nM (UM-SCC-6 is the most sensitive) and AZD1775 shows values of 31 nM to 149 nM (UM-SCC-6 is the most sensitive) at 72 h (Tables 4.1 and 4.2). 72 h appears to be the optimal time point for the compounds to result in the most effective inhibition of cell proliferation however, it could be that it takes a few turns of the cell cycle in order to see the effects of abrogating the G2/M checkpoint. This becomes apparent when we investigated the effect that the

compounds had alone and in combination with radiation or chemotherapeutics on colony formation of the cells.

Previous studies have shown that AZD1775 can sensitize oesophageal and HPV-negative HNSCC cancer cells to radiotherapy (Oetting et al., 2023; Yang et al., 2020). Most of the cell lines tested in these studies (apart from AGS) harboured p53 mutations. Our data showing AZD1775 sensitizing two further p53-deficient head and neck cell lines, A-253 and FaDu, support the findings of these publications. Furthermore, Yang et al., 2020 found no radiosensitization of p53-proficient cell line, AGS, when treated with AZD1775 which corresponds with our data where UM-SCC-6 (p53-WT) is also not radiosensitized. Wee1 PROTACs can radiosensitize cancer cells, however experiments including a larger range of *TP53* mutant cell lines need to be done to identify if the enhanced selectivity of Wee1 degradation by PROTACs increases radiation-induced cell death. To be able to determine if the enhancement of radiation-induced cell death by Wee1 PROTACs is a cell line specific observation in A-253 (p53-null) cells or if this is due to p53-deficiency, a p53 addback cell line could be created or more p53-null and p53-mutant cell lines should be tested. AZD1775 did not enhance radiation-induced cell death in UM-SCC-6 (p53-WT) cells but was able to enhance cytotoxicity of IR in A-253 (p53-null) and FaDu (p53-mutant) cells. Therefore, Wee1 inhibition could be considered more effective across varying cell types than Wee1 degradation with PROTACs when considering the combination with radiation.

Cisplatin is commonly used for head and neck cancers however, cisplatin-resistance is the main cause of relapse and death (Yamamoto et al., 2022). It is now standard practice to use cisplatin in combination with radiation or another chemotherapeutic in locally advanced HNSCC (Osman et al., 2015). Studies have demonstrated that AZD1775 chemosensitizes

p53-mutant head and neck cancer to cisplatin *in vivo* and *in vitro* and that AZD1775 can overcome cisplatin resistance (Osman et al., 2015; Yang et al., 2022). This correlates with our data in A-253 (p53-null) and FaDu (p53-mutant) cells. UM-SCC-17B and UM-SCC-2 have no reported p53 mutations and still showed that AZD1775 can chemosensitize the cells to cisplatin (Yang et al., 2022), similar to our findings in UM-SCC-6 (p53-WT) (Figure 4.7). From our data, we can conclude that the enhancement of cisplatin-induced cell death is not p53-dependent, whereas radiation-induced cell death is. The best compound to induce cell death was MA199 across all three cell lines and it would be interesting to investigate if VHL-recruiter Wee1 PROTACs are more effective with cisplatin treatment compared to AZD1775 or CRBN-recruiter Wee1 PROTACs in more cell types. A 2016 study (Lai et al., 2016) determined that CRBN-recruiting PROTACs against BCR-ABL exhibited better efficacy compared to VHL-recruiting PROTACs. Furthermore, resistance towards VHL-recruiting PROTACs has been reported more frequently than resistance to CRBN-recruiting PROTACs (Cieślak and Słowianek, 2023; Lai et al., 2016; Zhang et al., 2019). It seems that CRBN-recruiters are more favoured, even though our work suggests that the VHL-recruiter is more potent, however potency will be target specific. Perhaps the protein of interest is better degraded by certain E3 ligases and it could vary between cell lines and this has been when using BRD4-PROTACs, dBET1 (a CRBN-recruiter) and MZ1 (a VHL-recruiter), in multiple cancer types (Luo et al., 2022). This could explain why we see such variability between the PROTACs enhancing radiosensitization in A-253 (p53-null) but having no effect in FaDu (p53-mutant). Although there has been reported crosstalk between ATR-Chk1 and the ATM-Chk2 pathway (Maréchal and Zou, 2013), Wee1 inhibition or degradation will directly affect the downstream signalling of the ATR-Chk1 pathway, therefore, as cisplatin would cause ATR

activation, this may explain why this combination caused increased cell death across cell lines regardless of p53-status.

In A-253 (p53-null) and UM-SCC-6 (p53-WT) cells, there have been no previous reports whether irradiation, cisplatin or bleomycin treatment causes PARP-1 or caspase-3 cleavage. FaDu (p53-mutant) cells have shown that PARP-1 and caspase-3 cleavage can be induced by cisplatin treatment, however these treatments were either 33- or 1000-fold higher than the concentration that we tested (Chen et al., 2013; Li et al., 2022a). Therefore, the observation of PARP-1 and caspase-3 cleaved fragments is likely much more apoptosis induction from a greater treatment dose used. Our data suggest that AZD1775 and MA163 can induce apoptosis in the absence of IR, irrespective of p53 status (sections 4.3.3.3 and 4.3.4.3). In addition, less total PARP-1 was observed in AZD1775, MA163 and MA199 treatments as they cause apoptosis in the absence of cisplatin and bleomycin (Figures 4.12 and 4.25). The flow cytometry data in the cell lines is consistent with the western blot data that the combinations of Wee1-targeted treatment with chemotherapeutic is more effective at inducing apoptosis in comparison to DMSO or the chemotherapeutic alone, regardless of p53 status. However, the p53-deficient cell lines do see higher levels of apoptosis compared to p53-proficient cell line, UM-SCC-6 (p53-WT). Although the combination treatments increase the proportion of apoptotic cells compared to DMSO or the genotoxic agent alone, there is not much gain in apoptotic cells compared to the Wee1-targeting compound alone. Perhaps the action of inhibiting or degrading Wee1 is causing the initial induction of cell death rather than the genotoxic treatment. In both p53-deficient cells, the higher proportion of apoptotic cells was mainly as a result of an increase in late apoptotic cells, that stain for both Annexin V and PI. Necrotic cells will expose phosphatidylserine (PS), the substrate for Annexin V, on their surfaces and positively stain for PI, similarly to late

apoptotic cells (Furuta et al., 2021). Therefore, it would be interesting to investigate if AZD1775, MA163 and MA199 are inducing necrosis. Apoptosis is a complex mechanism, therefore testing these cells at more time points would enable us to draw more conclusions about how these compounds are causing cell death.

The data presented here has provided some preliminary insight into the mode of death in head and neck Wee1-deficient cancer cells however, investigations into other apoptotic and autophagic proteins, such as Bax, Beclin and LC-3, needs to be undertaken.

The impact of Wee1 PROTACs on HNSCC compared to Wee1i, AZD1775, on mitosis and the DNA damage response will be investigated in chapter 5.

5 Consequences of Wee1 PROTACs for mitosis and the DNA damage response

5.1 Introduction

5.1.1 The impact of p53 status on the effect of AZD1775 treatment on the cell cycle

Inhibition or degradation of Wee1 has shown to be cytotoxic as a single agent and has sensitized HNSCC cells to genotoxic agents in the previous chapter. Here we will highlight how the abrogation of the G2/M checkpoint by Wee1 inhibition and subsequent DDR signalling has been investigated.

It has been reported that AZD1775 abrogates radiation-induced G2/M arrest in oesophageal cancers (Yang et al., 2020). In FLO1 and OE33, both p53-mutant cell lines, 100 nM AZD1775 treatment decreased the proportion of cells in G2/M, indicating enforcement of cell cycle progression. Furthermore, AZD1775 radiosensitized both cell lines to X-ray irradiation and caused a significant decrease in radiation-induced G2/M arrest. AZD1775 with radiation also induced multi- and micro-nucleated cells, which are indicative of mitotic catastrophe.

AZD1775 has been reported to increase the number of cells entering normal mitosis and the rate of premature mitosis in Calu6 and H1703 KRAS-mutant cells, both p53-mutant lung cancer cell lines (Parsels et al., 2018). The % phospho-Histone H3 (Ser10) positive cells increased compared to irradiation alone when the combination of radiotherapy was used

with AZD1775. This implies that AZD1775 releases from a radiation-induced G2/M arrest, similarly to the Yang et al (2020) study in oesophageal cell lines discussed above.

AZD1775 radio- and chemosensitized hepatocellular carcinoma cells, Hep3B, Huh7 and HepG2 and induced replication stress, indicated by pan-nuclear γH2AX staining (Cuneo et al., 2016). Furthermore, AZD1775 released the radiation-induced G2/M checkpoint arrest in p53-deficient cell lines but not in the p53 wild-type cell line.

These three studies demonstrate that inhibition of Wee1 abrogates the radiation-induced G2/M checkpoint across multiple cancer cell lines. AZD1775 alone enforces mitotic progression compared to control cells. Most cancer types harbour p53 mutations, therefore most of these studies have used p53-mutant cell lines. It would be interesting to see whether, like HepG2 cells, p53 wild-type HNSCC cell lines show a similar absence of radiation-induced G2 arrest on treatment with AZD1775.

The increased specificity of Wee1 PROTAC, ZNL-02-096, compared to AZD1775 leads to an increase of MOLT4 cells in G2/M in ZNL-02-096-treated cells compared to AZD1775-treated cells (Li et al., 2020). The improved potency is due to the selective CRBN-dependent degradation of Wee1, and suggests that this is more advantageous to abrogate the G2/M checkpoint compared to AZD1775.

5.1.2 Activation of DDR by AZD1775

Abrogating the G2/M checkpoint and enforcing mitotic progression by targeting Wee1 has shown to be therapeutically advantageous (Mendez et al., 2018), however AZD1775 has also

shown to cause replication stress and inhibit DNA damage repair (Kausar et al., 2015; Pfister et al., 2015).

AZD1775 treatment leads to enhanced levels of γH2AX by immunoblot and pan-nuclear γH2AX was observed after 6 hr in hepatocellular carcinoma cells, suggesting replication fork collapse (Cuneo et al., 2016). AZD1775 has also shown to increase γH2AX levels in a wide variety of cancer types, including ovarian cancer, HNSCC and biliary tract cancer (Kao et al., 2017; Oku et al., 2018; Seo et al., 2022). Single agent AZD1775 appears to activate γH2AX at a similar intensity to AZD1775 with irradiation in oesophageal cancer cells (Yang et al., 2020) and it will be interesting to investigate this in other HNSCC cells with varying p53-status. Furthermore, it is well reported that AZD1775 treatment also activates DDR pathway proteins, such as Chk1 and ATR in various cancer types (Bukhari et al., 2019; Jin et al., 2018; Zhou et al., 2015).

5.2 Aims and objectives

In this chapter, the G2/M checkpoint will be abrogated using AZD1775 and Wee1 PROTACs and the impact of this on the cell cycle will be evaluated in HNSCC. It will also be determined if this causes a synthetic lethality effect in p53-deficient cells that lack a functional G1/S checkpoint. In addition, the activation of DDR pathways and presence of DNA damage as a result of Wee1-targeting compounds will be investigated. This will be assessed via the following aims:

1. Investigate how inhibition of Wee1 by AZD1775 changes the population of HNSCC cells in each cell cycle stage and to evaluate if more selective targeting of Wee1 by PROTACs has a different impact.

2. Determine if using a combination of ionizing radiation with Wee1-targeting treatments changes how cells progress through the cell cycle compared to the monotherapies and compare cell lines with differing p53-status.

3. Assess how targeting of Wee1 activates DDR pathways and causes DNA damage alone and in combination with ionizing radiation. The responses to these treatments will be compared between p53-proficient and p53-deficient cell lines.

5.3 Results and discussion

At the end of the second year of this project, generator issues led to the loss of our cell irradiator, therefore some of the cell cycle analysis experiments could only be carried out as an n = 1. This is the reason for introducing bleomycin treatments to the project, as bleomycin is a radiomimetic and induces DSBs.

5.3.1 Effects of Wee1 PROTACs on p53-proficient HNSCC cell lines

5.3.1.1 Cell cycle stage analysis of Wee1 PROTACs compared to AZD1775

In the previous chapter, it was observed that targeting Wee1, whether by classic inhibition or degradation, causes the same outcome on cytotoxicity or mode of death. To distinguish how both methods of targeting Wee1 affect the cell cycle, cells underwent monotherapy treatments for 18 h, 24 h or 48 h. Cells were treated with a DMSO control, AZD1775, MA163

or MA199 at 300 nM for the above-mentioned times. Cells were then incubated with 10 µM

EdU for 1 h before trypsinization and staining with Alexa Fluor™ 647 azide, for EdU

incorporation, and DAPI for DNA content (Figure 5.1). Cells were gated as seen in Figure 2.1.
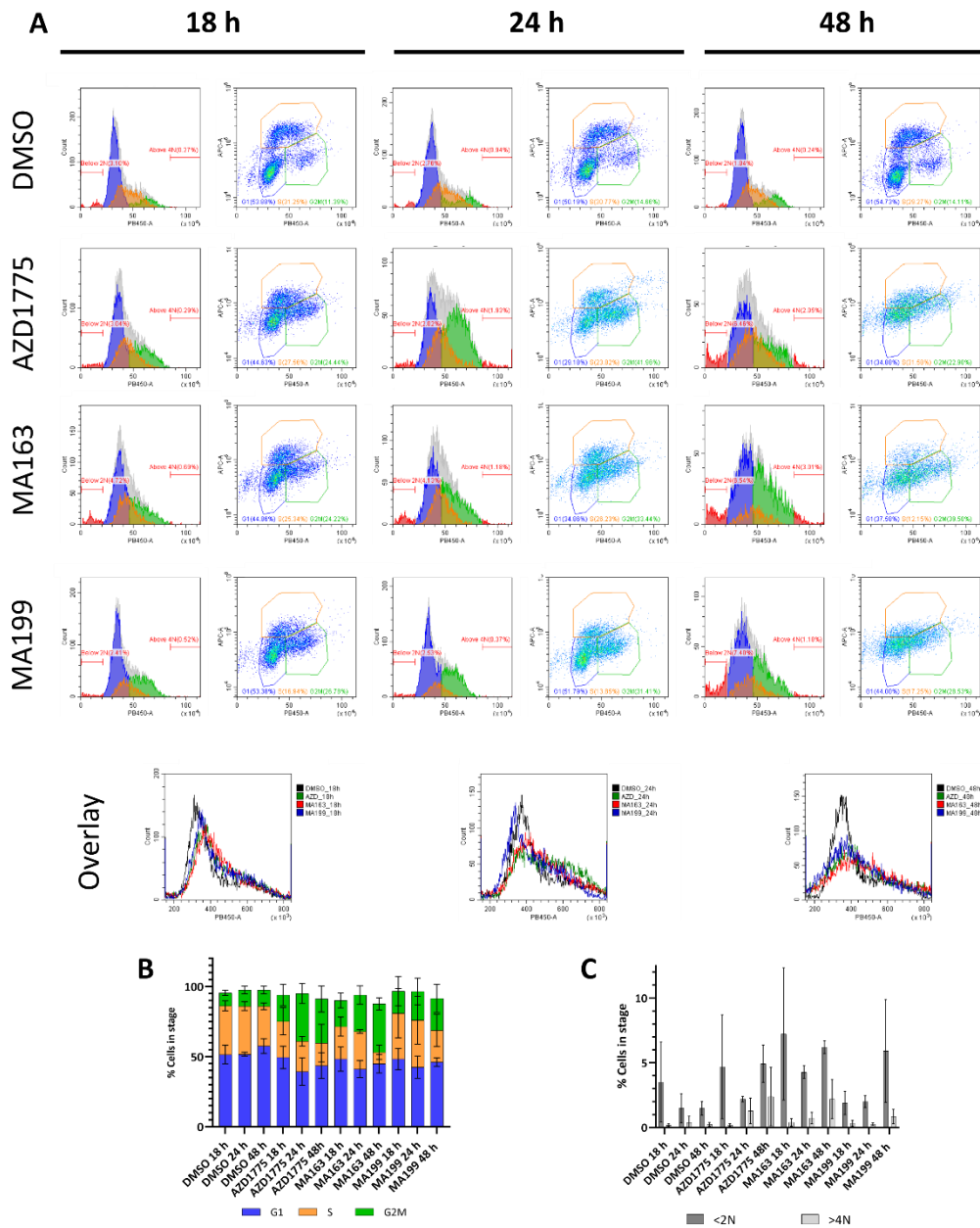
Figure 5.1 Cell cycle stage analysis of Wee1-targeting treatments on UM-SCC-6 cells over a 48 h time course.
Flow cytometry of UM-SCC-6 cells stained with Alexa Fluor™ 647 azide for EdU incorporation and DAPI for DNA content. (A) Representative dot plots and DNA content histograms for monotherapy treatments at 300 nM for 18 h, 24 h or 48 h, in addition to overlay histograms of the treatments at those time points. (B) Stacked bar graph showing mean ± SD of n = 3 biological replicates of cells in G1, S and G2/M (GraphPad Prism). (C) Bar graph showing mean ± SD of n = 3 biological replicates of cells with <2N or >4N DNA content (GraphPad Prism).

AZD1775, MA163 or MA199 treatment resulted in a progressive decrease in the actively

replicating S-phase population of cells over time in UM-SCC-6 (p53-WT) cells (Figure 5.1A).

Furthermore, when comparing treatments to the DMSO control, there was a loss of cells in G1 but an increase in G2/M phase (Figure 5.1B). However, as can be seen on the representative dot plots, over a longer time period of the compounds, there was a loss of clear defined G1 and G2/M populations. This suggests an increase of cells with 2<N<4 DNA content and replication stress. The G2/M gate includes cells that are in S phase, according to DNA content (2<N<4), however they are not incorporating EdU which suggests these cells are in S phase arrest. Therefore, targeting Wee1 does not cause a G1/S checkpoint arrest in this p53-proficient cell line. To test the hypothesis that 4 Gy irradiation and Wee1-targeting treatment would induce arrest at the G1/S checkpoint, cell cycle flow cytometry was performed (Figure 5.2).
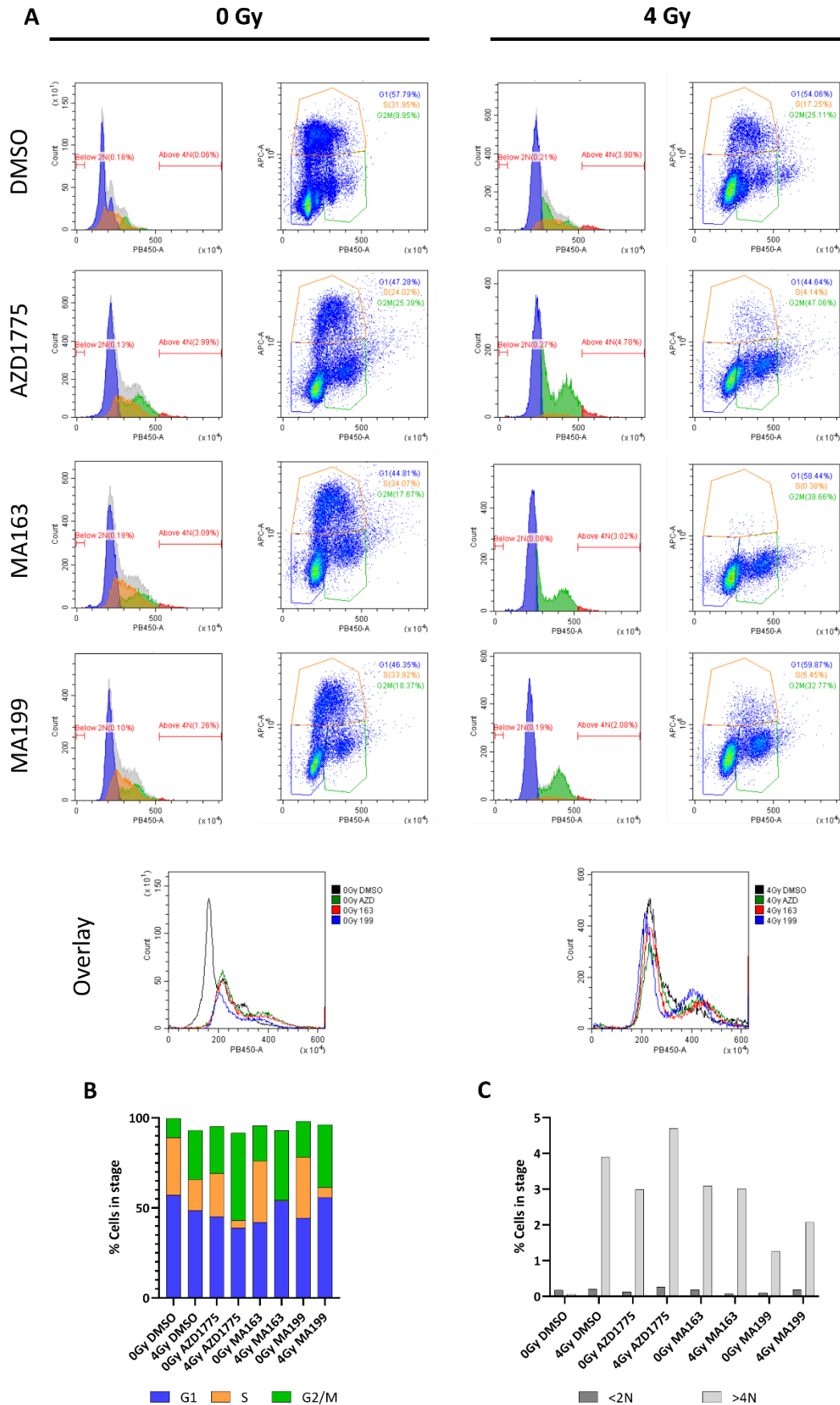
Figure 5.2 Cell cycle stage analysis of Wee1-targeting treatments alone and in combination with irradiation on UM-SCC-6 cells. Flow cytometry of UM-SCC-6 cells stained with Alexa Fluor™ 647 azide for EdU incorporation and DAPI for DNA content. (A) Representative dot plots and DNA content histograms for monotherapy treatments at 300 nM for 24 h or combination treatments with 300 nM compound and 4 Gy irradiation for 24 h, in addition to overlay histograms of the treatments at 0 Gy and 4 Gy. (B) Stacked bar graph showing values of n = 1 of cells in G1, S and G2/M (GraphPad Prism). (C) Bar graph showing values of n = 1 of cells with <2N or >4N DNA content (GraphPad Prism).

After 24 h, a increase in DNA content of all the cells can be seen in AZD1775, MA163 and MA199 treatments (Figure 5.2BA). This could be for a number of reasons. More cells could have grown in the DMSO control compared to the treated samples, as chapter 4 identified that, as monotherapies, AZD1775, MA163 and MA199 cause cytotoxicity. Potentially this is why the DAPI signal is showing up at a different part of the X-axis. At 0 Gy, AZD1775 causes the proportion of S phase cells to decrease from 32% to 24%, a loss of G1 cells from 57% to 45% and an increase in G2/M cells from 11% to 26% compared to the DMSO control. Treatment with MA163 or MA199 leads to a loss of G1 (from 57% to 42% and 44% for MA163 and MA199, respectively) and an increase in G2/M cells from 11% to 20% for both compounds, but the population of actively replicating S phase cells remains similar to the control (Figure 5.2B). When UM-SCC-6 (p53-WT) cells were irradiated, the cell cycle profile showed some similarities to using the Wee1-targeting drugs alone. AZD1775 with irradiation led to a large loss of actively-replicating (EdU-incorporating) cells. The same trend was seen in MA163 with irradiation and MA199 with irradiation. Furthermore, the combination treatments resulted in a bigger proportion of >4N DNA content cells compared to the single agents, except MA163 with irradiation compared to MA163 displayed the same proportion of >4N DNA content (Figure 5.2C). The overall trend, as can be observed by the histogram overlays, is that single agent targeting of Wee1 causes the whole population to display an increase in DNA content and the combination treatments result in a drop-in replicating S-phase cells compared to 4 Gy alone.

This experiment was also performed in UM-SCC-74A (p53-WT) cells to aim to support the trends seen in UM-SCC-6 (p53-WT) cells. Cells were treated and stained in the same way as can be seen in Figure 5.2 (Figure 5.3).
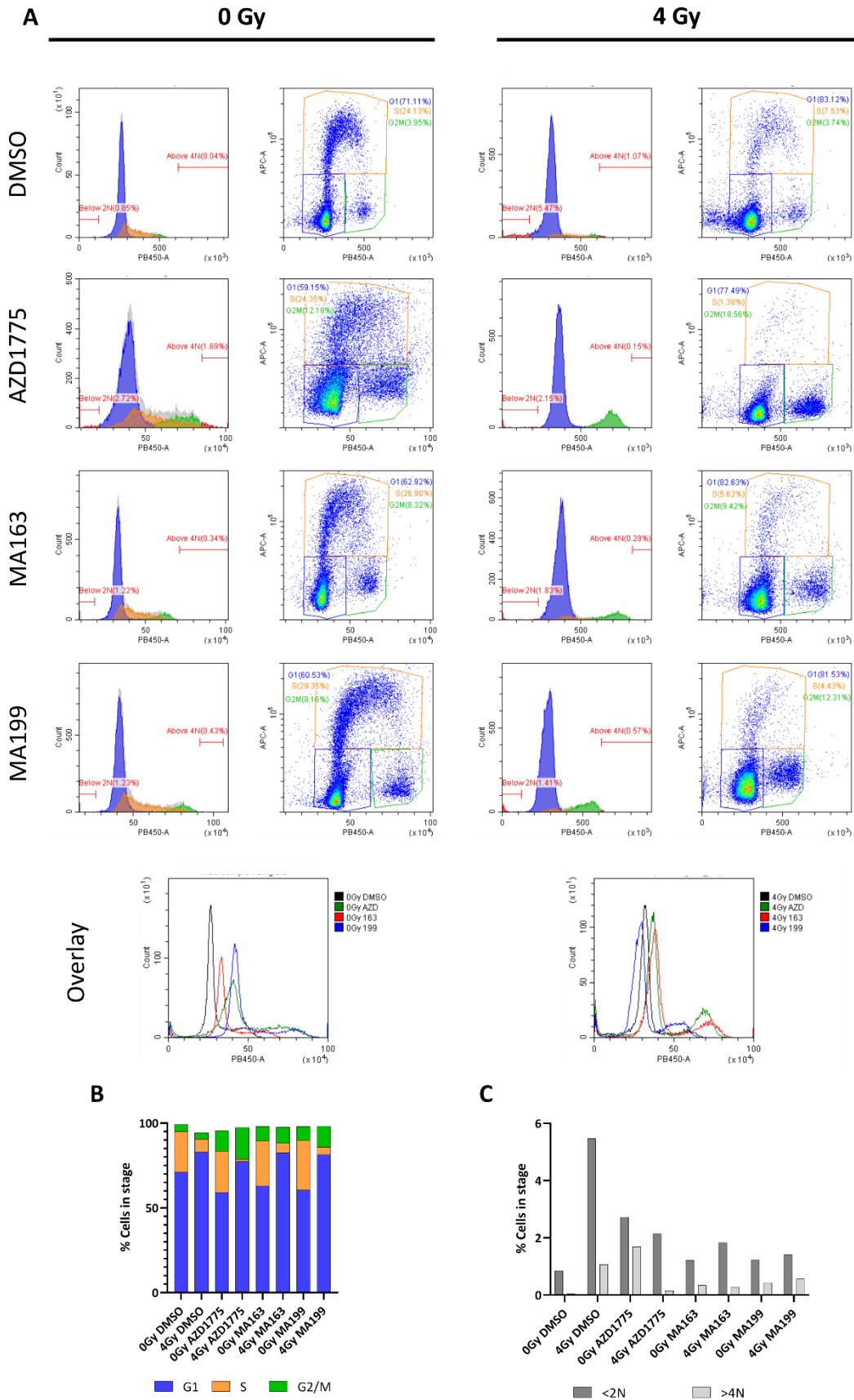
Figure 5.3 Cell cycle stage analysis of Wee1-targeting treatments alone and in combination with irradiation on UM-SCC-74A cells. Flow cytometry of UM-SCC-74A cells stained with Alexa Fluor™ 647 azide for EdU incorporation and DAPI for DNA content. (A) Representative dot plots and DNA content histograms for monotherapy treatments at 300 nM for 24 h or combination treatments with 300 nM compound and 4 Gy irradiation for 24 h, in addition to overlay histograms of the treatments at 0 Gy and 4 Gy. (B) Stacked bar graph showing values of n = 1 of cells in G1, S and G2/M (GraphPad Prism). (C) Bar graph showing values of n = 1 of cells with <2N or >4N DNA content (GraphPad Prism).

170

This experiment could not use gates from 0 Gy DMSO and apply those to the other samples due to issues with DAPI saturation. In treated samples, there will have been more cytotoxicity which would have caused a lower number of cells in the sample. This resulted in variable DAPI saturation across the samples. Due to this, each sample needed to be individually gated. UM-SCC-74A (p53-WT) appear to have a radiation-induced G1 arrest by ionizing radiation with a large decrease of S-phase and G2/M phase cells compared to DMSO, different from the other p53-WT cell line tested (Figure 5.3). This suggests that, in UM-SCC-6 (p53-WT), the radiation-induced G1 block does not rely on p53 function alone. The addition of AZD1775, MA163 and MA199 with irradiation results in a decrease in actively replicating cells and a larger proportion of G2/M compared to 4 Gy alone.

Overall, it is clear that these treatments are causing replication stress alone in p53 wild-type HNSCC cells and could potentially be leading to arrest of cells at the spindle assembly checkpoint in mitosis. To test these hypotheses, activation of ATR-Chk1 pathway, micronuclei detection and γH2AX intensity were investigated.

5.3.1.2 Activation of the DDR by Wee1-targeting treatments in wild-type TP53 HNSCC cells

Immunoblotting of DNA damage repair proteins Chk2 and Chk1 were performed in UM-SCC-6 (p53-WT) cells to determine if targeting Wee1 by inhibition, with AZD1775, or degradation, by Wee1 PROTACs, lead to activation of the DDR. This was investigated alone and with radiotherapy or chemotherapeutics, cisplatin and bleomycin. Cells were treated with 300 nM of Wee1-targeting drugs for 2 h prior to the addition of radiation, cisplatin or bleomycin for a further 1 h. Lysates were made and run on a western blot (Figure 5.4).
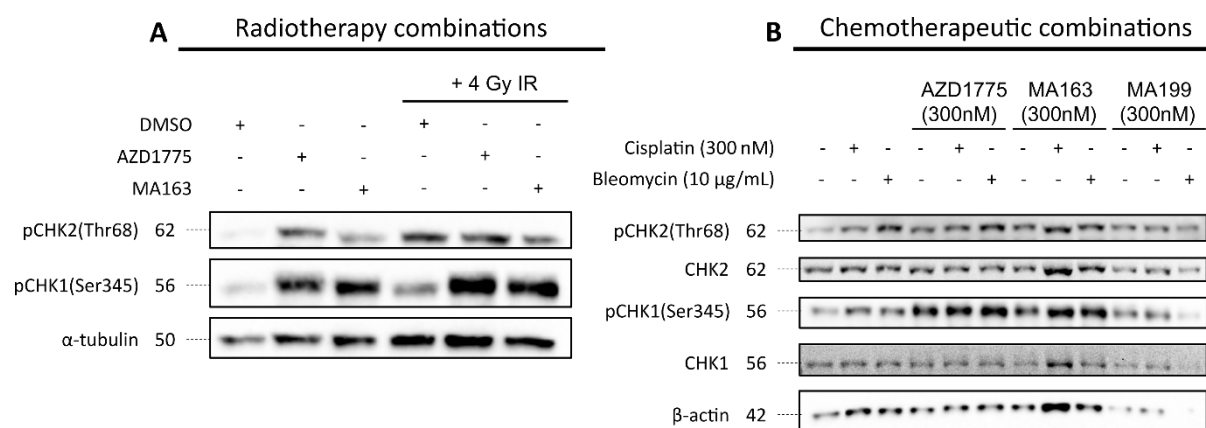
Figure 5.4 Activation of Chk1 and Chk2 by AZD1775. MA163 and MA199 as single agents and combinatorial treatments with irradiation, cisplatin or bleomycin in UM-SCC-6 cells. Cells were treated with 300 nM compounds for 3 h alone or in addition to 4 Gy irradiation, 300 nM cisplatin or 10 µg/mL bleomycin. Lysates were produced, ran and blots were probed for (A) pChk2(Thr68), pChk1(Ser345) and α-tubulin as a loading control or (B) pChk2(Thr68), Chk2, pChk1(Ser345), Chk1 and β-actin as a loading control. (A) Western blot where AZD1775 and MA163 were added to cells alone or in combination with 4 Gy IR (n = 1). (B) Western blot where AZD1775, MA163 or MA199 were added to cells alone or with cisplatin or bleomycin (n = 1).

Single treatment of UM-SCC-6 (p53-WT) cells with AZD1775 caused a 6.61-fold increase of phosphorylation of Chk2 at Threonine-68 compared to the DMSO control, indicative of activation of the ATM-Chk2 pathway (Figure 5.4A and Table 5.1). This trend was detected visually in Figure 5.4B and a further repeat of this would allow for better quantitation of

band intensity. Furthermore, total Chk1 or Chk2 protein should be blotted for to quantify the increase in phosphorylated protein. Increased activation of Chk1 was also seen and quantified from both blots (Figure 5.4). MA163 and MA199 showed an increase of pChk1 and pChk2 compared to DMSO. When AZD1775 and MA163 were used in combination with 4 Gy irradiation, there was a decrease in relative pChk2 (Thr68) levels from 5.02 in IR alone to 3.67 or 2.84 in the AZD1775 combination or MA163 combination, respectively (Table 5.1). Whereas, there was an increase in relative pChk1 (Ser345) levels when targeting Wee1 and inducing DSBs (Figure 5.4A).

Table 5.1 Quantitation of pChk1 and pChk2 from Figure 5.4A. Band intensity was calculated, normalised to tubulin and made relative to DMSO.

Treatment condition	pChk2 (Thr68)	pChk1 (Ser345)
DMSO	1.00	1.00
AZD1775	6.61	4.38
MA163	3.59	4.13
DMSO + 4 Gy	5.02	1.27
AZD1775 + 4 Gy	3.67	3.70
MA163 + 4 Gy	2.84	4.72

These same trends were seen with the chemotherapy combinations of AZD1775 however, MA163 and cisplatin or MA163 and bleomycin resulted in more intense bands for pChk1 and pChk2 compared to either MA163, cisplatin or bleomycin alone (Figure 5.4B). Unfortunately, the quantitation of these bands did not corroborate the qualitative trend, however this was only n = 1 and would need repeats (Table 5.2).

Table 5.2 Quantitation of pChk1 and pChk2 compared to total Chk1 and Chk2 respectively in Figure 5.4B.
Band intensity was calculated, normalised to tubulin and made relative to DMSO.

Protein	Band intensity relative total Chk1 or Chk2															
	- / + Cisplatin								- / + Bleomycin							
	DMSO		AZD1775		MA163		MA199		DMSO		AZD1775		MA163		MA199	
	-	+	-	+	-	+	-	+	-	+	-	+	-	+	-	+
pChk2 (Thr68)	0.56	0.46	0.56	0.62	0.62	0.41	0.71	0.54	0.56	0.61	0.56	1.08	0.62	0.47	0.71	0.83
pChk1 (Ser345)	1.13	1.82	5.99	6.14	5.80	2.65	2.90	1.98	1.13	2.49	5.99	7.55	5.80	4.05	2.90	1.13

These blots suggest activation of the ATR-Chk1 pathway is achieved by targeting Wee1 alone. The levels of pChk1 are similar in the single agent treatments and combination treatments with ionizing radiation, implying that Wee1 targeting is damaging to cells without a further genotoxic agent. To corroborate this data, immunoblotting of γH2AX was performed in UM-SCC-6 (p53-WT) and UM-SCC-74A (p53-WT) (Figure 5.5).
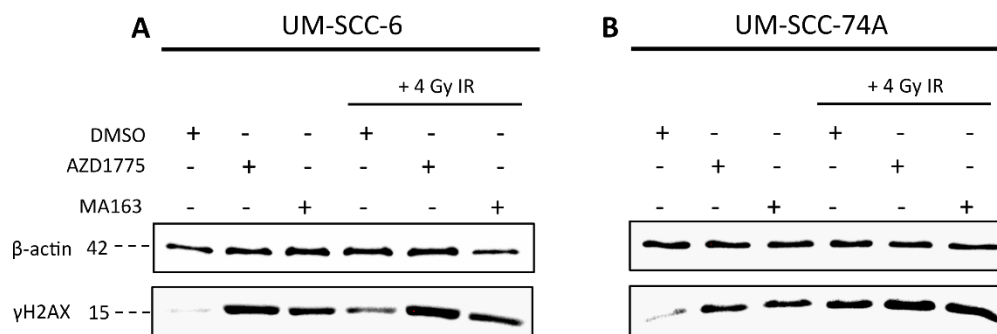
Figure 5.5 Activation of γH2AX by AZD1775 and MA163 as single agents and combinatorial treatments with irradiation in p53-proficicent cells. Cells were treated with 300 nM compounds for 3 h alone or in addition to 4 Gy irradiation. Lysates were produced, ran and blots were probed for γH2AX and β-actin as a loading control (n = 1 or n = 3 for blots A and B, respectively).

As hypothesized above, AZD1775 and MA163 as single agents led to increased activation of histone γH2AX, a sign of DNA damage or replication stress, by 23.4-fold and 9.9-fold respectively in UM-SCC-6 (p53-WT), and 6.1 ± 4.1-fold and 6.4 ± 4.5-fold respectively in UM-

SCC-74A (p53-WT) compared to DMSO (Figure 5.5 and Table 5.3). The combination of

AZD1775 with IR (27.0) or MA163 with IR (26.7) increases relative γH2AX levels by 4.8-fold

compared to 4 Gy alone (5.6) in UM-SCC-6 (p53-WT) (Figure 5.5A) and relative levels

increase from 9.7 ± 6.8 in IR alone to 22.2 ± 14.7 in the AZD1775 combination and 14.8 ±

13.9 in the MA163 combination in UM-SCC-74A (p53-WT) (Figure 5.5B).

Table 5.3 Quantitation of relative γH2AX levels from Figure 5.5 in p53-WT HNSCC cells after treatment with Wee1-targeting compounds alone or in combination with irradiation. Signal intensity was measured and normalised to actin before making levels relative to the DMSO control. In UM-SCC-74A, three repeats were performed and the mean ± SD was calculated from each repeat.

Treatment condition	Relative levels of phosphorylated H2AX	
	UM-SCC-6 (n = 1)	UM-SCC-74A (n = 3) (mean ± SD)
DMSO	1.00	1.00 ± 0.00
AZD1775	23.4	6.07 ± 4.12
MA163	9.90	6.44 ± 4.47
DMSO + 4 Gy	5.57	9.66 ± 6.81
AZD1775 + 4 Gy	27.0	22.2 ± 14.7
MA163 + 4 Gy	26.7	14.8 ± 13.9

These blots indicate that single agent targeting of Wee1 hyperactivates γH2AX. Confocal

immunofluorescent imaging was subsequently conducted to characterise γH2AX at the level

of individual nuclei. This was done in UM-SCC-6 (p53-WT) (Figure 5.6) and UM-SCC-74A

(p53-WT) (Figure 5.7).
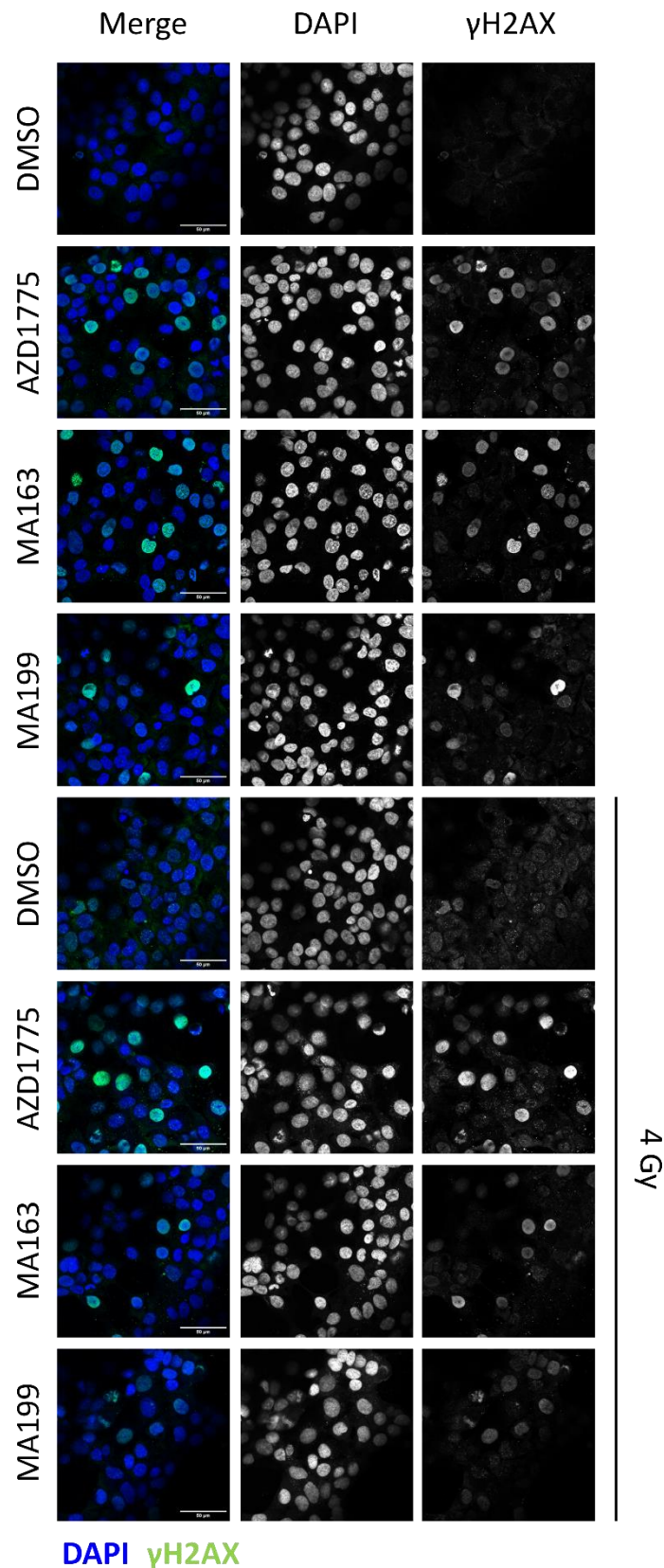
Figure 5.6 Activation of γH2AX by Wee1-targeting treatments in UM-SCC-6 cells. UM-SCC-6 cells were treated with 300 nM compound for 3 h alone or with 4 Gy IR after 2 h of initial treatment. Glass coverslips were then fixed and stained with DAPI and an anti-γH2AX antibody. Representative images of the treatments from n = 3 showing a colour merge tile with the separate grayscale channels of DAPI and γH2AX. Images were taken using a Leica Stellaris 5 microscope and LAS X software. Images were analysed using FIJI. Scale bar is 50 μm.

H2AX was not phosphorylated in the UM-SCC-6 (p53-WT) control cells treated with DMSO, and AZD1775 and MA163 results in activation of γH2AX, which corroborates the previous immunoblot data (Figure 5.5). Treatment with MA199 also showed phosphorylation of H2AX indicative of DNA damage; this further confirms that targeting of Wee1 leads to DNA damage. The same trend is observed when using the treatments with 4 Gy irradiation, Wee1 inhibition or degradation causes a larger increase of γH2AX signal in comparison to 4 Gy alone. These treatments seem to cause pan-nuclear staining of γH2AX rather than foci, therefore intensity of γH2AX was quantified and can be seen in Figure 5.8. The same experiment was performed in UM-SCC-74A (p53-WT) and the representative images can be seen in Figure 5.7.
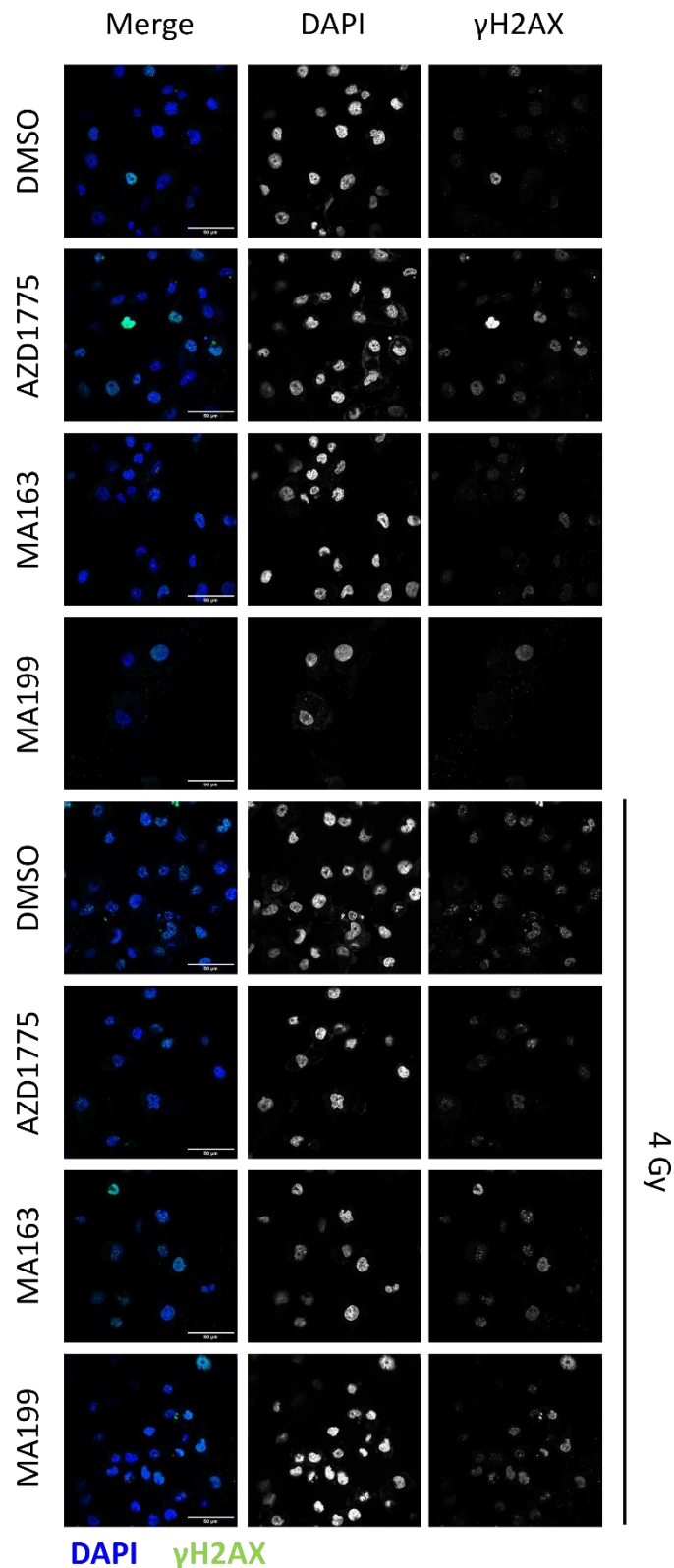
Figure 5.7 Activation of γH2AX by Wee1-targeting treatments alone and with ionizing radiation in UM-SCC-74A cells. UM-SCC-74A cells were treated with 300 nM compound for 3 h alone or with 4 Gy IR after 2 h of initial treatment. Glass coverslips were then fixed and stained with DAPI and an anti-γH2AX antibody. Representative images of the treatments from n = 3 showing a colour merge tile with the separate grayscale channels of DAPI and γH2AX. Images were taken using a Leica Stellaris 5 microscope and LAS X software. Images were analysed using FIJI. Scale bar is 50 μm.

Increased γH2AX is observed in all of the treatment conditions compared to DMSO in UM-

SCC-74A (p53-WT) (Figure 5.7), corresponding to the immunoblot seen in Figure 5.5. The

γH2AX intensity seen appeared similar between each condition, however, to confirm this,

the intensity was quantified and plots can be seen in Figure 5.8.
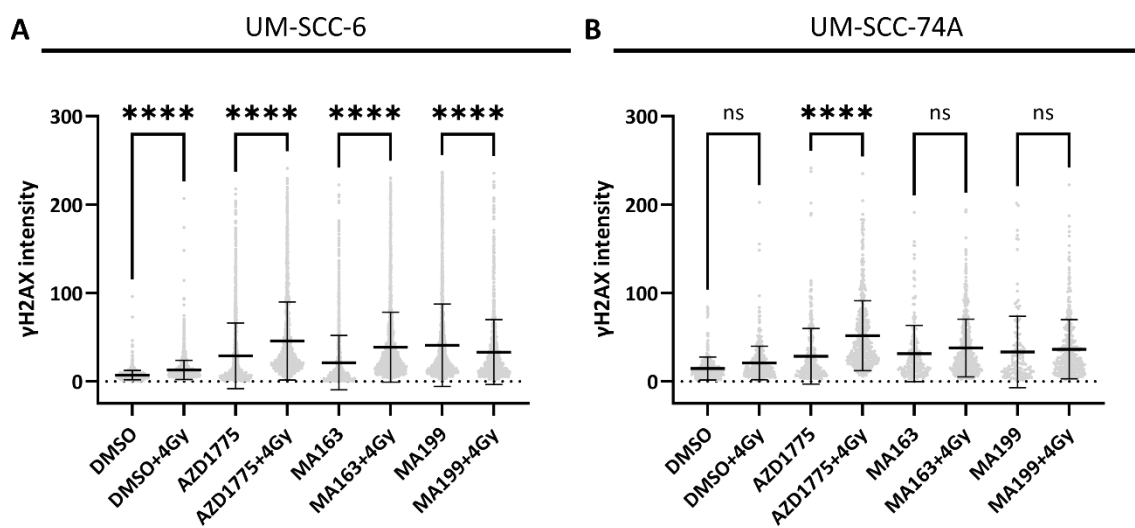
Figure 5.8 Bee swarm plots showing distribution of γH2AX intensity in p53-proficient HNSCC cells from Wee1 inhibition or degradation as a single agent or combinatorial strategy with ionizing radiation. Three fields of view from each condition were taken and analysed by creating masks on the DAPI channel and applying the mask to the γH2AX channel to collect the mean γH2AX intensity per cell. This was done across n = 3. All cell intensities (n>135 cells) were collated in each condition to create a Bee swarm to show the distribution of the cell population, plotting the median ± SD, and these were compared between each treatment condition (GraphPad Prism). A one-way ANOVA with a Tukey's multiple comparisons test was performed and the full p-values can be seen in tables 5.1 and 5.2 for UM-SCC-6 and UM-SCC-74A, respectively.

In UM-SCC-6 (p53-WT), all combination conditions showed a significant increase in γH2AX

levels in comparison to the drugs (except MA199) and 4 Gy alone (Figure 5.8A). This

corroborates the same trend observed in the immunoblot data (Figure 5.5). MA199

179

significantly induced the most activation of H2AX compared to AZD1775 or MA163 as single agents (Table 5.4). However, the combination of MA199 with 4 Gy decreased the γH2AX levels compared to MA199 alone. Interestingly, the entire population distribution for AZD1775 + 4 Gy combination treatment increased compared to the other treatments, suggesting that the highest levels of γH2AX in individual cells was in this condition.

Table 5.4 Table of adjusted p-vaules for the activation of γH2AX as a result of the monotherapy and combination with irradiation treatment comparisons in UM-SCC-6. Analysis of this data has been described in Figure 5.8 and representative images can be seen in Figure 5.6.

	DMSO 0 Gy	AZD1775 0 Gy	MA163 0 Gy	MA199 0 Gy	DMSO 4 Gy	AZD1775 4 Gy	MA163 4 Gy	MA 199 4 Gy
DMSO 0 Gy	-	<0.0001 (****)	<0.0001 (****)	<0.0001 (****)	<0.0001 (****)	<0.0001 (****)	<0.0001 (****)	<0.0001 (****)
AZD1775 0 Gy	<0.0001 (****)	-	<0.0001 (****)	<0.0001 (****)	<0.0001 (****)	<0.0001 (****)	<0.0001 (****)	0.0077 (**)
MA163 0 Gy	<0.0001 (****)	<0.0001 (****)	-	<0.0001 (****)	<0.0001 (****)	<0.0001 (****)	<0.0001 (****)	<0.0001 (****)
MA199 0 Gy	<0.0001 (****)	<0.0001 (****)	<0.0001 (****)	-	<0.0001 (****)	<0.0001 (****)	0.3455 (ns)	<0.0001 (****)
DMSO 4 Gy	<0.0001 (****)	<0.0001 (****)	<0.0001 (****)	<0.0001 (****)	-	<0.0001 (****)	<0.0001 (****)	<0.0001 (****)
AZD1775 4 Gy	<0.0001 (****)	<0.0001 (****)	<0.0001 (****)	<0.0001 (****)	<0.0001 (****)	-	<0.0001 (****)	<0.0001 (****)
MA163 4 Gy	<0.0001 (****)	<0.0001 (****)	<0.0001 (****)	0.3455 (ns)	<0.0001 (****)	<0.0001 (****)	-	<0.0001 (****)
MA199 4 Gy	<0.0001 (****)	0.0077 (**)	<0.0001 (****)	<0.0001 (****)	<0.0001 (****)	<0.0001 (****)	<0.0001 (****)	-

In UM-SCC-74A (p53-WT) cells, the quantification shows that the γH2AX intensity is similar

across all treatment conditions and is elevated compared to DMSO (Figure 5.8B). This bee

swarm plot corroborates the trend seen on the γH2AX immunoblot (Figure 5.5B). All

treatments with AZD1775, MA163 and MA199, alone or with 4 Gy irradiation, cause

significantly higher levels of γH2AX compared to DMSO alone and DMSO + 4 Gy (Table 5.5).

AZD1775 with 4 Gy is the only combination treatment with significantly more H2AX

phosphorylation in comparison to the Wee1 drug alone.

Table 5.5 Table of adjusted p-vaules for the activation of γH2AX as a result of the monotherapy and combination with irradiation treatment comparisons in UM-SCC-74A. Analysis of this data has been described in Figure 5.8 and representative images can be seen in Figure 5.7.

	DMSO 0 Gy	AZD1775 0 Gy	MA163 0 Gy	MA199 0 Gy	DMSO 4 Gy	AZD1775 4 Gy	MA163 4 Gy	MA199 4 Gy
DMSO 0 Gy	-	<0.0001 (****)	<0.0001 (****)	<0.0001 (****)	0.0629 (ns)	<0.0001 (****)	<0.0001 (****)	<0.0001 (****)
AZD1775 0 Gy	<0.0001 (****)	-	0.9214 (ns)	0.7263 (ns)	0.0051 (**)	<0.0001 (****)	<0.0001 (****)	0.0051 (**)
MA163 0 Gy	<0.0001 (****)	0.9214 (ns)	-	0.9994 (ns)	0.0004 (***)	<0.0001 (****)	0.1704 (ns)	0.5612 (ns)
MA199 0 Gy	<0.0001 (****)	0.7263 (ns)	0.9994 (ns)	-	0.0006 (***)	<0.0001 (****)	0.7999 (ns)	0.9756 (ns)
DMSO 4 Gy	0.0629 (ns)	0.0051 (**)	0.0004 (***)	0.0006 (***)	-	<0.0001 (****)	<0.0001 (****)	<0.0001 (****)
AZD1775 4 Gy	<0.0001 (****)	<0.0001 (****)	<0.0001 (****)	<0.0001 (****)	<0.0001 (****)	-	<0.0001 (****)	<0.0001 (****)
MA163 4 Gy	<0.0001 (****)	<0.0001 (****)	0.1704 (ns)	0.7999 (ns)	<0.0001 (****)	<0.0001 (****)	-	0.9967 (ns)
MA199 4 Gy	<0.0001 (****)	0.0051 (**)	0.5612 (ns)	0.9756 (ns)	<0.0001 (****)	<0.0001 (****)	0.9967 (ns)	-

The immunofluorescence data of γH2AX intensity, γH2AX western blots and western blots of phosphorylation of Chk1 and Chk2 all support that targeting Wee1 causes activation of the DDR, irrespective of additional genotoxic compound. Wee1-targeting in combination with irradiation significantly increases levels of DNA damage in both UM-SCC-74A (p53-WT) and UM-SCC-6 (p53-WT). Furthermore, this data is suggestive that these combination treatments and Wee1 drugs alone activate the ATR-Chk1 pathway compared to using 4 Gy irradiation alone. To further validate that these compounds increase DNA damage and to additionally investigate if this leads to mitotic problems, cells were treated with 300 nM compounds for 24 h with or without 4 Gy irradiation before fixing and staining.

UM-SCC-6 (p53-WT) cells were stained with DAPI, tubulin and CENP-A (Figure 5.9). It was observed that the longer treatment time was more cytotoxic to cells compared to the previous 3 h treatments for immunofluorescence experiments as fewer cells were seen on the coverslips. This impacted the data collected as we had to normalise the data to count per 100 cells, however even this normalisation has some issues. For example, in some fields of view no micronuclei were counted in MA163-treated condition as there were so few cells. This meant that, even with normalisation, there was no micronuclei counted for this condition. Perhaps if there were 100 cells in that field of view, we would have seen micronuclei in this treatment condition. Increased levels of CENP-A were observed in the irradiated only cells in comparison to the other conditions in UM-SCC-6 (p53-WT) (Figure 5.9). Micronuclei, multinucleated cells and mitotic cells were counted and quantified to be a measurement of DNA damage and mitotic deficiencies (Figure 5.10). Graphs of the analysed data for UM-SCC-6 (p53-WT) seen in figure 5.9 were produced (Figure 5.11).
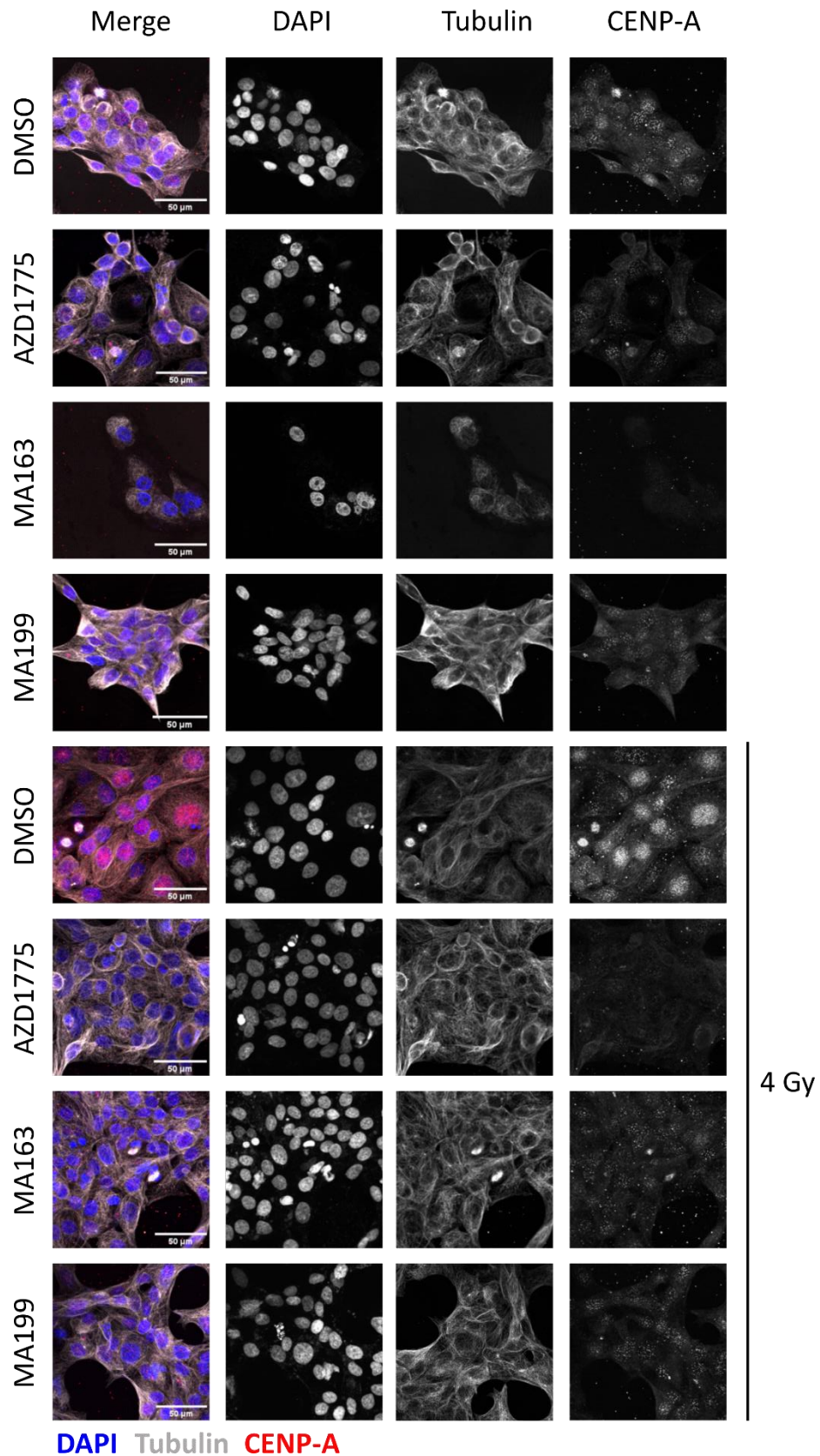
Figure 5.9 Representative images for micronuclei detection and mitotic index analysis of UM-SCC-6 cells. UM-SCC-6 cells were treated with 300 nM compounds for 24 h alone or with 4 Gy ionizing radiation before fixing and staining cells on glass coverslips with DAPI and antibodies to CENP-A and Tubulin. Three fields of view were taken for each treatment to analyse data in one repeat. Images were taken using a Leica Stellaris and LAS X software. Images were analysed using FIJI (n = 3). Scale bar is 50 μm.
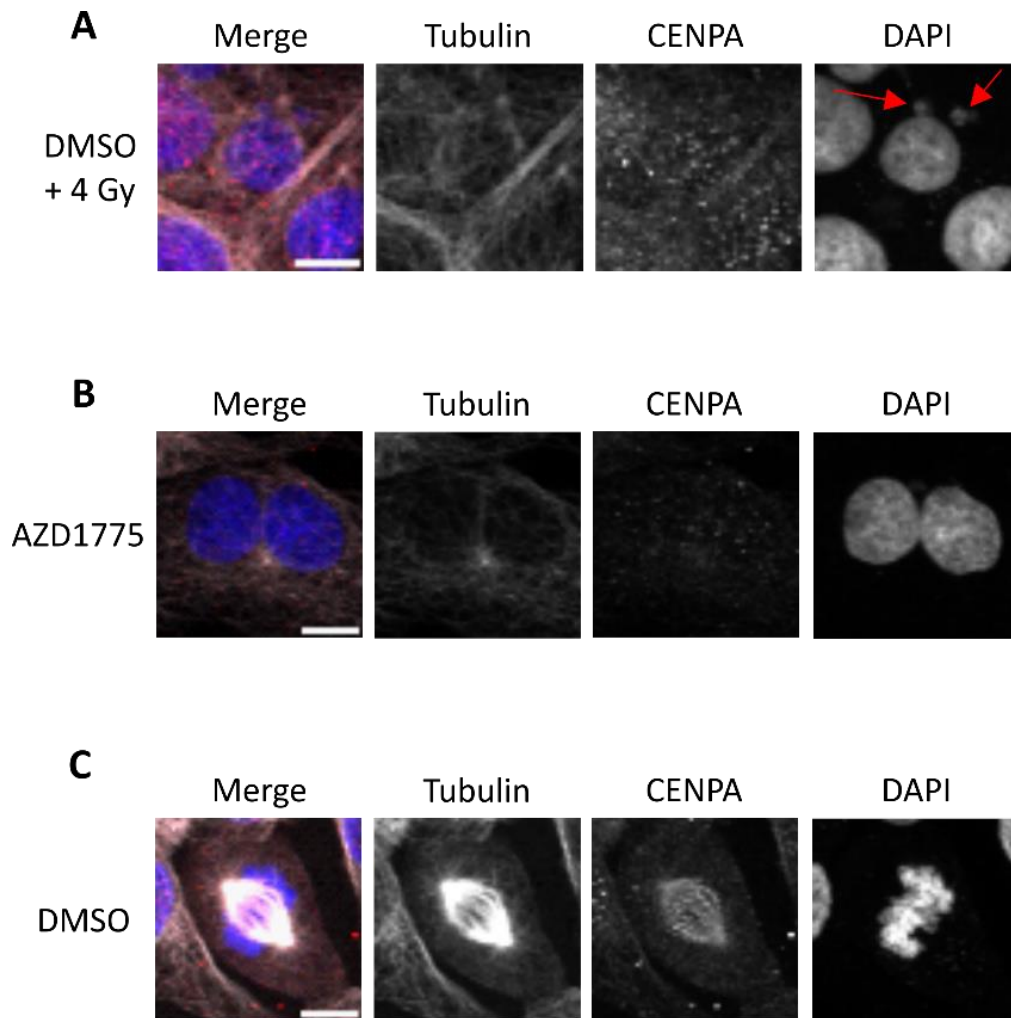
Figure 5.10 Representative images of micronuclei, binucleated and mitotic UM-SCC-6 cells. Representative images from the experiment seen in Figure 5.6 have been made to show what was considered micronuclei, a binucleated or multinucleated cell and a mitotic cell. (A) Zoomed image of an UM-SCC-6 cell treated with DMSO and 4 Gy irradiation that have two micronuclei indicated by red arrows. (B) Zoomed image of a UM-SCC-6 cell treated with AZD1775 that is binuclear. (C) Zoomed image of a mitotic UM-SCC-6 cell. Images were taken with a Leica Stellaris 5 and LAS X software and processed by FIJI. Scale bar is 20 μm.
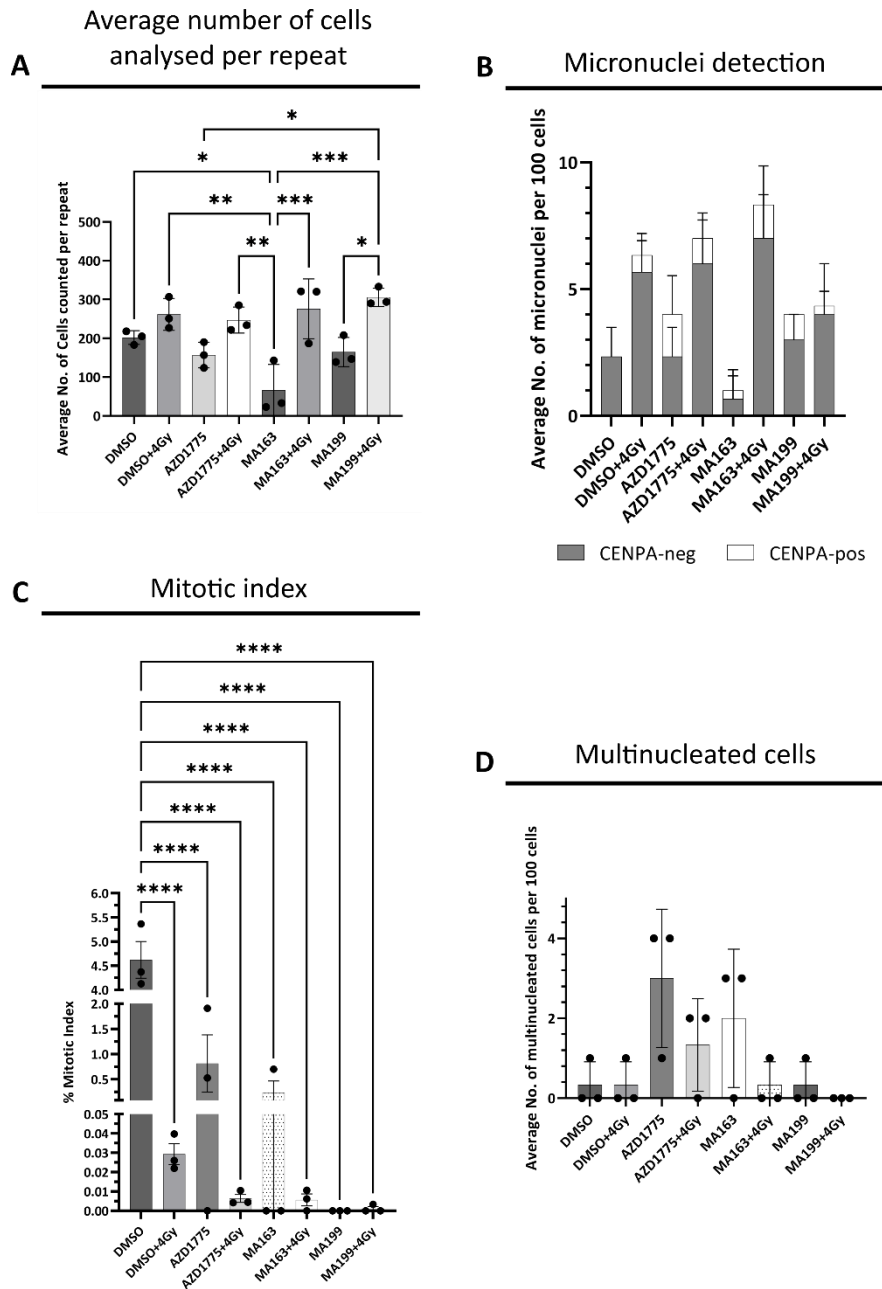
Figure 5.11 Graphs from micronuclei detection and mitotic index experiment of UM-SCC-6 cells.
Representative images from Figure 5.9 were quantified for (A) bar graph for mean ± SD of n = 3 biological replicates of average number of cells analysed per repeat in each treatment condition, (B) stacked bar column for mean ± SD number of CENPA-negative and CENPA-positive micronuclei per 100 cells, (C) bar graph of mean ± SD % mitotic index and (D) mean ± SD of multinucleated cells per 100 cells. Graphs were produced in GraphPad Prism and analysed by a one-way ANOVA with a Tukey's multiple comparisons test.

There were fewer cells on the coverslips treated with the single agent Wee1-targeting compounds compared to the combination treatment coverslips, suggesting that the monotherapies were more cytotoxic in this initial 24 h treatment compared to the combination conditions, especially with MA163 (Figure 5.11A). This observation was quantified as the smaller sample size for this condition could have led to fewer micronuclei, multinucleated or mitotic cells. Using 4 Gy irradiation on UM-SCC-6 (p53-WT) caused an increase in the average number of micronuclei per 100 cells compared to DMSO. The combination of 4 Gy with AZD1775 led to more micronuclei per 100 cells than either 4Gy or AZD1775 alone, although this is not statistically significant (Figure 5.11B). This trend was also observed with MA163 and MA163 + 4 Gy. MA199 and AZD1775 equally caused the largest increase of micronuclei out of the Wee1-targeting treatments compared to the DMSO control but the highest proportion of micronuclei was seen in MA163 + 4 Gy. Perhaps the number of micronuclei per 100 cells would have been higher in MA163 treated cells if this condition did not kill as many cells. All treatment conditions significantly reduced the mitotic index compared to DMSO alone (Figure 5.11C). Finally, an increase in multinucleated cells in AZD1775, AZD1775 with 4 Gy and MA163 treated cells compared to DMSO or DMSO with 4 Gy was seen, with the largest increase in AZD1775 only treated cells (Figure 5.11D).

These data suggest that in UM-SCC-6 (p53-WT) cells Wee1 inhibition is neither advantageous nor detrimental in comparison to Wee1 degradation in reducing the number of dividing cells and inducing DNA damage. Both methods are equally successful. Furthermore, the combinations of either AZD1775 or MA163 with irradiation are better at decreasing mitotic index and increasing micronuclei compared to irradiation or the drugs alone.

The same experiment was performed in the other p53 wild-type cell line, UM-SCC-74A (p53-WT) (Figure 5.12). It is clear from the representative images that there were less UM-SCC-74A (p53-WT) cells that remained adhered to the coverslips (Figure 5.12) in comparison to the representative images of UM-SCC-6 (p53-WT) (Figure 5.11).
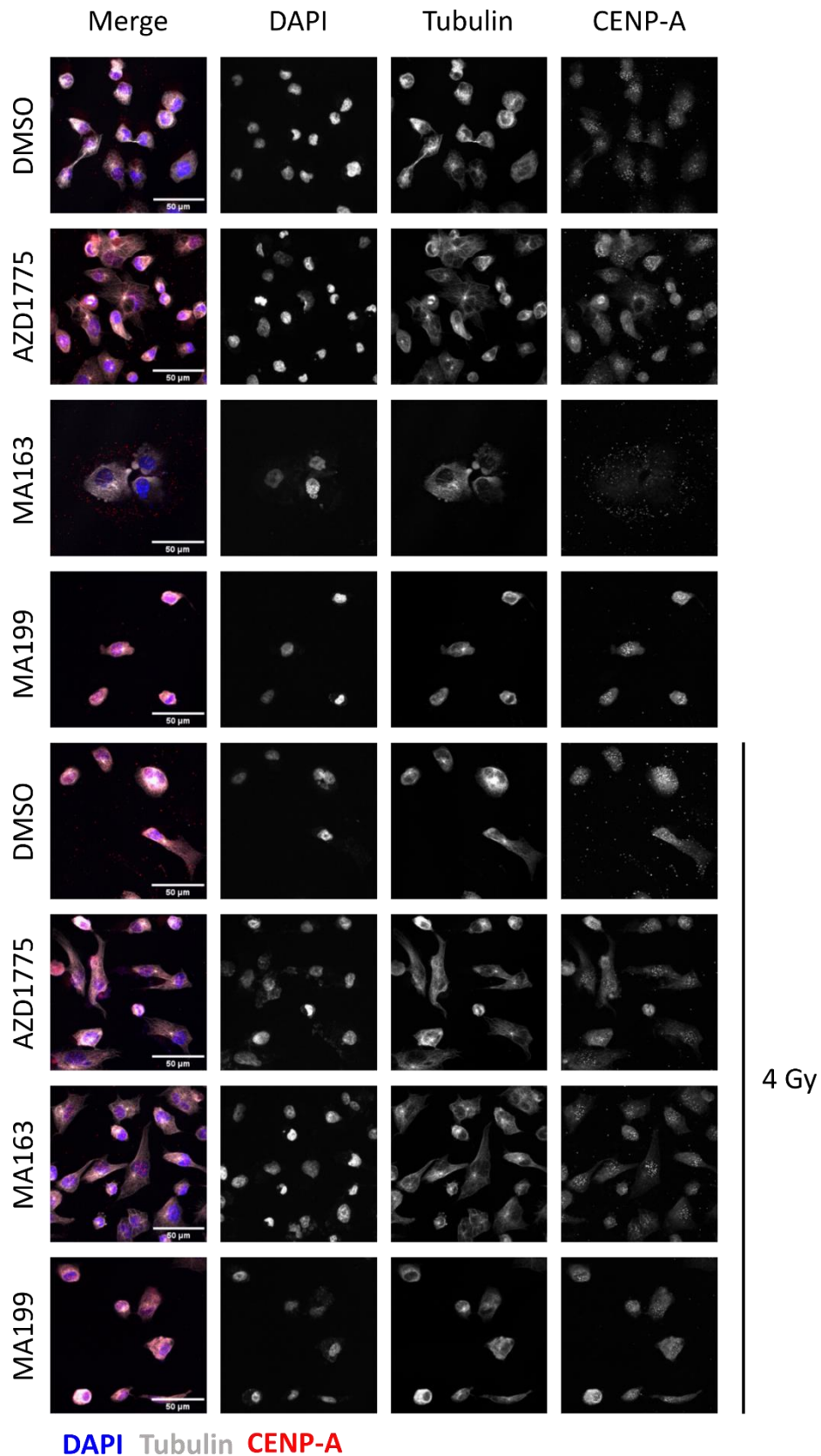
Figure 5.12 Representative images for micronuclei detection and mitotic index analysis of UM-SCC-74A cells. UM-SCC-74A cells were treated with 300 nM compounds for 24 h alone or with 4 Gy ionizing radiation before fixing and staining cells on glass coverslips with DAPI and antibodies to CENP-A and Tubulin. Three fields of view were taken for each treatment to analyse data in one repeat. Images were taken using a Leica Stellaris and LAS X software. Images were analysed using FIJI (n = 3). Scale bar is 50 μm.

MA163 seemed to be the most cytotoxic treatment condition at 24 h with the smallest average number of cells observed in UM-SCC-74A (p53-WT) (Figure 5.13A). This corroborates what was seen in UM-SCC-6 (p53-WT) cells (Figure 5.11A). The combinations of AZD1775, MA163 or MA199 with 4 Gy led to more micronuclei in comparison to DMSO and the compounds alone however, 4 Gy irradiation induced the most micronuclei and this was a significant increase compared to control cells (Figure 5.13B). As there were so few cells to count on these coverslips, and capturing mitosis is rare compared to normal cells, no mitotic cells could be found in many repeats (Figure 5.13C). Therefore, even though it appears that AZD1775, AZD1775 with 4 Gy, MA163 with 4 Gy and MA199 with 4 Gy increased the rate of mitosis, this is only by 0.01 % - 0.5 %. Although these data are obtained from three repeat experiments, a larger number of cells should be analysed to confirm these findings.

The majority of the conditions, other than MA163 and MA199, caused an increase of multinucleated cells compared to DMSO (Figure 5.13D). 4 Gy alone and MA199 with 4 Gy caused the largest increase of multinucleated cells compared to the DMSO control, in contrast to what was observed in UM-SCC-6 (p53-WT) cells (Figure 5.11D). Although both cells have functional p53, perhaps the formation of multinucleated cells in response to Wee1-targeting treatments is cell line-dependent.
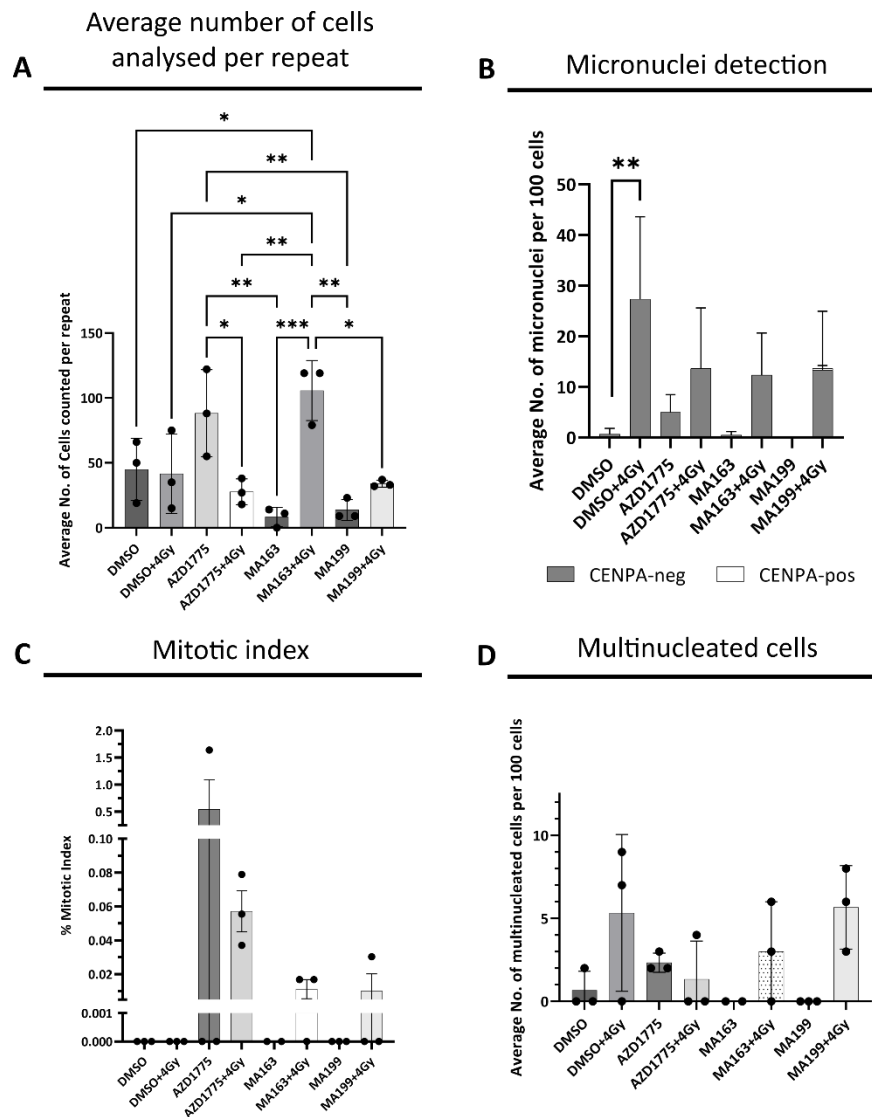
Figure 5.13 Graphs from micronuclei detection and mitotic index experiment of UM-SCC-74A cells.
Representative images from Figure 5.12 were quantified for (A) bar graph showing mean ± SD of average
number of cells analysed per repeat in each treatment condition, (B) stacked bar graph showing mean ± SD
CENPA-negative and CENPA-positive micronuclei per 100 cells, (C) bar graph showing mean ± SD % mitotic
index and (D) bar graph showing mean ± SD multinucleated cells per 100 cells. Graphs were produced in
GraphPad Prism and analysed by a one-way ANOVA with a Tukey's multiple comparisons test.

To evaluate if the nuclei changed size depending on treatment, the data obtained from the

micronuclei detection experiments (Figures 5.9 to 5.13) were re-analysed to measure nuclei

area (Figure 5.14). In UM-SCC-6 (p53-WT), MA163 or MA199 alone or in combination with

ionizing radiation caused a significant decrease in nuclei area compared to DMSO or DMSO

with 4 Gy (Figure 5.14A). Furthermore, MA163 and MA199 also significantly decreased

nuclei size compared to AZD1775 when used as single agents or AZD1775 with 4 Gy when

used as combination treatments. This was the opposite of the trend observed in UM-SCC-

74A (p53-WT). All combinations significantly increase nuclei area compared to 4 Gy alone

and MA163 significantly increased nuclei area compared to DMSO, AZD1775 or MA199

(Figure 5.14B). This further demonstrates that the effect of these treatments could be

heavily cell line-dependent. More p53-proficient cells lines should be observed to see if any

trends for nuclei size or multinucleated cells are apparent.
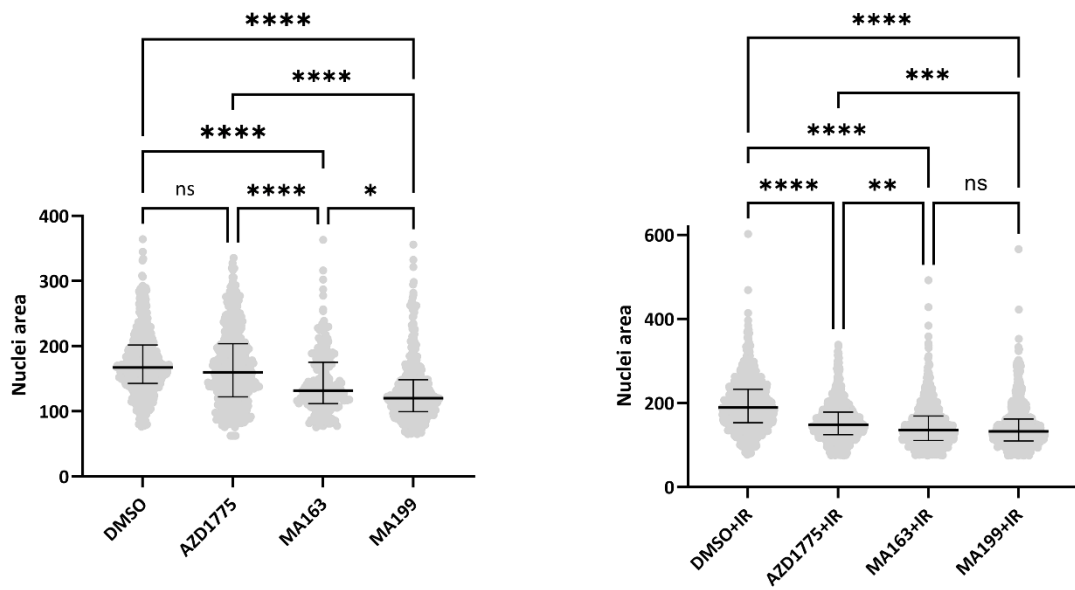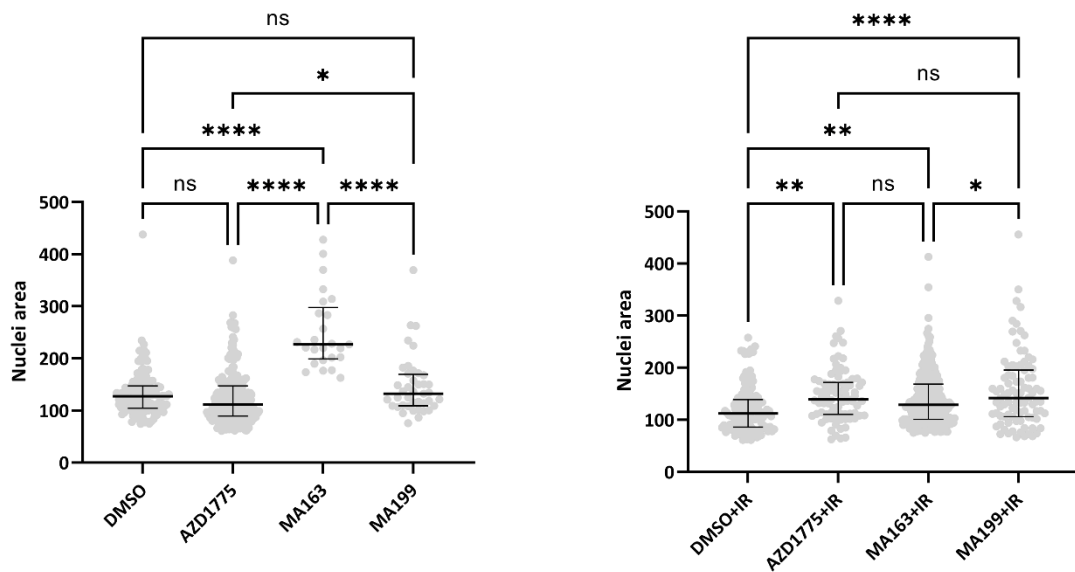
Figure 5.14 Bee swarm plots of nuclei area of p53-proficient cells treated with AZD1775 and Wee1 PROTACs alone and in combination with 4 Gy radiation. These plots were produced from the data collected from the micronuclei detection immunofluorescence experiment. Three fields of view from each condition was taken and analysed by creating regions of interest (ROIs) on the DAPI channel to measure the nuclei area. This was done across n = 3. All nuclei areas (n>25 cells) were collated in each condition to create Bee swarm plots to show the distribution of the nuclear size population, plotting the median and interquartile range, and these were compared between each treatment condition (GraphPad Prism). A one-way ANOVA with a Tukey's multiple comparisons test was performed.

5.3.2 Effects of Wee1 PROTACs on p53-deficient HNSCC cell lines

To determine if p53 status had any effect on the results seen thus far, the experiments in p53 wild type cell lines UM-SCC-6 (p53-WT) and UM-SCC-74A (p53-WT) discussed in Section 5.3.1 were also performed in p53-deficient cell lines, A-253 and FaDu.

5.3.2.1 Impact on cell cycle profile of Wee1 PROTACs compared to AZD1775

In Chapter 4, p53-deficient cells were shown to be more susceptible to radio- or chemosensitization compared to p53-proficient cell lines. Section 5.3.1 has explored how Wee1i, AZD1775, and Wee1 PROTACs affect the cell cycle and DNA damage response in p53-proficient cell lines. Therefore, this section will show data from the same experiments carried out with p53-deficient HNSCC cell lines, A-253 and FaDu.

A-253 (p53-null) and FaDu (p53-mutant) cells were treated with AZD1775, MA163 or MA199 at 300 nM for 18 h, 24 h and 48 h to investigate time points where cells that began the experiment in G1 would enter mitosis, complete one full cell cycle and complete two full cell cycles, respectively. The populations were asynchronous so all cells would not be going through these cell cycle points at the same time. Cells were then incubated with 10 μM EdU for 1 h before trypsinization and staining with Alexa Fluor™ 647 azide, for EdU incorporation, and DAPI for DNA content (Figure 5.15). Cells were gated as seen in Figure 2.1.
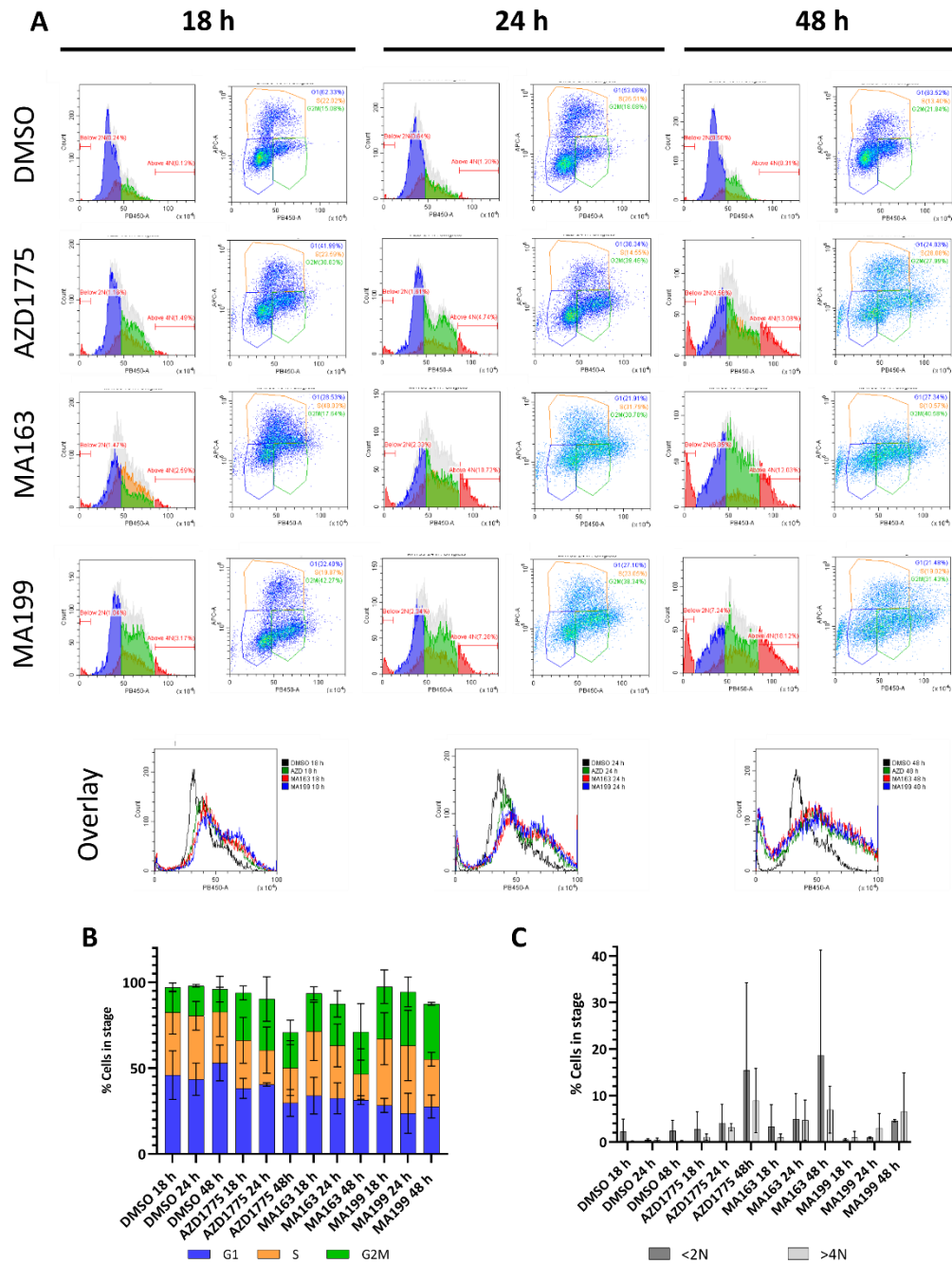
Figure 5.15 Cell cycle stage analysis of Wee1-targeting treatments on A-253 cells over a 48 h time course.
Flow cytometry of A-253 cells stained with Alexa Fluor™ 647 azide for EdU incorporation and DAPI for DNA content. (A) Representative dot plots and DNA content histograms for monotherapy treatments at 300 nM for 18 h, 24 h or 48 h, in addition to overlay histograms of the treatments at those time points. (B) Stacked bar graph showing mean ± SD of n = 3 biological replicates of cells in G1, S and G2/M (GraphPad Prism). (C) Bar graph showing mean ± SD of n = 3 biological replicates of cells with <2N or >4N DNA content (GraphPad Prism).

There is a substantial increase in >4N cells in A-253 (p53-null) when treated with AZD1775, MA163 and MA199 compared to the untreated sample (Figure 5.15A). AZD1775, MA163 and MA199 single treatment results in a loss of actively replicating S-phase population over time. The largest decrease was by 2.5-fold in S-phase population from 18 h to 48 h in MA163-treated cells. There were fewer cells in G1 when A-253 (p53-null) were treated with Wee1-targeting compounds compared to DMSO. For example, the mean G1 population at 48 h for DMSO is 53%, whereas this population drops to 29.8%, 31.4% and 27.7% for AZD1775, MA163 and MA199, respectively. There are no clear changes in the G1 population in each treatment over the treatment period (Figure 5.15B).

The single agent treatments caused an increase in the proportion of G2/M cells compared to DMSO, with the highest proportion at 48 h MA199 treatment. Populations of cells with inappropriate amount of DNA (>4N and <2N) are greatest at 48 h in each treatment condition (Figure 5.15C). Also, at this time point in treated cells, more EdU-negative cells with 2<N<4 DNA content are seen, which is indicative of replication stress. This suggests targeting Wee1 does not lead to a G1 or G2/M arrest in p53-deficient cells but could cause replication stress and an intra S-phase checkpoint activation. Furthermore, the increased >4N population is suggestive of a segregation defect (EdU-negative) and/or re-replication (EdU-positive) as a result of these treatments.

To observe how 4 Gy irradiation alone and in combination with Wee1-targeting compounds affected the cell cycle of G1/S checkpoint-dysfunctional cells, cell cycle stage analysis flow cytometry was performed on A253 treated cells (Figure 5.16).

Cells were treated with AZD1775, MA163 or MA199 for 24 h with or without 4 Gy

irradiation. The gating for G1, S and G2/M populations were originally based on 0 Gy DMSO

however, the movement of the cell cycle profile along the x-axis, due to incomplete

saturation of DNA with DAPI implied that most of the cells in the treated samples have >4N

DNA content. Due to this, it was decided that the G1, S and G2/M gates would be

individually applied to each sample (Figure 5.16).
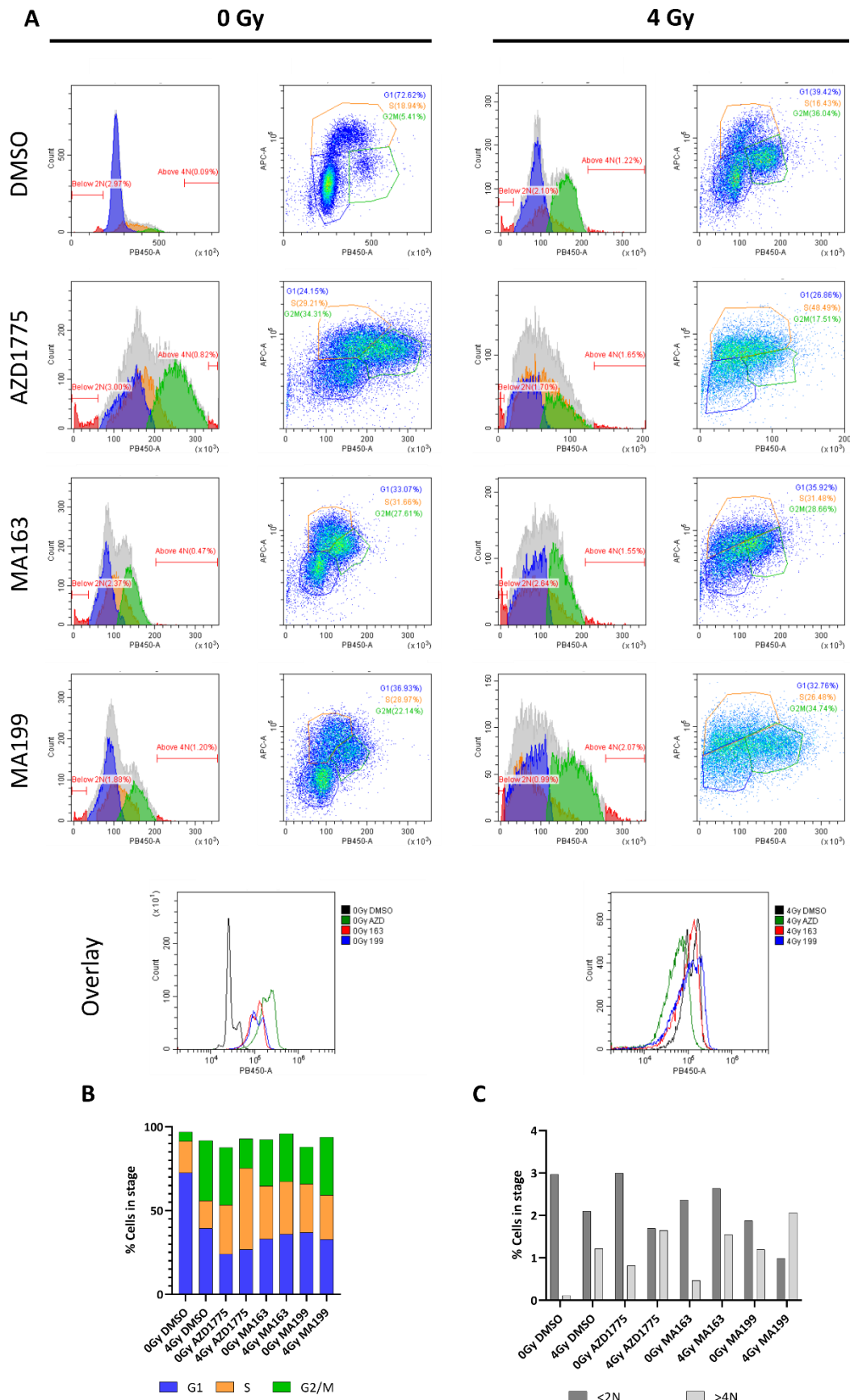
Figure 5.16 Cell cycle stage analysis of Wee1-targeting treatments alone and in combination with irradiation on A-253 cells with gating based on 4 Gy DMSO control. Flow cytometry of A-253 cells stained with Alexa Fluor™ 647 azide for EdU incorporation and DAPI for DNA content. (A) Representative dot plots and DNA content histograms for monotherapy treatments at 300 nM for 24 h or combination treatments with 300 nM compound and 4 Gy irradiation for 24 h, in addition to overlay histograms of the treatments at 0 Gy and 4 Gy. (B) Stacked bar graph showing values of n = 1 of cells in G1, S and G2/M (GraphPad Prism). (C) Bar graph showing values of n = 1 of cells with <2N or >4N DNA content (GraphPad Prism).

197

After the new gating, it remains difficult to draw conclusions from this preliminary experiment. As seen in UM-SCC-6 (p53-WT) (Figure 5.2), there is a loss of clear defined cell cycle stage populations when a Wee1-targeting treatment is added to the cells. Ionizing radiation did not cause a G1 arrest as A-253 (p53-null) are a p53-deficicent cell line and have a dysfunctional G1/S checkpoint. There is an increase in 2<N<4 cells, suggestive that these treatments is causing replicative stress.

To see if the trends observed in A-253 (p53-null) are cell-type specific or due to p53-deficiency, cell cycle stage analysis flow cytometry experiments in FaDu (p53-mutant) cells were carried out. The single agent Wee1-treatments over a 48 h time course were initially investigated (Figure 5.17).
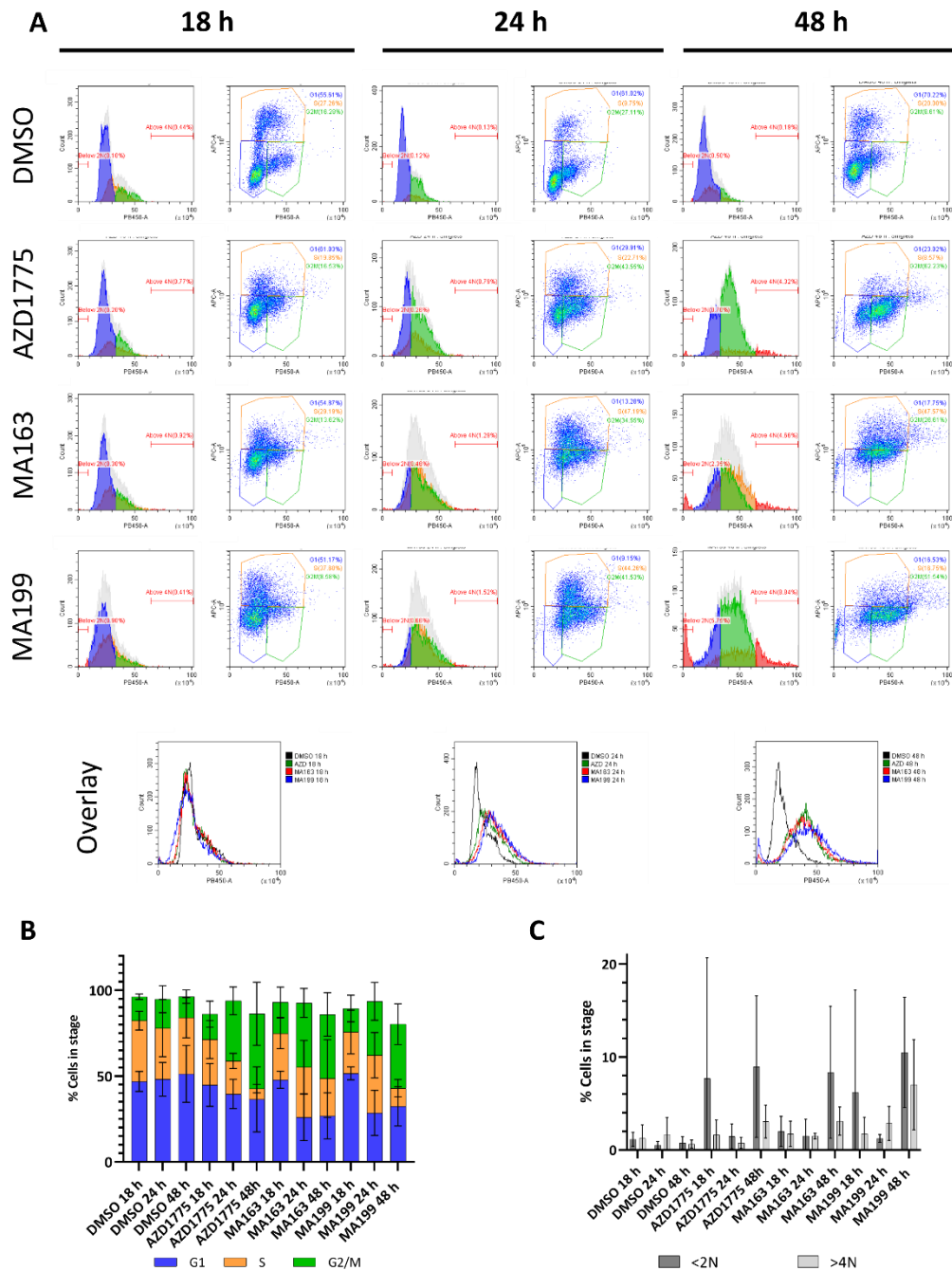
Figure 5.17 Cell cycle stage analysis of Wee1-targeting treatments on FaDu cells over a 48 h time course. Flow cytometry of FaDu cells stained with Alexa Fluor™ 647 azide for EdU incorporation and DAPI for DNA content. (A) Representative dot plots and DNA content histograms for monotherapy treatments at 300 nM for 18 h, 24 h or 48 h, in addition to overlay histograms of the treatments at those time points. (B) Stacked bar graph showing mean ± SD of n = 3 biological replicates of cells in G1, S and G2/M (GraphPad Prism). (C) Bar graph showing mean ± SD of n = 3 biological replicates of cells with <2N or >4N DNA content (GraphPad Prism).

The proportion of EdU-incorporating cells greatly decreases after roughly two cell cycle divisions at 48 h in AZD1775, MA163 and MA199 treated cells. 24 h and 48 h treatments of Wee1 PROTACs cause an equal loss of G1 cells (Figure 5.17B). AZD1775 also leads to loss of G1 cells. The largest population of <2N DNA content cells at 10.5 % and the largest >4N DNA content population at 7 % was observed in MA199 treated-cells (Figure 5.17C). To conclude from this time course, the Wee1-targeting treatments cause a progressive increase in DNA content for the whole cell cycle profile in FaDu (p53-mutant) and the same pattern is observed in UM-SCC-6 (p53-WT) and A-253 (p53-null), suggesting the effect of these compounds as single agents is not p53-dependent. Furthermore, the single agents cause an increase in cells with incorrect DNA content and the loss of clear defined G1 and G2/M populations, suggesting replication stress and S phase arrest with the population mostly distributed between >2N and <4N DNA content. 4 Gy irradiation in combination with the compounds changed the cell cycle profile in FaDu (p53-mutant) cells (Figure 5.18).
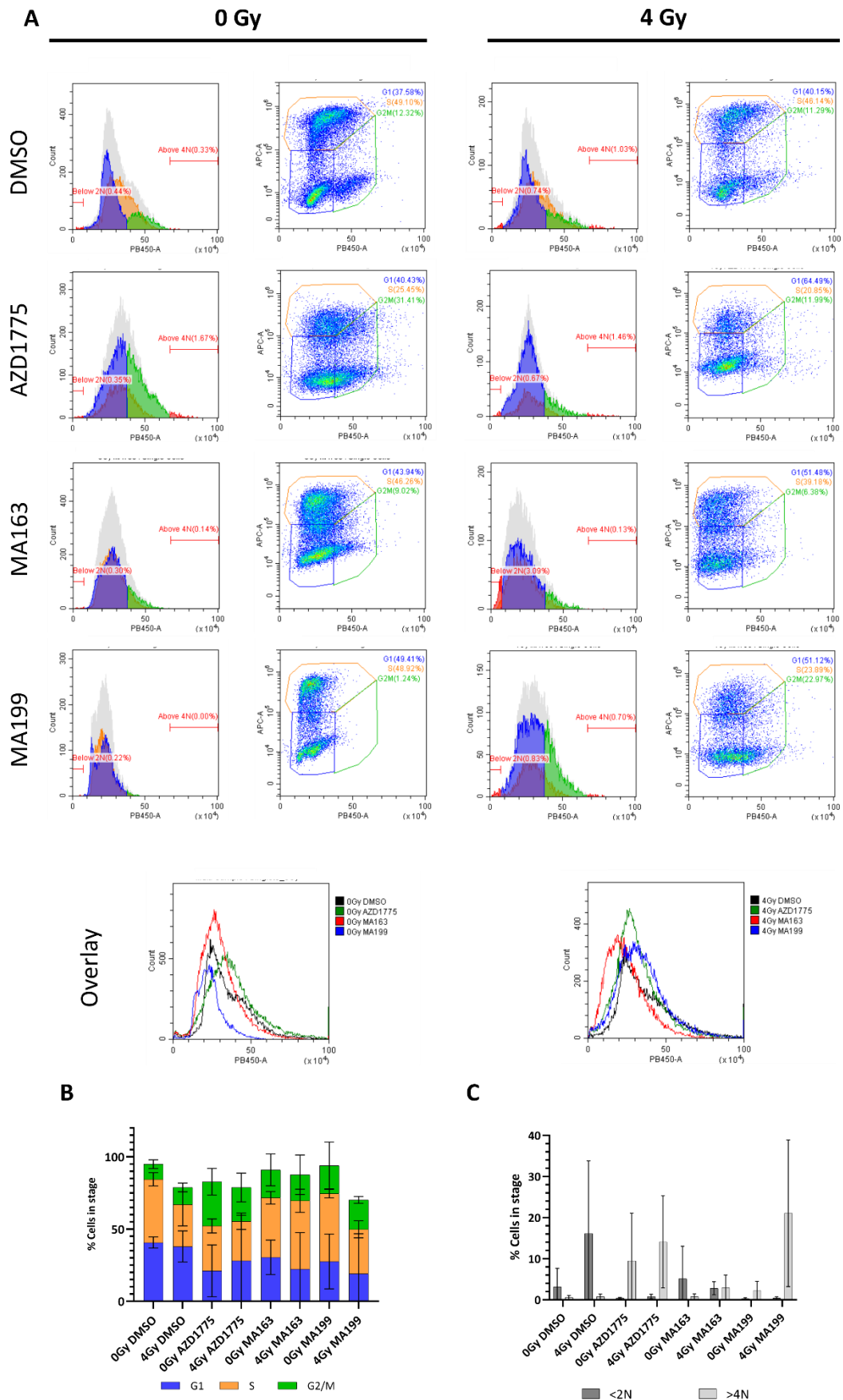
Figure 5.18 Cell cycle stage analysis of Wee1-targeting treatments alone and in combination with irradiation on FaDu cells. Flow cytometry of FaDu cells stained with Alexa Fluor™ 647 azide for EdU incorporation and DAPI for DNA content. (A) Representative dot plots and DNA content histograms for monotherapy treatments at 300 nM for 24 h or combination treatments with 300 nM compound and 4 Gy irradiation for 24 h, in addition to overlay histograms of the treatments at 0 Gy and 4 Gy. (B) Stacked bar graph showing values of mean ± SD of n = 3 biological replicates of cells in G1, S and G2/M (GraphPad Prism). (C) Bar graph showing values of mean ± SD of n = 3 biological replicates of cells with <2N or >4N DNA content (GraphPad Prism).

Treatments with AZD1775, MA163 and MA199 as single agents resulted in a loss of clear defined G1 and G2/M populations, and appeared to form a 2<N<4 population (Figure 5.18A). The addition of 4 Gy irradiation to each Wee1-monotreatment did not appear to change the proportion of cells in G1, S and G2/M (Figure 5.18B). MA199 had the highest >4N population at 21.1% and all of the Wee1-targeting treatment conditions, alone or with irradiation, had higher numbers of cells with >4N DNA content compared to DMSO (Figure 5.18C). The loss of clear defined G1 and G2/M populations in Wee1-targeting treatments with 4 Gy is seen in both p53-deficicent cell lines, whereas in p53-proficient cells there are G1 and G2/M populations.

Furthermore, the combination treatments cause near a complete loss of EdU-incorporating S phase cells in p53-proficient cells, whereas in A-253 (p53-null) and FaDu (p53-mutant) EdU is incorporated, but the signal is weaker. This suggests that as expected the p53 defective cells lines undergo radioresistant synthesis but with decreased efficiency relative to unirradiated cells.

To investigate if cells could be arresting at the anaphase checkpoint, FaDu (p53-mutant) cells were treated with 300 nM compounds for 24 h alone or irradiated with 4 Gy and stained for Cyclin B1 (Figure 5.19).

A

	Merge	DAPI	Tubulin	CycB1
DMSO				
AZD1775				
MA163				
MA199				
DMSO				
AZD1775				
MA163				
MA199				

4 Gy

DAPI Tubulin CyclinB1

B
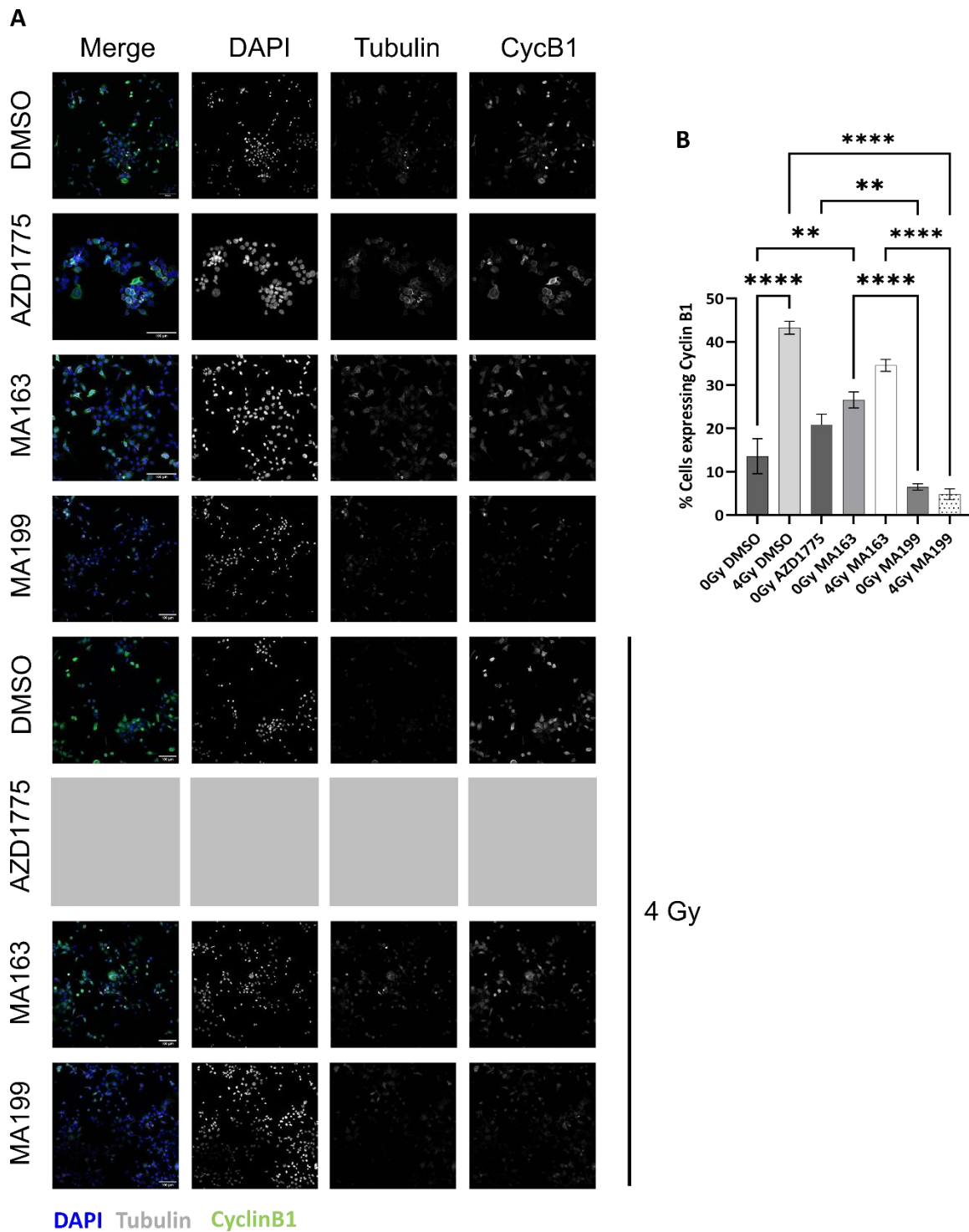
Figure 5.19 Effects of AZD1775 and Wee1 PROTACs on Cyclin-B1 expression levels as a monotherapy and combinatorial treatment. FaDu cells were treated with 300 nM compound for 24 h alone or with 4 Gy IR after 2 h of initial treatment. (A) Representative images of the treatments showing a colour merge tile with the separate grayscale channels of DAPI, tubulin and Cyclin-B1. Images were taken using a Zeiss LSM880 Airyscan and ZEN Blue 3.0 software. Images were analysed using FIJI. (B) Bar graph of mean ± SD of n = 3 fields of view from n = 1 biological repeat (GraphPad Prism).

AZD1775 and MA163 both increased Cyclin B1 levels from 13.6% in DMSO to 20.9% and 26.6%, respectively (Figure 5.19B). Conversely, MA199 decreased the % cells expressing Cyclin B1 by 7.1% compared to DMSO. A problem with the cells adhering to the AZD1775 and 4 Gy combination treatment coverslip resulted in no data being collected for this condition. The combination of 4 Gy with MA199 significantly decreased Cyclin B1 expression by 9-fold. MA163 with 4 Gy also caused a loss of cells expressing Cyclin B1. This data suggests that when FaDu (p53-mutant) cells are irradiated, they arrest at the spindle checkpoint, indicated by the build-up of Cyclin B1 that has not been broken down by the anaphase promoting complex (APC).

5.3.2.2 Activation of the DDR by Wee1-targeting treatments in TP53 mutant HNSCC cells

To assess activation of the DDR by Wee1-targeting drugs alone and in combination with ionizing radiation, cisplatin or bleomycin, the phosphorylation of Chk1, Chk2 and ATR in A-253 (p53-null) and FaDu (p53-mutant) cells was investigated by western blot. Cells were treated with 300 nM AZD1775, MA163 and MA199 for 2 h prior to the addition of radiation, cisplatin or bleomycin for a further 1 h. Lysates were made and run on a western blot for A-253 (p53-null) and FaDu (p53-mutant) (Figure 5.20 and Figure 5.21, respectively).
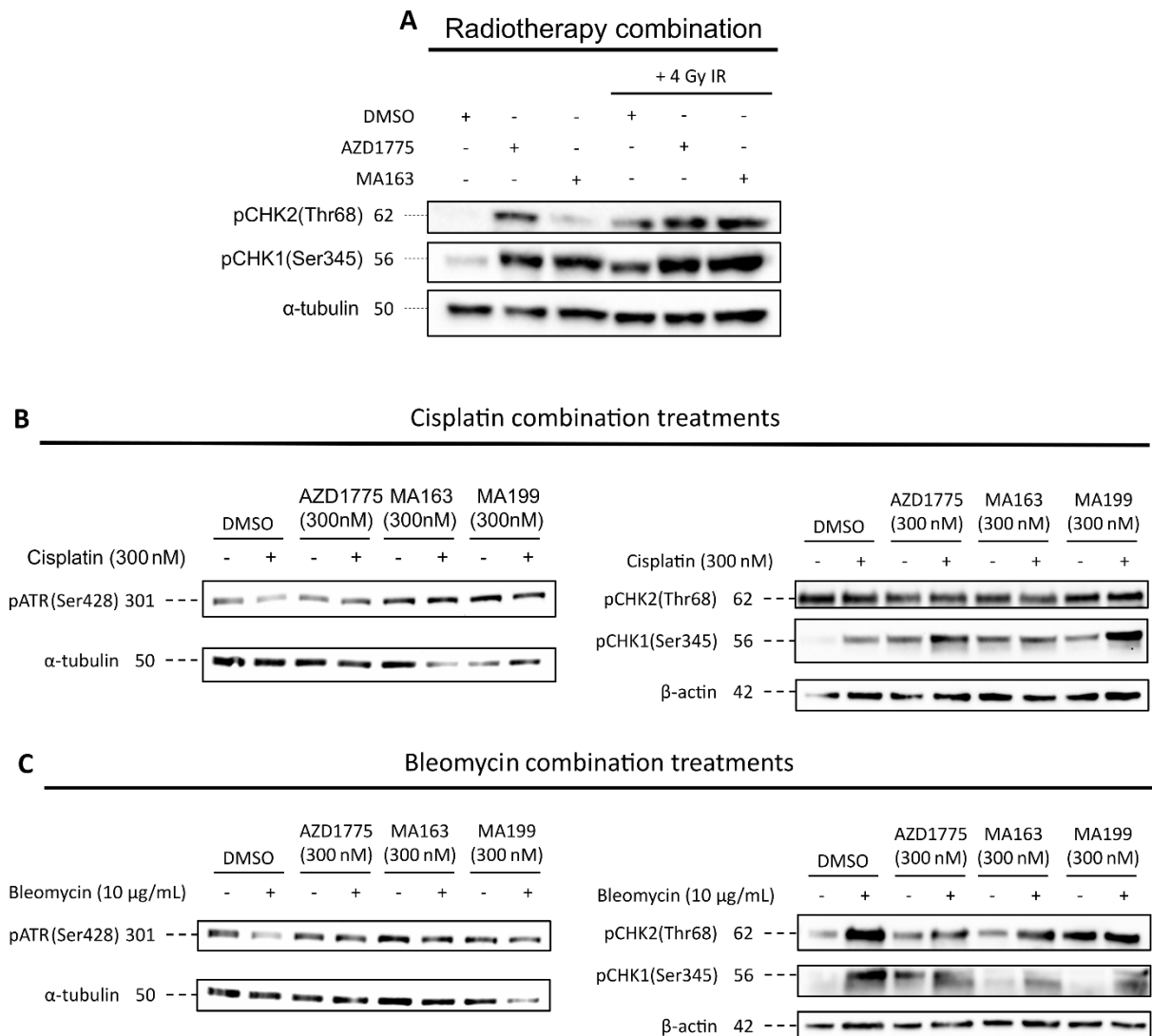
Figure 5.20 Activation of ATR, Chk1 and Chk2 by AZD1775. MA163 and MA199 as single agents and combinatorial treatments with irradiation, cisplatin or bleomycin in A-253 cells. Cells were treated with 300 nM compounds for 3 h alone or in addition to 4 Gy irradiation, 300 nM cisplatin or 10 μg/mL bleomycin. Lysates were produced, ran and blots were probed for (A) pChk2 (Thr68), pChk1 (Ser345) and α-tubulin as a loading control or (B & C) pATR, pChk2 (Thr68), pChk1 (Ser345), and α-tubulin or β-actin as a loading control. (A) Western blot where AZD1775 and MA163 were added to cells alone or in combination with 4 Gy IR (n = 1). (B) Western blots where AZD1775, MA163 or MA199 were added to cells alone or with cisplatin (n = 1). (C) Western blots where AZD1775, MA163 or MA199 were added to cells alone or with bleomycin (n = 1).

Phosphorylation of Chk1 is elevated in cells treated with AZD1775, MA163 and MA199 alone compared to DMSO in A-253 (p53-null) (Figure 5.20). AZD1775 with 4 Gy, MA163 with 4 Gy, AZD1775 with cisplatin and MA199 with cisplatin combinations also show higher levels of

pChk1 compared to the single genotoxic agent. Activation of pChk2 by Wee1-targeting

treatments, especially AZD1775, is more variable between repeats. It appears that the

phosphorylation of ATR at Ser428 is equal in the single Wee1-targeting compound

treatments compared to the combinations, therefore the activation of pChk1 appears to be

an effect independent of phosphorylation of ATR at this site. This data suggests that

AZD1775, MA163 and MA199 activate the ATR-Chk1 pathway as monotherapies and the

downstream of this pathway is hyperactivated with the combination of these treatments

with irradiation or cisplatin. The relative levels of pChk2, pChk1 and pATR were calculated

and can be found in Tables 5.6 and 5.7.

Table 5.6 Quantitation of pChk2 and pChk1 bands in Figure 5.20A of Wee1-targeted cells alone or in combination with IR in A-253 cells. Band intensity was measured, normalised to tubulin and made relative to DMSO.

Treatment condition	pChk2 (Thr68)	pChk1 (Ser345)
DMSO	1.00	1.00
AZD1775	11.1	8.00
MA163	2.35	6.54
DMSO + 4 Gy	6.51	3.83
AZD1775 + 4 Gy	13.1	8.16
MA163 + 4 Gy	9.35	8.00

Increased phosphorylation of Chk1 is observed in all treatment conditions in figure 5.20A,

with the largest relative increase in the combination of AZD1775 + 4 Gy. Furthermore,

pChk2 has increased 13-fold in the AZD1775 combination treatment compared to DMSO,

and shows higher relative levels in each sample. This quantitation supports the qualitative

increase in band intensity, suggesting that Wee1-targeting treatments can activate DDR

pathways independent of other genotoxic agents.

Table 5.7 Quantitation of pChk2 and pChk1 bands in Figure 5.20B and Figure 5.20C of Wee1-targeted cells alone or in combination with chemotherapeutics in A-253 cells. Band intensity was measured, normalised to tubulin and made relative to DMSO.

Protein	Band intensity relative to DMSO															
	+ / - Cisplatin								+ / - Bleomycin							
	DMSO		AZD1775		MA163		MA199		DMSO		AZD1775		MA163		MA199	
	-	+	-	+	-	+	-	+	-	+	-	+	-	+	-	+
pChk2 (Thr68)	1.00	0.32	0.36	0.22	0.23	0.37	0.32	0.22	1.00	3.77	1.40	2.00	0.84	1.78	2.75	3.95
pChk1 (Ser345)	1.00	0.53	1.54	0.50	0.43	0.45	2.02	1.28	1.00	2.41	2.32	2.50	0.60	1.40	0.67	2.58
pATR (Ser428)	1.00	0.74	1.11	1.59	1.67	6.40	6.38	2.82	1.00	0.58	1.16	0.95	0.81	1.02	1.19	2.19

Calculation of the relative band intensity for the chemotherapeutic blots supported that MA199 and cisplatin activates more pChk1 in comparison to cisplatin alone. Similarly, to UM-SCC-6 (p53-WT) cells, as these blots are only n = 1 and have some variability in the actin loading control, the quantitation of the blots does not corroborate all of the qualitative trends.
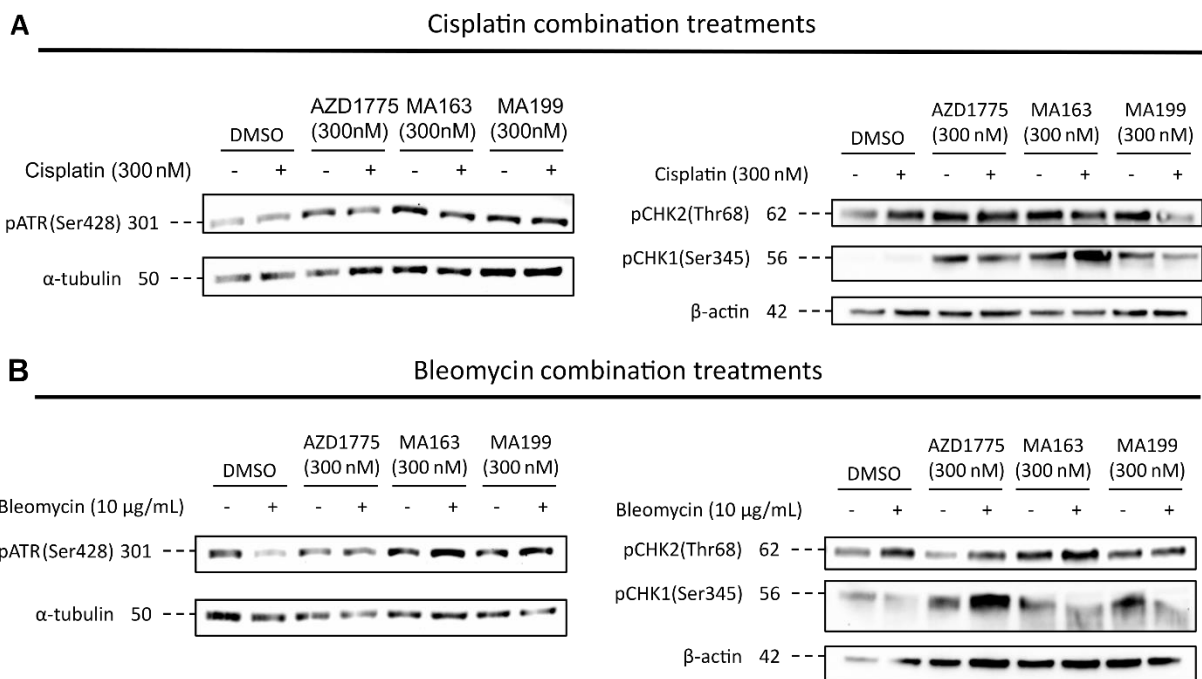
Figure 5.21 Phosphorylation of ATR, Chk1 and Chk2 following AZD1775, MA163 and MA199 administered as single agents and combinatorial treatments cisplatin or bleomycin in FaDu cells. Cells were treated with 300 nM compounds for 3 h alone or in addition to 300 nM cisplatin or 10 µg/mL bleomycin. Lysates were produced, ran and blots were probed for pATR, pCHK2(Thr68), pCHK1(Ser345), and α-tubulin or β-actin as a loading control. (A) Western blots where AZD1775, MA163 or MA199 were added to cells alone or with cisplatin (n = 1). (B) Western blots where AZD1775, MA163 or MA199 were added to cells alone or with bleomycin (n = 1).

pChk2 levels remain consistent between single agent or combinatorial cisplatin treatments in FaDu (p53-mutant) cells (Figure 5.21A and Table 5.8), as seen in A-253 (p53-null) cells (Figure 5.20). Bleomycin induces DSBs (Hecht, 2000), therefore the highest relative pChk2 levels in the treatment conditions are in the bleomycin-treated cells (Figure 5.21B). AZD1775, MA163 and MA199 increase activation of Chk1 alone and in combination with cisplatin or bleomycin compared to DMSO or the genotoxin alone. As previously described in A-253 (p53-null), ATR pSer428 levels remain consistent on the blots between all conditions, therefore the higher pChk1 levels in the treated cells is independent of ATR Ser428 phosphorylation. Quantitation of band intensity was performed (Table 5.8), however

as with the previous cell lines, more repeats would need to be conducted for accurate

relative levels.

Table 5.8 Quantitation of pChk2, pChk1 and pATR in Figure 5.21 of Wee1-targeted cells alone or in combination with chemotherapeutic agents in FaDu cells. Band intensity was measured, normalised to tubulin and made relative to DMSO.

Protein	Band intensity relative to DMSO															
	+ / - Cisplatin								+ / - Bleomycin							
	DMSO		AZD1775		MA163		MA199		DMSO		AZD1775		MA163		MA199	
	-	+	-	+	-	+	-	+	-	+	-	+	-	+	-	+
pChk2 (Thr68)	1.00	1.23	1.57	1.49	2.22	1.69	1.42	0.50	1.00	0.61	0.12	0.14	0.25	0.27	0.15	0.27
pChk1 (Ser345)	1.00	6.97	8.02	7.35	27.0	9.69	3.13	3.01	1.00	0.29	0.40	0.54	0.36	0.13	0.44	0.36
pATR (Ser428)	1.00	1.00	1.99	0.88	1.47	1.33	0.70	0.58	1.00	0.64	1.23	1.93	1.80	2.46	1.50	3.25

The phosphorylation of Chk1 and Chk2 show similar trends across UM-SCC-6 (p53-WT), A-253 (p53-null) and FaDu, suggesting activation of the DDR by these compounds is a p53-independent response. To investigate whether p53-deficient cells have more DNA damage, indicated by DNA damage marker γH2AX, compared to that observed in p53-proficient ones (Figure 5.5), γH2AX immunoblots were performed (Figure 5.22).
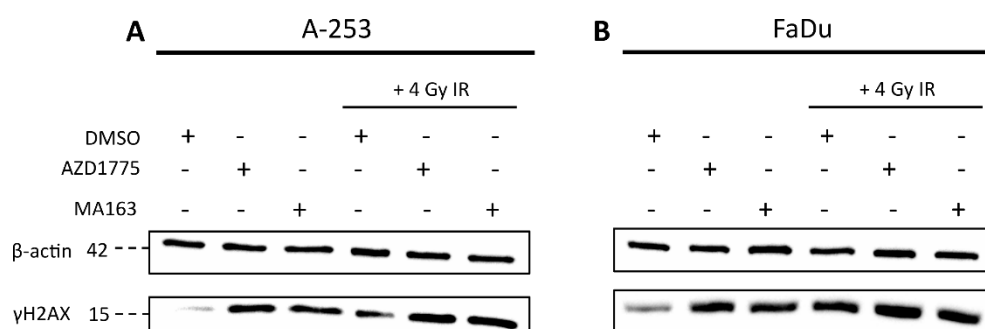
Figure 5.22 Activation of γH2AX by AZD1775 and MA163 as single agents and combinatorial treatments with irradiation in p53-deficient cells. Cells were treated with 300 nM compounds for 3 h alone or in addition to 4 Gy irradiation. Lysates were produced, ran and blots were probed for γH2AX and β-actin as a loading control (n = 3 or n = 1 for blots A and B, respectively).

γH2AX bands were more intense in all treatment conditions compared to the DMSO control in both A-253 (p53-null) and FaDu (p53-mutant) cells (Figure 5.22). There was an increase of ~4.00 relative levels in the combination of AZD1775 and MA163 with 4 Gy irradiation compared to IR alone in A-253 (p53-null) (Table 5.9). Although not as dramatic of an increase, the combination of AZD1775 with IR caused elevated phosphorylation of H2AX in comparison to radiation as a single agent.

Table 5.9 Quantitation of relative γH2AX levels from Figure 5.22 in p53-deficient HNSCC cells after treatment with Wee1-targeting compounds alone or in combination with irradiation. Signal intensity was measured and normalised to actin before making levels relative to the DMSO control. In A-253, three repeats were performed and the mean ± SD was calculated from each repeat.

Treatment condition	Relative levels of phosphorylated H2AX	
	A-253 (n = 3) (mean ± SD)	FaDu (n = 1)
DMSO	1.00 ± 0.00	1.00
AZD1775	7.05 ± 5.91	2.69
MA163	6.43 ± 4.40	1.58
DMSO + 4 Gy	6.03 ± 4.35	2.86
AZD1775 + 4 Gy	10.5 ± 7.75	3.12
MA163 + 4 Gy	10.9 ± 8.50	2.48

To better quantify γH2AX intensity and investigate differences between treatments, cells were treated for 2 h with compounds before irradiating with 4 Gy and left for 1 h prior to fixing and staining with anti-γH2AX antibody and DAPI. A-253 (p53-null) and FaDu (p53-mutant) coverslips were then imaged and representative images across three repeats were produced (Figures 5.23 and 5.24, respectively).

	Merge	DAPI	γH2AX
DMSO			
AZD1775			
MA163			
MA199			
DMSO			
AZD1775			
MA163			
MA199			

4 Gy

DAPI **γH2AX**
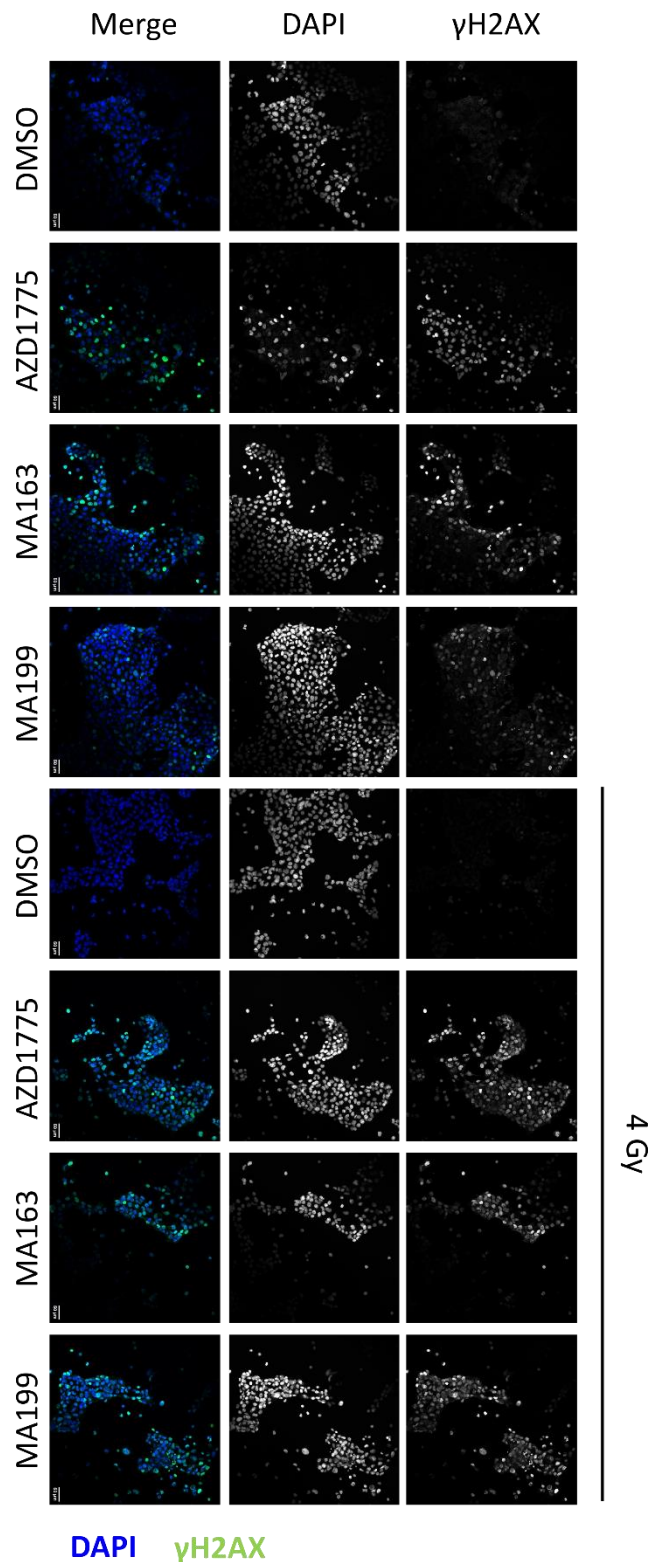
Figure 5.23 Activation of γH2AX as a result of Wee1 inhibition and degradation as single agents or combination treatments in A-253 cells. A-253 cells were treated with 300 nM compound for 3 h alone or with 4 Gy IR after 2 h of initial treatment. Glass coverslips were then fixed and stained with DAPI and γH2AX. Representative images of the treatments from n = 3 showing a colour merge tile with the separate grayscale channels of DAPI and γH2AX. Images were taken using a Leica Stellaris 5 microscope and LAS X software. Images were analysed using FIJI. Scale bar is 50 μm.

Targeting Wee1 increases γH2AX levels alone, compared to DMSO, and with irradiation, compared to DMSO with irradiation, in A-253 (p53-null) cells (Figure 5.23). Similarly, to UM-SCC-6 (p53-WT) (Figure 5.6) and UM-SCC-74A (p53-WT) (Figure 5.7), there was pan-nuclear staining of γH2AX rather than clear foci. Quantification of γH2AX intensity for A-253 (p53-null) was performed and a bee swarm plot was created (Figure 5.25A).

DAPI **γH2AX**
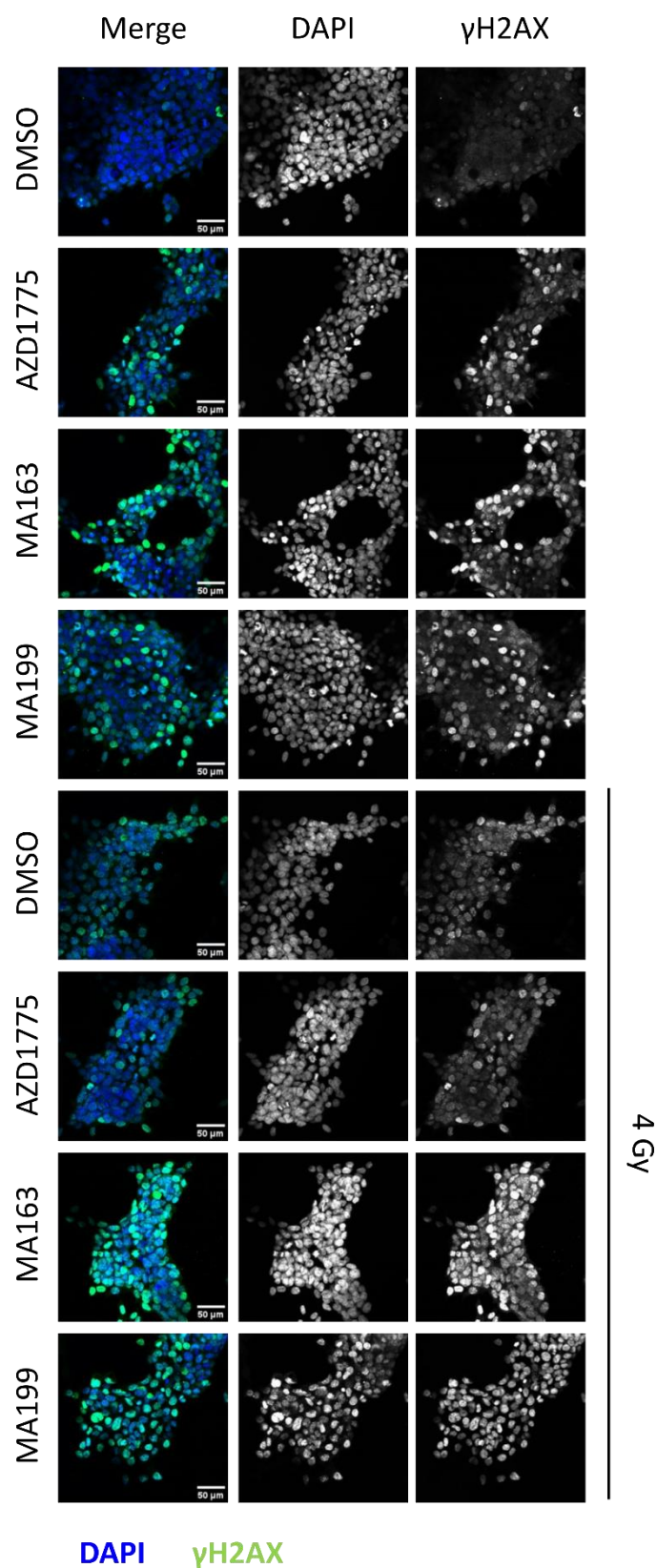
Figure 5.24 Activation of γH2AX due to treatment with Wee1i, AZD1775, or Wee1 PROTACs as a single or combinatorial strategy in FaDu cells. FaDu cells were treated with 300 nM compound for 3 h alone or with 4 Gy IR after 2 h of initial treatment. Glass coverslips were then fixed and stained with DAPI and γH2AX. Representative images of the treatments from n = 3 showing a colour merge tile with the separate grayscale channels of DAPI and γH2AX. Images were taken using a Leica Stellaris 5 microscope and LAS X software. Images were analysed using FIJI. Scale bar is 50 μM. 213

Phosphorylation of H2AX was increased in AZD1775, MA163 and MA199-treated cells alone and with ionizing radiation compared to their relative controls in FaDu (p53-mutant) cells (Figure 5.24). This is consistent with the trends observed in all four HNSCC cell lines tested. Furthermore, pan-nuclear staining of γH2AX was observed in FaDu (p53-mutant) cells. Quantification of γH2AX intensity for FaDu (p53-mutant) was performed and a bee swarm plot was created (Figure 5.25B).
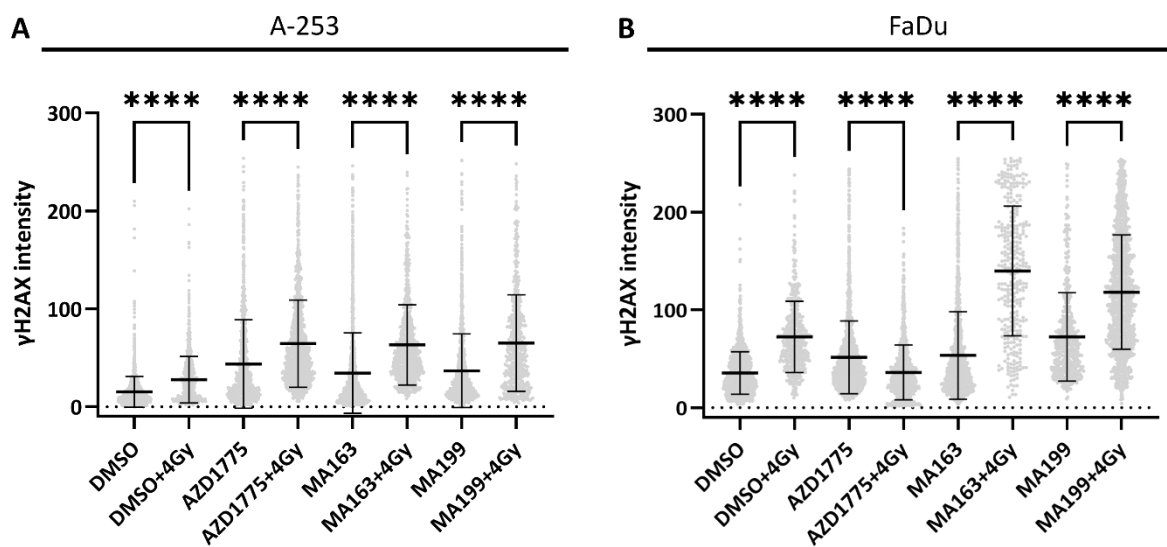
Figure 5.25 Bee swarm plots showing distribution of γH2AX intensity in p53-deficient HNSCC cells from AZD1775, MA163 or MA199 as single agents or with ionizing radiation. Three fields of view from each condition was taken and analysed by creating masks on the DAPI channel and applying the mask to the γH2AX channel to collect the mean γH2AX intensity per cell. This was done across n = 3. All cell intensities were collated (n>325 cells) in each condition to create a Bee swarm to show the distribution of the cell population, plotting the median ± SD, and these were compared between each treatment condition (GraphPad Prism). A one-way ANOVA with a Tukey's multiple comparisons test was performed and the full p-values can be seen in tables 5.3 and 5.4 for A-253 and FaDu, respectively.

All monotherapy treatments significantly increase the median intensity of γH2AX alone compared to DMSO in both A-253 (p53-null) and FaDu (p53-mutant) cells (Figure 5.25). Furthermore, MA163 or MA199 combination strategies caused significantly more γH2AX intensity indicated by a higher median compared to irradiation alone in both cell lines. The majority of combination strategies, except AZD1775 + 4 Gy in FaDu (p53-mutant), increased

phosphorylation of H2AX compared to the single Wee1-targeting drug in both cell lines. In A-253 (p53-null), MA163 and MA199 has a similar median intensity of γH2AX in single agent or combination conditions (Figure 5.25A), whereas, in FaDu (p53-mutant), MA163 showed significantly less γH2AX intensity alone compared to MA199 but significantly more as a combination compared to MA199 + 4 Gy (Figure 5.25B). The most diffuse population distribution was observed in the PROTAC combination treatment conditions in FaDu (p53-mutant) cells, and perhaps the PROTACs are inducing more pan-nuclear γH2AX staining, indicative of increased replication stress, than Wee1 inhibition in this cell line. The full tables of p-values comparing each treatment condition for A-253 (p53-null) and FaDu (p53-mutant) can be seen in table 5.10 and table 5.11, respectively.

Table 5.10 Table of adjusted p-vaules for the activation of γH2AX as a result of the monotherapy and combination with irradiation treatment comparisons in A-253. Analysis of this data has been described in Figure 5.25 and representative images can be seen in Figure 5.23.

	DMSO 0 Gy	AZD1775 0 Gy	MA163 0 Gy	MA199 0 Gy	DMSO 4 Gy	AZD1775 4 Gy	MA163 4 Gy	MA199 4 Gy
DMSO 0 Gy	-	<0.0001 (****)	<0.0001 (****)	<0.0001 (****)	<0.0001 (****)	<0.0001 (****)	<0.0001 (****)	<0.0001 (****)
AZD1775 0 Gy	<0.0001 (****)	-	<0.0001 (****)	<0.0001 (****)	<0.0001 (****)	<0.0001 (****)	<0.0001 (****)	<0.0001 (****)
MA163 0 Gy	<0.0001 (****)	<0.0001 (****)	-	0.4458 (ns)	<0.0001 (****)	<0.0001 (****)	<0.0001 (****)	<0.0001 (****)
MA199 0 Gy	<0.0001 (****)	<0.0001 (****)	0.4458 (ns)	-	<0.0001 (****)	<0.0001 (****)	<0.0001 (****)	<0.0001 (****)
DMSO 4 Gy	<0.0001 (****)	<0.0001 (****)	<0.0001 (****)	<0.0001 (****)	-	<0.0001 (****)	<0.0001 (****)	<0.0001 (****)
AZD1775 4 Gy	<0.0001 (****)	<0.0001 (****)	<0.0001 (****)	<0.0001 (****)	<0.0001 (****)	-	0.9917 (ns)	>0.9999 (ns)

| MA163 4 Gy | <0.0001 (****) | <0.0001 (****) | <0.0001 (****) | <0.0001 (****) | <0.0001 (****) | 0.9917 (ns) | - | 0.9810 (ns) |
| MA199 4 Gy | <0.0001 (****) | <0.0001 (****) | <0.0001 (****) | <0.0001 (****) | <0.0001 (****) | >0.9999 (ns) | 0.9810 (ns) | - |

Table 5.11 Table of adjusted p-values for comparison of the activation of γH2AX in FaDu cells following monotherapy and irradiation combination treatments. Analysis of these data has been described in Figure 5.25 and representative images can be seen in Figure 5.24.

	DMSO 0 Gy	AZD1775 0 Gy	MA163 0 Gy	MA199 0 Gy	DMSO 4 Gy	AZD1775 4 Gy	MA163 4 Gy	MA199 4 Gy
DMSO 0 Gy	-	<0.0001 (****)	<0.0001 (****)	<0.0001 (****)	<0.0001 (****)	>0.9999 (ns)	<0.0001 (****)	<0.0001 (****)
AZD1775 0 Gy	<0.0001 (****)	-	0.8580 (ns)	<0.0001 (****)	<0.0001 (****)	<0.0001 (****)	<0.0001 (****)	<0.0001 (****)
MA163 0 Gy	<0.0001 (****)	0.8580 (ns)	-	<0.0001 (****)	<0.0001 (****)	<0.0001 (****)	<0.0001 (****)	<0.0001 (****)
MA199 0 Gy	<0.0001 (****)	<0.0001 (****)	<0.0001 (****)	-	>0.9999 (ns)	<0.0001 (****)	<0.0001 (****)	<0.0001 (****)
DMSO 4 Gy	<0.0001 (****)	<0.0001 (****)	<0.0001 (****)	>0.9999 (ns)	-	<0.0001 (****)	<0.0001 (****)	<0.0001 (****)
AZD1775 4 Gy	>0.9999 (ns)	<0.0001 (****)	<0.0001 (****)	<0.0001 (****)	<0.0001 (****)	-	<0.0001 (****)	<0.0001 (****)
MA163 4 Gy	<0.0001 (****)	<0.0001 (****)	<0.0001 (****)	<0.0001 (****)	<0.0001 (****)	<0.0001 (****)	-	<0.0001 (****)
MA199 4 Gy	<0.0001 (****)	<0.0001 (****)	<0.0001 (****)	<0.0001 (****)	<0.0001 (****)	<0.0001 (****)	<0.0001 (****)	-

To summarise, the DNA damage response is activated when using a Wee1-targeting

treatment. This trend is also seen in p53 wild-type cell lines, therefore activation of the DDR

by these compounds is not dependent on p53. To elucidate the types of DNA damage that could occur as a result of these treatments, immunofluorescent staining of CENP-A, tubulin and DAPI were undertaken to aim to detect micronuclei, mitotic index and multinucleated cells. This was first performed in A-253 (p53-null) (Figure 5.26).
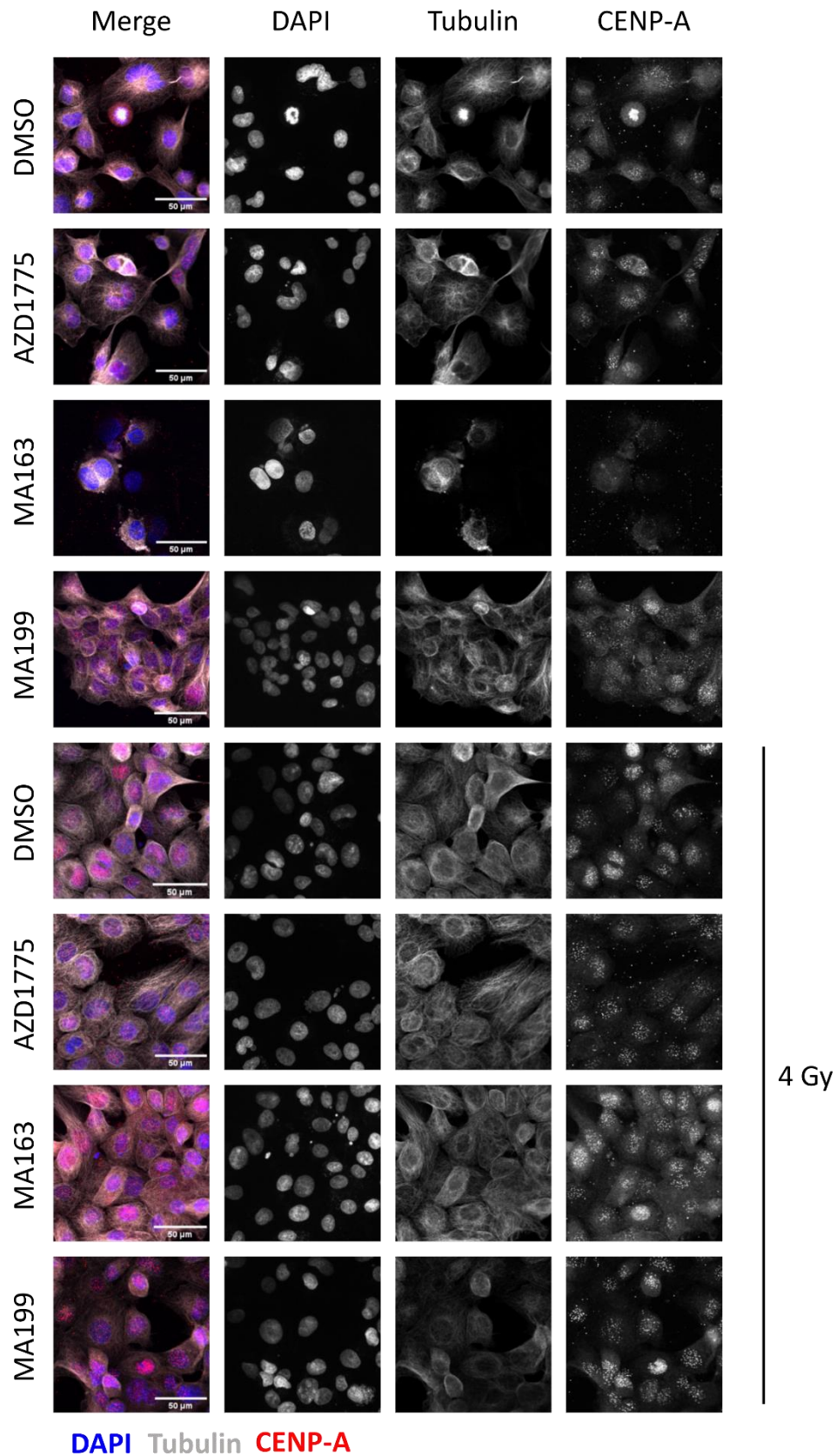
Figure 5.26 Representative images for micronuclei detection and mitotic index analysis of A-253 cells. A-253 cells were treated with 300 nM compounds for 24 h alone or with 4 Gy ionizing radiation before fixing and staining cells on glass coverslips with DAPI and antibodies to CENP-A and Tubulin. Three fields of view were taken for each treatment to analyse data in one repeat. Images were taken using a Leica Stellaris and LAS X software. Images were analysed using FIJI (n = 3). Scale bar is 50 μm.

Initial observations whilst capturing images of the coverslips were that the MA163 single treatment had the lowest number of cells in A-253 (p53-null) (Figure 5.26). Examples of what was considered to be micronuclei, mitotic cells or multinucleated cells can be seen in Figure 5.10. Data was collected and quantified to produce bar graphs for mitotic index, average number of cells analysed per repeat, micronuclei detection and multinucleated cells in A-253 (p53-null) (Figure 5.27).
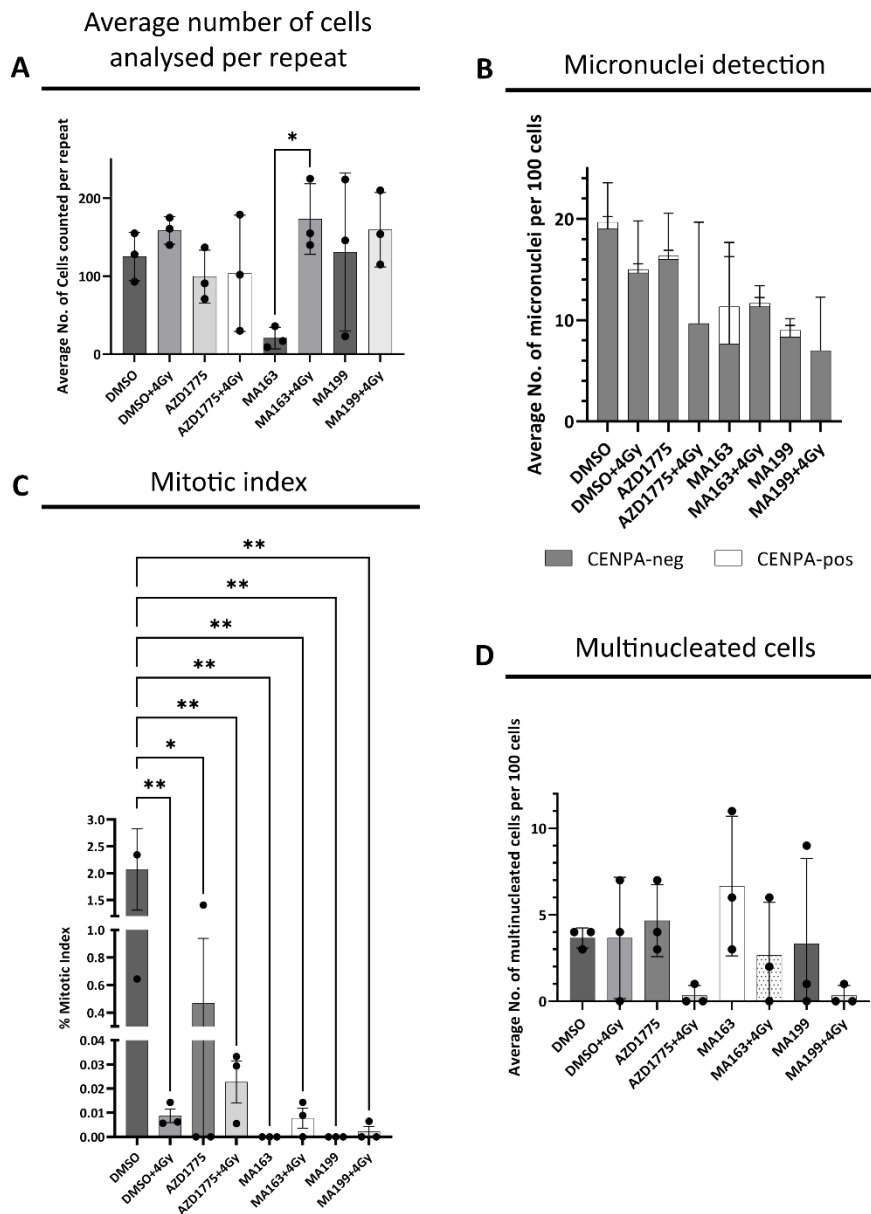
Figure 5.27 Graphs from micronuclei detection and mitotic index experiment of A-253 cells. Representative images from Figure 5.26 were quantified for (A) bar graph showing mean ± SD of n = 3 biological repeats for average number of cells analysed per repeat in each treatment condition, (B) mean ± SD of n = 3 biological repeats for CENPA-negative and CENPA-positive micronuclei per 100 cells, (C) bar graph showing mean ± SD % mitotic index from n = 3 and (D) mean ± SD multinucleated cells per 100 cells across n = 3. cells. Graphs were produced in GraphPad Prism and analysed by a one-way ANOVA with a Tukey's multiple comparisons test. Scale bar is 50 µM.

MA163 had the lowest average number of cells in each treatment condition (Figure 5.27A), as observed in Figure 5.26. The most CENPA-negative micronuclei were seen in the control cells with an average of 19 micronuclei per 100 cells and the least CENPA-negative micronuclei were seen in MA199 with a 63.2% decrease compared to DMSO (Figure 5.27B). Conversely, the treatments generally caused an increase in frequency of micronuclei compared to control cells in UM-SCC-6 (p53-WT) (Figure 5.9) and UM-SCC-74A (p53-WT) (Figure 5.12). However, it is uncertain whether this contradictory response observed in A-253 (p53-null) cells is due to the differing p53 status or a cell line specific effect. As seen with UM-SCC-6 (p53-WT), all treatment conditions of the compounds alone and in combination with irradiation significantly decrease the mitotic index (Figure 5.27C). Fewer multinucleated cells were observed in AZD1775, MA163 or MA199 with 4 Gy compared to the drugs alone (Figure 5.27D).

The same experiment seen in A-253 (p53-null) was then performed in FaDu (p53-mutant) cells and representative images were produced (Figure 5.28). FaDu (p53-mutant) cells are very clustered in cell culture and tend to grow on top of each other in colonies, therefore it was difficult to visualize the CENP-A staining as it was very diffuse (Figure 5.28). It was clear that MA163 was the most cytotoxic to cells at 24 h before fixing and staining as fewer cells were observed on the MA163-treated coverslips compared to the other treatments. as seen in all three other cell lines. Analysed data of mitotic index, multinucleated cells, average number of cells per repeat and micronuclei was collated and produced bar graphs (Figure 5.29).
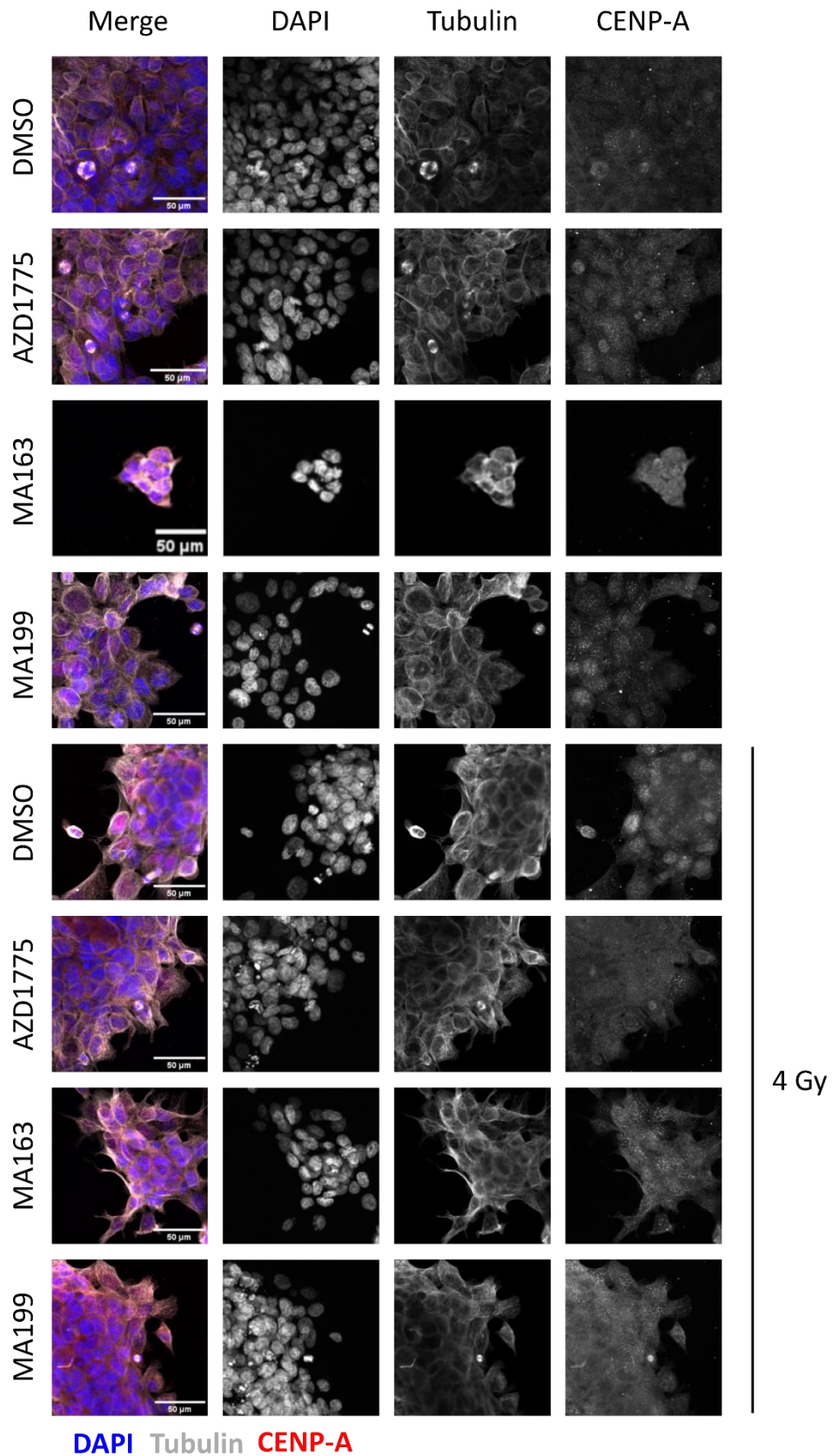
Figure 5.28 Representative images for micronuclei detection and mitotic index analysis of FaDu cells. FaDu cells were treated with 300 nM compounds for 24 h alone or with 4 Gy ionizing radiation before fixing and staining cells on glass coverslips with DAPI, CENP-A or Tubulin. Three fields of view were taken for each treatment to analyse data in one repeat. Images were taken using a Leica Stellaris and LAS X software. Images were analysed using FIJI (n = 3).
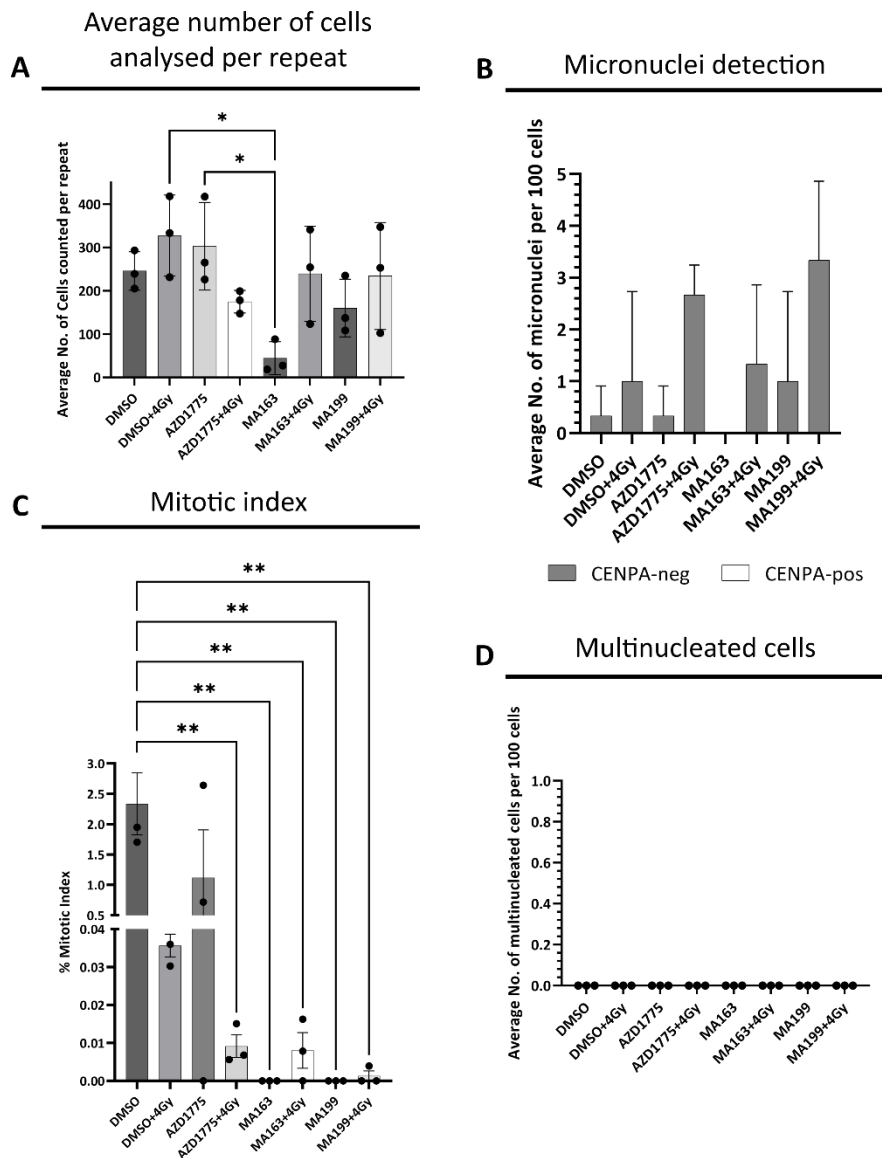
Figure 5.29 Graphs from micronuclei detection and mitotic index experiment of FaDu cells. Representative images from Figure 5.28 were quantified for (A) bar graph showing mean ± SD of n = 3 biological repeats for average number of cells analysed per repeat in each treatment condition, (B) mean ± SD of n = 3 biological repeats for CENPA-negative and CENPA-positive micronuclei per 100 cells, (C) bar graph showing mean ± SD % mitotic index from n = 3 and (D) mean ± SD multinucleated cells per 100 cells across n = 3. cells. Graphs were produced in GraphPad Prism and analysed by a one-way ANOVA with a Tukey's multiple comparisons test.

MA163 was consistently the treatment condition that resulted in the least average number of cells per repeat (Figure 5.29A), suggesting that the initial action of MA163 is much more potent across all cell lines in comparison to the other treatments. All combination

treatments induced more micronuclei formation in FaDu (p53-mutant), supporting that the combination inflicts more DSBs on cells than either the single agent or irradiation alone (Figure 5.29B). The decrease of micronuclei per 100 cells in A-253 (p53-null) cells is likely to be a cell line specific effect and another p53-deficient cell line should be tested to confirm this. The combination of AZD1775, MA163 or MA199 with ionizing radiation or MA163 or MA199 alone causes a significant loss of dividing FaDu (p53-mutant) cells (Figure 5.29C), consistent with previous findings. Finally, no multinucleated cells were detected in any of the repeats (Figure 5.29D).

The final data collected to evaluate how these compounds affect chromosome segregation and if they cause an increase in DNA content was to measure the nuclei size of these cells (Figure 5.30). The proposed hypothesis is that more signs of DNA damage and >4N DNA content would cause larger nuclei. However, this was not necessarily the case in p53-proficient cells (Figure 5.14).
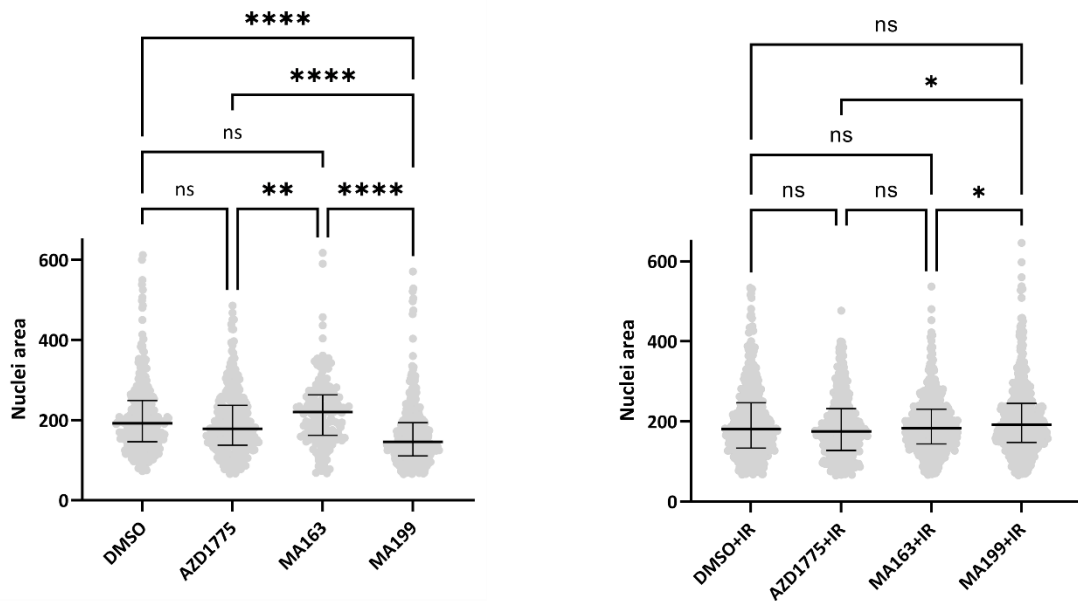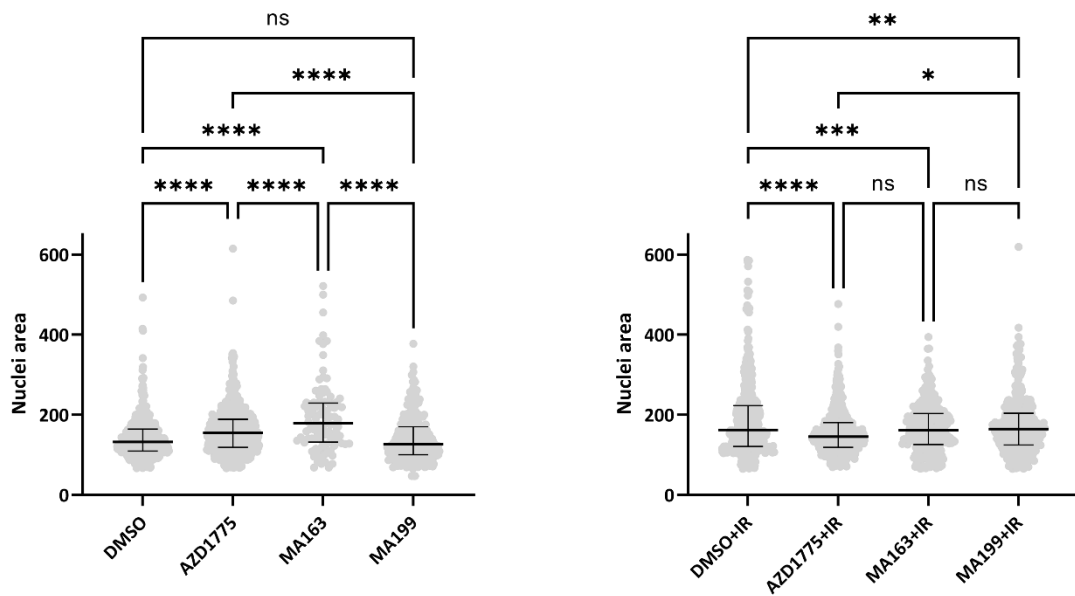
Figure 5.30 Bee swarm plots of nuclear area of p53-deficient cells treated Wee1-targeting drugs alone and in combination with 4 Gy radiation. These plots were produced from the data collected from the micronuclei detection immunofluorescence experiment (Figures 5.26 and 5.28). Three fields of view from each condition were taken and analysed by creating regions of interest (ROIs) on the DAPI channel to measure the nuclear area. This was done across n = 3. All nuclear areas (n>100 cells) were collated in each condition to create Bee swarm plots to show the distribution of the nuclear size population, plotting the median and interquartile range, and these were compared between each treatment condition (GraphPad Prism). A one-way ANOVA with a Tukey's multiple comparisons test was performed.

In A-253 (p53-null), AZD1775 and MA163 did not significantly change the nuclear area compared to DMSO, however MA199 significantly decreased the nuclei size (Figure 5.30A). The combination of Wee1-targetnig treatment with 4 Gy irradiation did not change the nuclear size compared to irradiation alone. In FaDu (p53-mutant) cells, AZD1775 and MA163 significantly increase nuclear area as single agents compared to DMSO but significantly decrease nuclear area as combinations with IR compared to DMSO + 4 Gy (Figure 5.30B). This suggests that the effect that these compounds have as single or combinatorial strategies on nuclear size is cell line-dependent as all four cell lines have not shown any similar trends.

5.3.3 Discussion

This chapter showed that AZD1775 or Wee1 PROTACs can target cells to change how they progress through the cell cycle. In the introduction to this chapter, it was discussed that Wee1 inhibition with or without radiation leads to a decrease of cells in G2 (Yang et al., 2020), which would be expected as inhibition of Wee1 leads to progression past the G2/M checkpoint and into mitosis. Irrespective of p53-status, AZD1775 caused a progressive increase in the G2/M population in UM-SCC-6 (p53-WT) (Figure 5.1), A-253 (p53-null) (Figure 5.15) and FaDu (p53-mutant) (Figure 5.17). Our experiment could not distinguish between G2 and M phase cells; it is hypothesized that this effect in HNSCC cells is due to AZD1775 forcing cells to pass the G2/M checkpoint and the % mitotic cells increases as this has previously been observed in other cell lines (Cuneo et al., 2016; Yang et al., 2020). This was not observed via immunofluorescence in the data presented here, and an explanation for this could be that mitotic cells can be washed away during the processing steps of the experiment. This is even more of an issue with coverslips that have a low cell density, therefore perhaps this is why there is a low mitotic index in the majority of the treatment conditions tested in this chapter. If time had allowed, Histone H3 pSer10 flow cytometry could have been performed to overcome this experimental issue and to determine if these findings support or contradict previously published data. Furthermore, there was a decrease in actively replicating S-phase population over the 48 h time period in all cell lines, indicating replication stress as a result of inhibiting Wee1. These same trends were seen when degrading Wee1 with PROTACs and there were no obvious cell cycle stage differences between Wee1 degradation and inhibition at 300 nM.

Cell cycle analysis of Wee1i and irradiation-treated UM-SCC-6 (p53-WT) cells revealed a nearly complete absence of any actively replicating cells compared to Wee1i-treated cells alone (Figure 5.2) and this was also observed in the other p53-proficient cell line, UM-SCC-74A (p53-WT) (Figure 5.3). This effect appears to have some p53-dependence, as p53-deficient cell lines did not show a complete loss of the EdU-incorporating population (Figures 5.16 and 5.18 for A-253 and FaDu, respectively). The populations of G1, S and G2/M cells were much harder to gate in A-253 (p53-null) and FaDu (p53-mutant) and it appeared that these populations merged to form one large 2<N<4 population when Wee1-targeting treatments were used in combination with irradiation. Although the single agents appear to have the same cellular response, regardless of p53-status, the combination of these compounds with irradiation appears to cause more genomic instability for p53-deficient cell lines. This combination in cells without a G1/S checkpoint leads to replication stress that causes the appearance of cells with intermediate DNA content (2<N<4), whereas cells with 2<N<4 DNA content will likely be arrested at the G1/S transition in p53-proficient cells and killed before they were fixed, stained and analysed.

When degrading Wee1 with PROTACs, this does not inhibit PLK1 and allows cells with DNA damage to progress through mitosis, implied by the decrease in Cyclin B1 levels seen in FaDu (p53-mutant) (Figure 5.19). It would be interesting to see if the combination of AZD1775 and 4 Gy has the same effect as AZD1775 inhibits PLK1. In addition, it would be good to investigate this trend in UM-SCC-6 (p53-WT), UM-SCC-74A (p53-WT) and A-253 (p53-null) to test the hypothesis that this trend would be the same in all cells, irrespective of p53-status. This is because the spindle checkpoint is a p53-independent checkpoint (Meek, 2000).

Analysing the mitotic index highlighted that the monotherapies caused a significant decrease in actively dividing cells in UM-SCC-6 (p53-WT) (Figure 5.11), A-253 (p53-null) (Figure 5.27) and FaDu (p53-mutant) (Figure 5.29). This suggests that targeting Wee1 prevents metaphase to be carried out. To aim to elucidate how these monotherapies cause this, live cell microscopy with mitotic markers, such as using a fluorescent probe that can allow visualisation of chromatin condensation, may help to conclude how these treatments impact metaphase and the spindle assembly checkpoint. Furthermore, using another mitotic marker as well as CENP-A may make it easier to count mitotic cells, such as using pH3(ser10). This marker can then be used in immunofluorescence and flow cytometry to compare trends between techniques. The length of mitosis should also be investigated as if these treatments are causing difficulties at the spindle assembly checkpoint, this could result in G2/M checkpoint abrogated cells showing longer mitosis.

AZD1775, MA163 and MA199 caused pan-nuclear staining of γH2AX alone and in combination with 4 Gy in all HNSCC cell lines (Figures 5.6, 5.7, 5.23 and 5.24), which is consistent with previous studies that AZD1775 leads to pan-nuclear staining (Parsels et al., 2018). This is indicative of replication stress and supports the hypothesis that these compounds cause replication stress made from observing an intermediary 2<N<4 EdU-negative cells in the cell cycle profile experiments. This pan-nuclear staining increases in intensity when the combination of 4 Gy and Wee1-targeting treatment is used in comparison to the single agent or 4 Gy alone in most instances across all cell lines (Figures 5.8 and 5.25). The activation of γH2AX levels was equal in AZD1775 and AZD1775 + IR treatment on a western blot in oesophageal cancer cells and our findings (Figures 5.5 and 5.22) were consistent in each cell line with this previous study (Yang et al., 2020). Our data showed that in some cases, PROTACs caused significantly more γH2AX activation compared

to AZD1775, such as in FaDu (p53-mutant) (Figure 5.25 and Table 5.4), however it appeared to be cell line dependent if AZD1775 or Wee1 PROTACs caused more pan-nuclear staining, and therefore replication stress. Phosphorylation of ATR and Chk1 was elevated in Wee1-treated cells compared to 0 Gy or 4 Gy alone in all cell lines, further suggesting replication stress. In some cases, pChk1 was present in the absence of pATR, however it is likely due to experimental set-up. Immunoblotting of pATR was performed with pATR Ser428, which is an established marker of ATR activation, but pATR Thr1989 may have been a more suitable marker as this autophosphorylation event is crucial for ATR activation (Liu et al., 2011).

Previous studies have shown AZD1775 increases radiation-induced mitotic catastrophe by measuring micro- and multi-nucleated cells (Yang et al., 2020). In 75% of the cell lines tested, our data supports this finding by seeing an increase of micronuclei. Furthermore, <2N DNA content cells progressively increased over time in UM-SCC-6 (p53-WT), A-253 (p53-null) and FaDu (p53-mutant). CENP-A was used to determine if the micronuclei contain a whole chromosome (CENP-A positive) or chromosomal fragments indicative of DSBs (CENP-A negative). The majority of micronuclei found in the AZD1775, MA163 or MA199 treated cells were CENP-A negative and this did not change when adding 4 Gy irradiation. These findings, consistent with mitotic catastrophe, were found in both p53-proficient and p53-deficient cell lines. There appeared to be no clear consistent trends with multinucleated cells across the cell lines, however, in the cell cycle flow cytometry, there was an increase in treated cells with >4N DNA content.

The findings in this chapter suggest that Wee1 inhibition causes a progressive increase in the G2/M population in HNSCC cells, irrespective of p53-status. Furthermore, this observation is seen when Wee1 is degraded, implying that selectively targeting Wee1 does

not enforce progression past the G2/M checkpoint any more than Wee1 inhibition at 300 nM. Using irradiation with Wee1-targeting treatments could result in more replication stress compared to Wee1 treatments as single therapies, however as we are unsure if the irradiator was operating correctly during these experiments, they would need to be repeated to draw these conclusions. In both p53-proficicent and p53-deficient cell lines, we see blocking of EdU incorporation, however we do not see the presence of 2<N<4 DNA content cells in p53-proficient cells treated with Wee1-targeting compound + IR that we see in p53-deficient cell types. Targeting Wee1 leads to the activation of ATR-Chk1 pathway, which is more intensely activated when treating cells with the combination of drug and radiotherapy. The induction of the DNA damage response is seen in all cell lines and does not depend on p53-dependecy in HNSCC cells. The data presented here has supported findings of the effect of Wee1 inhibition in the literature and has provided details on how Wee1 PROTACs could affect S-phase and mitosis in the cell cycle and cause a DDR in HNSCC cells.

To further elucidate the capabilities of Wee1 PROTACs, the next chapter will investigate whether selective targeting using Wee1 PROTACs causes more or less inhibition of cell proliferation compared to AZD1775 in lung and kidney cancer cell lines. Furthermore, we wanted to investigate if the choice of E3 ligase used in the PROTAC had a bearing on the efficacy of the compound.

6 The impact of varying E3 ubiquitin ligase status on Wee1 PROTACs in lung and kidney cancer cell lines

6.1 Introduction

6.1.1 Wee1 as a drug target in lung and kidney cancers

The discussion of if expression of E3 ligase had an impact on PROTAC potency was mentioned in sections 3.3.5 and 4.3.5. Here we discuss a study that stated that the efficacy of PROTACs is largely affected by the choice of E3 ligase recruited and focus on how Wee1 inhibition has previously been reported to impact the selected cell lines.

During this project, a report found that VHL- and CRBN-based BRD4 PROTACs show differing efficacy to their target (Luo et al., 2022). For example, the CRBN-BRD4 PROTAC, dBET1, shows a very high DC50 in NCI-H23 whereas the PROTAC shows potency with a DC50 of 507 nM in A549, both lung cancer cell lines. There were no reported mutations of CRBN, therefore we hypothesised that the choice of E3 ligase ligand has an impact on efficacy. As both A549 and NCI-H23 were accessible to us, these were selected to investigate. Kidney cancers have frequently reported mutations in VHL, therefore to further confirm that the potency of the PROTACs is dependent on E3 ligase levels, two RCC cell lines were selected with varying VHL status to confirm if a VHL PROTAC will not work in a VHL mutant cell line. Mutational analysis of the NCI-60 cell line set revealed that A-498 possesses mutations in VHL causing loss of VHL (Ikediobi et al., 2006), therefore this was selected as the VHL-mutant cell line and SN12C, with no reported mutations in VHL, was the wild type cell line.

To determine if Wee1 PROTACs would be efficacious in the cell lines selected, initial literature searches were performed. A study has reported that renal cell carcinoma cells are sensitive to Wee1 inhibition, with EC50 values of 87 nM in A-498 (Pfister et al., 2015). Furthermore, AZD1775 caused tumour regression in A-498 tumour xenografts, indicating that Wee1 inhibition can cause cytotoxicity in renal cell carcinoma (RCC) cells. Wee1 inhibition in A-498 caused replication stress, which was signified by pan-nuclear γH2AX staining, a similar effect as seen in HNSCC cells in Chapter 5. This suggested that although the VHL-Wee1 PROTAC may not degrade Wee1, we should still see loss of cell viability and reduction of pCDK1.

Wee1i, AZD1775, has demonstrated to increase late S-phase and G2/M populations in HeLa and NSCLC, NCI-H1299, cell lines (Mak et al., 2014). Furthermore, it has been shown to sensitize NCI-H1299 to gemcitabine treatments as a combinatorial strategy by reducing cell viability, inducing apoptosis and a sub-G1 population (Hirai et al., 2009). Single agent treatment with AZD1775 in the murine LLC (lung cancer cell) line shows some induction of DNA damage by slightly elevated γH2AX levels, however the combination with irradiation significantly enhances γH2AX levels (Patel et al., 2019). Therefore, Wee1 PROTACs are likely to have some effect on cell viability in lung cancer cells.

This clearly demonstrates that lung and kidney cancer cell lines can be sensitized to other genotoxic treatments with AZD1775. Wee1 inhibition reduces cell viability of lung and kidney cancer cell lines, therefore it will be interesting to investigate if Wee1 PROTACs can degrade Wee1 and reduce cell viability, equally to AZD1775. In addition, the differing efficacy of CRBN- or VHL-based PROTACs within cancer types were investigated to see if the expression levels of the E3 ligases had a bearing on the potency of the molecule.

6.2 Aims and objectives

In this chapter, Wee1 PROTACs will be characterized in lung and kidney cancer cell lines with varying levels of E3 ubiquitin ligase expression and this will be assessed via a number of aims:

1. Investigate the relative expression levels of CRBN and VHL in lung and kidney cell lines and determine if the levels of the E3 ubiquitin ligases affect the potency of the Wee1 PROTACs.

2. Compare the degradation profiles of MA163 and MA199 in lung and kidney cancer cell lines.

3. Assess AZD1775, MA163 and MA199 as single agent treatments on cell viability.

6.3 Results and discussion

6.3.1 Expression levels of E3 ubiquitin ligases in Lung and Kidney cell lines

It has previously been discussed that expression and mutation of VHL and CRBN were predictors of PROTAC activity (Luo et al., 2022). To further investigate this with VHL- and CRBN-based Wee1 PROTACs, kidney cancer cell lines, SN12C and A-498, and lung cancer cell lines, A-549 and NCI-H23, were allowed to grow under normal growth conditions to observe the relative expression levels of E3 ubiquitin ligases, CRBN and VHL. This was performed before assessing the degraders degradation profile in these cells. This was to evaluate the ability of the PROTACs to cause degradation and if this depended on varying levels of the E3 ubiqutin ligase. Western blots were probed for CRBN, α-Tubulin and VHL. α-Tubulin was

used as the loading control for this experiment as there was less variability in α-Tubulin

levels across the cell lines in comparison to β-actin (Figure 6.1).
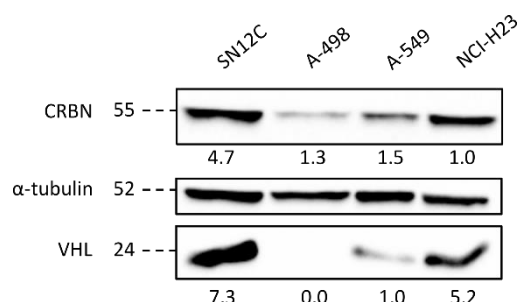
Figure 6.1 Relative expression levels of E3 ubiquitin ligases, CRBN and VHL, in Lung and Kidney cell lines. Western blot showing levels of CRBN and VHL in untreated lysates of Kidney cancer cells, SN12C and A-498, and Lung cancer cells, A-549 and NCI-H23. The membrane was blotted for CRBN, α-Tubulin (as the loading control) and VHL, n = 1. Relative levels of CRBN or VHL normalised to tubulin are shown for each protein underneath the band that the value corresponds to.

SN12C contained 3.6-fold more CRBN compared to the other kidney cell line, A-498 (Figure

6.1). It was hypothesized that A-498 would not show a band for VHL, as this kidney cell line

is VHL-mutant, and this was what was observed and quantified. A-549 showed ~ 5-fold less

VHL compared to the alternative lung cancer cell line, NCI-H23 and similar levels of CRBN.

No known CRBN or VHL mutations have been noted for either lung cancer cell line. Chapter

3 suggests that the PROTACs are efficient even when E3 ubiquitin ligases are at their lowest

levels. Previous published data suggested that we would not see degradation with a CRBN-

based PROTAC in NCI-H23 (Luo et al., 2022), however as there is an intense band for

presence of CRBN in NCI-H23, it was anticipated that MA163 will be able to degrade. We

hypothesize that MA199 will not degrade Wee1 in A-498 as this cell line is VHL-mutant. This

hypothesis will be tested by dose response western blots, similar to those performed in

HNSCC cells in section 3.3.3 (Figure 3.7).

6.3.2 Assessment of second generation Wee1 PROTACs in Ling and Kidney cell lines

6.3.2.1 Dose response of MA163 and MA199 in Lung and Kidney cells

Lung and kidney cancer cells were treated with MA163 or MA199 for 24 h prior to the production of lysates to examine the Wee1 degradation profiles. Cell lines were selected with one exhibiting higher expression levels of the E3 ubiquitin ligases and one with lower expression levels (or mutations) to test if this effected the potency of the PROTACs in different cancer types. Western blots of PROTAC-treated lung and kidney cancer cells were probed for Wee1, β-actin and pCDK1 (Tyr15) (Figure 6.2 & Figure 6.3, respectively).
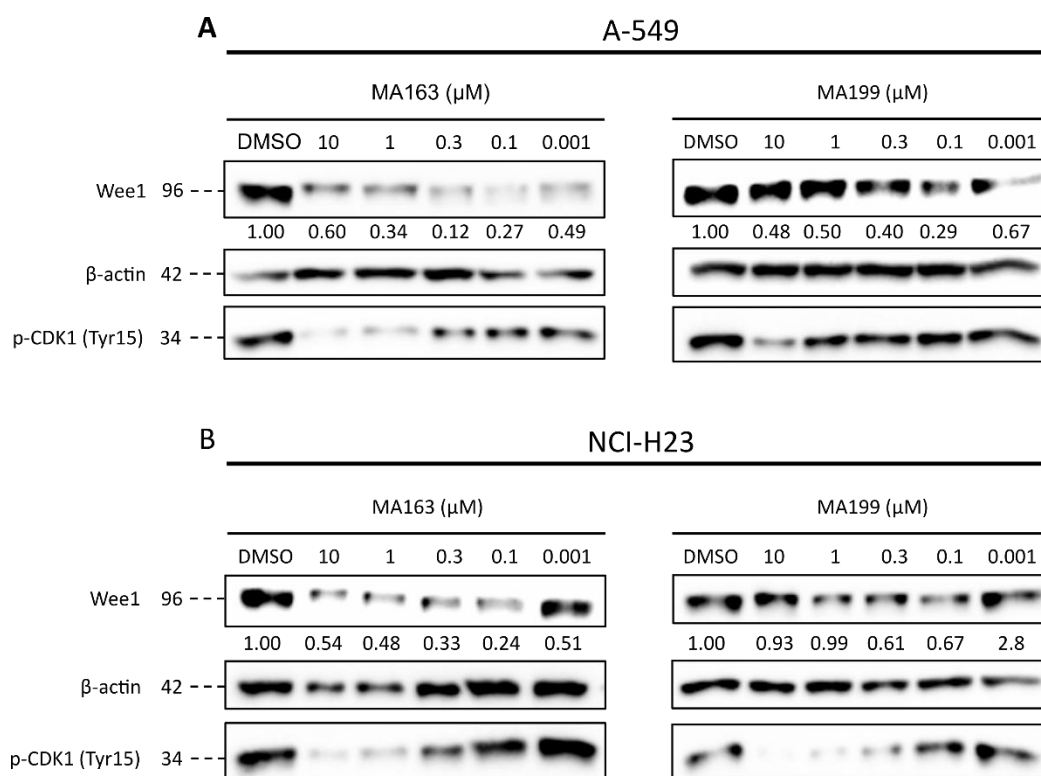
Figure 6.2 Degradation profiles of MA163 and MA199 in lung cancer cell lines, A549 and NCI-H23. Western blots of lung cancer cells that were treated with either MA163 or MA199 for 24 h prior to the production of lysates. The membrane was blotted for Wee1, β-actin (as the loading control) and pCDK1 (Tyr15), n = 1. Quantitation of relative levels of Wee1 to DMSO control normalised to actin are underneath the corresponding band.

MA163, a CRBN-recruiter Wee1 PROTAC, was able to degrade Wee1 from 10 µM to 100 nM and inhibit its substrate, pCDK1, in both lung cancer cell lines (Figure 6.2). The most degradation was observed at 300 nM with 12 % Wee1 remaining in A-549 and was at 100 nM with 24 % Wee1 remaining in NCI-H23. MA199 was a particularly poor degrader and was not able to reduce levels of pCDK1 in A549 cells compared to NCI-H23 (Figure 6.2). Furthermore, MA199 was also not effective at degrading Wee1 in NCI-H23, however it was able to inhibit Wee1 and cause loss of pCDK1 more effectively than A549 cells. MA163 was a better Wee1 degrader in both A549 and NCI-H23 compared to the VHL-based degrader. This finding is contradicting of previously shown data where VHL-based PROTAC, MZ1, was more potent in both cell lines compared to the CRBN-based PROTAC tested (Luo et al., 2022). MA163 appears to induce more degradation in A549 in comparison to NCI-H23, which was a similar trend observed in Luo et al., (2022).
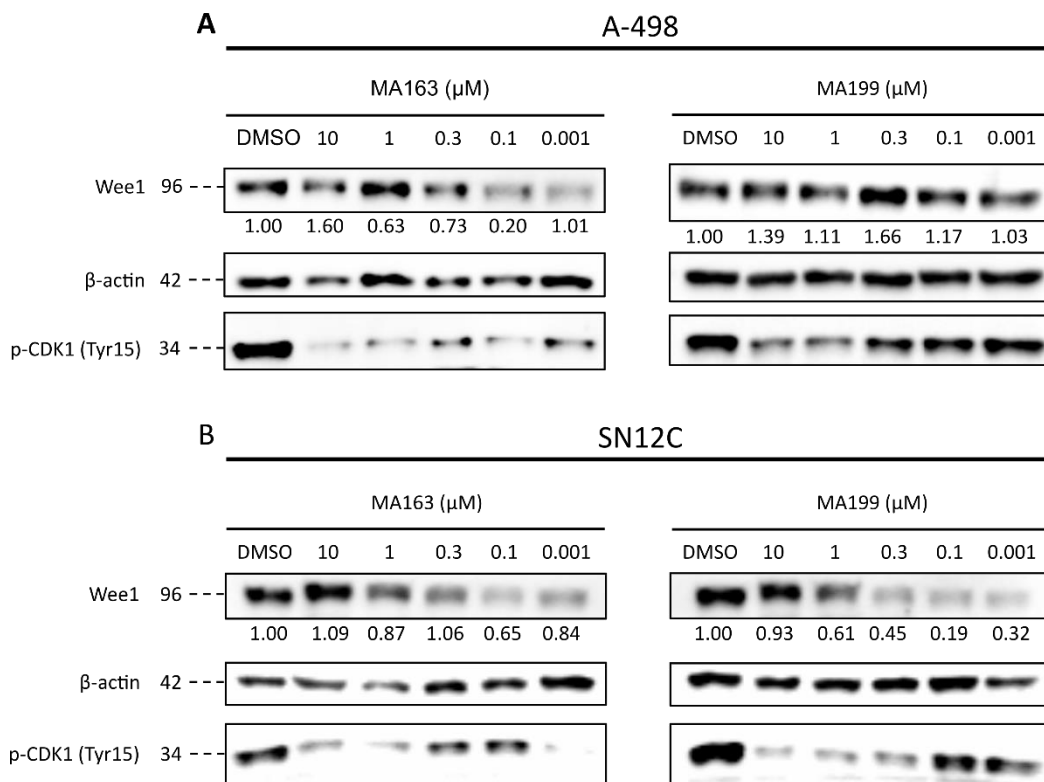
Figure 6.3 Degradation profiles of MA163 and MA199 in A-498 and SN12C kidney cancer cell lines. Western blots of MA163 and MA199-treated kidney cancer cells that were treated with either MA163 or MA199 for 24 h prior to the production of lysates. The membrane was blotted for Wee1, β-actin (as the loading control) and pCDK1 (Tyr15), n = 1. Quantitation of relative levels of Wee1 to DMSO control normalised to actin are underneath the corresponding band.

MA199, a VHL-recruiter Wee1 PROTAC, was not able to degrade Wee1 in VHL-mutant kidney cancer cell line, A-498, however it was able to inhibit Wee1 and reduce levels of pCDK1 (Figure 6.3A). MA199 degraded Wee1 at nanomolar concentrations in SN12C, sustained reduced pCDK1 levels and demonstrated the hook effect at high doses of the compound (Figure 6.3B). MA163 formed unproductive binary complexes at high concentrations in kidney cell lines and was unable to degrade Wee1 at 10 µM but was able to target Wee1 for degradation at the lower doses.

These data further corroborated that relative expression levels of the E3 ubiquitin ligases do not affect the PROTACs ability to degrade its target and that variations in the degradation profiles could be more cell line dependent. The exception is VHL-mutant kidney cell line A-498 which showed no degradation with MA199, confirming that the degradation of Wee1 seen by these PROTACs is as a result of targeting Wee1 for degradation by the UPS via VHL.

6.3.2.2 Effect of single agent treatment of Wee1 PROTACs on cell viability in lung and kidney cancer cell lines

To compare the potency of MA163 and MA199 in the lung and kidney cancer cell lines to that observed in the HNSCC cell lines investigated in previous chapters, their EC50 values were calculated. A-549, NCI-H23, A-498 and SN12C cells were treated for 72h with varying doses of MA163 and MA199, ranging from 20 µM to 0.1 nM. The plates were incubated with MTS reagent and dose response curves were produced (Figure 6.4).
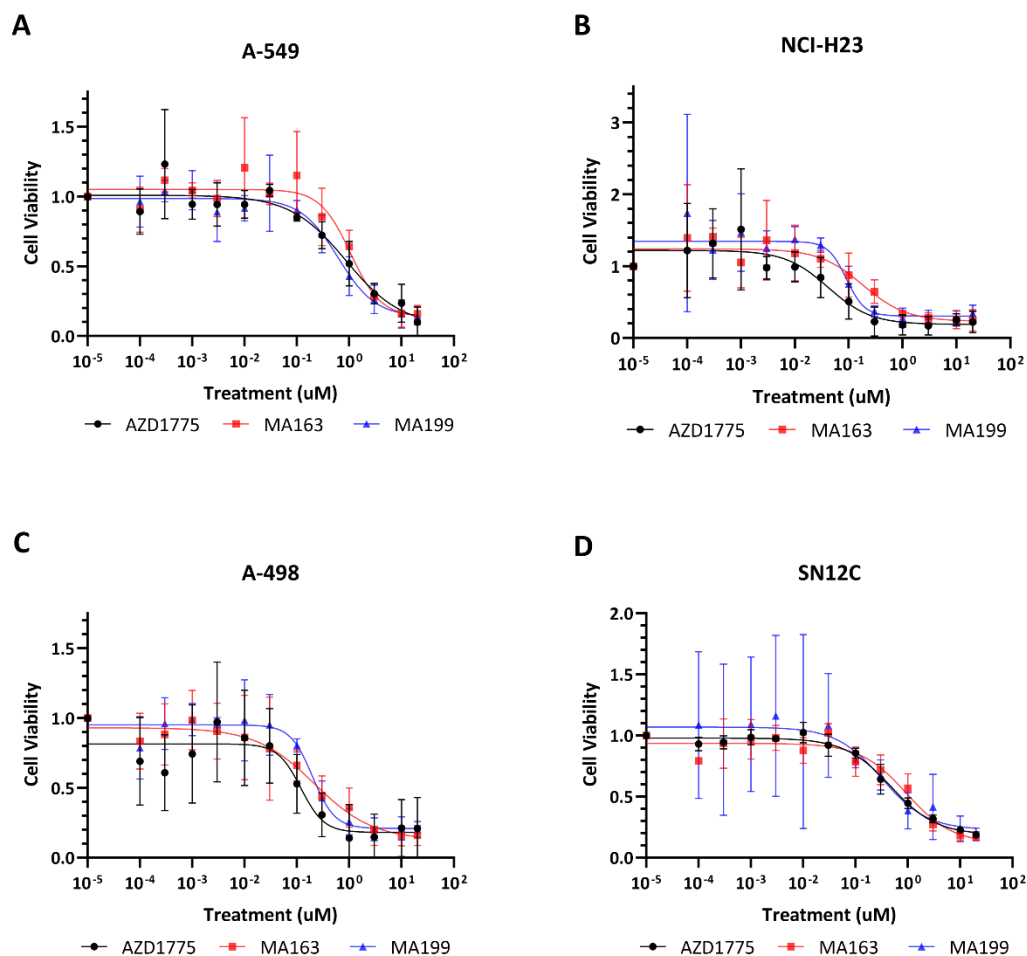
Figure 6.4 Cell viability assays of Wee1 PROTACs in Lung and Kidney cancer cell lines. Cells were treated for 72 h with Wee1i, AZD1775, CRBN-recruiter, MA163, and VHL-recruiter, MA199. Cell viability assays were normalised with vehicle control, DMSO. Plots are presented as mean ± SD of n = 3 biological repeats.

All cell lines showed sensitivity to AZD1775, MA163 and MA199 and compounds showed varying degrees of potency between cell lines (Figure 6.4). The highest EC50 was MA163 in SN12C and A-549 at 1.17 µM, whereas the most potent EC50 was AZD1775 in NCI-H23 (Table 6.1). NCI-H23 and A-498 were most sensitive to AZD1775, whereas A-549 and SN12C were most sensitive to MA199. Although A-498 harbours VHL mutations, it is still sensitive to MA199 as the PROTAC can bind and inhibit Wee1, like AZD1775.

Table 6.1 Table of EC50 values of cell viability assays (MTS) in Lung and Kidney cancer lines for Wee1 PROTACs. Cells were treated with AZD1775, MA163 and MA199. All treatments were 72 h (n = 3) and dose response curves for these values can be seen in Figure 6.4.

Treatment	EC50 (µM) ± SD			
	A-549	NCI-H23	A-498	SN12C
AZD1775	1.01 ± 0.13	0.06 ± 0.01	0.15 ± 0.01	0.57 ± 0.12
MA163	1.17 ± 0.163	0.29 ± 0.08	0.31 ± 0.01	1.17 ± 0.33
MA199	0.93 ± 0.26	0.10 ± 0.02	0.26 ± 0.04	0.29 ± 0.08

This data demonstrates that the expression levels of VHL and CRBN does not affect the potency of the compound at inhibiting cell proliferation. Even when the cell line is unable to recruit the E3 ubiquitin ligase, the PROTAC can still act as a small molecule inhibitor and halt cell proliferation. Furthermore, the compounds appear to work cell line specifically and do not greatly differ between cancer types. This provides insight that these compounds can be versatile between different cancer types, which is useful when considering moving these to the clinic.

6.3.3 Discussion

As seen in Chapter 3 in HNSCC cell lines, Wee1 PROTACs can successfully degrade Wee1 levels and reduce pCDK1 in lung and kidney cancer cell lines that do not harbour mutations in CRBN or VHL (Figures 6.2 and 6.3). MA199 does not degrade Wee1 in A-498 as this cell line is VHL-mutant, therefore MA199 cannot form a ternary complex with VHL to target Wee1 to the UPS.

The relative expression levels of CRBN or VHL in each cell line suggest that the potency of PROTACs does not depend on absolute levels of the E3 ligase that they are recruiting, but

that their potency depends on other factors. This was seen and discussed in HNSCC in section 3.3.5.

There were some contradictions between these results and data observed in the literature (Luo et al., 2022). For example, figure 6.2 showed that CRBN-based degraders were more effective in the lung cell lines tested in comparison to VHL-based degraders, whereas this was the opposite result as what was observed in the literature (Luo et al., 2022). Perhaps these discrepancies are due to variations in treatment time with the PROTACs (our experiments utilised a 24 h treatment time and Luo et al., (2022) used a maximum of 10 h treatment). Furthermore, CRBN and VHL expression could be sensitive to cell culture conditions, such as medium and cell density.

The PROTACs had similar efficacy in comparison to AZD1775 in most of the lung and kidney cancer cell lines tested at inhibiting cell proliferation (Table 6.1). This suggests that Wee1 PROTACs may be able to sensitize lung and kidney cancer cells to genotoxic treatments, like AZD1775 has demonstrated (Hirai et al., 2009; Mak et al., 2014; Patel et al., 2019; Pfister et al., 2015). This work has provided insight that we cannot predict that using, for example, CRBN-recruiting PROTACs in tissue types with high expression of CRBN would be more potent than using VHL-recruiters. These two cancer types suggest that CRBN-recruiters are more likely to be able to degrade Wee1 over a range of concentrations, however the response of cell line to PROTAC cannot be definitively predicted based on cancer type or E3 ligase expression levels. Furthermore, it has been demonstrated that Wee1 inhibition is not cancer type specific and this work has contributed to the field by demonstrating that Wee1 degradation is also not cancer type specific. Trends observed in lung and kidney cancer cell lines reflect those seen in early experiments (Chapter 3) of HNSCC cell lines, therefore a

natural progression of this work is to use Wee1 PROTACs in lung and kidney cancer cell lines

to determine their cytotoxicity alone and in combination with radiotherapy or

chemotherapy.

7 General discussion

Cancer causes approximately 25% of all deaths in England annually and one-year survival rates are less than 50% for people with lung, liver, oesophageal, stomach and pancreatic cancer (Baker and Mansfield, 2023). It is well known that cancer is often caused by genome instability and mutation and proliferation in the absence of mitogen signalling, which makes targeting the cell cycle an attractive treatment modality (Hanahan, 2022; Sherr and Bartek, 2017). Radiotherapy (Handley, 1919) and chemotherapy (Zhang et al., 2022) have been well documented treatments for killing cancer cells, however these methods are usually damaging to healthy cells of the patients which leads to significant side effects. Therefore, there is a great need to find and implement more effective methods to selectively kill cancer cells.

Radiotherapy and chemotherapy in combination with SMIs that target the cell cycle and DDR have been used in the treatment of HNSCC to further sensitize head and neck cancers to genotoxic treatments (Hintelmann et al., 2021; Oetting et al., 2023; Osman et al., 2015). Head and neck cancers have a poor prognoses and the current gold standard treatments of surgery followed up by radiotherapy or platinum-based chemotherapeutics are not effective at eradicating HNSCC tumours (Alsahafi et al., 2019; Denaro et al., 2018). Thus, it is crucial to develop more effective combinatorial strategies to kill head and neck tumour cells.

Targeted protein degradation with PROTACs has become an attractive field of study, especially as a tool for targeted cancer therapies over the last few decades (Li et al., 2022b). These compounds have demonstrated the ability to degrade previously "undruggable" proteins and overcome therapeutic challenges, such as selectivity issues, which reiterates the potential of these molecules as treatments (Nalawansha and Crews, 2020). PROTACs are

heterobifunctional molecules that form productive ternary complexes with the target

protein and an E3 ubiquitin ligase to induce polyubiquitylation of the target protein and

subsequent degradation by the UPS (Sakamoto et al., 2003). PROTACs utilise well

characterised inhibitors to the targeted protein as the warhead and the PROTACs often

show enhanced selectivity to their targets compared to the small molecule inhibitor due to

increased serendipitous interactions that the PROTAC creates. Drug resistance to well

characterised inhibitors is a problem and it will be interesting to discover if this is seen when

utilising PROTACs (Burslem et al., 2018).

7.1.1 Wee1 PROTACs can degrade Wee1 and decrease cell viability in HNSCC, lung and kidney cancer cell lines

7.1.1.1 Successful degradation of Wee1 and reduction of its substrate, pCDK1

I characterised first and second generation CRBN- and VHL-based PROTACs against Wee1

kinase, synthesised by Marine Aublette (Aublette et al., 2022), in head and neck, lung and

kidney cancer cells in Chapters 3 and 6. This assessment was conducted by determining

their degradation profiles in both chapters, as well as examining the effect of linker length

and washout of PROTACs on the profiles in HNSCC in Chapter 3. These PROTACs successfully

degrade Wee1 in HNSCC, lung and kidney cells irrespective of p53 status and with varying

maximal degradation. Second generation PROTACs were ~10-fold more potent in HNSCC

compared to the first generation synthesised.

It has been shown that some of these PROTACs selectively degrade Wee1 and negative

control PROTACs have proved that the degradation is PROTAC-dependent (Aublette et al.,

2022; Li et al., 2020), however future work should conclusively determine if this is true for VHL-recruiter, MA199. A negative control for MA199 should be synthesised and to confirm that degradation of Wee1 by MA199 is as a result of the PROTAC, no degradation would be seen on a dose response western blot.

A dose response experiment was performed using AZD1775 which displayed that relative Wee1 levels did not drop below those in the DMSO control, however more repeats of AZD1775 in A-253 (p53-null) and other cell lines, particularly UM-SCC-74A (p53-WT) and FaDu (p53-mutant), should be performed to conclude this. Changes in relative Wee1 levels observed in the negMA163 dose response treatments of UM-SCC-74A (p53-WT) and FaDu (p53-mutant) suggest that Wee1 inhibition could affect expression levels of Wee1 and the previously mentioned experiment would help to understand this. Previous studies have shown that Wee1 PROTACs selectively degrade Wee1 and do not degrade other off-targets, such as PLK1, that AZD1775 inhibits (Aublette et al., 2022; Li et al., 2020). Future work could utilise Western blotting for pCdc25c(Ser198), the product of PLK1 kinase activity, to investigate if Wee1 PROTACs are as selective at inhibiting Wee1, or if they inhibit PLK1-dependent phosphorylation of Cdc25c. Finally, the permeability of the PROTACs and how they enter or exit the cell is largely unknown, therefore this should be investigated as it may provide some insight into why washout experiments showed variability between cell lines. For example, fluorescently-tagged versions (such as with Alexa-Fluor molecules) of the Wee1 PROTACs could be synthesised to indirectly assess the permeability of Wee1 PROTACs by looking at Wee1 degradation across spheroids and flow cytometry.

7.1.1.2 Efficacy of Wee1 PROTACs is not reliant on absolute levels of E3 ligase

This thesis and previous literature has shown data to suggest that the absolute levels of E3 ligase is not important for maximal degradation (Luo et al., 2022), therefore efforts to understand how linker length and proximity to the proteins changes the degradation potential should be pursued. The key to PROTAC optimisation has shown to be understanding the ternary complex (Nowak and Jones, 2020) and perhaps, for maximal effectiveness, PROTAC linkers should be optimised for the individual cancer type and high throughput screening could help to analyse this for one target. For example, using TR-FRET, a fluorescence-based assay, to investigate how the linker affects ternary complex formation or an AlphaScreen, an amplified luminescent proximity-based assay that quantifies ternary complex formation would accomplish this (Wurz et al., 2018; Zorba et al., 2018).

7.1.2 Wee1 PROTACs are cytotoxic to cells, induce apoptosis and, in some cases, sensitize cells to radiotherapy or cisplatin

7.1.2.1 Targeting of Wee1 can sensitize HNSCC cells to cisplatin or radiotherapy

This work demonstrated that Wee1 PROTACs cause a progressive loss of cell viability over time, radiosensitize p53-deficient HNSCC, A-253, and induce apoptosis alone and in combination with radiotherapy or chemotherapeutics, irrespective of p53 status in Chapter 4. AZD1775 has previously shown to sensitize p53-deficient HNSCC cells to cisplatin (Osman et al., 2015), a trend that has been observed in other p53-deficient HNSCC cell lines tested as part of this work. Furthermore, this thesis has demonstrated that Wee1 inhibition can also sensitize p53 wild-type HNSCC cells to cisplatin, correlating with results in UM-SCC-17B

and UM-SCC-2 (Yang et al., 2022). This work has provided insight that Wee1 PROTACs can sensitize HNSCC cell lines, irrespective of p53 status, to cisplatin treatment as effectively as AZD1775. The continuation of this work should investigate if Wee1 PROTACs could overcome cisplatin resistance, dependent on resistance mechanism, a common problem for treating HNSCC (Osman et al., 2015; Yang et al., 2022), and if there are any advantages to using Wee1 PROTACs with cisplatin over longer time periods in comparison to AZD1775 and cisplatin.

Chapter 4 showed that Wee1 PROTACs can radiosensitize some p53-deficient HNSCC cell lines, but not p53 wild-type cell lines, similarly to previous findings in the literature that demonstrate Wee1 inhibition has the same effect (Oetting et al., 2023; Yang et al., 2020). There is less variability when using AZD1775 to radiosensitize cell lines in the two that were tested, however the enhancement of radiation-induced cell death by Wee1 PROTACs should be further investigated. Unfortunately, the HNSCC cells tested were from different tumour sites (Section 2.4.1), therefore to examine p53-dependence more specifically, isogenic cell lines should be used that contain a p53-WT, p53-null and p53-mutant version to eliminate cell to cell variability.

The results from the ongoing WISTERIA dose escalation clinical trial will be interesting to see and the data could help to guide how we should use/investigate the applications of Wee1 PROTACs (Kong et al., 2020). As Wee1 PROTACs show enhanced selectivity (Aublette et al., 2022; Li et al., 2020), and this work has provided preliminary insight that they may be as effective as AZD1775 at radiosensitization of p53-deficient tumours, the field should use these compounds in a trial similar to WISTERIA to determine if the enhanced selectivity leads to less side effects in patients.

7.1.2.2 Single agent treatment with Wee1i or Wee1 PROTACs appears to induce apoptosis in the absence of a genotoxic agent

AZD1775 has been shown to induce apoptosis in varying cancer cell types as a single agent treatment (Bi et al., 2019; Sand et al., 2020; Webster et al., 2017). In chapter 4, I have shown that some HPV- HNSCC cells can be forced to enter apoptosis by AZD1775 treatment, in contrast to previous studies (Tanaka et al., 2015). Perhaps AZD1775 induction of apoptosis is more cell line specific or the cell lines tested in the above study, HN30 and HN31, had differing mutations that made them more resistant to apoptosis induction by AZD1775. This thesis determined that, in the absence of an additional genotoxic agent, the Wee1 PROTACs were able to induce apoptosis at similar rates to AZD1775 in all the cell lines at the 24 h timepoint. Furthermore, the combination of AZD1775, MA163 or MA199 with cisplatin or bleomycin resulted in a larger increase in the apoptotic population compared to DMSO or the chemotherapy alone. When the % apoptotic population was plotted as separate early and late apoptotic populations, this highlighted that perhaps these treatments are inducing necrosis.

Necrotic cells can appear as late apoptotic cells as they can bind PI but also present the Annexin V substrate (phosphatidylserine) on their surface (Furuta et al., 2021; Lecoeur et al., 2001). It has not previously been reported that AZD1775 could induce necrosis, however future work could investigate this in a number of ways. The TUNEL assay, an assay that utilises the activity of the terminal deoxynucleotidyl transferase enzyme to label the 3'-OH ends of ssDNA breaks, is an alternative method to detect nuclei of apoptotic cells, however it has been discussed that necrotic cells also exhibit TUNEL-positive nuclei (Fink and Cookson, 2005). Therefore, to further investigate this hypothesis, the apoptotic and necrotic

cascade should be immunoblotted. For example, more optimisation of the PARP blots performed in this thesis, blotting for lamins and other caspases could help to underpin caspase-mediated apoptosis (McCarthy and Evan, 1998). Bax, Beclin and LC-3 immunoblotting could identify if these treatments are inducing an autophagic response (Singh and Bhaskar, 2019). One method of troubleshooting could be to treat cells with AZD1775 or Wee1 PROTACs, DMSO as a negative control and staurosporine as a positive control prior to staining with Annexin-V/PI and subsequently cell sorting these before immunoblotting. This could allow for clearer visualisation of PARP cleavage in these cell lines. Furthermore, optimisation of treatment times, perhaps shorter before degradation of cleavage fragments, should be considered.

7.1.3 Degradation of Wee1 causes replicative stress and could be inducing chromosome missegregation

7.1.3.1 Treatment with Wee1-targeting compounds increases cells with aberrant DNA content, suggestive of replicative stress or missegregation

Work in Chapter 5 confirmed that AZD1775 and Wee1 PROTACs increase the G2/M population in HNSCC cell lines. It was hypothesized that Wee1 inhibition or degradation by these compounds would lead to mitotic progression, however the data presented here show an increase of treated cells in G2/M. More specific detection of mitosis, such as phospho-Histone-H3 (Ser10) staining could identify if treated cells are passing through the G2/M checkpoint and are progressing slower or arresting in mitosis. This work was not able

to determine if AZD1775 or Wee1 PROTACs could release the radiation-induced G2/M arrest, therefore this hypothesis should be further investigated. Furthermore, the cell cycle stage analysis showed an increase in >4N and <2N DNA content cells across cell lines in each Wee1-targeted treatment condition, suggestive of mitotic missegregation and genome instability. Furthermore, >4N DNA content could be indicative of endoreduplication, where the nuclear genome is further replicated in the absence of mitosis, leading to increased DNA content and polyploidy (Ullah et al., 2009).

7.1.3.2 Wee1-inhibited or -depleted cells with above 4N DNA content could be indicative of endoreduplication

Cells experiencing endoreduplication lose expression of Cyclin B1 (Gandarillas et al., 2018); chapter 5 showed that FaDu (p53-mutant) cells treated with Wee1 PROTACs and IR had decreased levels of Cyclin B1 in comparison to IR alone. Perhaps targeting of Wee1 with another genotoxic agent enforces progression past the G2/M checkpoint and skipping of M phase. It has previously been discussed that AZD1775 as a single agent causes an increase in >4N DNA content, a finding that has been demonstrated in HNSCC in this work, and this has been linked to endoreduplication (Heijink et al., 2015). To develop the hypothesis that AZD1775, MA163 and MA199 may cause endoreduplication in HNSCC cells, the Cyclin B1 expression levels and activity of S-phase CDKs should be further examined. The incidence of endoreduplication may be simply as a result of a reduction in CyclinB-CDK1 activity and activity of S-phase CDKs, and as targeting of Wee1 manipulates the former, it is plausible that our findings are suggestive of endoreduplication (Larkins et al., 2001). Another study highlights that p53 promotes mitotic bypass which contributes to whole genome duplication

by endoreduplication, therefore it would be interesting to investigate this further in HNSCC with varying p53 status (Zeng et al., 2023).

7.1.3.3 Inhibition or degradation of Wee1 increases pan-nuclear γH2AX staining and activates ATR-Chk1 pathway, indicative of replication stress

This work has shown that AZD1775 and Wee1 PROTACs cause pan-nuclear staining of γH2AX in HNSCC cells, regardless of p53 status, indicative of replication stress. This corroborates findings in hepatocellular carcinoma cells (Cuneo et al., 2016). Our data shows a reduction in actively replicating cells (S-phase) and the presence of 2<N<4 DNA content cells increases, which suggests that these treatments cause replication stress alone and in combination with radiotherapy (Saxena and Zou, 2022). It has been shown that AZD1775 increases CDK1-dependent dormant origin firing, which will reduce fork speed as a result of depleting dNTPs (Moiseeva et al., 2019). The effect of restoring the dNTP pool by adding exogenous dNTPs into the cells when the drug treatment is applied should be studied to gain a better understanding of if this is how AZD1775 and Wee1 PROTACs are causing replication stress in HNSCC cells. Furthermore, DNA combing, a methodology that stretches out EdU or BrdU-incorporated dsDNA to investigate DNA replication, could be utilised to investigate how the treatments alter fork rate, stalled forks and origin firing (Fu and Aladjem, 2022). As these HNSCC cells were not incorporating much EdU at the time points tested, this would require some optimisation.

Activation of γH2AX, activation of Chk1 and signs of replication stress suggest that AZD1775 and Wee1 PROTACs induce the DDR as single agent treatments, as seen in Chapter 5. This activation of γH2AX is usually heightened on the addition of IR and the combinations usually

show the most unresolved DNA damage. The micronuclei experiments, although variable, showed that overall there was an increase in micronuclei in the treated cells in comparison to DMSO as well as significant differences in the nuclei area of the treated cells in comparison to the control. Perhaps the detection of micronuclei and multinucleated cells is cell-line specific and more cell lines would need to be tested in order to draw conclusions about how these treatments are creating problems in mitosis. However, investigating if the individual cell lines partake in endoreduplication may deepen our understanding of why we see varying results regarding nuclei area, multinucleated cells and micronuclei in each cell line.

Final Summary

- Wee1 degradation shows similar effectiveness to Wee1 inhibition in HNSCC. With the current Wee1 PROTACs synthesised, the potency of these compounds are equal to Wee1 inhibitor, AZD1775.

- Wee1 PROTACs induce similar levels of replication stress and DNA damage compared to Wee1i, AZD1775, and gave similar effects on the loss of clear defined cell cycle stages. These main points have been illustrated in figure 7.1.

- CRBN-based and VHL-based PROTACs are not limited to the absolute levels of E3 ligase in order to be effective and they show varying potencies dependent on cell line. This work has provided insight into how we could overcome resistance issues when treating cancers by using PROTACs that recruit different E3 ligases to their desired POI.

- PROTACs have great potential to be used as treatment strategies, in place of inhibitors in some cases, and targeting Wee1 is a good treatment strategy in head and neck cancer.
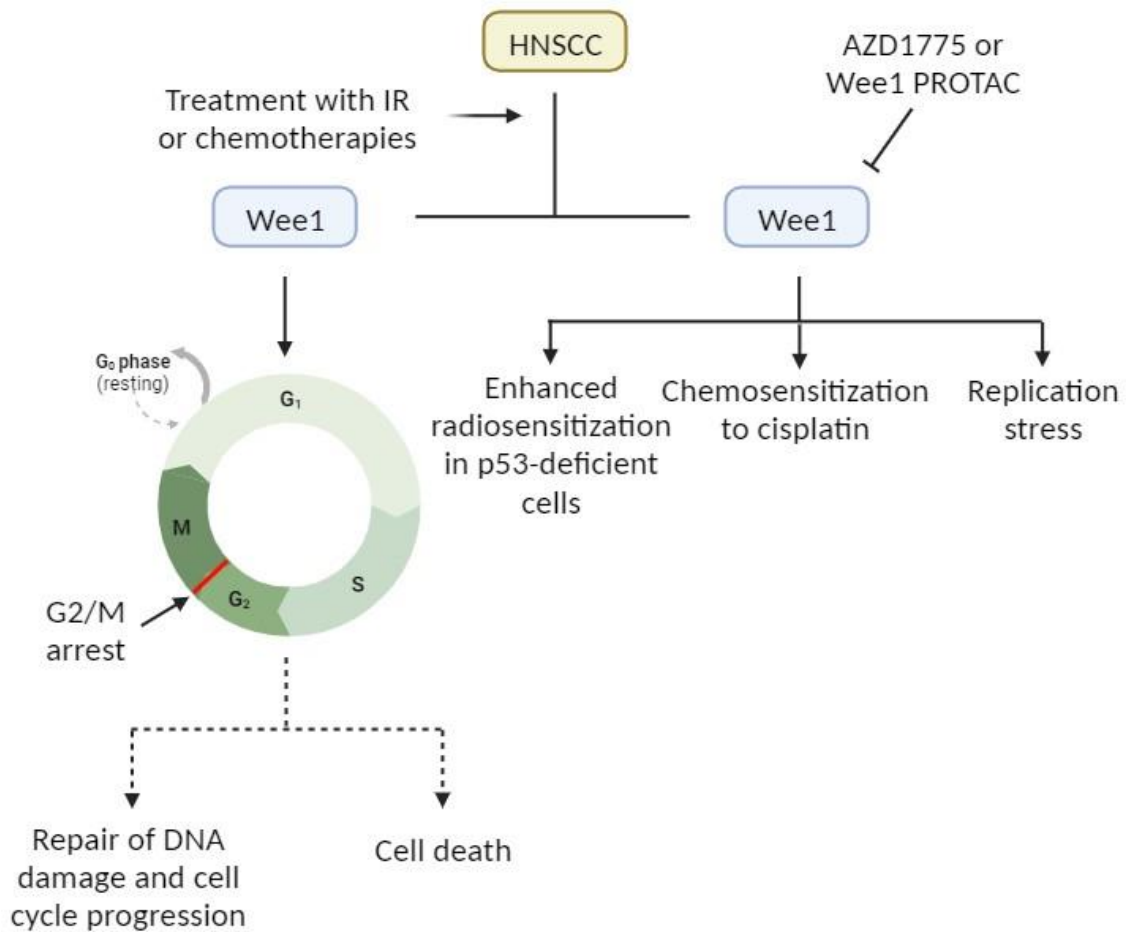
Figure 7.1 Effects of inhibition or degradation of Wee1 in head and neck cancer. Main findings to propose the impact that manipulation of Wee1 has on radio- or chemotherapy treated HNSCC cells. Figure made using biorender.com.

8 References

Abraham, R. T. (2001) Cell cycle checkpoint signaling through the ATM and ATR kinases. *Genes Dev,* 15(17)**,** 2177-96.

Alberts, B., Johnson, A., Lewis, J., Raff, M., Roberts, K. & Walter, P. (2002) Mitosis. *Molecular Biology of the Cell. 4th edition.* New York: Garland Science.

Alho, O. P., Teppo, H., Mantyselka, P. & Kantola, S. (2006) Head and neck cancer in primary care: presenting symptoms and the effect of delayed diagnosis of cancer cases. *Canadian Medical Association Journal,* 174(6)**,** 779-784.

Alsahafi, E., Begg, K., Amelio, I., Raulf, N., Lucarelli, P., Sauter, T. & Tavassoli, M. (2019) Clinical update on head and neck cancer: molecular biology and ongoing challenges. *Cell Death & Disease,* 10.

An, S. & Fu, L. (2018) Small-molecule PROTACs: An emerging and promising approach for the development of targeted therapy drugs. *Ebiomedicine,* 36**,** 553-562.

Anacker, D. C., Aloor, H. L., Shepard, C. N., Lenzi, G. M., Johnson, B. A., Kim, B. & Moody, C. A. (2016) HPV31 utilizes the ATR-Chk1 pathway to maintain elevated RRM2 levels and a replication-competent environment in differentiating Keratinocytes. *Virology,* 499**,** 383-396.

Angius, G., Tomao, S., Stati, V., Vici, P., Bianco, V. & Tomao, F. (2020) Prexasertib, a checkpoint kinase inhibitor: from preclinical data to clinical development. *Cancer Chemother Pharmacol,* 85(1)**,** 9-20.

Araujo, A. R., Gelens, L., Sheriff, R. S. & Santos, S. D. (2016) Positive Feedback Keeps Duration of Mitosis Temporally Insulated from Upstream Cell-Cycle Events. *Mol Cell,* 64(2)**,** 362-375.

Arooz, T., Yam, C. H., Siu, W. Y., Lau, A., Li, K. K. W. & Poon, R. Y. C. (2000) On the concentrations of cyclins and cyclin-dependent kinases in extracts of cultured human cells. *Biochemistry,* 39(31)**,** 9494-9501.

Artios, P. (2022) *ART0380 (ATR inhibitor)*. Available at: https://www.artios.com/science/pipeline/art0380-atr-inhibitor/ [Accessed 04/10/2022 2022].

Aublette, M. C., Harrison, T. A., Thorpe, E. J. & Gadd, M. S. (2022) Selective Wee1 degradation by PROTAC degraders recruiting VHL and CRBN E3 ubiquitin ligases. *Bioorg Med Chem Lett,* 64**,** 128636.

Baker, C. & Mansfield, Z. (2023) Cancer statistics for England. House of Commons library.

Bakkenist, C. J. & Kastan, M. B. (2003) DNA damage activates ATM through intermolecular autophosphorylation and dimer dissociation. *Nature,* 421(6922)**,** 499-506.

Barlow, C., Hirotsune, S., Paylor, R., Liyanage, M., Eckhaus, M., Collins, F., Shiloh, Y., Crawley, J. N., Ried, T., Tagle, D. & Wynshaw-Boris, A. (1996) Atm-deficient mice: a paradigm of ataxia telangiectasia. *Cell,* 86(1)**,** 159-71.

Barnum, K. J. & O'connell, M. J. (2014) Cell Cycle Regulation by Checkpoints. *Cell Cycle Control: Mechanisms and Protocols, 2nd Edition,* 1170**,** 29-40.

Bartek, J., Falck, J. & Lukas, J. (2001) CHK2 kinase--a busy messenger. *Nat Rev Mol Cell Biol,* 2(12)**,** 877-86.

Bartek, J. & Lukas, J. (2003) Chk1 and Chk2 kinases in checkpoint control and cancer. *Cancer Cell,* 3(5)**,** 421-9.

Bartlett, J. B., Dredge, K. & Dalgleish, A. G. (2004) The evolution of thalidomide and its IMiD derivatives as anticancer agents. *Nat Rev Cancer,* 4(4)**,** 314-22.

Baschnagel, A. M., Elnaggar, J. H., Vanbeek, H. J., Kromke, A. C., Skiba, J. H., Kaushik, S., Abel, L., Clark, P. A., Longhurst, C. A., Nickel, K. P., Leal, T. A., Zhao, S. G. & Kimple, R. J. (2021) ATR Inhibitor M6620 (VX-970) Enhances the Effect of Radiation in Non-Small Cell Lung Cancer Brain Metastasis Patient-Derived Xenografts. *Mol Cancer Ther,* 20(11)**,** 2129-2139.

Batey, M. A., Zhao, Y., Kyle, S., Richardson, C., Slade, A., Martin, N. M., Lau, A., Newell, D. R. & Curtin, N. J. (2013) Preclinical evaluation of a novel ATM inhibitor, KU59403, in vitro and in vivo in p53 functional and dysfunctional models of human cancer. *Mol Cancer Ther,* 12(6)**,** 959-67.

Bauer, T. M., Moore, K. N., Rader, J. S., Simpkins, F., Mita, A. C., Beck, J. T., Hart, L., Chu, Q., Oza, A., Tinker, A. V., Imedio, E. R., Kumar, S., Mugundu, G., Jenkins, S., Chmielecki, J., Jones, S., Spigel, D. & Fu, S. (2023) A Phase Ib Study Assessing the Safety, Tolerability, and Efficacy of the First-in-Class Wee1 Inhibitor Adavosertib (AZD1775) as Monotherapy in Patients with Advanced Solid Tumors. *Target Oncol,* 18(4)**,** 517-530.

Bennett, C. N., Tomlinson, C. C., Michalowski, A. M., Chu, I. M., Luger, D., Mittereder, L. R., Aprelikova, O., Shou, J., Piwinica-Worms, H., Caplen, N. J., Hollingshead, M. G. & Green, J. E. (2012) Cross-species genomic and functional analyses identify a combination therapy using a CHK1 inhibitor and a ribonucleotide reductase inhibitor to treat triple-negative breast cancer. *Breast Cancer Research,* 14(4)**,** R109.

Bensimon, A., Aebersold, R. & Shiloh, Y. (2011) Beyond ATM: the protein kinase landscape of the DNA damage response. *FEBS Lett,* 585(11)**,** 1625-39.

Bertoli, C., Klier, S., Mcgowan, C., Wittenberg, C. & De Bruin, R. A. (2013a) Chk1 inhibits E2F6 repressor function in response to replication stress to maintain cell-cycle transcription. *Curr Biol,* 23(17)**,** 1629-37.

Bertoli, C., Skotheim, J. M. & De Bruin, R. A. M. (2013b) Control of cell cycle transcription during G1 and S phases. *Nature Reviews Molecular Cell Biology,* 14(8)**,** 518-528.

Bi, S., Wei, Q., Zhao, Z., Chen, L., Wang, C. & Xie, S. (2019) Wee1 Inhibitor AZD1775 Effectively Inhibits the Malignant Phenotypes of Esophageal Squamous Cell Carcinoma In Vitro and In Vivo. *Frontiers in Pharmacology,* 10.

Blaquiere, N., Villemure, E. & Staben, S. T. (2020) Medicinal Chemistry of Inhibiting RING-Type E3 Ubiquitin Ligases. *Journal of Medicinal Chemistry,* 63(15)**,** 7957-7985.

Bond, M. J., Chu, L., Nalawansha, D. A., Li, K. & Crews, C. M. (2020) Targeted Degradation of Oncogenic KRAS(G12C) by VHL-Recruiting PROTACs. *Acs Central Science,* 6(8)**,** 1367-1375.

Boulares, A. H., Yakovlev, A. G., Ivanova, V., Stoica, B. A., Wang, G., Iyer, S. & Smulson, M. (1999) Role of poly(ADP-ribose) polymerase (PARP) cleavage in apoptosis. Caspase 3-resistant PARP mutant increases rates of apoptosis in transfected cells. *J Biol Chem,* 274(33)**,** 22932-40.

Bouvard, V., Baan, R., Straif, K., Grosse, Y., Secretan, B., El Ghissassi, F., Benbrahim-Tallaa, L., Guha, N., Freeman, C., Galichet, L., Cogliano, V. & Wo, W. H. O. I. A. R. C. M. (2009) A review of human carcinogens-Part B: biological agents. *Lancet Oncology,* 10(4)**,** 321-322.

Boyce, R. P. & Howard-Flanders, P. (1964) RELEASE OF ULTRAVIOLET LIGHT-INDUCED THYMINE DIMERS FROM DNA IN E. COLI K-12. *Proc Natl Acad Sci U S A,* 51(2)**,** 293-300.

Bradbury, A., Hall, S., Curtin, N. & Drew, Y. (2020) Targeting ATR as Cancer Therapy: A new era for synthetic lethality and synergistic combinations? *Pharmacol Ther,* 207**,** 107450.

Brand, M., Jiang, B., Bauer, S., Donovan, K. A., Liang, Y., Wang, E. S., Nowak, R. P., Yuan, J. C., Zhang, T., Kwiatkowski, N., Müller, A. C., Fischer, E. S., Gray, N. S. & Winter, G. E. (2019) Homolog-Selective Degradation as a Strategy to Probe the Function of CDK6 in AML. *Cell Chem Biol,* 26(2)**,** 300-306.e9.

Bridges, K. A., Hirai, H., Buser, C. A., Brooks, C., Liu, H., Buchholz, T. A., Molkentine, J. M., Mason, K. A. & Meyn, R. E. (2011) MK-1775, a Novel Wee1 Kinase Inhibitor, Radiosensitizes p53-Defective Human Tumor Cells. *Clinical Cancer Research,* 17(17)**,** 5638-5648.

Brill, E., Yokoyama, T., Nair, J., Yu, M., Ahn, Y. R. & Lee, J. M. (2017) Prexasertib, a cell cycle checkpoint kinases 1 and 2 inhibitor, increases. *Oncotarget,* 8(67)**,** 111026-111040.

Brown, E. J. & Baltimore, D. (2000) ATR disruption leads to chromosomal fragmentation and early embryonic lethality. *Genes Dev,* 14(4)**,** 397-402.

Buckley, D. L., Van Molle, I., Gareiss, P. C., Tae, H. S., Michel, J., Noblin, D. J., Jorgensen, W. L., Ciulli, A. & Crews, C. M. (2012) Targeting the von Hippel-Lindau E3 Ubiquitin Ligase Using Small Molecules To Disrupt the VHL/HIF-1 alpha Interaction. *Journal of the American Chemical Society,* 134(10)**,** 4465-4468.

Buganim, Y., Solomon, H., Rais, Y., Kistner, D., Nachmany, I., Brait, M., Madar, S., Goldstein, I., Kalo, E., Adam, N., Gordin, M., Rivlin, N., Kogan, I., Brosh, R., Sefadia-Elad, G., Goldfinger, N., Sidransky, D., Kloog, Y. & Rotter, V. (2010) p53 Regulates the Ras Circuit to Inhibit the Expression of a Cancer-Related Gene Signature by Various Molecular Pathways. *Cancer Research,* 70(6)**,** 2274-2284.

Bukhari, A. B., Lewis, C. W., Pearce, J. J., Luong, D., Chan, G. K. & Gamper, A. M. (2019)
Inhibiting Wee1 and ATR kinases produces tumor-selective synthetic lethality and
suppresses metastasis. *J Clin Invest,* 129(3)**,** 1329-1344.

Bunch, R. T. & Eastman, A. (1996) Enhancement of cisplatin-induced cytotoxicity by 7-
hydroxystaurosporine (UCN-01), a new G2-checkpoint inhibitor. *Clin Cancer Res,*
2(5)**,** 791-7.

Burma, S., Chen, B. P., Murphy, M., Kurimasa, A. & Chen, D. J. (2001) ATM phosphorylates
histone H2AX in response to DNA double-strand breaks. *Journal of Biological
Chemistry,* 276(45)**,** 42462-42467.

Burslem, G. M., Smith, B. E., Lai, A. C., Jaime-Figueroa, S., Mcquaid, D. C., Bondeson, D. P.,
Toure, M., Dong, H., Qian, Y., Wang, J., Crew, A. P., Hines, J. & Crews, C. M. (2018)
The Advantages of Targeted Protein Degradation Over Inhibition: An RTK Case Study.
Cell Chemical Biology, 25(1)**,** 67-+.

Byun, T. S., Pacek, M., Yee, M. C., Walter, J. C. & Cimprich, K. A. (2005) Functional
uncoupling of MCM helicase and DNA polymerase activities activates the ATR-
dependent checkpoint. *Genes Dev,* 19(9)**,** 1040-52.

Cancer Research, U. (2021) *Head and neck cancers statistics*. Available at:
https://www.cancerresearchuk.org/health-professional/cancer-statistics/statistics-
by-cancer-type/head-and-neck-cancers [Accessed 18/07/2021 2021].

Cao, C., Yang, J., Chen, Y., Zhou, P., Wang, Y., Du, W. & Zhao, L. (2020) Discovery of SK-575 as
a Highly Potent and Efficacious Proteolysis-Targeting Chimera Degrader of PARP1 for
Treating Cancers. *J Med Chem,* 63(19)**,** 11012-11033.

Chatterjee, N. & Walker, G. C. (2017) Mechanisms of DNA Damage, Repair, and
Mutagenesis. *Environmental and Molecular Mutagenesis,* 58(5)**,** 235-263.

Chen, H., Zhou, Y., Xu, W., Yu, J., Xu, Y. & Zhou, F. (2023) Comparative efficacy of novel-drugs combined therapeutic regimens on relapsed/refractory multiple myeloma: a network meta-analysis. *Hematology,* 28(1)**,** 2225342.

Chen, T., Stephens, P. A., Middleton, F. K. & Curtin, N. J. (2012) Targeting the S and G2 checkpoint to treat cancer. *Drug Discovery Today,* 17(5-6)**,** 194-202.

Chen, Y. H., Wang, J. Y., Pan, B. S., Mu, Y. F., Lai, M. S., So, E. C., Wong, T. S. & Huang, B. M. (2013) Cordycepin enhances cisplatin apoptotic effect through caspase/MAPK pathways in human head and neck tumor cells. *Onco Targets Ther,* 6**,** 983-98.

Chera, B. S., Sheth, S. H., Patel, S. A., Goldin, D., Douglas, K. E., Green, R. L., Shen, C. J., Gupta, G. P., Moore, D. T., Grilley Olson, J. E. & Weiss, J. M. (2021) Phase 1 trial of adavosertib (AZD1775) in combination with concurrent radiation and cisplatin for intermediate-risk and high-risk head and neck squamous cell carcinoma. *Cancer*.

Ciardo, D., Goldar, A. & Marheineke, K. (2019) On the Interplay of the DNA Replication Program and the Intra-S Phase Checkpoint Pathway. *Genes (Basel),* 10(2).

Cieślak, M. & Słowianek, M. (2023) Cereblon-Recruiting PROTACs: Will New Drugs Have to Face Old Challenges? *Pharmaceutics,* 15(3).

Cliby, W. A., Roberts, C. J., Cimprich, K. A., Stringer, C. M., Lamb, J. R., Schreiber, S. L. & Friend, S. H. (1998) Overexpression of a kinase-inactive ATR protein causes sensitivity to DNA-damaging agents and defects in cell cycle checkpoints. *Embo Journal,* 17(1)**,** 159-169.

Cohen, P. & Tcherpakov, M. (2010) Will the Ubiquitin System Furnish as Many Drug Targets as Protein Kinases? *Cell,* 143(5)**,** 686-693.

Cuneo, K. C., Morgan, M. A., Davis, M. A., Parcels, L. A., Parcels, J., Karnak, D., Ryan, C., Liu, N., Maybaum, J. & Lawrence, T. S. (2016) Wee1 Kinase Inhibitor AZD1775

Radiosensitizes Hepatocellular Carcinoma Regardless of TP53 Mutational Status Through Induction of Replication Stress. *International Journal of Radiation Oncology Biology Physics,* 95(2)**,** 782-790.

Curigliano, G., Loibl, S., Müller, V., Pivot, X., Wardley, A. & Cameron, D. (2016) 312TiP - A phase 2 randomized, double-blinded, controlled study of ONT-380 vs. placebo in combination with capecitabine (C) and trastuzumab (T) in patients with pretreated HER2+ unresectable locally advanced or metastatic breast carcinoma (MBC). *Annals of Oncology,* 27**,** vi98.

Dasari, S. & Tchounwou, P. B. (2014) Cisplatin in cancer therapy: molecular mechanisms of action. *Eur J Pharmacol,* 740**,** 364-78.

De Keukeleire, S. J., Vermassen, T., Hilgert, E., Creytens, D., Ferdinande, L. & Rottey, S. (2021) Immuno-Oncological Biomarkers for Squamous Cell Cancer of the Head and Neck: Current State of the Art and Future Perspectives. *Cancers,* 13(7).

Denaro, N., Russi, E. G. & Merlano, M. C. (2018) Pros and Cons of the New Edition of TNM Classification of Head and Neck Squamous Cell Carcinoma. *Oncology,* 95(4)**,** 202-210.

Desouky, O., Ding, N. & Zhou, G. (2015) Targeted and non-targeted effects of ionizing radiation. *Journal of Radiation Research and Applied Sciences,* 8(2)**,** 247-254.

Dietz, A., Rudat, V., Dreyhaupt, J., Pritsch, M., Hoppe, F., Hagen, R., Pfreundner, L., Schroeder, U., Eckel, H., Hess, M., Schroeder, M., Schneider, P., Jens, B., Zenner, H. P., Werner, J. A., Engenhardt-Cabillic, R., Vanselow, B., Plinkert, P., Niewald, M., Kuhnt, T., Budach, W. & Flentje, M. (2009) Induction chemotherapy with paclitaxel and cisplatin followed by radiotherapy for larynx organ preservation in advanced laryngeal and hypopharyngeal cancer offers moderate late toxicity outcome (DeLOS-I-trial). *European Archives of Oto-Rhino-Laryngology,* 266(8)**,** 1291-1300.

Dimaio, D. & Petti, L. M. (2013) The E5 proteins. *Virology,* 445(1-2)**,** 99-114.

Do, K., Wilsker, D., Ji, J., Zlott, J., Freshwater, T., Kinders, R. J., Collins, J., Chen, A. P., Doroshow, J. H. & Kummar, S. (2015) Phase I Study of Single-Agent AZD1775 (MK-1775), a Wee1 Kinase Inhibitor, in Patients With Refractory Solid Tumors. *Journal of Clinical Oncology,* 33(30)**,** 3409-+.

Dredge, K., Marriott, J. B., Todryk, S. M., Muller, G. W., Chen, R., Stirling, D. I. & Dalgleish, A. G. (2002) Protective antitumor immunity induced by a costimulatory thalidomide analog in conjunction with whole tumor cell vaccination is mediated by increased Th1-type immunity. *J Immunol,* 168(10)**,** 4914-9.

Dréan, A., Williamson, C. T., Brough, R., Brandsma, I., Menon, M., Konde, A., Garcia-Murillas, I., Pemberton, H. N., Frankum, J., Rafiq, R., Badham, N., Campbell, J., Gulati, A., Turner, N. C., Pettitt, S. J., Ashworth, A. & Lord, C. J. (2017) Modeling Therapy Resistance in. *Mol Cancer Ther,* 16(9)**,** 2022-2034.

Durant, S. T., Zheng, L., Wang, Y., Chen, K., Zhang, L., Zhang, T., Yang, Z., Riches, L., Trinidad, A. G., Fok, J. H. L., Hunt, T., Pike, K. G., Wilson, J., Smith, A., Colclough, N., Reddy, V. P., Sykes, A., Janefeldt, A., Johnström, P., Varnäs, K., Takano, A., Ling, S., Orme, J., Stott, J., Roberts, C., Barrett, I., Jones, G., Roudier, M., Pierce, A., Allen, J., Kahn, J., Sule, A., Karlin, J., Cronin, A., Chapman, M., Valerie, K., Illingworth, R. & Pass, M. (2018) The brain-penetrant clinical ATM inhibitor AZD1390 radiosensitizes and improves survival of preclinical brain tumor models. *Sci Adv,* 4(6)**,** eaat1719.

Economopoulou, P., De Bree, R., Kotsantis, I. & Psyrri, A. (2019) Diagnostic Tumor Markers in Head and Neck Squamous Cell Carcinoma (HNSCC) in the Clinical Setting. *Frontiers in Oncology,* 9.

Elson, A., Wang, Y., Daugherty, C. J., Morton, C. C., Zhou, F., Campos-Torres, J. & Leder, P. (1996) Pleiotropic defects in ataxia-telangiectasia protein-deficient mice. *Proc Natl Acad Sci U S A,* 93(23)**,** 13084-9.

Errico, A. & Costanzo, V. (2012) Mechanisms of replication fork protection: a safeguard for genome stability. *Crit Rev Biochem Mol Biol,* 47(3)**,** 222-35.

Estevao, D., Costa, N. R., Gil Da Costa, R. M. & Medeiros, R. (2019) Hallmarks of HPV carcinogenesis: The role of E6, E7 and E5 oncoproteins in cellular malignancy. *Biochimica Et Biophysica Acta-Gene Regulatory Mechanisms,* 1862(2)**,** 153-162.

Falck, J., Petrini, J. H. J., Williams, B. R., Lukas, J. & Bartek, J. (2002) The DNA damage-dependent intra-S phase checkpoint is regulated by parallel pathways. *Nature Genetics,* 30(3)**,** 290-294.

Fink, S. L. & Cookson, B. T. (2005) Apoptosis, pyroptosis, and necrosis: mechanistic description of dead and dying eukaryotic cells. *Infect Immun,* 73(4)**,** 1907-16.

Flanagan, J. J., Qian, Y., Gough, S. M., Andreoli, M., Bookbinder, M., Cadelina, G., Bradley, J., Rousseau, E., Willard, R., Pizzano, J., Crews, C. M., Crew, A. P., Taylor, I. & Houston, J. (2019) ARV-471, an oral estrogen receptor PROTAC degrader for breast cancer. *Cancer Research,* 79(4).

Fokas, E., Prevo, R., Pollard, J. R., Reaper, P. M., Charlton, P. A., Cornelissen, B., Vallis, K. A., Hammond, E. M., Olcina, M. M., Gillies Mckenna, W., Muschel, R. J. & Brunner, T. B. (2012) Targeting ATR in vivo using the novel inhibitor VE-822 results in selective sensitization of pancreatic tumors to radiation. *Cell Death Dis,* 3**,** e441.

Fousteri, M. & Mullenders, L. H. (2008) Transcription-coupled nucleotide excision repair in mammalian cells: molecular mechanisms and biological effects. *Cell Res,* 18(1)**,** 73-84.

Frost, J., Galdeano, C., Soares, P., Gadd, M. S., Grzes, K. M., Ellis, L., Epemolu, O., Shimamura, S., Bantscheff, M., Grandi, P., Read, K. D., Cantrell, D. A., Rocha, S. & Ciulli, A. (2016) Potent and selective chemical probe of hypoxic signalling downstream of HIF-α hydroxylation via VHL inhibition. *Nat Commun,* 7**,** 13312.

Frost, J., Rocha, S. & Ciulli, A. (2021) Von Hippel-Lindau (VHL) small-molecule inhibitor binding increases stability and intracellular levels of VHL protein. *J Biol Chem,* 297(2)**,** 100910.

Fu, H. & Aladjem, M. I. (2022) DNA replication profiling by molecular combing on single DNA fibers. *STAR Protoc,* 3(2)**,** 101290.

Fu, R., Zhao, B., Chen, M., Fu, X., Zhang, Q., Cui, Y., Hu, X. & Zhou, W. (2023) Moving beyond cisplatin resistance: mechanisms, challenges, and prospects for overcoming recurrence in clinical cancer therapy. *Med Oncol,* 41(1)**,** 9.

Fu, S., Pasic, A., Richardson, G., Vranjes, Z. J., Meniawy, T., De Jong, P. R., Donate, F., Samatar, A. A., Rodriguez, J., Pultar, P. & Voliotis, D. (2021) A phase Ib dose-escalation study of ZN-c3, a WEE1 inhibitor, in combination with chemotherapy in patients with platinum-resistant or -refractory ovarian, peritoneal, or fallopian tube cancer. *Annals of Oncology,* 32**,** S618-S618.

Fuchss, T., Mederski, W. W., Zenke, F. T., Dahmen, H., Zimmermann, A. & Blaukat, A. (2018) Highly potent and selective ATM kinase inhibitor M3541: A clinical candidate drug with strong antitumor activity in combination with radiotherapy. *Cancer Research,* 78(13).

Furuta, Y., Pena-Ramos, O., Li, Z., Chiao, L. & Zhou, Z. (2021) Calcium ions trigger the exposure of phosphatidylserine on the surface of necrotic cells. *PLoS Genet,* 17(2)**,** e1009066.

Gadd, M. S., Testa, A., Lucas, X., Chan, K. H., Chen, W. Z., Lamont, D. J., Zengerle, M. & Ciulli, A. (2017) Structural basis of PROTAC cooperative recognition for selective protein degradation. *Nature Chemical Biology,* 13(5)**,** 514-+.

Gandarillas, A., Molinuevo, R. & Sanz-Gómez, N. (2018) Mammalian endoreplication emerges to reveal a potential developmental timer. *Cell Death Differ,* 25(3)**,** 471-476.

Gao, H., Sun, X. & Rao, Y. (2020) PROTAC Technology: Opportunities and Challenges. *ACS Med Chem Lett,* 11(3)**,** 237-240.

García, M. E. G., Kirsch, D. G. & Reitman, Z. J. (2022) Targeting the ATM Kinase to Enhance the Efficacy of Radiotherapy and Outcomes for Cancer Patients. *Semin Radiat Oncol,* 32(1)**,** 3-14.

Gately, D. P., Hittle, J. C., Chan, G. K. & Yen, T. J. (1998) Characterization of ATM expression, localization, and associated DNA-dependent protein kinase activity. *Mol Biol Cell,* 9(9)**,** 2361-74.

Gerry, C. J. & Schreiber, S. L. (2020) Unifying principles of bifunctional, proximity-inducing small molecules. *Nature Chemical Biology,* 16(4)**,** 369-378.

Golding, S. E., Rosenberg, E., Khalil, A., Mcewen, A., Holmes, M., Neill, S., Povirk, L. F. & Valerie, K. (2004) Double strand break repair by homologous recombination is regulated by cell cycle-independent signaling via ATM in human glioma cells. *J Biol Chem,* 279(15)**,** 15402-10.

Golding, S. E., Rosenberg, E., Valerie, N., Hussaini, I., Frigerio, M., Cockcroft, X. F., Chong, W. Y., Hummersone, M., Rigoreau, L., Menear, K. A., O'connor, M. J., Povirk, L. F., Van Meter, T. & Valerie, K. (2009) Improved ATM kinase inhibitor KU-60019 radiosensitizes glioma cells, compromises insulin, AKT and ERK prosurvival signaling, and inhibits migration and invasion. *Mol Cancer Ther,* 8(10)**,** 2894-902.

Gormley, M., Creaney, G., Schache, A., Ingarfield, K. & Conway, D. I. (2022) Reviewing the epidemiology of head and neck cancer: definitions, trends and risk factors. *Br Dent J,* 233(9)**,** 780-786.

Grabowska, A. K. & Riemer, A. B. (2012) The invisible enemy - how human papillomaviruses avoid recognition and clearance by the host immune system. *The open virology journal,* 6**,** 249-56.

Graves, P. R., Yu, L., Schwarz, J. K., Gales, J., Sausville, E. A., O'connor, P. M. & Piwnica-Worms, H. (2000) The Chk1 protein kinase and the Cdc25C regulatory pathways are targets of the anticancer agent UCN-01. *J Biol Chem,* 275(8)**,** 5600-5.

Guizard, A.-V. N., Dejardin, O. J., Launay, L. C., Bara, S., Lapotre-Ledoux, B. M., Babin, E. B., Launoy, G. D. & Ligier, K. A. (2017) Diagnosis and management of head and neck cancers in a high-incidence area in France: A population-based study. *Medicine,* 96(26).

Gusho, E. & Laimins, L. (2021) Human Papillomaviruses Target the DNA Damage Repair and Innate Immune Response Pathways to Allow for Persistent Infection. *Viruses-Basel,* 13(7).

Ha, D. H., Min, A., Kim, S., Jang, H., Kim, S. H., Kim, H. J., Ryu, H. S., Ku, J. L., Lee, K. H. & Im, S. A. (2020) Antitumor effect of a WEE1 inhibitor and potentiation of olaparib sensitivity by DNA damage response modulation in triple-negative breast cancer. *Sci Rep,* 10(1)**,** 9930.

Han, J. H. J., Kim, K., Im, J., Park, S., Choi, M. K., Kim, I., Nam, K. Y. & Yoon, J. (2021) PHI-101, a potent and novel inhibitor of CHK2 in ovarian and breast cancer cells. *Cancer Research,* 81(13).

Hanahan, D. (2022) Hallmarks of Cancer: New Dimensions. *Cancer Discov,* 12(1)**,** 31-46.

Hanahan, D. & Weinberg, R. A. (2011) Hallmarks of cancer: the next generation. *Cell,* 144(5)**,** 646-74.

Handley, W. S. (1919) On the Mode of Spread of Cancer in relation to its Treatment by Radiation. *Proc R Soc Med,* 12(Electro Ther Sect)**,** 41-51.

Harris, S. L. & Levine, A. J. (2005) The p53 pathway: positive and negative feedback loops. *Oncogene,* 24(17)**,** 2899-2908.

Hashibe, M., Brennan, P., Chuang, S.-C., Boccia, S., Castellsague, X., Chen, C., Curado, M. P., Dal Maso, L., Daudt, A. W., Fabianova, E., Fernandez, L., Wuensch-Filho, V., Franceschi, S., Hayes, R. B., Herrero, R., Kelsey, K., Koifman, S., La Vecchia, C., Lazarus, P., Levi, F., Lence, J. J., Mates, D., Matos, E., Menezes, A., Mcclean, M. D., Muscat, J., Eluf-Neto, J., Olshan, A. F., Purdue, M., Rudnai, P., Schwartz, S. M., Smith, E., Sturgis, E. M., Szeszenia-Dabrowska, N., Talamini, R., Wei, Q., Winn, D. M., Shangina, O., Pilarska, A., Zhang, Z.-F., Ferro, G., Berthiller, J. & Boffetta, P. (2009) Interaction between Tobacco and Alcohol Use and the Risk of Head and Neck Cancer: Pooled Analysis in the International Head and Neck Cancer Epidemiology Consortium. *Cancer Epidemiology Biomarkers & Prevention,* 18(2)**,** 541-550.

Hashimoto, S., Anai, H. & Hanada, K. (2016) Mechanisms of interstrand DNA crosslink repair and human disorders. *Genes Environ,* 38**,** 9.

Hatakeyama, M. & Weinberg, R. A. (1995) The role of RB in cell cycle control. *Prog Cell Cycle Res,* 1**,** 9-19.

Hatcher, J. M., Wang, E. S., Johannessen, L., Kwiatkowski, N., Sim, T. & Gray, N. S. (2018) Development of Highly Potent and Selective Steroidal Inhibitors and Degraders of CDK8. *ACS Med Chem Lett,* 9(6)**,** 540-545.

Hecht, S. M. (2000) Bleomycin: new perspectives on the mechanism of action. *J Nat Prod,* 63(1)**,** 158-68.

Heijink, A. M., Blomen, V. A., Bisteau, X., Degener, F., Matsushita, F. Y., Kaldis, P., Foijer, F. & Van Vugt, M. A. (2015) A haploid genetic screen identifies the G1/S regulatory machinery as a determinant of Wee1 inhibitor sensitivity. *Proc Natl Acad Sci U S A,* 112(49)**,** 15160-5.

Helin, K. (1998) Regulation of cell proliferation by the E2F transcription factors. *Curr Opin Genet Dev,* 8(1)**,** 28-35.

Helin, K., Harlow, E. & Fattaey, A. (1993) Inhibition of E2F-1 transactivation by direct binding of the retinoblastoma protein. *Mol Cell Biol,* 13(10)**,** 6501-8.

Hershko, A. & Ciechanover, A. (1992) THE UBIQUITIN SYSTEM FOR PROTEIN-DEGRADATION. *Annual Review of Biochemistry,* 61**,** 761-807.

Hershko, A., Heller, H., Elias, S. & Ciechanover, A. (1983) COMPONENTS OF UBIQUITIN-PROTEIN LIGASE SYSTEM - RESOLUTION, AFFINITY PURIFICATION, AND ROLE IN PROTEIN BREAKDOWN. *Journal of Biological Chemistry,* 258(13)**,** 8206-8214.

Hickson, I., Pike, K. G. & Durant, S. T. (2018) Targeting ATM for Cancer Therapy: Prospects for Drugging ATM. In: Pollard, J. & Curtin, N. (eds.) *Targeting the DNA Damage Response for Anti-Cancer Therapy.* Cham: Springer International Publishing.

Hickson, I., Zhao, Y., Richardson, C. J., Green, S. J., Martin, N. M., Orr, A. I., Reaper, P. M., Jackson, S. P., Curtin, N. J. & Smith, G. C. (2004) Identification and characterization of a novel and specific inhibitor of the ataxia-telangiectasia mutated kinase ATM. *Cancer Res,* 64(24)**,** 9152-9.

Hintelmann, K., Berenz, T., Kriegs, M., Christiansen, S., Gatzemeier, F., Struve, N., Petersen, C., Betz, C., Rothkamm, K., Oetting, A. & Rieckmann, T. (2021) Dual Inhibition of

PARP and the Intra-S/G2 Cell Cycle Checkpoints Results in Highly Effective
Radiosensitization of HPV-Positive HNSCC Cells. *Frontiers in Oncology,* 11.

Hirai, H., Iwasawa, Y., Okada, M., Arai, T., Nishibata, T., Kobayashi, M., Kimura, T., Kaneko,
N., Ohtani, J., Yamanaka, K., Itadani, H., Takahashi-Suzuki, I., Fukasawa, K., Oki, H.,
Nambu, T., Jiang, J., Sakai, T., Arakawa, H., Sakamoto, T., Sagara, T., Yoshizumi, T.,
Mizuarai, S. & Kotani, H. (2009) Small-molecule inhibition of Wee1 kinase by MK-
1775 selectively sensitizes p53-deficient tumor cells to DNA-damaging agents.
Molecular Cancer Therapeutics, 8(11)**,** 2992-3000.

Hsieh, C. C., Hsu, S. H., Lin, C. Y., Liaw, H. J., Li, T. W., Jiang, K. Y., Chiang, N. J., Chen, S. H.,
Lin, B. W., Chen, P. C., Chan, R. H., Lin, P. C., Yeh, Y. M. & Shen, C. H. (2022) CHK2
activation contributes to the development of oxaliplatin resistance in colorectal
cancer. *Br J Cancer*.

Huang, H. T., Dobrovolsky, D., Paulk, J., Yang, G., Weisberg, E. L., Doctor, Z. M., Buckley, D.
L., Cho, J. H., Ko, E., Jang, J., Shi, K., Choi, H. G., Griffin, J. D., Li, Y., Treon, S. P.,
Fischer, E. S., Bradner, J. E., Tan, L. & Gray, N. S. (2018) A Chemoproteomic Approach
to Query the Degradable Kinome Using a Multi-kinase Degrader. *Cell Chem Biol,*
25(1)**,** 88-99.e6.

Huang, P. Q., Boren, B. C., Hegde, S. G., Liu, H., Unni, A. K., Abraham, S., Hopkins, C. D.,
Paliwal, S., Samatar, A. A., Li, J. & Bunker, K. D. (2021) Discovery of ZN-c3, a Highly
Potent and Selective Wee1 Inhibitor Undergoing Evaluation in Clinical Trials for the
Treatment of Cancer. *J Med Chem,* 64(17)**,** 13004-13024.

Hughes, S. J. & Ciulli, A. (2017) Molecular recognition of ternary complexes: a new
dimension in the structure-guided design of chemical degraders. *Structure-Based
Drug Design: Insights from Academia and Industry,* 61(5)**,** 505-516.

Hwang, B. J., Adhikary, G., Eckert, R. L. & Lu, A. L. (2018) Chk1 inhibition as a novel therapeutic strategy in melanoma. *Oncotarget,* 9(54)**,** 30450-30464.

Ikediobi, O. N., Davies, H., Bignell, G., Edkins, S., Stevens, C., O'meara, S., Santarius, T., Avis, T., Barthorpe, S., Brackenbury, L., Buck, G., Butler, A., Clements, J., Cole, J., Dicks, E., Forbes, S., Gray, K., Halliday, K., Harrison, R., Hills, K., Hinton, J., Hunter, C., Jenkinson, A., Jones, D., Kosmidou, V., Lugg, R., Menzies, A., Mironenko, T., Parker, A., Perry, J., Raine, K., Richardson, D., Shepherd, R., Small, A., Smith, R., Solomon, H., Stephens, P., Teague, J., Tofts, C., Varian, J., Webb, T., West, S., Widaa, S., Yates, A., Reinhold, W., Weinstein, J. N., Stratton, M. R., Futreal, P. A. & Wooster, R. (2006) Mutation analysis of 24 known cancer genes in the NCI-60 cell line set. *Mol Cancer Ther,* 5(11)**,** 2606-12.

Ishida, T. & Ciulli, A. (2021) E3 Ligase Ligands for PROTACs: How They Were Found and How to Discover New Ones. *Slas Discovery,* 26(4)**,** 484-502.

Ito, T., Ando, H., Suzuki, T., Ogura, T., Hotta, K., Imamura, Y., Yamaguchi, Y. & Handa, H. (2010) Identification of a Primary Target of Thalidomide Teratogenicity. *Science,* 327(5971)**,** 1345-1350.

Iyer, D. R. & Rhind, N. (2017) The Intra-S Checkpoint Responses to DNA Damage. *Genes (Basel),* 8(2).

Jacobs, A. L. & Schär, P. (2012) DNA glycosylases: in DNA repair and beyond. *Chromosoma,* 121(1)**,** 1-20.

Jiang, B., Gao, Y., Che, J., Lu, W., Kaltheuner, I. H., Dries, R., Kalocsay, M., Berberich, M. J., Jiang, J., You, I., Kwiatkowski, N., Riching, K. M., Daniels, D. L., Sorger, P. K., Geyer, M., Zhang, T. & Gray, N. S. (2021) Discovery and resistance mechanism of a selective CDK12 degrader. *Nat Chem Biol,* 17(6)**,** 675-683.

Jiang, B., Wang, E. S., Donovan, K. A., Liang, Y., Fischer, E. S., Zhang, T. & Gray, N. S. (2019) Development of Dual and Selective Degraders of Cyclin-Dependent Kinases 4 and 6. *Angew Chem Int Ed Engl,* 58(19)**,** 6321-6326.

Jin, J., Fang, H., Yang, F., Ji, W., Guan, N., Sun, Z., Shi, Y., Zhou, G. & Guan, X. (2018) Combined Inhibition of ATR and WEE1 as a Novel Therapeutic Strategy in Triple-Negative Breast Cancer. *Neoplasia,* 20(5)**,** 478-488.

Jin, S. K. & Levine, A. J. (2001) The p53 functional circuit. *Journal of Cell Science,* 114(23)**,** 4139-4140.

Johnson, D. E., Burtness, B., Leemans, C. R., Lui, V. W. Y., Bauman, J. E. & Grandis, J. R. (2020) Head and neck squamous cell carcinoma. *Nature Reviews Disease Primers,* 6(1).

Kang, J. W., Eun, Y. G. & Lee, Y. C. (2021) Diagnostic Value of Salivary miRNA in Head and Neck Squamous Cell Cancer: Systematic Review and Meta-Analysis. *International Journal of Molecular Sciences,* 22(13).

Kao, M., Green, C., Sidorova, J. & Mendez, E. (2017) Strategies for Targeted Therapy in Head and Neck Squamous Cell Carcinoma Using WEE1 Inhibitor AZD1775. *Jama Otolaryngology-Head & Neck Surgery,* 143(6)**,** 631-633.

Kastan, M. B., Onyekwere, O., Sidransky, D., Vogelstein, B. & Craig, R. W. (1991) PARTICIPATION OF P53 PROTEIN IN THE CELLULAR-RESPONSE TO DNA DAMAGE. *Cancer Research,* 51(23)**,** 6304-6311.

Kausar, T., Schreiber, J. S., Karnak, D., Parsels, L. A., Parsels, J. D., Davis, M. A., Zhao, L., Maybaum, J., Lawrence, T. S. & Morgan, M. A. (2015) Sensitization of Pancreatic Cancers to Gemcitabine Chemoradiation by WEE1 Kinase Inhibition Depends on Homologous Recombination Repair. *Neoplasia,* 17(10)**,** 757-66.

Khan, S., Zhang, X., Lv, D., Zhang, Q., He, Y., Zhang, P., Liu, X., Thummuri, D., Yuan, Y.,

    Wiegand, J. S., Pei, J., Zhang, W., Sharma, A., Mccurdy, C. R., Kuruvilla, V. M., Baran,

    N., Ferrando, A. A., Kim, Y.-M., Rogojina, A., Houghton, P. J., Huang, G., Hromas, R.,

    Konopleva, M., Zheng, G. & Zhou, D. (2019) A selective BCL-X-L PROTAC degrader

    achieves safe and potent antitumor activity. *Nature Medicine,* 25(12)**,** 1938-+.

King, C., Diaz, H. B., Mcneely, S., Barnard, D., Dempsey, J., Blosser, W., Beckmann, R., Barda,

    D. & Marshall, M. S. (2015) LY2606368 Causes Replication Catastrophe and

    Antitumor Effects through CHK1-Dependent Mechanisms. *Mol Cancer Ther,* 14(9)**,**

    2004-13.

King, R. W., Jackson, P. K. & Kirschner, M. W. (1994) MITOSIS IN TRANSITION. *Cell,* 79(4)**,**

    563-571.

Kleiger, G. & Mayor, T. (2014) Perilous journey: a tour of the ubiquitin-proteasome system.

    Trends in Cell Biology, 24(6)**,** 352-359.

Komander, D. & Rape, M. (2012) The Ubiquitin Code. *Annual Review of Biochemistry, Vol 81,*

    81**,** 203-229.

Kong, A., Good, J., Kirkham, A., Savage, J., Mant, R., Llewellyn, L., Parish, J., Spruce, R.,

    Forster, M., Schipani, S., Harrington, K., Sacco, J., Murray, P., Middleton, G., Yap, C. &

    Mehanna, H. (2020) Phase I trial of WEE1 inhibition with chemotherapy and

    radiotherapy as adjuvant treatment, and a window of opportunity trial with cisplatin

    in patients with head and neck cancer: the WISTERIA trial protocol. *Bmj Open,* 10(3).

Kong, A. & Mehanna, H. (2021) WEE1 Inhibitor: Clinical Development. *Curr Oncol Rep,* 23(9)**,**

    107.

Konstantinidou, M., Li, J., Zhang, B., Wang, Z., Shaabani, S., Ter Brake, F., Essa, K. & Dömling, A. (2019) PROTACs- a game-changing technology. *Expert Opin Drug Discov,* 14(12)**,** 1255-1268.

Kostic, M. & Jones, L. H. (2020) Critical Assessment of Targeted Protein Degradation as a Research Tool and Pharmacological Modality. *Trends in pharmacological sciences,* 41(5)**,** 305-317.

Kottemann, M. C. & Smogorzewska, A. (2013) Fanconi anaemia and the repair of Watson and Crick DNA crosslinks. *Nature,* 493(7432)**,** 356-63.

Kusakabe, M., Onishi, Y., Tada, H., Kurihara, F., Kusao, K., Furukawa, M., Iwai, S., Yokoi, M., Sakai, W. & Sugasawa, K. (2019) Mechanism and regulation of DNA damage recognition in nucleotide excision repair. *Genes Environ,* 41**,** 2.

Lai, A. C., Toure, M., Hellerschmied, D., Salami, J., Jaime-Figueroa, S., Ko, E., Hines, J. & Crews, C. M. (2016) Modular PROTAC Design for the Degradation of Oncogenic BCR-ABL. *Angew Chem Int Ed Engl,* 55(2)**,** 807-10.

Lane, D. P. (1992) CANCER - P53, GUARDIAN OF THE GENOME. *Nature,* 358(6381)**,** 15-16.

Lane, D. P. & Crawford, L. V. (1979) T-ANTIGEN IS BOUND TO A HOST PROTEIN IN SV40-TRANSFORMED CELLS. *Nature,* 278(5701)**,** 261-263.

Larkins, B. A., Dilkes, B. P., Dante, R. A., Coelho, C. M., Woo, Y. M. & Liu, Y. (2001) Investigating the hows and whys of DNA endoreduplication. *Journal of Experimental Botany,* 52(355)**,** 183-192.

Lazaro, J.-B., Parmar, K., Shapiro, G. I. & D'andrea, A. D. (2016) Abstract 2729: Estrogen receptor-negative breast cancer cell lines exhibit hypersensitivity to the CHK1 inhibitor LY2606368. *Cancer Research,* 76(14 Supplement)**,** 2729.

Lecoeur, H., Prévost, M. C. & Gougeon, M. L. (2001) Oncosis is associated with exposure of phosphatidylserine residues on the outside layer of the plasma membrane: a reconsideration of the specificity of the annexin V/propidium iodide assay. *Cytometry,* 44(1)**,** 65-72.

Lee, J. W., Parameswaran, J., Sandoval-Schaefer, T., Eoh, K. J., Yang, D. H., Zhu, F., Mehra, R., Sharma, R., Gaffney, S. G., Perry, E. B., Townsend, J. P., Serebriiskii, I. G., Golemis, E. A., Issaeva, N., Yarbrough, W. G., Koo, J. S. & Burtness, B. (2019) Combined Aurora Kinase A (AURKA) and WEE1 Inhibition Demonstrates Synergistic Antitumor Effect in Squamous Cell Carcinoma of the Head and Neck. *Clin Cancer Res,* 25(11)**,** 3430-3442.

Lee, T. H. & Kang, T. H. (2019) DNA Oxidation and Excision Repair Pathways. *Int J Mol Sci,* 20(23).

Leijen, S., Van Geel, R. M., Sonke, G. S., De Jong, D., Rosenberg, E. H., Marchetti, S., Pluim, D., Van Werkhoven, E., Rose, S., Lee, M. A., Freshwater, T., Beijnen, J. H. & Schellens, J. H. (2016) Phase II Study of WEE1 Inhibitor AZD1775 Plus Carboplatin in Patients With TP53-Mutated Ovarian Cancer Refractory or Resistant to First-Line Therapy Within 3 Months. *J Clin Oncol,* 34(36)**,** 4354-4361.

Leonard, B. C., Lee, E. D., Bhola, N. E., Li, H., Sogaard, K. K., Bakkenist, C. J., Grandis, J. R. & Johnson, D. E. (2019) ATR inhibition sensitizes HPV. *Oral Oncol,* 95**,** 35-42.

Levine, A. J. (1997) p53, the cellular gatekeeper for growth and division. *Cell,* 88(3)**,** 323-331.

Li, J., Duan, B., Cheng, Z. & Kou, M. (2022a) Costunolide enhances cisplatin-induced cytotoxicity in hypopharyngeal SCC FaDu cells by increasing the production of reactive oxygen species. *Pathol Res Pract,* 236**,** 153966.

Li, X., Pu, W., Zheng, Q., Ai, M., Chen, S. & Peng, Y. (2022b) Proteolysis-targeting chimeras (PROTACs) in cancer therapy. *Mol Cancer,* 21(1)**,** 99.

Li, Z., Pinch, B. J., Olson, C. M., Donovan, K. A., Nowak, R. P., Mills, C. E., Scott, D. A., Doctor, Z. M., Eleuteri, N. A., Chung, M., Sorger, P. K., Fischer, E. S. & Gray, N. S. (2020) Development and Characterization of a Wee1 Kinase Degrader. *Cell Chem Biol,* 27(1)**,** 57-65.e9.

Lin, X., Chen, D., Zhang, C., Zhang, X., Li, Z., Dong, B., Gao, J. & Shen, L. (2018) Augmented antitumor activity by olaparib plus AZD1775 in gastric cancer through disrupting DNA damage repair pathways and DNA damage checkpoint. *J Exp Clin Cancer Res,* 37(1)**,** 129.

Lindahl, T. (1974) An N-glycosidase from Escherichia coli that releases free uracil from DNA containing deaminated cytosine residues. *Proc Natl Acad Sci U S A,* 71(9)**,** 3649-53.

Lindemann, A., Patel, A. A., Tang, L., Tanaka, N., Gleber-Netto, F. O., Bartels, M. D., Wang, L., Mcgrail, D. J., Lin, S. Y., Frank, S. J., Frederick, M. J., Myers, J. N. & Osman, A. A. (2021) Combined Inhibition of Rad51 and Wee1 Enhances Cell Killing in HNSCC Through Induction of Apoptosis Associated With Excessive DNA Damage and Replication Stress. *Mol Cancer Ther,* 20(7)**,** 1257-1269.

Linzer, D. I. H. & Levine, A. J. (1979) CHARACTERIZATION OF A 54K DALTON CELLULAR SV40 TUMOR-ANTIGEN PRESENT IN SV40-TRANSFORMED CELLS AND UNINFECTED EMBRYONAL CARCINOMA-CELLS. *Cell,* 17(1)**,** 43-52.

Liu, S., Shiotani, B., Lahiri, M., Maréchal, A., Tse, A., Leung, C. C., Glover, J. N., Yang, X. H. & Zou, L. (2011) ATR autophosphorylation as a molecular switch for checkpoint activation. *Mol Cell,* 43(2)**,** 192-202.

Liu, W., Palovcak, A., Li, F., Zafar, A., Yuan, F. & Zhang, Y. (2020) Fanconi anemia pathway as a prospective target for cancer intervention. *Cell Biosci,* 10**,** 39.

Luo, X., Archibeque, I., Dellamaggiore, K., Smither, K., Homann, O., Lipford, J. R. & Mohl, D. (2022) Profiling of diverse tumor types establishes the broad utility of VHL-based ProTaCs and triages candidate ubiquitin ligases. *iScience,* 25(3)**,** 103985.

Lücking, U., Wortmann, L., Wengner, A. M., Lefranc, J., Lienau, P., Briem, H., Siemeister, G., Bömer, U., Denner, K., Schäfer, M., Koppitz, M., Eis, K., Bartels, F., Bader, B., Bone, W., Moosmayer, D., Holton, S. J., Eberspächer, U., Grudzinska-Goebel, J., Schatz, C., Deeg, G., Mumberg, D. & Von Nussbaum, F. (2020) Damage Incorporated: Discovery of the Potent, Highly Selective, Orally Available ATR Inhibitor BAY 1895344 with Favorable Pharmacokinetic Properties and Promising Efficacy in Monotherapy and in Combination Treatments in Preclinical Tumor Models. *J Med Chem,* 63(13)**,** 7293-7325.

Madariaga, A., Mitchell, S. A., Pittman, T., Wang, L., Bowering, V., Kavak, N., Quintos, J., Chang, K., Ramsahai, J., Karakasis, K., Welch, S. A., Dhani, N. C., Lheureux, S. & Oza, A. M. (2022) Patient self-reporting of tolerability using PRO-CTCAE in a randomized double-blind, placebo-controlled phase II trial comparing gemcitabine in combination with adavosertib or placebo in patients with platinum resistant or refractory epithelial ovarian carcinoma. *Gynecol Oncol*.

Mak, J. P., Man, W. Y., Ma, H. T. & Poon, R. Y. (2014) Pharmacological targeting the ATR-CHK1-WEE1 axis involves balancing cell growth stimulation and apoptosis. *Oncotarget,* 5(21)**,** 10546-57.

Maniaci, C. & Ciulli, A. (2019) Bifunctional chemical probes inducing protein-protein interactions. *Current Opinion in Chemical Biology,* 52**,** 145-156.

Martín-Acosta, P. & Xiao, X. (2021) PROTACs to address the challenges facing small molecule inhibitors. *Eur J Med Chem,* 210**,** 112993.

Maréchal, A. & Zou, L. (2013) DNA damage sensing by the ATM and ATR kinases. *Cold Spring Harb Perspect Biol,* 5(9).

Matheson, C. J., Backos, D. S. & Reigan, P. (2016) Targeting WEE1 Kinase in Cancer. *Trends in Pharmacological Sciences,* 37(10)**,** 872-881.

Matsuoka, S., Rotman, G., Ogawa, A., Shiloh, Y., Tamai, K. & Elledge, S. J. (2000) Ataxia telangiectasia-mutated phosphorylates Chk2 in vivo and in vitro. *Proceedings of the National Academy of Sciences of the United States of America,* 97(19)**,** 10389-10394.

Matthews, H. K., Bertoli, C. & De Bruin, R. A. M. (2021) Cell cycle control in cancer. *Nat Rev Mol Cell Biol*.

Maya, R., Balass, M., Kim, S. T., Shkedy, D., Leal, J. F., Shifman, O., Moas, M., Buschmann, T., Ronai, Z., Shiloh, Y., Kastan, M. B., Katzir, E. & Oren, M. (2001) ATM-dependent phosphorylation of Mdm2 on serine 395: role in p53 activation by DNA damage. *Genes Dev,* 15(9)**,** 1067-77.

Mccarthy, N. J. & Evan, G. I. (1998) Methods for detecting and quantifying apoptosis. *Curr Top Dev Biol,* 36**,** 259-78.

Mccurdy, A. R. & Lacy, M. Q. (2013) Pomalidomide and its clinical potential for relapsed or refractory multiple myeloma: an update for the hematologist. *Ther Adv Hematol,* 4(3)**,** 211-6.

Meek, D. W. (2000) The role of p53 in the response to mitotic spindle damage. *Pathol Biol (Paris),* 48(3)**,** 246-54.

Mei, L., Zhang, J. & He, K. (2019) Ataxia telangiectasia and Rad3-related inhibitors and cancer therapy: where we stand. *J Hematol Oncol,* 12(1)**,** 43.

Mendez, E., Rodriguez, C. P., Kao, M. C., Raju, S., Diab, A., Harbison, R. A., Konnick, E. Q., Mugundu, G. M., Santana-Davila, R., Martins, R., Futran, N. D. & Chow, L. Q. M.

(2018) A Phase I Clinical Trial of AZD1775 in Combination with Neoadjuvant Weekly Docetaxel and Cisplatin before Definitive Therapy in Head and Neck Squamous Cell Carcinoma. *Clinical Cancer Research,* 24(12)**,** 2740-2748.

Mi, D., Li, Y., Gu, H. & Chen, Y. (2023) Current advances of small molecule E3 ligands for proteolysis-targeting chimeras design. *Eur J Med Chem,* 256**,** 115444.

Min, A., Im, S. A., Jang, H., Kim, S., Lee, M., Kim, D. K., Yang, Y., Kim, H. J., Lee, K. H., Kim, J. W., Kim, T. Y., Oh, D. Y., Brown, J., Lau, A., O'connor, M. J. & Bang, Y. J. (2017) AZD6738, A Novel Oral Inhibitor of ATR, Induces Synthetic Lethality with ATM Deficiency in Gastric Cancer Cells. *Mol Cancer Ther,* 16(4)**,** 566-577.

Moiseeva, T. N., Qian, C., Sugitani, N., Osmanbeyoglu, H. U. & Bakkenist, C. J. (2019) WEE1 kinase inhibitor AZD1775 induces CDK1 kinase-dependent origin firing in unperturbed G1-and S-phase cells. *Proceedings of the National Academy of Sciences of the United States of America,* 116(48)**,** 23891-23893.

Nalawansha, D. A. & Crews, C. M. (2020) PROTACs: An Emerging Therapeutic Modality in Precision Medicine. *Cell Chem Biol,* 27(8)**,** 998-1014.

Neklesa, T., Snyder, L. B., Willard, R. R., Vitale, N., Pizzano, J., Gordon, D. A., Bookbinder, M., Macaluso, J., Dong, H., Ferraro, C., Wang, G., Wang, J., Crews, C. M., Houston, J., Crew, A. P. & Taylor, I. (2019) ARV-110: An oral androgen receptor PROTAC degrader for prostate cancer. *Journal of Clinical Oncology,* 37(7).

Ngoi, N. Y. L., Pham, M. M., Tan, D. S. P. & Yap, T. A. (2021) Targeting the replication stress response through synthetic lethal strategies in cancer medicine. *Trends Cancer,* 7(10)**,** 930-957.

Niraj, J., Färkkilä, A. & D'andrea, A. D. (2019) The Fanconi Anemia Pathway in Cancer. *Annu Rev Cancer Biol,* 3**,** 457-478.

Norbury, C. & Nurse, P. (1992) ANIMAL-CELL CYCLES AND THEIR CONTROL. *Annual Review of Biochemistry,* 61**,** 441-470.

Nowak, R. P. & Jones, L. H. (2020) Target Validation Using PROTACs: Applying the Four Pillars Framework. *SLAS discovery : advancing life sciences R & D***,** 2472555220979584-2472555220979584.

Nurse, P. (1975) GENETIC-CONTROL OF CELL-SIZE AT CELL-DIVISION IN YEAST. *Nature,* 256(5518)**,** 547-551.

Oetting, A., Christiansen, S., Gatzemeier, F., Köcher, S., Bußmann, L., Böttcher, A., Stölzel, K., Hoffmann, A. S., Struve, N., Kriegs, M., Petersen, C., Betz, C., Rothkamm, K., Zech, H. B. & Rieckmann, T. (2023) Impaired DNA double-strand break repair and effective radiosensitization of HPV-negative HNSCC cell lines through combined inhibition of PARP and Wee1. *Clin Transl Radiat Oncol,* 41**,** 100630.

Oku, Y., Nishiya, N., Tazawa, T., Kobayashi, T., Umezawa, N., Sugawara, Y. & Uehara, Y. (2018) Augmentation of the therapeutic efficacy of WEE1 kinase inhibitor AZD1775 by inhibiting the YAP-E2F1-DNA damage response pathway axis. *FEBS Open Bio,* 8(6)**,** 1001-1012.

Olivier, M., Eeles, R., Hollstein, M., Khan, M. A., Harris, C. C. & Hainaut, P. (2002) The IARC TP53 database: New Online mutation analysis and recommendations to users. *Human Mutation,* 19(6)**,** 607-614.

Olson, C. M., Jiang, B., Erb, M. A., Liang, Y., Doctor, Z. M., Zhang, Z., Zhang, T., Kwiatkowski, N., Boukhali, M., Green, J. L., Haas, W., Nomanbhoy, T., Fischer, E. S., Young, R. A., Bradner, J. E., Winter, G. E. & Gray, N. S. (2018) Pharmacological perturbation of CDK9 using selective CDK9 inhibition or degradation. *Nat Chem Biol,* 14(2)**,** 163-170.

Oren, M. & Levine, A. J. (1983) MOLECULAR-CLONING OF A CDNA SPECIFIC FOR THE MURINE P53 CELLULAR TUMOR-ANTIGEN. *Proceedings of the National Academy of Sciences of the United States of America-Biological Sciences,* 80(1)**,** 56-59.

Osman, A. A., Monroe, M. M., Ortega Alves, M. V., Patel, A. A., Katsonis, P., Fitzgerald, A. L., Neskey, D. M., Frederick, M. J., Woo, S. H., Caulin, C., Hsu, T. K., Mcdonald, T. O., Kimmel, M., Meyn, R. E., Lichtarge, O. & Myers, J. N. (2015) Wee-1 kinase inhibition overcomes cisplatin resistance associated with high-risk TP53 mutations in head and neck cancer through mitotic arrest followed by senescence. *Mol Cancer Ther,* 14(2)**,** 608-19.

Paiva, S.-L. & Crews, C. M. (2019) Targeted protein degradation: elements of PROTAC design. *Current Opinion in Chemical Biology,* 50**,** 111-119.

Parada, L. F., Land, H., Weinberg, R. A., Wolf, D. & Rotter, V. (1984) COOPERATION BETWEEN GENE ENCODING P53 TUMOR-ANTIGEN AND RAS IN CELLULAR-TRANSFORMATION. *Nature,* 312(5995)**,** 649-651.

Parker, L. L. & Piwnicaworms, H. (1992) INACTIVATION OF THE P34(CDC2)-CYCLIN-B COMPLEX BY THE HUMAN WEE1 TYROSINE KINASE. *Science,* 257(5078)**,** 1955-1957.

Parkin, D. M., Bray, F., Ferlay, J. & Pisani, P. (2005) Global cancer statistics, 2002. *Ca-a Cancer Journal for Clinicians,* 55(2)**,** 74-108.

Parsels, L. A., Karnak, D., Parsels, J. D., Zhang, Q., Vélez-Padilla, J., Reichert, Z. R., Wahl, D. R., Maybaum, J., O'connor, M. J., Lawrence, T. S. & Morgan, M. A. (2018) PARP1 Trapping and DNA Replication Stress Enhance Radiosensitization with Combined WEE1 and PARP Inhibitors. *Mol Cancer Res,* 16(2)**,** 222-232.

Patel, P., Sun, L., Robbins, Y., Clavijo, P. E., Friedman, J., Silvin, C., Van Waes, C., Cook, J., Mitchell, J. & Allen, C. (2019) Enhancing direct cytotoxicity and response to immune

checkpoint blockade following ionizing radiation with Wee1 kinase inhibition. *Oncoimmunology,* 8(11)**,** e1638207.

Paulsen, R. D. & Cimprich, K. A. (2007) The ATR pathway: fine-tuning the fork. *DNA Repair (Amst),* 6(7)**,** 953-66.

Petitjean, A., Mathe, E., Kato, S., Ishioka, C., Tavtigian, S. V., Hainaut, P. & Olivier, M. (2007) Impact of mutant p53 functional properties on TP53 mutation patterns and tumor phenotype: Lessons from recent developments in the IARC TP53 database. *Human Mutation,* 28(6)**,** 622-629.

Pettersson, M. & Crews, C. M. (2019) PROteolysis TArgeting Chimeras (PROTACs) - Past, present and future. *Drug Discov Today Technol,* 31**,** 15-27.

Pfister, S. X., Markkanen, E., Jiang, Y., Sarkar, S., Woodcock, M., Orlando, G., Mavrommati, I., Pai, C. C., Zalmas, L. P., Drobnitzky, N., Dianov, G. L., Verrill, C., Macaulay, V. M., Ying, S., La Thangue, N. B., D'angiolella, V., Ryan, A. J. & Humphrey, T. C. (2015) Inhibiting WEE1 Selectively Kills Histone H3K36me3-Deficient Cancers by dNTP Starvation. *Cancer Cell,* 28(5)**,** 557-568.

Pfizer & Arvinas (2021) *ARVINAS AND PFIZER ANNOUNCE GLOBAL COLLABORATION TO DEVELOP AND COMMERCIALIZE PROTAC® PROTEIN DEGRADER ARV-471*. Available at: https://www.pfizer.com/news/press-release/press-release-detail/arvinas-and-pfizer-announce-global-collaboration-develop [Accessed 23/07/2021].

Pico, C. X. C., Li, D., Lanier, C. D., Evans, K., Raso, M. G., Diperi, T., Rizvi, Y., Ha, M. J., Chen, H., Zhao, M., Akcakanat, A., Zheng, X., Toruner, G., Yuca, E., Scott, S., Wengner, A. M., Yap, T. A. & Meric-Bernstam, F. (2021) Anti-tumor activity of ATR inhibitor BAY 1895344 in patient-derived xenograft (PDX) models with DNA damage response (DDR) pathway alterations. *Molecular Cancer Therapeutics,* 20(12).

Pike, K. G., Barlaam, B., Cadogan, E., Campbell, A., Chen, Y., Colclough, N., Davies, N. L., De-Almeida, C., Degorce, S. L., Didelot, M., Dishington, A., Ducray, R., Durant, S. T., Hassall, L. A., Holmes, J., Hughes, G. D., Macfaul, P. A., Mulholland, K. R., Mcguire, T. M., Ouvry, G., Pass, M., Robb, G., Stratton, N., Wang, Z., Wilson, J., Zhai, B., Zhao, K. & Al-Huniti, N. (2018) The Identification of Potent, Selective, and Orally Available Inhibitors of Ataxia Telangiectasia Mutated (ATM) Kinase: The Discovery of AZD0156 (8-{6-[3-(Dimethylamino)propoxy]pyridin-3-yl}-3-methyl-1-(tetrahydro-2 H-pyran-4-yl)-1,3-dihydro-2 H-imidazo[4,5- c]quinolin-2-one). *J Med Chem,* 61(9)**,** 3823-3841.

Plummer, E. R., Dean, E. J., Evans, T. R. J., Greystoke, A., Herbschleb, K., Ranson, M., Brown, J., Zhang, Y., Karan, S., Pollard, J., Penney, M. S., Asmal, M., Fields, S. Z. & Middleton, M. R. (2016) Phase I trial of first-in-class ATR inhibitor VX-970 in combination with gemcitabine (Gem) in advanced solid tumors (NCT02157792). *Journal of Clinical Oncology,* 34(15_suppl)**,** 2513-2513.

Reinhardt, H. C. & Yaffe, M. B. (2009) Kinases that control the cell cycle in response to DNA damage: Chk1, Chk2, and MK2. *Curr Opin Cell Biol,* 21(2)**,** 245-55.

Rickman, K. A., Lach, F. P., Abhyankar, A., Donovan, F. X., Sanborn, E. M., Kennedy, J. A., Sougnez, C., Gabriel, S. B., Elemento, O., Chandrasekharappa, S. C., Schindler, D., Auerbach, A. D. & Smogorzewska, A. (2015) Deficiency of UBE2T, the E2 Ubiquitin Ligase Necessary for FANCD2 and FANCI Ubiquitination, Causes FA-T Subtype of Fanconi Anemia. *Cell Rep,* 12(1)**,** 35-41.

Robertson, M. S. & Hornibrook, J. (1982) THE PRESENTING SYMPTOMS OF HEAD AND NECK-CANCER. *New Zealand Medical Journal,* 95(708)**,** 337-341.

Rodier, F. & Campisi, J. (2011) Four faces of cellular senescence. *Journal of Cell Biology,* 192(4)**,** 547-556.

Roulston, A., Zimmermann, M., Papp, R., Skeldon, A., Pellerin, C., Dumas-Bérube, É., Dumais, V., Dorich, S., Fader, L. D., Fournier, S., Li, L., Leclaire, M. E., Yin, S. Y., Chefson, A., Alam, H., Yang, W., Fugère-Desjardins, C., Vignini-Hammond, S., Skorey, K., Mulani, A., Rimkunas, V., Veloso, A., Hamel, M., Stocco, R., Mamane, Y., Li, Z., Young, J. T. F., Zinda, M. & Black, W. C. (2022) RP-3500: A Novel, Potent, and Selective ATR Inhibitor that is Effective in Preclinical Models as a Monotherapy and in Combination with PARP Inhibitors. *Mol Cancer Ther,* 21(2)**,** 245-256.

Roy, M. J., Winkler, S., Hughes, S. J., Whitworth, C., Galant, M., Farnaby, W., Rumpel, K. & Ciulli, A. (2019) SPR-Measured Dissociation Kinetics of PROTAC Ternary Complexes Influence Target Degradation Rate. *Acs Chemical Biology,* 14(3)**,** 361-368.

Russell, P. & Nurse, P. (1987) NEGATIVE REGULATION OF MITOSIS BY WEE1+, A GENE ENCODING A PROTEIN-KINASE HOMOLOG. *Cell,* 49(4)**,** 559-567.

Sakamoto, K. M., Kim, K. B., Kumagai, A., Mercurio, F., Crews, C. M. & Deshaies, R. J. (2001) Protacs: Chimeric molecules that target proteins to the Skp1-Cullin-F box complex for ubiquitination and degradation. *Proceedings of the National Academy of Sciences of the United States of America,* 98(15)**,** 8554-8559.

Sakamoto, K. M., Kim, K. B., Verma, R., Ransick, A., Stein, B., Crews, C. M. & Deshaies, R. J. (2003) Development of protacs to target cancer-promoting proteins for ubiquitination and degradation. *Molecular & Cellular Proteomics,* 2(12)**,** 1350-1358.

Saldivar, J. C., Cortez, D. & Cimprich, K. A. (2017) The essential kinase ATR: ensuring faithful duplication of a challenging genome. *Nat Rev Mol Cell Biol,* 18(10)**,** 622-636.

Sand, A., Piacsek, M., Donohoe, D. L., Duffin, A. T., Riddell, G. T., Sun, C., Tang, M., Rovin, R. A., Tjoe, J. A. & Yin, J. (2020) WEE1 inhibitor, AZD1775, overcomes trastuzumab

resistance by targeting cancer stem-like properties in HER2-positive breast cancer. *Cancer Lett,* 472**,** 119-131.

Sarkar, S., Davies, A. A., Ulrich, H. D. & Mchugh, P. J. (2006) DNA interstrand crosslink repair during G1 involves nucleotide excision repair and DNA polymerase zeta. *EMBO J,* 25(6)**,** 1285-94.

Sarkaria, J. N., Busby, E. C., Tibbetts, R. S., Roos, P., Taya, Y., Karnitz, L. M. & Abraham, R. T. (1999) Inhibition of ATM and ATR kinase activities by the radiosensitizing agent, caffeine. *Cancer Res,* 59(17)**,** 4375-82.

Satyanarayana, A. & Kaldis, P. (2009) Mammalian cell-cycle regulation: several Cdks, numerous cyclins and diverse compensatory mechanisms. *Oncogene,* 28(33)**,** 2925-2939.

Saxena, S. & Zou, L. (2022) Hallmarks of DNA replication stress. *Mol Cell,* 82(12)**,** 2298-2314.

Scheffner, M., Huibregtse, J. M., Vierstra, R. D. & Howley, P. M. (1993) THE HPV-16 E6 AND E6-AP COMPLEX FUNCTIONS AS A UBIQUITIN-PROTEIN LIGASE IN THE UBIQUITINATION OF P53. *Cell,* 75(3)**,** 495-505.

Schneekloth, J. S., Fonseca, F. N., Koldobskiy, M., Mandal, A., Deshaies, R., Sakamoto, K. & Crews, C. M. (2004) Chemical genetic control of protein levels: Selective in vivo targeted degradation. *Journal of the American Chemical Society,* 126(12)**,** 3748-3754.

Schulman, B. A. & Harper, J. W. (2009) Ubiquitin-like protein activation by E1 enzymes: the apex for downstream signalling pathways. *Nature Reviews Molecular Cell Biology,* 10(5)**,** 319-331.

Schutte, H. W., Heutink, F., Wellenstein, D. J., Van Den Broek, G. B., Van Den Hoogen, F. J. A., Marres, H. A. M., Van Herpen, C. M. L., Kaanders, J. H. A. M., Merkx, T. M. A. W. & Takes, R. P. (2020) Impact of Time to Diagnosis and Treatment in Head and Neck

Cancer: A Systematic Review. *Otolaryngology-Head and Neck Surgery,* 162(4)**,** 446-457.

Schärer, O. D. (2013) Nucleotide excision repair in eukaryotes. *Cold Spring Harb Perspect Biol,* 5(10)**,** a012609.

Semlow, D. R. & Walter, J. C. (2021) Mechanisms of Vertebrate DNA Interstrand Cross-Link Repair. *Annu Rev Biochem,* 90**,** 107-135.

Sen, T., Tong, P., Stewart, C. A., Cristea, S., Valliani, A., Shames, D. S., Redwood, A. B., Fan, Y. H., Li, L., Glisson, B. S., Minna, J. D., Sage, J., Gibbons, D. L., Piwnica-Worms, H., Heymach, J. V., Wang, J. & Byers, L. A. (2017) CHK1 Inhibition in Small-Cell Lung Cancer Produces Single-Agent Activity in Biomarker-Defined Disease Subsets and Combination Activity with Cisplatin or Olaparib. *Cancer Res,* 77(14)**,** 3870-3884.

Seo, H. R., Nam, A. R., Bang, J. H., Oh, K. S., Kim, J. M., Yoon, J., Kim, T. Y. & Oh, D. Y. (2022) Inhibition of WEE1 Potentiates Sensitivity to PARP Inhibitor in Biliary Tract Cancer. *Cancer Res Treat,* 54(2)**,** 541-553.

Serpico, A. F., D'alterio, G., Vetrei, C., Della Monica, R., Nardella, L., Visconti, R. & Grieco, D. (2019) Wee1 Rather Than Plk1 Is Inhibited by AZD1775 at Therapeutically Relevant Concentrations. *Cancers (Basel),* 11(6).

Setlow, R. B. & Carrier, W. L. (1964) THE DISAPPEARANCE OF THYMINE DIMERS FROM DNA: AN ERROR-CORRECTING MECHANISM. *Proc Natl Acad Sci U S A,* 51(2)**,** 226-31.

Shadfar, S., Parakh, S., Jamali, M. S. & Atkin, J. D. (2023) Redox dysregulation as a driver for DNA damage and its relationship to neurodegenerative diseases. *Transl Neurodegener,* 12(1)**,** 18.

Sheng, H., Huang, Y., Xiao, Y., Zhu, Z., Shen, M., Zhou, P., Guo, Z., Wang, J., Wang, H., Dai, W., Zhang, W., Sun, J. & Cao, C. (2020) ATR inhibitor AZD6738 enhances the

antitumor activity of radiotherapy and immune checkpoint inhibitors by potentiating the tumor immune microenvironment in hepatocellular carcinoma. *J Immunother Cancer,* 8(1).

Sherr, C. J. & Bartek, J. (2017) Cell Cycle–Targeted Cancer Therapies. *Annual Review of Cancer Biology,* 1(1)**,** 41-57.

Shi, C., Zhang, H., Wang, P., Wang, K., Xu, D., Wang, H., Yin, L., Zhang, S. & Zhang, Y. (2019) PROTAC induced-BET protein degradation exhibits potent anti-osteosarcoma activity by triggering apoptosis. *Cell Death & Disease,* 10.

Shiloh, Y. (2003) ATM and related protein kinases: safeguarding genome integrity. *Nat Rev Cancer,* 3(3)**,** 155-68.

Silva, M. C., Ferguson, F. M., Cai, Q., Donovan, K. A., Nandi, G., Patnaik, D., Zhang, T., Huang, H.-T., Lucente, D. E., Dickerson, B. C., Mitchison, T. J., Fischer, E. S., Gray, N. S. & Haggarty, S. J. (2019) Targeted degradation of aberrant tau in frontotemporal dementia patient-derived neuronal cell models. *Elife,* 8.

Singh, B. & Bhaskar, S. (2019) Methods for Detection of Autophagy in Mammalian Cells. *Methods Mol Biol,* 2045**,** 245-258.

Skotheim, J. M., Di Talia, S., Siggia, E. D. & Cross, F. R. (2008) Positive feedback of G1 cyclins ensures coherent cell cycle entry. *Nature,* 454(7202)**,** 291-6.

Stakyte, K., Rotheneder, M., Lammens, K., Bartho, J. D., Grädler, U., Fuchß, T., Pehl, U., Alt, A., Van De Logt, E. & Hopfner, K. P. (2021) Molecular basis of human ATM kinase inhibition. *Nat Struct Mol Biol,* 28(10)**,** 789-798.

Sun, X., Gao, H., Yang, Y., He, M., Wu, Y., Song, Y., Tong, Y. & Rao, Y. (2019) PROTACs: great opportunities for academia and industry. *Signal Transduct Target Ther,* 4**,** 64.

Swift, L. H. & Golsteyn, R. M. (2014) Genotoxic anti-cancer agents and their relationship to

DNA damage, mitosis, and checkpoint adaptation in proliferating cancer cells. *Int J*

Mol Sci, 15(3)**,** 3403-31.

Takebe, N., Naqash, A. R., O'sullivan Coyne, G., Kummar, S., Do, K., Bruns, A., Juwara, L.,

Zlott, J., Rubinstein, L., Piekarz, R., Sharon, E., Streicher, H., Mittra, A., Miller, S. B., Ji,

J., Wilsker, D., Kinders, R. J., Parchment, R. E., Chen, L., Chang, T. C., Das, B.,

Mugundu, G., Doroshow, J. H. & Chen, A. P. (2021) Safety, Antitumor Activity, and

Biomarker Analysis in a Phase I Trial of the Once-daily Wee1 Inhibitor Adavosertib

(AZD1775) in Patients with Advanced Solid Tumors. *Clin Cancer Res,* 27(14)**,** 3834-

3844.

Talamini, R., Bosetti, C., La Vecchia, C., Dal Maso, L., Levi, F., Bidoli, E., Negri, E., Pasche, C.,

Vaccarella, S., Barzan, L. & Franceschi, S. (2002) Combined effect of tobacco and

alcohol on laryngeal cancer risk: a case-control study. *Cancer Causes & Control,*

13(10)**,** 957-964.

Tanaka, N., Patel, A. A., Wang, J., Frederick, M. J., Kalu, N. N., Zhao, M., Fitzgerald, A. L., Xie,

T.-X., Silver, N. L., Caulin, C., Zhou, G., Skinner, H. D., Johnson, F. M., Myers, J. N. &

Osman, A. A. (2015) Wee-1 Kinase Inhibition Sensitizes High-Risk HPV+ HNSCC to

Apoptosis Accompanied by Downregulation of MCl-1 and XIAP Antiapoptotic

Proteins. *Clinical Cancer Research,* 21(21)**,** 4831-4844.

Tang, S., Li, Z., Yang, L., Shen, L. & Wang, Y. (2020) A potential new role of ATM inhibitor in

radiotherapy: suppressing ionizing Radiation-Activated EGFR. *Int J Radiat Biol,* 96(4)**,**

461-468.

Testino, G. (2011) The burden of cancer attributable to alcohol consumption. *Maedica,* 6(4)**,**

313-20.

Thomas, A., Manchella, S., Koo, K., Tiong, A., Nastri, A. & Wiesenfeld, D. (2021) The impact

of delayed diagnosis on the outcomes of oral cancer patients: a retrospective cohort

study. *International Journal of Oral and Maxillofacial Surgery,* 50(5)**,** 585-590.

Thompson, R. & Eastman, A. (2013) The cancer therapeutic potential of Chk1 inhibitors: how

mechanistic studies impact on clinical trial design. *Br J Clin Pharmacol,* 76(3)**,** 358-69.

Tibbetts, R. S., Brumbaugh, K. M., Williams, J. M., Sarkaria, J. N., Cliby, W. A., Shieh, S. Y.,

Taya, Y., Prives, C. & Abraham, R. T. (1999) A role for ATR in the DNA damage-

induced phosphorylation of p53. *Genes Dev,* 13(2)**,** 152-7.

Toledo, L., Neelsen, K. J. & Lukas, J. (2017) Replication Catastrophe: When a Checkpoint Fails

because of Exhaustion. *Molecular Cell,* 66(6)**,** 735-749.

Tu, X., Kahila, M. M., Zhou, Q., Yu, J., Kalari, K. R., Wang, L., Harmsen, W. S., Yuan, J.,

Boughey, J. C., Goetz, M. P., Sarkaria, J. N., Lou, Z. & Mutter, R. W. (2018) ATR

Inhibition Is a Promising Radiosensitizing Strategy for Triple-Negative Breast Cancer.

Mol Cancer Ther, 17(11)**,** 2462-2472.

Tuma, A. M., Zhong, W., Liu, L., Burgenske, D. M., Carlson, B. L., Bakken, K. K., Hu, Z.,

Connors, M. A. & Sarkaria, J. N. (2022) Abstract 3305: WSD-0628, a novel brain

penetrant ATM inhibitor, radiosensitizes GBM and melanoma patient derived

xenografts. *Cancer Research,* 82(12)**,** 3305.

Ullah, Z., Lee, C. Y., Lilly, M. A. & Depamphilis, M. L. (2009) Developmentally programmed

endoreduplication in animals. *Cell Cycle,* 8(10)**,** 1501-9.

Uziel, T., Lerenthal, Y., Moyal, L., Andegeko, Y., Mittelman, L. & Shiloh, Y. (2003)

Requirement of the MRN complex for ATM activation by DNA damage. *EMBO J,*

22(20)**,** 5612-21.

Valas, R. E. & Bourne, P. E. (2008) Rethinking proteasome evolution: Two novel bacterial proteasomes. *Journal of Molecular Evolution,* 66(5)**,** 494-504.

Van Engeland, M., Nieland, L. J., Ramaekers, F. C., Schutte, B. & Reutelingsperger, C. P. (1998) Annexin V-affinity assay: a review on an apoptosis detection system based on phosphatidylserine exposure. *Cytometry,* 31(1)**,** 1-9.

Vassilev, L. T., Vu, B. T., Graves, B., Carvajal, D., Podlaski, F., Filipovic, Z., Kong, N., Kammlott, U., Lukacs, C., Klein, C., Fotouhi, N. & Liu, E. A. (2004) In vivo activation of the p53 pathway by small-molecule antagonists of MDM2. *Science,* 303(5659)**,** 844-848.

Vendetti, F. P., Lau, A., Schamus, S., Conrads, T. P., O'connor, M. J. & Bakkenist, C. J. (2015) The orally active and bioavailable ATR kinase inhibitor AZD6738 potentiates the anti-tumor effects of cisplatin to resolve ATM-deficient non-small cell lung cancer in vivo. *Oncotarget,* 6(42)**,** 44289-305.

Vermeulen, K., Van Bockstaele, D. R. & Berneman, Z. N. (2003) The cell cycle: a review of regulation, deregulation and therapeutic targets in cancer. *Cell Proliferation,* 36(3)**,** 131-149.

Vignard, J., Mirey, G. & Salles, B. (2013) Ionizing-radiation induced DNA double-strand breaks: a direct and indirect lighting up. *Radiother Oncol,* 108(3)**,** 362-9.

Visconti, R., Della Monica, R. & Grieco, D. (2016) Cell cycle checkpoint in cancer: a therapeutically targetable double-edged sword. *Journal of Experimental & Clinical Cancer Research,* 35.

Walton, M. I., Eve, P. D., Hayes, A., Henley, A. T., Valenti, M. R., De Haven Brandon, A. K., Box, G., Boxall, K. J., Tall, M., Swales, K., Matthews, T. P., Mchardy, T., Lainchbury, M., Osborne, J., Hunter, J. E., Perkins, N. D., Aherne, G. W., Reader, J. C., Raynaud, F. I., Eccles, S. A., Collins, I. & Garrett, M. D. (2016) The clinical development candidate

CCT245737 is an orally active CHK1 inhibitor with preclinical activity in RAS mutant NSCLC and Eμ-MYC driven B-cell lymphoma. *Oncotarget,* 7(3)**,** 2329-42.

Walworth, N. C. & Bernards, R. (1996) rad-dependent response of the chk1-encoded protein kinase at the DNA damage checkpoint. *Science,* 271(5247)**,** 353-6.

Wang, L., Bharti, Kumar, R., Pavlov, P. F. & Winblad, B. (2021a) Small molecule therapeutics for tauopathy in Alzheimer's disease: Walking on the path of most resistance. *European Journal of Medicinal Chemistry,* 209.

Wang, Q., Fan, S., Eastman, A., Worland, P. J., Sausville, E. A. & O'connor, P. M. (1996) UCN-01: a potent abrogator of G2 checkpoint function in cancer cells with disrupted p53. *J Natl Cancer Inst,* 88(14)**,** 956-65.

Wang, W., Zhou, Q., Jiang, T., Li, S., Ye, J., Zheng, J., Wang, X., Liu, Y., Deng, M., Ke, D., Wang, Q., Wang, Y. & Wang, J.-Z. (2021b) A novel small-molecule PROTAC selectively promotes tau clearance to improve cognitive functions in Alzheimer-like models. *Theranostics,* 11(11)**,** 5279-5295.

Waqar, S. N., Robinson, C., Olszanski, A. J., Spira, A., Hackmaster, M., Lucas, L., Sponton, L., Jin, H., Hering, U., Cronier, D., Grinberg, M., Seithel-Keuth, A., Diaz-Padilla, I. & Berlin, J. (2022) Phase I trial of ATM inhibitor M3541 in combination with palliative radiotherapy in patients with solid tumors. *Invest New Drugs,* 40(3)**,** 596-605.

Ward, I. M. & Chen, J. J. (2001) Histone H2AX is phosphorylated in an ATR-dependent manner in response to replicational stress. *Journal of Biological Chemistry,* 276(51)**,** 47759-47762.

Webster, P. J., Littlejohns, A. T., Gaunt, H. J., Prasad, K. R., Beech, D. J. & Burke, D. A. (2017) AZD1775 induces toxicity through double-stranded DNA breaks independently of

chemotherapeutic agents in p53-mutated colorectal cancer cells. *Cell Cycle,* 16(22)**,** 2176-2182.

Wengner, A. M., Siemeister, G., Lücking, U., Lefranc, J., Wortmann, L., Lienau, P., Bader, B., Bömer, U., Moosmayer, D., Eberspächer, U., Golfier, S., Schatz, C. A., Baumgart, S. J., Haendler, B., Lejeune, P., Schlicker, A., Von Nussbaum, F., Brands, M., Ziegelbauer, K. & Mumberg, D. (2020) The Novel ATR Inhibitor BAY 1895344 Is Efficacious as Monotherapy and Combined with DNA Damage-Inducing or Repair-Compromising Therapies in Preclinical Cancer Models. *Mol Cancer Ther,* 19(1)**,** 26-38.

Wright, G., Golubeva, V., Rix, L. L. R., Bemdt, N., Luo, Y., Ward, G. A., Gray, J. E., Schonbrunn, E., Lawrence, H. R., Monteiro, A. N. A. & Rix, U. (2017) Dual Targeting of WEE1 and PLK1 by AZD1775 Elicits Single Agent Cellular Anticancer Activity. *Acs Chemical Biology,* 12(7)**,** 1883-1892.

Wurz, R. P., Dellamaggiore, K., Dou, H., Javier, N., Lo, M. C., Mccarter, J. D., Mohl, D., Sastri, C., Lipford, J. R. & Cee, V. J. (2018) A "Click Chemistry Platform" for the Rapid Synthesis of Bispecific Molecules for Inducing Protein Degradation. *J Med Chem,* 61(2)**,** 453-461.

Yamamoto, K., Wang, Y., Jiang, W., Liu, X., Dubois, R. L., Lin, C. S., Ludwig, T., Bakkenist, C. J. & Zha, S. (2012) Kinase-dead ATM protein causes genomic instability and early embryonic lethality in mice. *J Cell Biol,* 198(3)**,** 305-13.

Yamamoto, V., Wang, B. & Lee, A. S. (2022) Suppression of head and neck cancer cell survival and cisplatin resistance by GRP78 small molecule inhibitor YUM70. *Front Oncol,* 12**,** 1044699.

Yanagida, M. (2014) The Role of Model Organisms in the History of Mitosis Research. *Cold Spring Harbor Perspectives in Biology,* 6(9).

Yang, L., Shen, C., Pettit, C. J., Li, T., Hu, A. J., Miller, E. D., Zhang, J., Lin, S. H. & Williams, T. M. (2020) Wee1 Kinase Inhibitor AZD1775 Effectively Sensitizes Esophageal Cancer to Radiotherapy. *Clinical Cancer Research,* 26(14)**,** 3740-3750.

Yang, Z., Liao, J., Lapidus, R. G., Fan, X., Mehra, R., Cullen, K. J. & Dan, H. (2022) Targeting Wee1 kinase to suppress proliferation and survival of cisplatin-resistant head and neck squamous cell carcinoma. *Cancer Chemother Pharmacol,* 89(4)**,** 469-478.

Yap, T. A., Tolcher, A. W., Plummer, E. R., Becker, A., Fleuranceau-Morel, P., Goddemeier, T., Locatelli, G., Gounaris, I. & De Bono, J. S. (2021) A first-in-human phase I study of ATR inhibitor M1774 in patients with solid tumors. *Journal of Clinical Oncology,* 39(15).

Ye, Y. & Rape, M. (2009) Building ubiquitin chains: E2 enzymes at work. *Nature Reviews Molecular Cell Biology,* 10(11)**,** 755-764.

Yin, Y., Shen, Q., Tao, R., Chang, W., Li, R., Xie, G., Liu, W., Zhang, P. & Tao, K. (2018) Wee1 inhibition can suppress tumor proliferation and sensitize p53 mutant colonic cancer cells to the anticancer effect of irinotecan. *Mol Med Rep,* 17(2)**,** 3344-3349.

Zeng, J., Hills, S. A., Ozono, E. & Diffley, J. F. X. (2023) Cyclin E-induced replicative stress drives p53-dependent whole-genome duplication. *Cell,* 186(3)**,** 528-542.e14.

Zeng, L., Beggs, R. R., Cooper, T. S., Weaver, A. N. & Yang, E. S. (2017) Combining Chk1/2 Inhibition with Cetuximab and Radiation Enhances. *Mol Cancer Ther,* 16(4)**,** 591-600.

Zengerle, M., Chan, K. H. & Ciulli, A. (2015) Selective Small Molecule Induced Degradation of the BET Bromodomain Protein BRD4. *Acs Chemical Biology,* 10(8)**,** 1770-1777.

Zenke, F. T., Zimmermann, A., Dahmen, H., Elenbaas, B., Pollard, J., Reaper, P., Bagrodia, S., Spilker, M. E., Amendt, C. & Blaukat, A. (2019) Antitumor activity of M4344, a potent

and selective ATR inhibitor, in monotherapy and combination therapy. *Cancer Research,* 79(13).

Zhang, C., Xu, C., Gao, X. & Yao, Q. (2022) Platinum-based drugs for cancer therapy and anti-tumor strategies. *Theranostics,* 12(5)**,** 2115-2132.

Zhang, L., Riley-Gillis, B., Vijay, P. & Shen, Y. (2019) Acquired Resistance to BET-PROTACs (Proteolysis-Targeting Chimeras) Caused by Genomic Alterations in Core Components of E3 Ligase Complexes. *Mol Cancer Ther,* 18(7)**,** 1302-1311.

Zhang, Y. & Xiong, Y. (2001) A p53 amino-terminal nuclear export signal inhibited by DNA damage-induced phosphorylation. *Science,* 292(5523)**,** 1910-5.

Zhao, J. H., Xu, Q. L., Ma, S., Li, C. Y., Zhang, H. C., Zhao, L. J. & Zhang, Z. Y. (2023) Recent advance of small-molecule drugs for clinical treatment of multiple myeloma. *Eur J Med Chem,* 257**,** 115492.

Zhou, G., Liu, Z. Y. & Myers, J. N. (2016) TP53 Mutations in Head and Neck Squamous Cell Carcinoma and Their Impact on Disease Progression and Treatment Response. *Journal of Cellular Biochemistry,* 117(12)**,** 2682-2692.

Zhou, H., Bai, L., Xu, R., Zhao, Y., Chen, J., Mceachern, D., Chinnaswamy, K., Wen, B., Dai, L., Kumar, P., Yang, C.-Y., Liu, Z., Wang, M., Liu, L., Meagher, J. L., Yi, H., Sun, D., Stuckey, J. A. & Wang, S. (2019) Structure-Based Discovery of SD-36 as a Potent, Selective, and Efficacious PROTAC Degrader of STAT3 Protein. *Journal of Medicinal Chemistry,* 62(24)**,** 11280-11300.

Zhou, L., Zhang, Y., Chen, S., Kmieciak, M., Leng, Y., Lin, H., Rizzo, K. A., Dumur, C. I., Ferreira-Gonzalez, A., Dai, Y. & Grant, S. (2015) A regimen combining the Wee1 inhibitor AZD1775 with HDAC inhibitors targets human acute myeloid leukemia cells harboring various genetic mutations. *Leukemia,* 29(4)**,** 807-18.

Zhou, X. Y., Wang, X., Hu, B., Guan, J., Iliakis, G. & Wang, Y. (2002) An ATM-independent S-phase checkpoint response involves CHK1 pathway. *Cancer Res,* 62(6)**,** 1598-603.

Zhu, J. Y., Cuellar, R. A., Berndt, N., Lee, H. E., Olesen, S. H., Martin, M. P., Jensen, J. T., Georg, G. I. & Schonbrunn, E. (2017) Structural Basis of Wee Kinases Functionality and Inactivation by Diverse Small Molecule Inhibitors. *Journal of Medicinal Chemistry,* 60(18)**,** 7863-7875.

Ziemann, F., Arenz, A., Preising, S., Wittekindt, C., Klussmann, J. P., Engenhart-Cabillic, R. & Wittig, A. (2015) Increased sensitivity of HPV-positive head and neck cancer cell lines to x-irradiation ± Cisplatin due to decreased expression of E6 and E7 oncoproteins and enhanced apoptosis. *Am J Cancer Res,* 5(3)**,** 1017-31.

Zimmermann, A., Zenke, F. T., Chiu, L. Y., Dahmen, H., Pehl, U., Fuchss, T., Grombacher, T., Blume, B., Vassilev, L. T. & Blaukat, A. (2022) A New Class of Selective ATM Inhibitors as Combination Partners of DNA Double-Strand Break Inducing Cancer Therapies. *Mol Cancer Ther,* 21(6)**,** 859-870.

Zorba, A., Nguyen, C., Xu, Y., Starr, J., Borzilleri, K., Smith, J., Zhu, H., Farley, K. A., Ding, W., Schiemer, J., Feng, X., Chang, J. S., Uccello, D. P., Young, J. A., Garcia-Irrizary, C. N., Czabaniuk, L., Schuff, B., Oliver, R., Montgomery, J., Hayward, M. M., Coe, J., Chen, J., Niosi, M., Luthra, S., Shah, J. C., El-Kattan, A., Qiu, X., West, G. M., Noe, M. C., Shanmugasundaram, V., Gilbert, A. M., Brown, M. F. & Calabrese, M. F. (2018) Delineating the role of cooperativity in the design of potent PROTACs for BTK. *Proc Natl Acad Sci U S A,* 115(31)**,** E7285-E7292.

Zou, L. & Elledge, S. J. (2003) Sensing DNA damage through ATRIP recognition of RPA-ssDNA complexes. *Science,* 300(5625)**,** 1542-8.